



# **CFD Analysis of FDA Round Robin Benchmark #1**

## **Final Year Project - Final Report**

**Bearach Byrne**

**C15379616**

**DT022**

Submitted to the Technological University Dublin in partial fulfilment of the requirements for the degree of Bachelor of Engineering (Hons) in Mechanical Engineering (DT022)

Supervisor: Professor Fergal J. Boyle

School of Mechanical & Design Engineering

College of Engineering & Built Environment

Technological University Dublin

*April 2019*

# DECLARATION

I hereby certify that this material, which I now submit for assessment on the programme of study leading to the award of BEng in Mechanical Engineering is entirely my own work and has not been submitted for assessment for any academic purpose other than in partial fulfilment for that stated above

*Signed Bearach Byrne...*

Bearach Byrne - C15379616

*29th April 2019*  
*Date .....*

29/04/2019

# **ACKNOWLEDGEMENTS**

I would like to thank first and foremost my supervisor Professor Fergal Boyle for his help and guidance throughout the entirety of this project.

I would also like to thank all of the staff at CADFEM Ireland for their help and expertise when it comes to all things ANSYS. In my 2 month internship during the summer of 2018 I learned a huge amount about computer aided engineering and computational fluid dynamics, which helped to inspire my choice of final year project and also provided me with a great starting point for the project.

A special thanks goes to Adrian Dunne at CADFEM, who was always more than happy to help guide me through any problems and issues I faced over the course of this project.

- Bearach Byrne

# TABLE OF CONTENTS

Declaration .....	i
Acknowledgements .....	ii
Table of Contents .....	iii
List of Figures .....	vii
List of Tables .....	xiii
Nomenclature .....	xiv
Abstract .....	1
Chapter 1 Introduction .....	2
1.1 Aim .....	2
1.2 Objectives .....	2
1.3 Project Timeline .....	3
1.3.1 Gantt Chart .....	3
1.4 Methods .....	4
1.4.1 Research .....	4
Chapter 2 Literature Review .....	6
2.1 Medical Devices .....	6
2.1.1 Classification of Medical Devices .....	6
2.1.2 Blood Contacting Medical Devices .....	7
2.2 Paper Reviews .....	9
2.2.1 Title of Paper: “Computational Fluid Dynamics for Medical Device Design and Evaluation: Are We There Yet?” .....	9
2.2.2 Title of Paper: “CFD Validations with FDA Benchmarks of Medical Devices Flows” .....	11
2.2.3 Title of Paper: “FDA’s Nozzle Numerical Simulation Challenge: Non-Newtonian Fluid Effects and Blood Damage” .....	12
Chapter 3 Computational Fluid Dynamics .....	15

3.1	ANSYS CFX .....	15
3.2	Navier-Stokes Equations .....	16
3.3	Reynolds Averaged Navier-Stokes Equations (RANS) .....	17
3.4	Direct Numerical Simulation (DNS).....	18
3.5	Large Eddy Simulation (LES).....	18
	Chapter 4 FDA Round Robin .....	19
4.1	Critical Path Initiative .....	19
4.1.1	Benchmark 1 / Computational Round Robin 1 .....	20
4.1.2	Benchmark 2 / Computational Round Robin 2.....	22
4.2	Test Case .....	22
4.3	Validation.....	22
4.3.1	Particle Image Velocimetry (PIV) .....	22
4.3.2	CFD Model Validation .....	25
4.3.3	Data.....	26
	Chapter 5 Laminar Pipe Flow Model.....	28
5.1	Introduction .....	28
5.2	Geometry.....	28
5.3	Mesh.....	29
5.3.1	Geometry Decomposition .....	29
5.3.2	Mesh Controls.....	31
5.3.3	Final Meshes .....	34
5.4	Theoretical Calculations.....	40
5.4.1	Hand Calculations.....	40
5.4.2	Excel Workbook Calculations .....	41
5.5	Model Setup .....	42
5.5.1	Working Fluid.....	42
5.5.2	Boundary Conditions .....	44

5.5.3	Solver Control.....	49
5.5.4	Expressions .....	50
5.6	Solution .....	51
5.7	Model Validation.....	53
5.8	Mesh Convergence Study.....	54
5.8.1	Mesh Details .....	54
5.8.2	Mesh Convergence Results.....	56
5.8.3	Conclusion .....	60
5.9	Conclusion.....	60
Chapter 6	Final Model .....	62
6.1	Introduction .....	62
6.2	Geometry.....	62
6.3	Mesh .....	63
6.3.1	Mesh Controls.....	64
6.3.2	Area of Interest .....	65
6.3.3	Final Meshes .....	67
6.4	Model Setup .....	79
6.4.1	Working Fluid.....	79
6.4.2	Theoretical Calculations .....	79
6.4.3	Boundary Conditions .....	80
6.4.4	Solver Control.....	85
6.4.5	Expressions .....	86
6.5	Model Solution.....	87
6.6	Mesh Convergence.....	90
6.6.1	Mesh Details .....	91
6.6.2	Mesh Convergence Results.....	91
6.6.3	Conclusion .....	93

Chapter 7 Results .....	94
7.1 Velocity .....	94
7.2 Pressure .....	102
7.3 Results Validation .....	103
7.3.1 Centreline Velocity .....	103
7.3.2 Centreline Pressure .....	105
7.3.3 Wall Pressure .....	106
7.3.4 Axial Velocity Slices .....	107
Chapter 8 Conclusions & Recommendations .....	114
8.1 Conclusions .....	114
8.1.1 Comparison of Results.....	114
8.2 Recommendations .....	115
8.2.1 Normalised Pressure Comparison.....	115
8.2.2 Further Test Cases.....	115
8.2.3 Two Dimensional Simulations.....	116
8.2.4 Wedge Simulations .....	117
8.2.5 Larger Meshes.....	119
8.2.6 More Strict Convergence Criteria.....	119
8.2.7 Critical Path Initiative .....	119
References.....	I
Appendix A - Gantt Chart.....	V
Appendix B - FDA Dataset.....	VI
Appendix C - CFD Dataset.....	VII
Appendix D - Final Model Centreline Velocity .....	VIII
Appendix E - Final Model Centreline Pressure .....	IX

# LIST OF FIGURES

Figure 1 - Project Gantt Chart created using Microsoft Excel at the start of the project.....	3
Figure 2 - Final Gantt chart.....	4
Figure 3 - A flowchart examining some of the key areas of research for this project.....	5
Figure 4- An example of a modern coronary stent designed by Boston Scientific [5].....	8
Figure 5 - An example of a modern pulsatile artificial blood pump system [6].....	8
Figure 6 - Workbench toolbox showing the CFX analysis system.....	15
Figure 7 - A blank CFX module in Workbench .....	15
Figure 8 - The general CFX workflow [11].....	16
Figure 9 - The website detailing the round robin study .....	19
Figure 10 - Benchmark 1 geometry provided by The FDA [20] .....	20
Figure 11 - Benchmark 1 geometry rendered in Solidworks 2018 Photoview 360 .....	21
Figure 12 - Dimensioned 2D drawing of Benchmark 1 [1] .....	21
Figure 13 - The geometry provided for the blood pump benchmark [21] .....	22
Figure 14 - Simplified schematic diagram showing the layout of the experimental model ....	23
Figure 15 - An example of a machined acrylic tube, similar to the model used in the PIV experiments [22] .....	24
Figure 16 - An example of flow analysis around a cylinder using Particle Image Velocimetry (PIV) [23].....	24
Figure 17 - A schematic diagram showing how PIV is carried out [24] .....	24
Figure 18 - The NCIP Hub website showing where the data sets were downloaded for .....	26
Figure 19 - The text file containing experimental data.....	26
Figure 20 - The velocity data after being imported into Excel .....	27
Figure 21 - The 12 locations where experimental axial velocity readings were taken .....	27
Figure 22 - The final geometry showing the section used in this analysis, render generated in Solidworks Photoview 360 .....	28
Figure 23 - Showing the sketch used to create the outer portion of the cylinder .....	29
Figure 24 - Showing the sketch and dimensions used to create the central prism.....	30
Figure 25 - The ANSYS Meshing tree, showing the structure of the mesh .....	31
Figure 26 - The details tab of the mesh overview.....	31
Figure 27 - Selecting different physics preferences can have a large impact on the final mesh generated [26] .....	32

Figure 28 - Isometric view of the model showing the guide lines used for the mesh sizing ...	32
Figure 29 - The face sizing used on the central prism .....	32
Figure 30 - The edge sizing method used on the outer circular edge .....	33
Figure 31 - The edge sizing method used on the top and right guide lines .....	33
Figure 32 - The edge sizing method used on the bottom and left guide lines .....	33
Figure 33 - Front view of mesh 1.....	34
Figure 34 - Isometric view showing cutaway of mesh 1 .....	35
Figure 35 - Front view of mesh 2.....	36
Figure 36 - Isometric view showing cutaway of mesh 2 .....	36
Figure 37 - Front view of mesh 3.....	37
Figure 38 - Isometric view showing cutaway of mesh 3 .....	37
Figure 39 - Front view of mesh 4.....	38
Figure 40 - Isometric view showing cutaway of mesh 4 .....	38
Figure 41 - Front view of mesh 5.....	39
Figure 42 - Isometric view showing cutaway of mesh 5 .....	39
Figure 43 - The workbook created to keep track of multiple theoretical calculations .....	42
Figure 44 - The properties settings for the new fluid.....	43
Figure 45 - The fluid selection menu.....	44
Figure 46 - Outline tree structure in CFX-Pre .....	44
Figure 47 - Isometric view of the model with all boundaries highlighted in green. The black vector arrows show the inlet and outlet of the fluid domain.....	45
Figure 48 - The inlet boundary details .....	46
Figure 49 - The inlet velocity profile shown plotted within CFX-Pre using CEL .....	46
Figure 50 - A boundary contour plot showing the velocity profile of the fluid as it enters the domain. Note - red denotes a minimum velocity and blue denotes a maximum velocity .....	47
Figure 51 - The inlet velocity profile plotted using vector arrows .....	47
Figure 52 - The outlet boundary details .....	48
Figure 53 - A closeup of the outlet boundary .....	48
Figure 54 - The wall boundary details .....	49
Figure 55 - Isometric view highlighting the wall boundary in green .....	49
Figure 56 - The solver control menu.....	50
Figure 57 - The CEL expressions used for this model.....	50

Figure 58 - The "Define Run" dialog box allows the user to easily set the number of CPU cores to be used when solving the CFD code. Along with the option of “Double Precision” mode and “Large Problem” mode .....	51
Figure 59 - Windows Task Manager showing the laptop CPU under 100% load on all 4 virtual CPU cores while solving a CFD model .....	52
Figure 60 - The RMS values plotted against the accumulated time step of the crudest mesh.	52
Figure 61 - The total wall clock time needed for the crudest mesh to achieve RMS values of $1 \times 10^{-7}$ .....	53
Figure 62 - The final iteration of the crudest mesh, showing that convergence of the RMS residuals was achieved .....	53
Figure 63 - Screenshot from Workbench showing the output parameters table view .....	56
Figure 64 - Plot of pressure drop against number of nodes in mesh.....	57
Figure 65 - Plot of pressure drop against number of nodes in mesh (with adjusted Y axis) ...	58
Figure 66 - Plot of the % change in pressure drop against mesh size.....	58
Figure 67 - Plot of mass flow rate against mesh size.....	59
Figure 68 - Plot showing the % change in mass flow rate against size of mesh .....	59
Figure 69 - Plot showing the mass imbalance plotted against mesh size .....	60
Figure 70 - Isometric view showing streamlines coloured by velocity .....	61
Figure 71 - Flowchart showing the steps taken to create the geometry.....	62
Figure 72 - Benchmark #1 geometry .....	62
Figure 73 - The geometry modelled in Solidworks .....	63
Figure 74 - The geometry opened in Design Modeler after being imported to Workbench ...	63
Figure 75 - The outline tree in ANSYS Meshing .....	64
Figure 76 - Mesh details .....	65
Figure 77 - Sphere of influence body sizing around the area of interest .....	66
Figure 78 - Profile view of the mesh .....	66
Figure 79 - Profile view of mesh 1 .....	68
Figure 80 - Isometric view of mesh 1 .....	68
Figure 81 - Isometric cutaway view of mesh 1 .....	69
Figure 82 - Profile view of mesh 2 .....	69
Figure 83 - Isometric view of mesh 2 .....	70
Figure 84 - Isometric cutaway view of mesh 2 .....	70
Figure 85 - Profile view of mesh 3 .....	71
Figure 86 - Profile view of mesh 3 .....	71

Figure 87 - Isometric view of mesh 3 .....	72
Figure 88 - Isometric view of mesh 3 .....	72
Figure 89 - Isometric cutaway view of mesh 3 .....	73
Figure 90 - Profile view of mesh 4 .....	73
Figure 91 - Profile view of mesh 4 .....	74
Figure 92 - Isometric view of mesh 4 .....	74
Figure 93 - Isometric view of mesh 4 .....	75
Figure 94 - Isometric cutaway view of mesh 4 .....	75
Figure 95 - Profile view of mesh 5 .....	76
Figure 96 - Profile view of mesh 5 .....	76
Figure 97 - Profile view of mesh 5 .....	77
Figure 98 - Isometric view of mesh 5 .....	77
Figure 99 - Isometric view of mesh 5 .....	78
Figure 100 - Isometric view of mesh 5 .....	78
Figure 101 - Isometric cutaway view of mesh 5 .....	79
Figure 102 - Outline tree structure in CFX-Pre .....	80
Figure 103 - Isometric view of the model with all boundaries highlighted in green. The black vector arrows show the inlet and outlet of the fluid domain.....	81
Figure 104 - The CEL expression used to define the inlet velocity profile .....	81
Figure 105 - The inlet boundary details .....	82
Figure 106 - The inlet velocity profile shown plotted within CFX-Pre using CEL .....	82
Figure 107 - A boundary contour plot showing the velocity profile of the fluid as it enters the domain. Note - red denotes a minimum velocity and blue denotes a maximum velocity .....	83
Figure 108 - The inlet velocity profile plotted using vector arrows .....	83
Figure 109 - The outlet boundary details .....	84
Figure 110 - A closeup of the outlet boundary .....	84
Figure 111 - The wall boundary details .....	85
Figure 112 - Isometric view highlighting the wall boundary in green .....	85
Figure 113 - The solver control menu.....	86
Figure 114 - The CEL expressions used for this model.....	87
Figure 115 - The "Define Run" dialog box allows the user to easily set the number of CPU cores to be used when solving the CFD code. Along with the option of “Double Precision” mode and “Large Problem” mode.....	88

Figure 116 - Windows Task Manager showing the laptop CPU under 100% load on all 8 virtual CPU cores while solving a CFD model .....	88
Figure 117 - - The RMS values plotted against the accumulated time step for the final mesh	89
Figure 118 - The total wall clock time needed for the crudest mesh to achieve RMS values of $1 \times 10^{-8}$ .....	90
Figure 119 - Pressure drop plotted against number of nodes in mesh .....	92
Figure 120 - Variation from theoretical mass flow rate Vs number of nodes in mesh.....	92
Figure 121 - Variation in mass flow flow rate Vs number of nodes in mesh .....	93
Figure 122 - Geometry showing the 12 slice locations.....	94
Figure 123 - Showing the 12 slices in CFD post .....	94
Figure 124 - Axial velocity at $Z = -0.088$ m .....	95
Figure 125 - Axial velocity at $Z = -0.064$ m .....	95
Figure 126 - Axial velocity at $Z = -0.048$ m .....	96
Figure 127 - Axial velocity at $Z = -0.02$ m .....	96
Figure 128 - Axial velocity at $Z = -0.008$ m .....	97
Figure 129 - Axial velocity at $Z = 0.0$ m .....	97
Figure 130 - Axial velocity at $Z = 0.008$ m .....	98
Figure 131 - Axial velocity at $Z = 0.016$ m .....	98
Figure 132 - Axial velocity at $Z = 0.024$ m .....	99
Figure 133 - Axial velocity at $Z = 0.032$ m .....	99
Figure 134 - Axial velocity at $Z = 0.060$ m .....	100
Figure 135 - Axial velocity at $Z = 0.088$ m .....	100
Figure 136 - Slice showing the velocity along the centre of the geometry.....	101
Figure 137 - The 12 axial velocity profile locations that will be compared against the expeirmental measurements.....	101
Figure 138 - Streamline visualisation that coloured to show velocity.....	102
Figure 139 - Pressure along the centreline of geometry .....	102
Figure 140 - Centreline velocity, comparison of CFD and experimental.....	103
Figure 141 - Centreline slice of velocity.....	104
Figure 142 - Centreline pressure distribution .....	105
Figure 143 - Centreline slice of pressure .....	105
Figure 144 - Wall pressure distribution along the length of the geometery .....	106
Figure 145 - CFD vs experimental velocity @ $Z = -0.088$ m.....	107
Figure 146 - CFD vs experimental velocity @ $Z = -0.064$ m.....	108

Figure 147 - CFD vs experimental velocity @ Z = -0.048 m.....	108
Figure 148 - CFD vs experimental velocity @ Z = -0.020 m.....	109
Figure 149 - CFD vs experimental velocity @ Z = -0.008 m.....	109
Figure 150 - CFD vs experimental velocity @ Z = 0.000 m .....	110
Figure 151 - CFD vs experimental velocity @ Z = 0.008 m .....	110
Figure 152 - CFD vs experimental velocity @ Z = 0.016 m .....	111
Figure 153 - CFD vs experimental velocity @ Z = 0.024 m .....	111
Figure 154 - CFD vs experimental velocity @ Z = 0.032 m .....	112
Figure 155 - CFD vs experimental velocity @ Z = 0.060 m .....	112
Figure 156 - CFD vs experimental velocity @ Z = 0.080 m .....	113
Figure 157 - An example of a 2D simulation created in ANSYS Fluent [31].....	117
Figure 158 - View of the 10 degree wedge of the geometry .....	118
Figure 159 - View of the 10 degree wedge of the geometry .....	118
Figure 160 - Profile view of the 10 degree wedge of the geometry .....	119

# LIST OF TABLES

Table 1 - PIV Experimental parameters.....	21
Table 2 - The test cases that were completed in the FDA study.....	22
Table 3 - PIV Experimental parameters.....	25
Table 4 - The assumed information about the pipe and fluid .....	40
Table 5 - Table created in Excel that was used to compare the model values with theoretical values .....	54
Table 6 - The mesh sizing chart created in Excel .....	55
Table 7 - Tabulated results from the 5 meshes .....	56
Table 8 - The sizing and element/node counts for each of the final meshes .....	67
Table 9 - Mesh convergence study results .....	91
Table 10 - Centreline velocity CFD Vs PIV .....	104
Table 11 - Centreline pressure - CFD Vs Experimental .....	106
Table 12 - The experimental test cases .....	115

# NOMENCLATURE

510(K)

A type of form that may need to be submitted to the CDRH in order to achieve classification of a medical device, 9, 10

CDRH

Centre for Devices & Radiological Health (sub office of the FDA), 9, 10

CFD

Computational Fluid Dynamics, 30

DNS

Direct Numerical Simulation, 19

Excel

Microsoft Excel, 3, 30, 42, 54, 55

FDA

US Food and Drug Administration, 1

hemodynamics

General term referring to the flow of blood, 11

LES

Large Eddy Simulation, 19

PIV

Particle Image Velocimetry, 2, 6, 8, 22, 24, 25, 26, 40

RANS

Reynolds Averaged Navier Stokes [Equations], 18

RMS

Root mean square, 49, 52, 53, 83

Round Robin

A study that is started by one group and successively continued by other groups in turn, 1, 2, 20, 21, 23, 24

Workbench

ANSYS Workbench, 16, 30, 43, 55, 59, 61, 91

# ABSTRACT

CFD can provide massive cost and time savings if it can be successfully leveraged in the design of products. This project focuses on the use of CFD in the design of blood carrying medical devices. The project centres around the FDA Benchmark #1 geometry. The geometry was designed by the FDA to give rise to various fluid flow phenomena that commonly occur in blood carrying medical devices, such as:

- Flow separation
- Intense shear layers
- Transition from laminar to turbulent flow
- Favourable and adverse pressure gradients [1]

In being able to reproduce these phenomena in a known geometry, the study provides a useful testbed for validating CFD models of medical devices.

The purpose of this project is to create an accurate CFD model simulating fluid flow through the given FDA Round Robin Benchmark #1 geometry for test case where the Reynolds number at the narrowest point in the geometry is equal to 500.

Once the CFD analysis was carried out, the results were compared against measurements from physical experiments on the geometry that were carried out by the FDA. The experimental measurements consist of velocity information captured using PIV methods, and pressure information measured using pressure taps.

These CFD velocity results presented very good agreement with the experimental measurements. The CFD pressure results present good agreement with the experimental measurements.

Recommendations were then made about how to potentially improve the results, along with some directions that future projects related to this project could proceed in.

# Chapter 1

## INTRODUCTION

The following chapter seeks to provide an understanding for the basis of the project, the aims of the project, the timeline of the project, how the project will be completed, what results were obtained and what validation methods were used to verify the results.

### 1.1 AIM

The overarching aim for this project is to create a true to life CFD model of fluid flow through the FDA Round Robin conical nozzle geometry, using the experimental particle image velocimetry data to validate the CFD model.

### 1.2 OBJECTIVES

In order to create this CFD model, a number of separate steps are necessary:

- Research
  - Research medical devices
  - Research CFD
  - Research CFD for medical devices
  - Papers released on the FDA Round Robin
- Modelling
  - Model geometry creation
  - Meshing
  - Mesh convergence study
- Analysis
  - Comparison of CFD model results to FDA PIV experimental measurements (velocity)
  - Comparison of CFD model results to FDA experimental pressure measurements

## 1.3 PROJECT TIMELINE

The timeline of this project was dictated by the terms of the Technological University Dublin, in agreement with the academic year of the University. The project began in the second week of September 2018 (the week of the 17<sup>th</sup>) and continued until its completion at the beginning of April. This gives a duration of approximately 29 weeks, not including exam weeks or holidays.

### 1.3.1 Gantt Chart

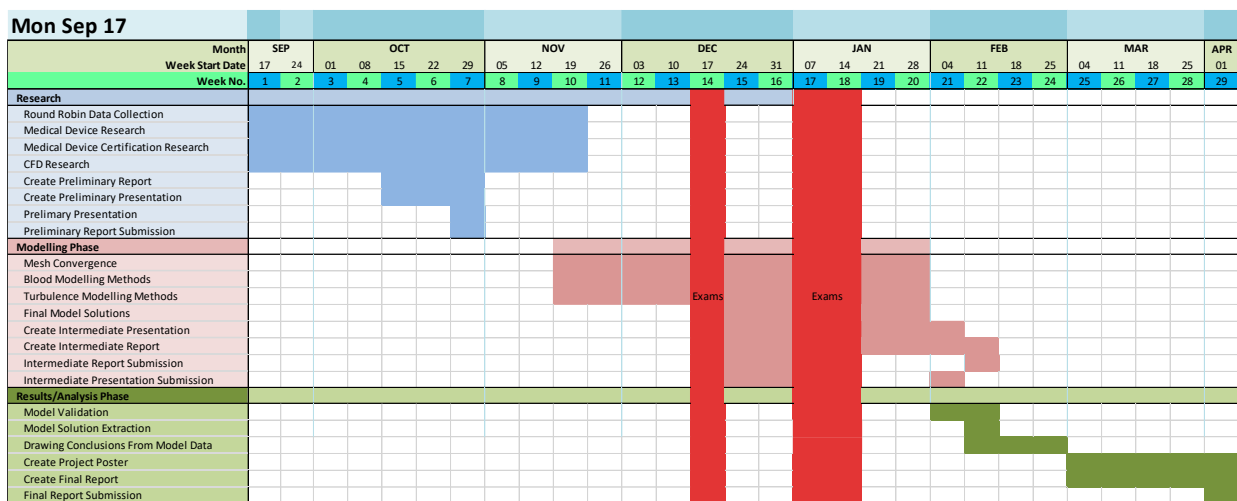
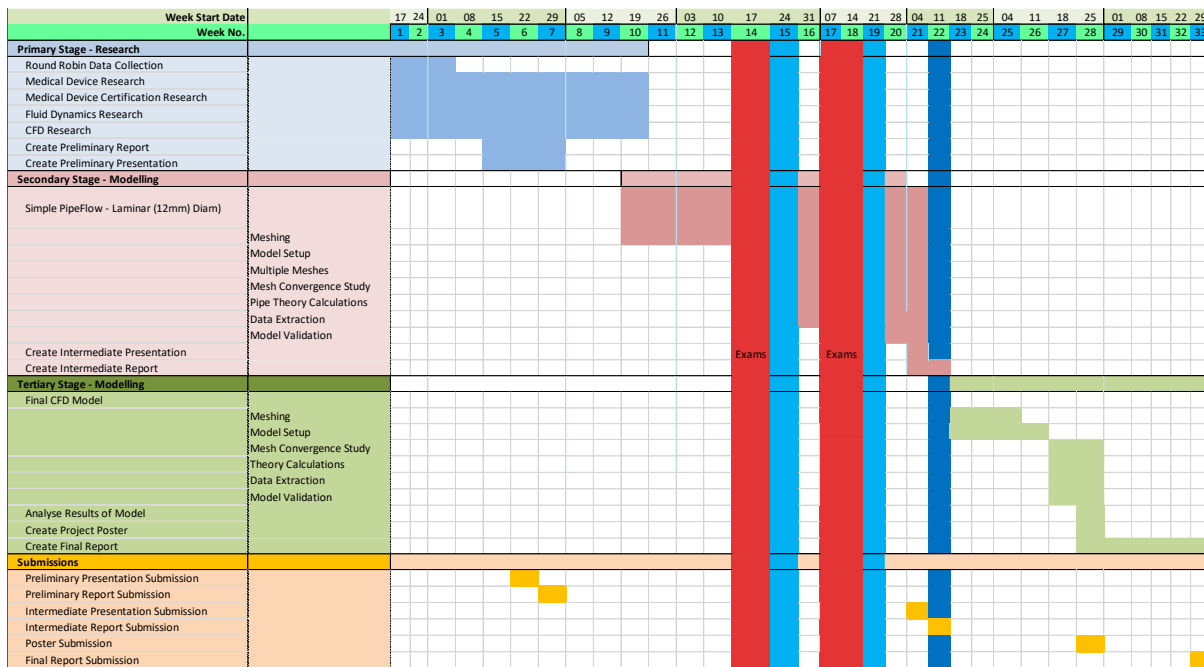


Figure 1 - Project Gantt Chart created using Microsoft Excel at the start of the project

The Gantt chart was created in Microsoft Excel using the provided submission dates for this project. The project took place over approximately 29 weeks, beginning in the 3<sup>rd</sup> week of September and continued until April 2019. For a full-page version of this chart, please see appendix.

The project was divided into three distinct stages, the first being the research stage, the second being the modelling phase, and the third being the results/analysis stage. There is some overlap between the first two phases of the project, as some research will be conducted concurrently with the modelling phase.

This Gantt chart is the basis of the project time management plan and was continuously updated throughout the duration of the project as tasks were completed and as new tasks were added.



*Figure 2 - Final Gantt chart*

## 1.4 METHODS

In order to effectively complete this project, it was divided into 3 main stages:

The first, the research stage, can be seen below. The second deals with the first model that was created, which is detailed in chapter 5. And finally, the third stage deals with the final CFD model of the FDA geometry, which is detailed in chapter 6 and 7.

#### 1.4.1 Research

The research for this project was mostly completed using the TUD Library resources that are provided to all students. The main resources that are available are:

- Physical
    - The physical books available within the TUD campus libraries
    - The dissertations completed by past students available in the library
  - Digital
    - The E-books available through the TUD library website
    - The scientific paper/ journal databases provided by TUD:
      - Science Direct
      - Arrow@TUD
      - Summon@TUD

- JSTOR
- Online websites
- Free to view scientific paper resources
- The FDA website ([www.fda.gov](http://www.fda.gov))
- The NCIP Hub ([www.nciphub.org](http://www.nciphub.org))

The above list is not a comprehensive list of all resources used. If a source is referenced in this report it will be clearly marked where it was taken from.

Once a clear objective was set out for what was needed to be researched, data collection began on the various topics (as shown in section 1.2 Objectives). This data collection involved searching all of the above stated resources for any books/papers/websites that appeared to have relevant information. All the information that was collected was then carefully read and summarised, to determine which information collected was relevant to the project.

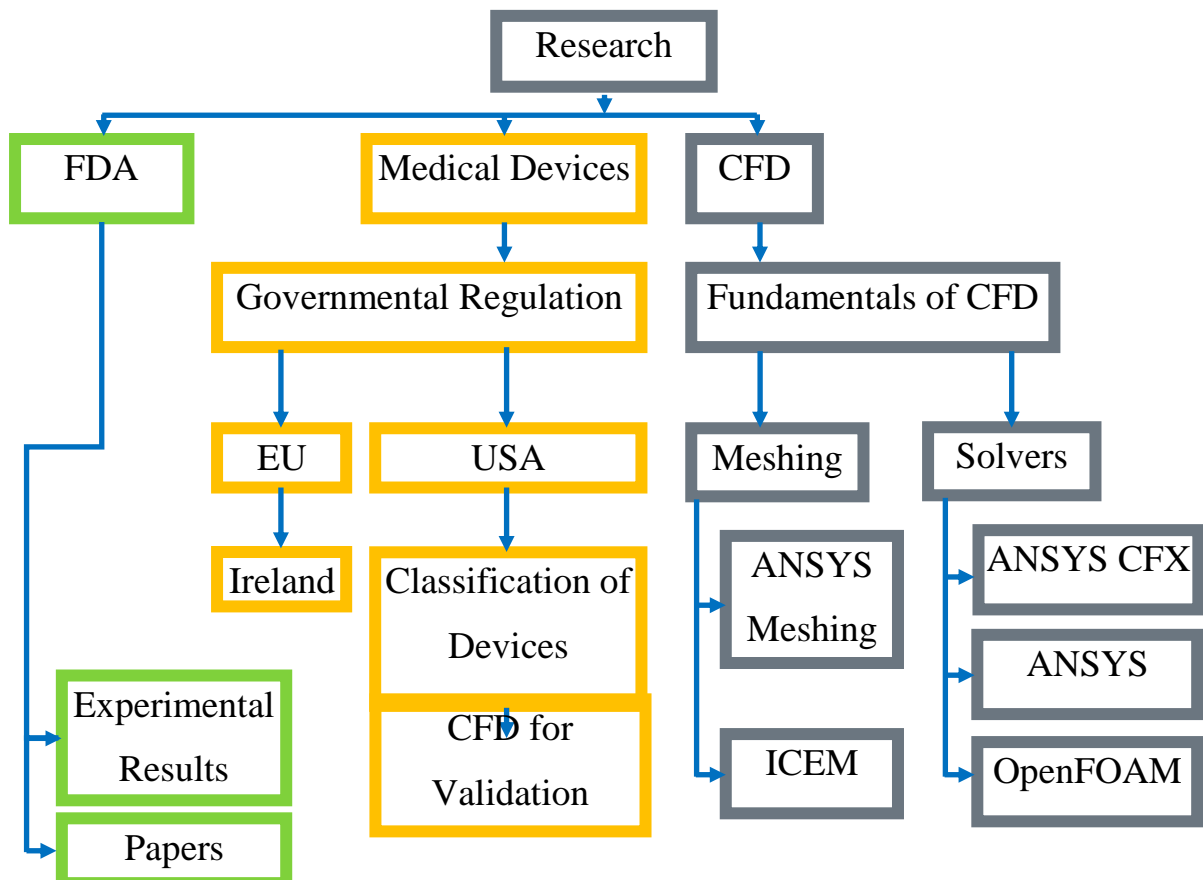


Figure 3 - A flowchart examining some of the key areas of research for this project

# Chapter 2

## LITERATURE REVIEW

This chapter will provide an overview and some commentary on the research that was conducted throughout this project. The main focus of the background research was that of medical devices and FDA Round Robin 1, the research that was conducted with respect to CFD can be seen in Chapter 3 - Computational Fluid Dynamics. The research that was conducted on the FDA Round Robin study can be seen in Chapter 4 - FDA Round Robin.

### 2.1 MEDICAL DEVICES

#### 2.1.1 Classification of Medical Devices

##### *2.1.1.1 Government Bodies*

Each nation across the world has their own national body that deals with the regulation of medical devices; some examples are shown below:

- USA - US Food and Drug Administration (FDA)
- Japan - Ministry of Health, Labour and Welfare (MHLW)
- Canada – Health Canada
- Ireland – Health Products Regulatory Authority (HPRA)

The European Union (EU) is an interesting case as they provide a framework to all member states to allow them to develop their own governmental body to take charge of medical device regulation in that country. This framework is known as the European Union Medical Device Regulation Framework and is issued by the EU Council. [2]

##### *2.1.1.2 FDA Classification*

Within the FDA, the office that deals with the regulation and classification of medical devices is that of the Centre for Devices and Radiological Health (CDRH), it divides all medical devices into 3 broad categories:

- Class 1 – Low risk - Everyday items (e.g. electric toothbrushes, bandages, manual stethoscopes), these make up 47% of medical devices for sale in the United States of America. 95% of class 1 devices are exempt from needing to submit a 510(K) or Premarket Notification (PMN) to the CDRH.

- Class 2 – Medium risk (e.g. pregnancy testing kits, electric wheelchairs) – These make up 43% of medical devices for sale in the USA. Class 2 devices require a 510(K) (aka PMN) to be submitted to the CDRH.
- Class 3 – High risk - Implantable medical devices (e.g. stents, pacemakers, breast implants). These devices make up the remaining 10% of medical devices currently for sale in the USA. Class 3 devices require a Pre-Market Approval (PMA) to be submitted to the CDRH, which is a much more detailed application than the 510(K), the contents of which go beyond the scope of this project. [3] [4] [5]

### 2.1.2 Blood Contacting Medical Devices

Blood contacting medical device is a general term that is used to refer to any implantable medical device that comes into physical contact with blood. This includes blood carrying devices such as cardiovascular stents, blood pumps, artificial cardiovascular valves.

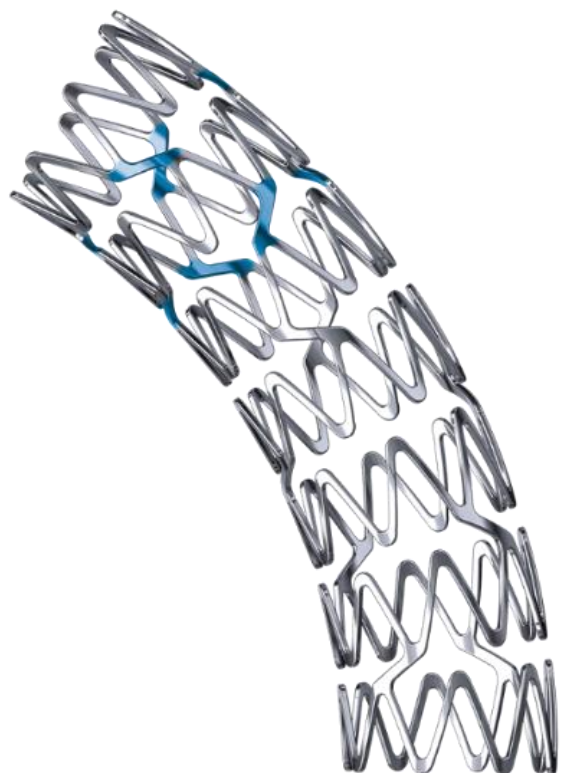


Figure 4- An example of a modern coronary stent designed by Boston Scientific [5]

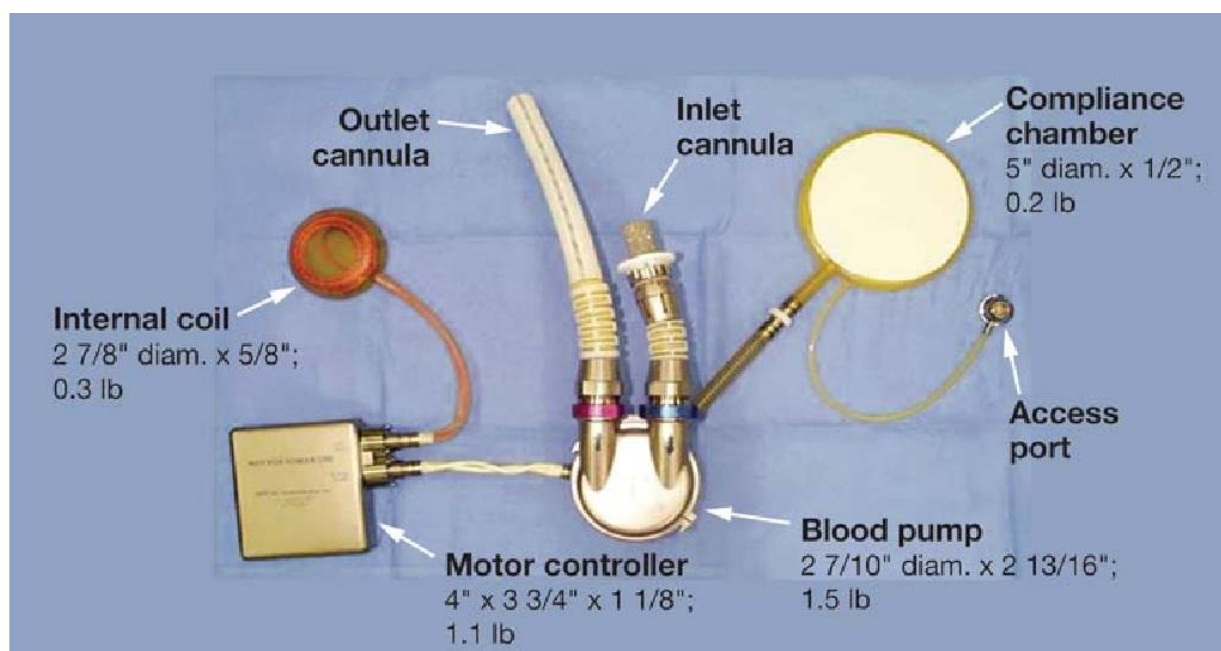


Figure 5 - An example of a modern pulsatile artificial blood pump system [6]

## 2.2 PAPER REVIEWS

This section features a number of summaries of papers related to the topics dealt with in this project.

### 2.2.1 Title of Paper: “Computational Fluid Dynamics for Medical Device Design and Evaluation: Are We There Yet?”

*Author(s) of Paper: Fotis Sotiropoulos, Director St. Anthony Falls Laboratory*

*Professor James L. Record, Department of Civil Engineering,  
University of Minnesota*

*Published in Cardiovascular Engineering and Technology (CVET), Vol. 3, No. 2, June 2012 (2012)  
pp. 137–138 [7]*

#### 2.2.1.1 Summary

CFD analysis of medical devices is not yet a required component of premarket notifications & applications, however it has already established itself as a useful tool in cardiovascular hemodynamics. This is evidenced by: numerous papers published in Cardiovascular Engineering and Technology (CVET), other journals in the field, and at conferences and workshops.

These are all papers employing CFD to analyse flow patterns and draw conclusions about performance of devices.

CFD is so widespread that papers may refer to CFD or ‘Standard CFD’ as the main method employed to carry out simulations, without any specifics about the CFD methods/assumptions used. Thus, it is believed by many that CFD is a mature, universally accepted technology. This leads many to the conclusion that CFD can be used with little scrutiny in the design of medical devices.

The authors Sotiropoulos and Record believe that because of the prevalence of CFD in industry, the results of Stewart et Al 2012 (“Assessment of CFD Performance in Simulations of an Idealized Medical Device - Results of FDA’s First Computational Interlaboratory Study”) are so shocking.

Complexities commonly encountered with medical device simulations were ignored. Issues such as:

- Complex 3D geometries with moving boundaries
- Fluid Structure interaction
- Flow pulsatility
- Small gaps

The CFD phase was accompanied by Particle Image Velocimetry (PIV) experiments carried out in 3 FDA labs. These experimental measurements provided benchmark data for validating the CFD results.

The authors go on to state that in Stewart et Al (2012) show that none of the 28 CFD simulations contributed by an international group of researchers yielded results that agreed with the PIV results. All simulations showed scatter and variation not only the PIV results, but also with each other.

These CFD simulations are not cutting edge, however they serve to challenge the notion of ‘standard CFD’.

Sotiropoulos and Record go on to say that not all CFD codes are created equal. Different CFD codes/solvers deal with certain issues in very different ways. Issues such as:

- The order of accuracy of spatial and temporal discretization techniques
- The iterative solvers and schemes used to achieve convergence
- The level of convergence achieved
- The quality of the mesh and the sensitivity of the solver to mesh quality and density
- The treatment of inflow, outflow and wall boundaries
- The manner in which laminar-to-turbulence transition and fully turbulent flow regimes are handled by the code

The authors believe that all of the above mentioned issues are of great importance and deserve attention and extensive discussion in CFD studies. The authors go on to say that this study underscores the need for continuous, systematic validation of CFD techniques.

A common feature of all CFD models in this study is the use of statistical turbulence modelling approaches i.e. Reynolds Averaged Navier-Stokes (RANS) equations closed with 1 or 2 equation turbulence models. Such models have been developed and calibrated mainly for use

in the aeronautical sector. As clearly shown in Stewart et al (2012), these are not adequate for transitional cardiovascular flows. Another downside of RANS, inherent to the model is that it can only yield information about the Reynolds stresses, which do not represent the mechanical loads experienced by the blood cells.

The instantaneous viscous stresses provide a more relevant metric for quantifying blood damage but Direct Numerical Simulation (DNS) is needed for this. While DNS simulations of stenotic flows are within reach in certain limited situations, they are far too computationally demanding to be routine. However, this level of flow resolution is required if we are to use CFD as a reliable tool in medical device design.

Sotiropoulos and Record go on to say however, that there is some good news when it comes to the topic of CFD for medical device design. Two of the biggest positive factors in this regard are:

- The largest Reynolds numbers encountered in cardiovascular flow are generally less than  $R_e = 10,000$
- The exponential growth of computing power

Both of these factors have brought us closer to DNS/Large Eddy Simulation (LES) being feasible for routine use.

## 2.2.2 Title of Paper: “CFD Validations with FDA Benchmarks of Medical Devices Flows”

*Author(s) of Paper: Chien-Jung Huang*

*Inaki Caldichoury*

*Facundo Del Pin*

*Rodrigo R. Paz*

*Published at the 15<sup>th</sup> International LS-DYNA User’s Conference, June 2018 [8]*

### 2.2.2.1 Summary

CFD has proven itself to be a very powerful tool in engineering. As computers get more powerful, capability of CFD has skyrocketed. CFD is used widely in simulations of blood

flow/airflow in lungs. It is also used in design and analysis of medical devices. It is a relatively cheap and fast option for medical device development (compared to in vitro).

The authors state that hemolysis is a very important factor in medical device design. Hemolysis is prolonged large local shear stress in a vessel/cell, which can cause the destruction of blood cells. Under transitional/turbulent flow regimes, the accuracy of the CFD model has a huge amount to do with the setup of that model. Hence, it is crucial to set up proper numerical models in order to estimate the ratio of hemolysis.

The FDA is trying to standardise use of CFD in the design of blood-contacting devices. They are trying to standardise the methods for the analysis of the ratio of hemolysis in them.

To establish guidelines for applying CFD to evaluation/optimisation of medical devices, two benchmarks were created - the sudden expansion geometry & the centrifugal blood pump geometry. Experiments were carried out in various institutes and compared. In this paper, they were analysed using LS-DYNA ICFD solver.

At  $Re = 500$ , their results have good agreement with the experimental results. Velocity distribution in the throat matches well with the experimental values.

At  $Re= 3,500$  the flow fields have good agreement with experimental results, and the velocity distributions also have good agreement.

The rest of the paper is dedicated to analysing the pump benchmark, and as such was not summarised.

### 2.2.3 Title of Paper: “FDA’s Nozzle Numerical Simulation Challenge: Non-Newtonian Fluid Effects and Blood Damage”

*Author(s) of Paper:*

*Miquel Trias*

*Antonio Arbona*

*Joan Masso*

*Borja Minano*

*Carles Bona*

*The Institute of Applied Computing & Community Code  
(IAC3), University of the Balearic Islands, Palma, Spain [9]*

*Published in PLOS ONE, March 2014*

#### *2.2.3.1 Abstract*

“Data from FDA’s nozzle challenge—a study to assess the suitability of simulating fluid flow in an idealized medical device—is used to validate the simulations obtained from a numerical, finite-differences code. Various physiological indicators are computed and compared with experimental data from three different laboratories, getting a very good agreement. Special care is taken with the derivation of blood damage (hemolysis). The paper is focused on the laminar regime, in order to investigate non-Newtonian effects (non-constant fluid viscosity). The code can deal with these effects with just a small extra computational cost, improving Newtonian estimations up to a ten percent. The relevance of non-Newtonian effects for hemolysis parameters is discussed.” [9]

#### *2.2.3.2 Summary*

Data from FDA’s tests is used to validate simulations obtained from numerical and finite difference codes. Various physiological indicators are computed and compared with good agreement.

The geometry used is a simplified, idealised medical device with a small nozzle. The geometry shares characteristics with blood carrying devices such as: blood tubing, hemodialysis sets, catheters, cannulas, syringes and hypodermic needles. The device was designed to include accelerating flow, decelerating flow, variations in shear stress and velocities, and recirculating flow.

The authors state that all of these flow regimes may be related to hemolysis (i.e. blood damage) in medical devices. Five different Reynolds numbers in the throat were proposed. Lowest Reynolds number of  $Re = 500$  is selected, so DNS can be applied. At lower Reynolds numbers, lower shear rates are present, so non-Newtonian effects become more relevant.

The flow conditions for this setup are as follows:

- $Re_{in} = 167$
- $Q_{in} = 5.21 \times 10^{-3} \text{ m}^3/\text{s}$

## Numerical Scheme Used

The model used by the authors is given by Navier Stokes Eq.'s (a set of PDE's for the time evolution of density and linear momentum). In comparison to simpler Euler equations, Navier Stokes adds the possibility of including viscosity.

In hemodynamics, viscosity plays an important role. Viscosity of blood cannot be assumed to be constant as it has some non-Newtonian behaviour [10]. In combination with Navier Stokes, one must apply an equation that relates pressure with the remaining fields.

The authors go on to explain that there are some mass conservation errors, these are concentrated in the nozzle because inherently, the conical shape is harder to fit in a regular orthogonal mesh. These errors are  $\sim 0.5\%$  from the expected values.

Axial velocity profile along centreline is a key indicator of validation. The results generated agree very well with experimental findings. Another metric for validation is that of pressure along the centreline. Again, results generated agree well with experimental values. For this study, non-Newtonian effects have a limited effect on pressure values obtained.

# Chapter 3

## COMPUTATIONAL FLUID DYNAMICS

This chapter will provide a background on some fundamental information about CFD and CFD solvers that was crucial for completion of this project.

### 3.1 ANSYS CFX

CFX is a CFD software package that is integrated fully into the ANSYS Workbench suite. The module can be selected from the “Analysis Systems” section of the “Toolbox” menu. Each CFX project consists of 5 separate components: geometry, mesh, setup (CFX-Pre database), solution (CFX Solver output file), and results (CFD Post state/session file). These separate files are all obfuscated from the user, housed within a single ANSYS Workbench file (.wbpj), unless the user chooses to manually go in and view the files separately.

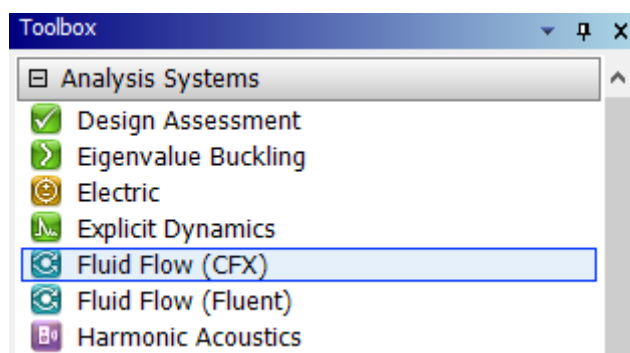


Figure 6 - Workbench toolbox showing the CFX analysis system

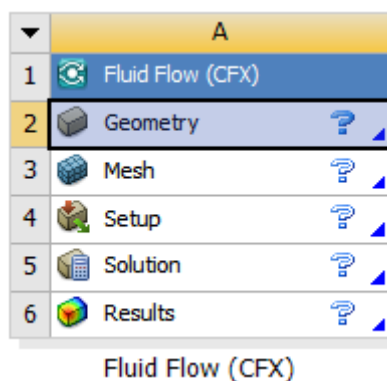
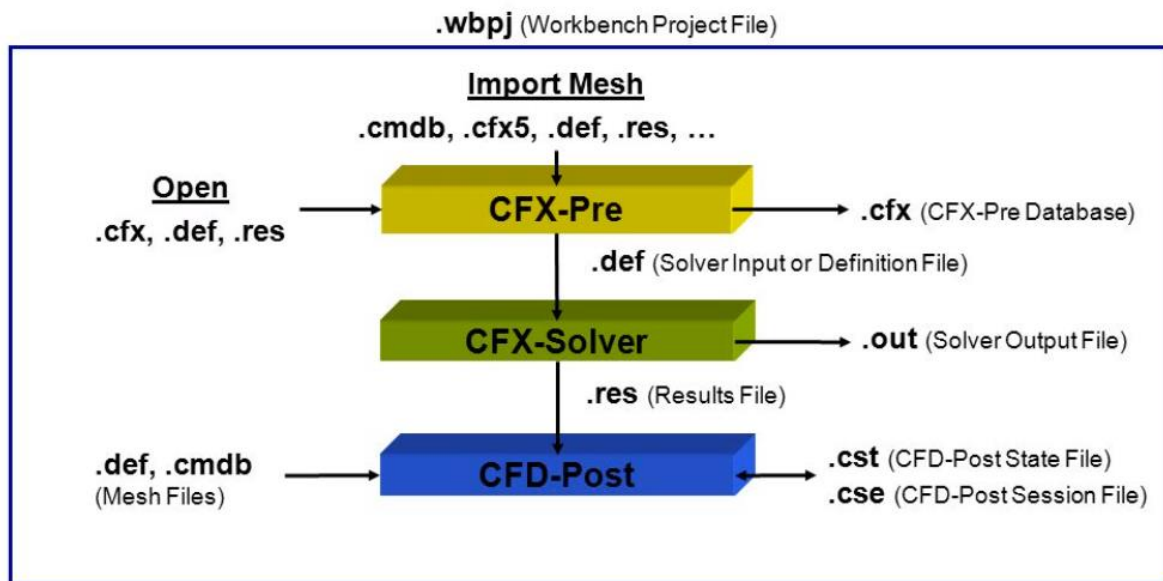


Figure 7 - A blank CFX module in Workbench

The general workflow for CFX files is shown below. Geometry creation is not shown in this image, however it could be included above “Import Mesh” while still being within the blue border.



*Figure 8 - The general CFX workflow [11]*

### 3.2 NAVIER-STOKES EQUATIONS

The Navier-Stokes equations are used to describe how the velocity, pressure, temperature, and density of a moving, incompressible fluid are related. They were independently derived by Sir George Gabriel Stokes and Claude-Louis Navier in the early 19<sup>th</sup> century. The equations are a set of coupled differential equations meaning that they are very hard to solve analytically. The field of CFD has its basis in using computers to solve approximations of these equations.

ANSYS CFX uses the unsteady Navier-Stokes equations in their conservation form. This non-dimensional form of the continuity, X, Y and Z momentum equations can be seen below.

$$\frac{\partial \rho}{\partial t} + \frac{\partial(\rho u)}{\partial x} + \frac{\partial(\rho v)}{\partial y} + \frac{\partial(\rho w)}{\partial z} = 0$$

(Eqn. 1)

$$\frac{\partial(\rho u)}{\partial t} + \frac{\partial(\rho u^2)}{\partial x} + \frac{\partial(\rho uv)}{\partial y} + \frac{\partial(\rho uw)}{\partial z} = -\frac{\partial p}{\partial x} + \frac{1}{R_e} \left[ \frac{\partial \tau_{xx}}{\partial x} + \frac{\partial \tau_{xy}}{\partial y} + \frac{\partial \tau_{xz}}{\partial z} \right]$$

(Eqn. 2)

$$\frac{\partial(\rho v)}{\partial t} + \frac{\partial(\rho uv)}{\partial x} + \frac{\partial(\rho v^2)}{\partial y} + \frac{\partial(\rho vw)}{\partial z} = -\frac{\partial p}{\partial y} + \frac{1}{R_e} \left[ \frac{\partial \tau_{xy}}{\partial x} + \frac{\partial \tau_{yy}}{\partial y} + \frac{\partial \tau_{yz}}{\partial z} \right]$$

(Eqn. 3)

$$\frac{\partial(\rho w)}{\partial t} + \frac{\partial(\rho uw)}{\partial x} + \frac{\partial(\rho vw)}{\partial y} + \frac{\partial(\rho w^2)}{\partial z} = -\frac{\partial p}{\partial z} + \frac{1}{R_e} \left[ \frac{\partial \tau_{xz}}{\partial x} + \frac{\partial \tau_{yz}}{\partial y} + \frac{\partial \tau_{zz}}{\partial z} \right]$$

(Eqn. 4)

where:

Coordinates:  $(x, y, z)$

Velocity components:  $(u, v, w)$

Time:  $t$

Pressure:  $p$

Density:  $\rho$

Stress:  $\tau$

Reynolds Number:  $Re$

[12] [13] [14]

### 3.3 REYNOLDS AVERAGED NAVIER-STOKES EQUATIONS (RANS)

The RANS equations are a statistical turbulence modelling approach.

According to [10], using the RANS equations to model blood flow is not an adequate method, as this can only yield information about the Reynolds stresses being experienced by the fluid, as opposed to the mechanical loads that are physically being exerted in the fluid. Sotiropoulos

suggests that a better method for the modelling of blood would be to use the direct numerical simulation method.

A description of why the RANS equations are used is provided in the CFX 17.0 user guide [15]. The author describes turbulence models as being used to “solve a modified set of transport equations by introducing average and fluctuating components.”

### 3.4 DIRECT NUMERICAL SIMULATION (DNS)

Direct numerical simulation is a method first proposed by [16], in which the Navier-Stokes equations are numerically solved without any turbulence model being used. Instead of using a turbulence model to parametrise the influence of turbulent eddies on the model, every eddy is computed. This applies from the largest eddy to the smallest, and as a result this method is extremely computational demanding and has only become a viable method for computing fluid flow in recent years, with thanks the rapidly increasing computational power available as described by Moore’s law.

One of the benefits of using the DNS method is that it provides the instantaneous viscous stresses in the fluids, which can be a relevant metric for quantifying blood damage (hemolysis for example).

While DNS simulations for stenotic flows are within reach in very specific circumstances [10], they are still too computationally demanding to be standard procedure, however the level of flow resolution provided by DNS is required if CFD is to be used as a reliable tool in the design of blood contacting medical devices. As DNS models are inherently less computationally demanding to solve at lower Reynolds numbers, this somewhat lends itself to being used in the design of medical device design because generally the highest Reynolds number typically found in cardiovascular flow is under  $Re = 10,000$ . [9]

### 3.5 LARGE EDDY SIMULATION (LES)

Large eddy simulation is a mathematical method for modelling turbulence first described by Joseph Smagorinsky in 1963 as a method for simulating atmospheric air currents. The main idea behind the use of LES is to reduce the computational cost of fluid modelling by ignoring the smallest length scales of the fluid model. These are the most computationally expensive scales to solve and are generally solved for by using low pass filtering of the Navier-Stokes equations. [17] [18]

# Chapter 4

## FDA ROUND ROBIN

### 4.1 CRITICAL PATH INITIATIVE

The ““Critical Path” Computational Fluid Dynamics (CFD)/ Blood Damage Project’ was a study designed by the US Food & Drug Administration to provide a useful testbed for the validation of CFD models, and to “assess the state of the art in biomedical fluid dynamics”. The study consisted of 2 benchmarks, the first of which (Benchmark 1 / Computational Round Robin 1) is a theoretical generic blood carrying medical device (which is the focus of this dissertation). [19]

The screenshot shows the homepage of the NCI P-HUB website. At the top, there is a navigation bar with links for 'DISCOVER', 'RESOURCES', 'COMMUNITY', 'ABOUT', 'SUPPORT', 'Login/Register', 'Help', and a search bar. Below the navigation bar, the page title 'Computational Fluid Dynamics Round Robin Study' is displayed. The main content area features a banner with the text 'Computational Fluid Dynamics: An FDA Critical Path Initiative' and the caBIG logo. A sub-banner below it says 'Welcome to the FDA's "Critical Path" Computational Fluid Dynamics (CFD)/Blood Damage Project.' A note states that data on CFD and blood damage validation studies is available here. A section titled 'Benchmark 1:' describes the nozzle study, mentioning it was an international effort to assess the state of the art in biomedical computational fluid dynamics. It includes a link to click for data from Benchmark 1 and an image of a nozzle.

Figure 9 - The website detailing the round robin study

#### 4.1.1 Benchmark 1 / Computational Round Robin 1

The Benchmark #1 study, also referred to as the Computational Round Robin 1 was a study focused on a geometry designed by the FDA to mimic some characteristics of fluid flow in a blood contacting medical device. The geometry is a pipe shape with varying diameters, starting at 12 mm at the inlet, going through a gradual reduction in diameter (the conical shape) to a minimum diameter of 4 mm (the throat). The throat is 40 mm in length and leads to the sudden increase in diameter to 12 mm (the sudden expansion).



**Benchmark 1: Nozzle**

*Figure 10 - Benchmark 1 geometry provided by The FDA [20]*



Figure 11 - Benchmark 1 geometry rendered in Solidworks 2018 Photoview 360

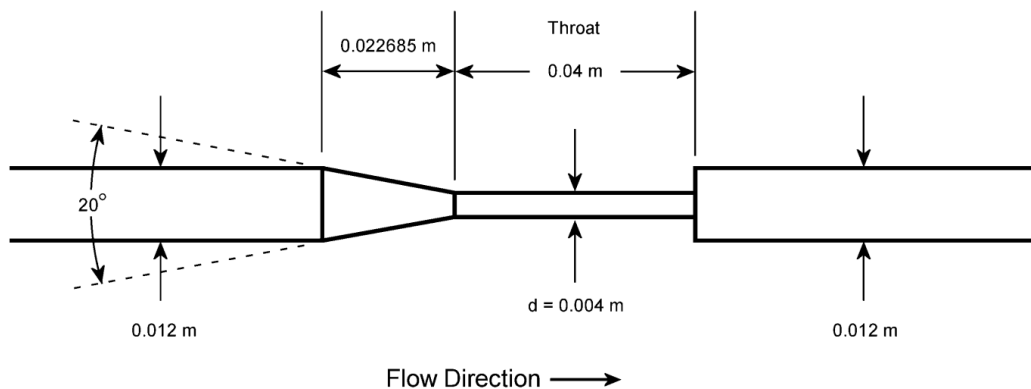


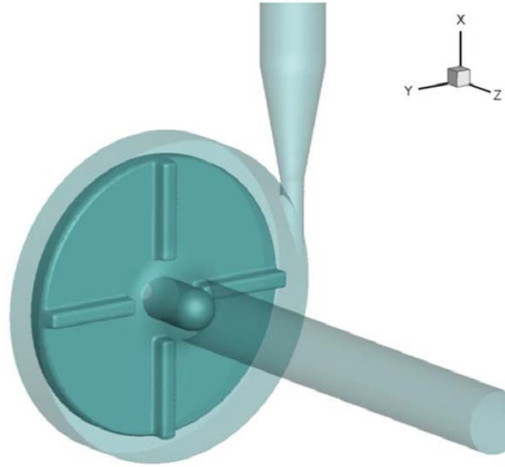
Figure 12 - Dimensioned 2D drawing of Benchmark 1 [1]

Fluid Data		
Density	$\rho$	1056 kg/m <sup>3</sup>
Dynamic Viscosity	$\mu$	0.0035 Ns/m <sup>2</sup>
Acrylic Data		
Surface Roughness	$R_a$	0.5 $\mu m$
Radius of Curvature of Sudden Expansion	$R$	25 $\mu m$
Model Length	$L$	0.25 m

Table 1 - PIV Experimental parameters

#### 4.1.2 Benchmark 2 / Computational Round Robin 2

The second benchmark for this study was that of an axial blood pump. As this project is focusing on benchmark 1, the blood pump will not be discussed in detail.



**Benchmark 2: Blood Pump**

*Figure 13 - The geometry provided for the blood pump benchmark [21]*

## 4.2 TEST CASE

The primary test case that is examined in this project, is the sudden expansion orientation of the geometry with the Reynolds number in the throat being 500. However, the conical diffuser orientation for the same Reynolds number was also examined.

Case	$R_e$
Case 1	500
Case 2	2000
Case 3	3500
Case 4	5000
Case 5	6500

*Table 2 - The test cases that were completed in the FDA study*

## 4.3 VALIDATION

### 4.3.1 Particle Image Velocimetry (PIV)

The validation for this project is based upon the experimental findings of the various Particle Image Velocimetry (PIV) tests carried out by three anonymous FDA laboratories in the United

States. The results from the PIV experiments are provided in the form of text files (.txt), on the FDA Round Robin data website ([https://nciphub.org/wiki/FDA\\_CFD](https://nciphub.org/wiki/FDA_CFD)), and they contain experimental readings of velocity along the length of the geometry, along with pressures along the length of the model. To achieve both of the results, 2 separate physical models had to be constructed, one with wall pressure taps along the length to measure pressures, and the other with a smooth wall finish. Both models were made from transparent acrylic.

The geometry for the experiments was first designed in a Computer Aided Design (CAD) program, then milled out of acrylic using a Computer Numerical Control (CNC) mill. The acrylic was then polished thoroughly by hand to produce a smooth surface finish on the inside walls of the acrylic (the walls that would be in contact with the working fluid).

The models measure 250mm total in length, with additional acrylic extenders of an unspecified length added to each end in order to extend the range of flow analysis. Beyond these acrylic extenders, stainless steel adapter tubes were fixed to each acrylic extender to act as the working fluid inlet to the model. Both sets of additional tubes (acrylic extender tubes, and stainless-steel adapter tubes) had the same internal diameter as the ends of the model (12mm) in order to allow for fully developed flow of the fluid prior to entering the model proper.

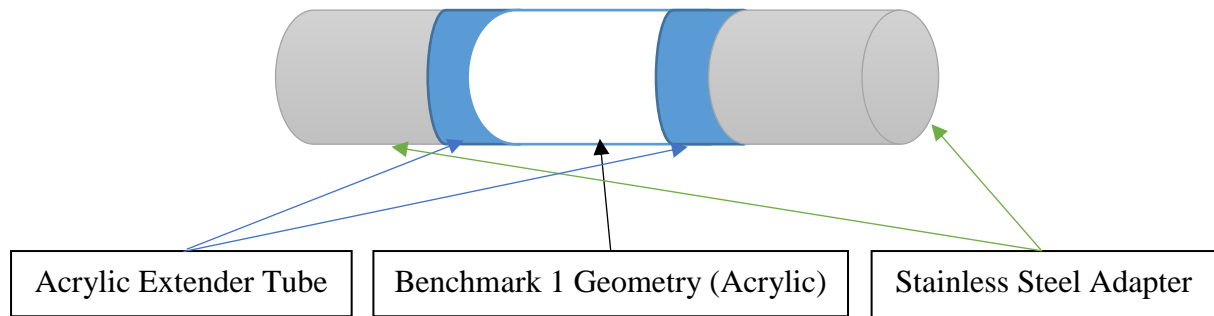


Figure 14 - Simplified schematic diagram showing the layout of the experimental model



Figure 15 - An example of a machined acrylic tube, similar to the model used in the PIV experiments [22]

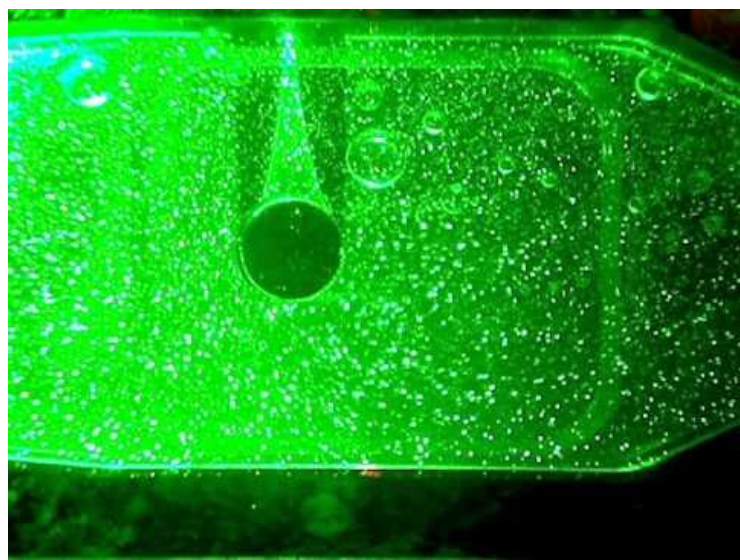


Figure 16 - An example of flow analysis around a cylinder using Particle Image Velocimetry (PIV) [23]

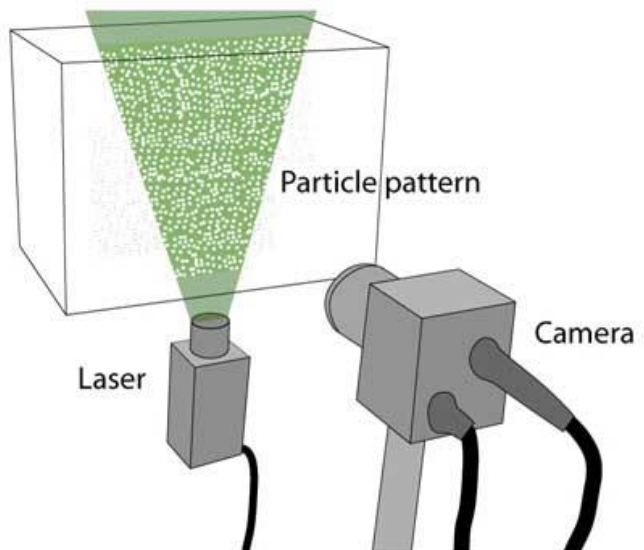


Figure 17 - A schematic diagram showing how PIV is carried out [24]

The working fluid used for the PIV tests was a solution of water, glycerine and sodium iodide. This solution was designed so that the refractive index of the solution would be the same as that of the acrylic used (1.489), in an effort to remove optical distortion caused by the curved surface of the acrylic. The density and dynamic viscosity are shown below. These values were chosen to mimic the properties of blood.

<b>Fluid Data</b>		
<b>Density</b>	$\rho$	1056 kg/m <sup>3</sup>
<b>Dynamic Viscosity</b>	$\mu$	0.0035 Pa.s
<b>Acrylic Data</b>		
<b>Surface Roughness</b>	$R_a$	0.5 $\mu m$
<b>Radius of Curvature of Sudden Expansion</b>	$R$	25 $\mu m$
<b>Model Length</b>	$L$	0.25 m

*Table 3 - PIV Experimental parameters*

#### 4.3.2 CFD Model Validation

The results that will be obtained from the CFD model will be compared against the experimental results from the physical tests carried out by the FDA. This is explained in the section below.

### 4.3.3 Data

The datasets for each of the five FDA labs were taken directly from the NCIP Hub website. The data was provided in the form of text files with all of the pressure and velocity data as plain text. Due to the data being provided in this form, it had to be converted into an Excel file, and then processed into a form where it could be compared with the CFD data.

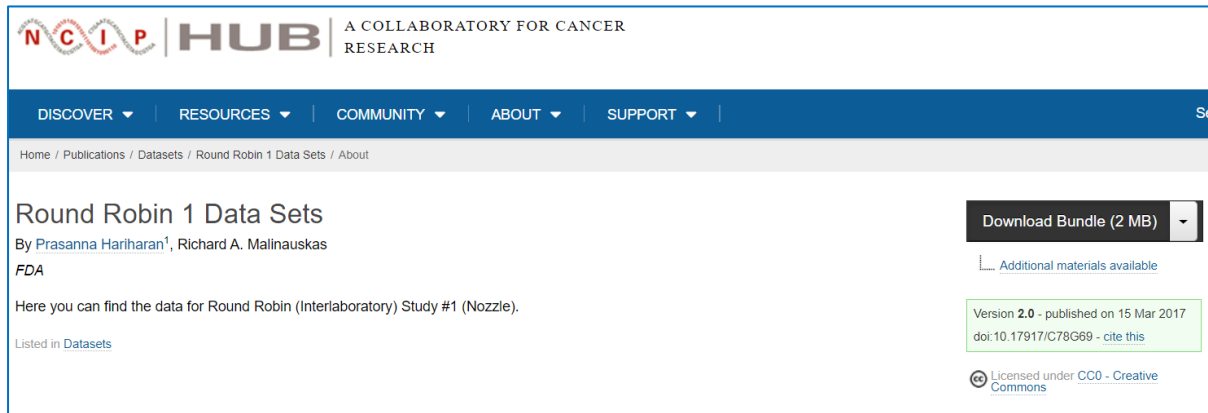


Figure 18 - The NCIP Hub website showing where the data sets were downloaded for

A screenshot of a Windows Notepad window titled "PIV\_Sudden\_Expansion\_500\_297 - Notepad". The window contains a large amount of text representing experimental data. The data is structured with various parameters and numerical values. Parameters include dataset-comment, dataset-description, dataset-orientation, dataset-reynolds, dataset-laminar-turbulent, dataset-experiment, dataset-code, dataset-experiment, geometry-flow-z-direction, geometry-throat-outlet-expansion-type, geometry-sudden-z, fluid-density, fluid-viscosity, fluid-volumetric-flow-rate, deleted-plot-wall-distribution-pressure, and deleted-plot-z-distribution-pressure. Numerical values are given in scientific notation, such as 1.31804E+002, 4.64005E+002, etc.

Figure 19 - The text file containing experimental data

	A	B	C	D	E	F	G	H
1	dataset-comment							
2	dataset-description	Sudden Expansion 500	-0.005861663	0.00452241	-0.005861663	0.00433674	-0.00326484	0.069478
3	dataset-orientation	Sudden Expansion	-0.005677225	0.00940381	-0.005677225	0.00912771	-0.003089016	0.0965919
4	dataset-reynolds	500	-0.005492787	0.0148128	-0.005492787	0.0146127	-0.002913192	0.125764
5	dataset-laminar-turbulent		-0.005308348	0.0196668	-0.005308348	0.0194092	-0.002737368	0.145495
6	dataset-experiment	1	-0.00512391	0.024505	-0.00512391	0.0243296	-0.002561544	0.159426
7	dataset-code	243	-0.004939471	0.0290719	-0.004939471	0.0287821	-0.00238572	0.167714
8	dataset-experiment	1	-0.004755033	0.0334977	-0.004755033	0.0331538	-0.00209896	0.172771
9	geometry-flow-z-direction	1	-0.004570595	0.0378235	-0.004570595	0.0375693	-0.002034072	0.176678
10	geometry-throat-outlet-expansion-type	sudden	-0.004386156	0.0415471	-0.004386156	0.0413607	-0.001858248	0.180147
11	geometry-sudden-z	0	-0.004201718	0.0455057	-0.004201718	0.0454488	-0.001682424	0.183185
12	fluid-density	1056	-0.004017279	0.0493745	-0.004017279	0.0493512	-0.0015066	0.185789
13	fluid-viscosity	0.0035	-0.003832841	0.052565	-0.003832841	0.0526048	-0.001330776	0.187099
14	fluid-volumetric-flow-rate	5.21E-06	-0.003648403	0.056018	-0.003648403	0.0560954	-0.001154952	0.187732

Figure 20 - The velocity data after being imported into Excel

#### 4.3.3.1 Axial Velocity

The data provided contained experimental velocity profiles at 12 locations along the Z axis of the part. The 12 locations can be seen below in the schematic diagram. For each velocity slice, the information provided a number of X, Y, and Z coordinates and the velocity at those coordinates.

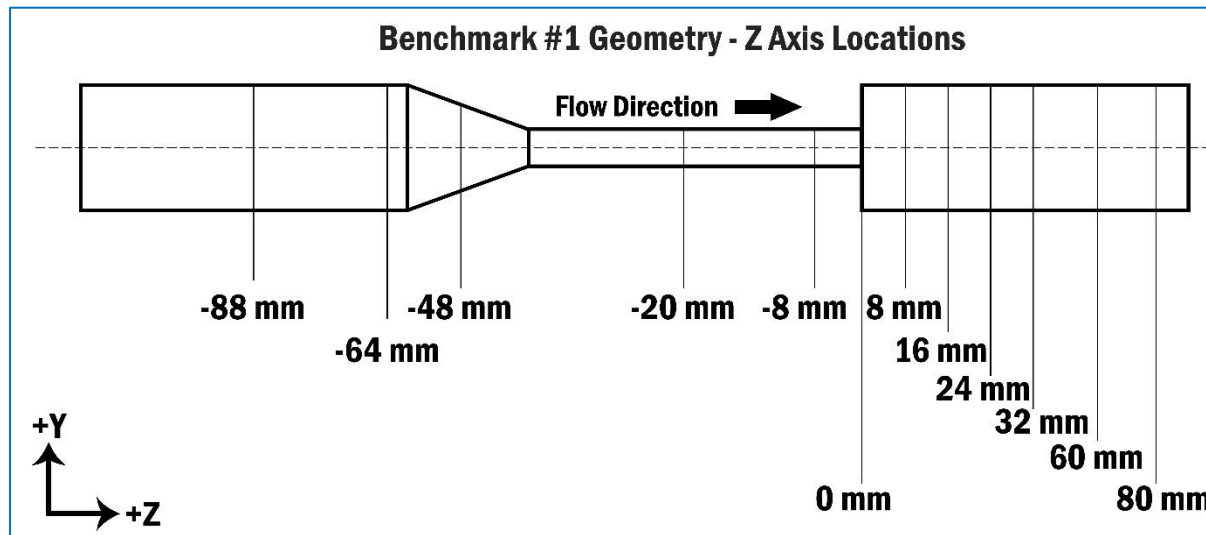


Figure 21 - The 12 locations where experimental axial velocity readings were taken

#### 4.3.3.2 Centreline Velocity

The data provided contained velocity readings along the centre of the geometry.

#### 4.3.3.3 Centreline Pressure

The data provided also contained pressure measurements along the length of the geometry, both at the wall, and at the centreline.

# Chapter 5

## LAMINAR PIPE FLOW MODEL

### 5.1 INTRODUCTION

Prior to the creation of the CFD model of the final geometry, an idealised model of fully laminar pipe flow was created to introduce many aspects of CFD model creation that were encountered when creating the final model. The idea was to start with a simple model that could be created and then built upon after.

This chapter deals with a CFD model of fluid flow through a pipe measuring 12 mm in diameter (0.012 m). This diameter corresponds to the inlet and outlet diameter of the Benchmark #1 geometry, which is the geometry used for the final CFD model.

The software used for this chapter was: Microsoft Excel 2016, ANSYS Workbench 19.1, ANSYS Design Modeler, ANSYS Meshing Utility, ANSYS CFX-Solver, ANSYS CFD Post.

### 5.2 GEOMETRY

The geometry chosen for this model was derived from the final Benchmark #1 geometry, in order to keep the content of this model similar to what will be encountered in the final model.

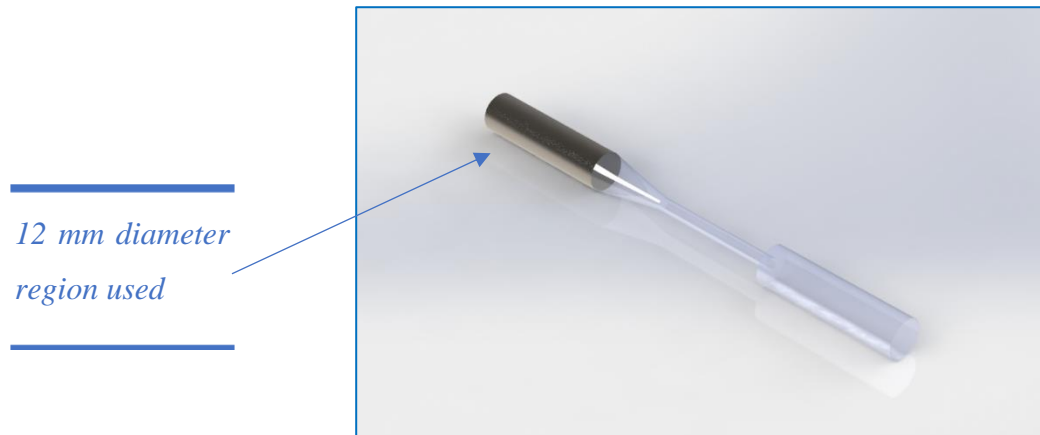


Figure 22 - The final geometry showing the section used in this analysis, render generated in Solidworks Photoview 360

The

geometry was created in ANSYS Design Modeler, which is a module integrated into ANSYS Workbench.

## 5.3 MESH

### 5.3.1 Geometry Decomposition

In order to place adequate mesh controls on the cylinder, care was taken to draw the geometry in a specific way, with a rectangular prism placed in the centre, and lines joining the outer diameter to the vertices of the prism. This meant that the geometry was divided into 5 separate volumes. The size of the prism was arbitrarily chosen, as it does not have a huge impact on the final mesh. The only criteria being that the prism needed to fit fully inside the outer circle, so that the lines joining the vertices of the prism to the circle can be used in mesh sizing.

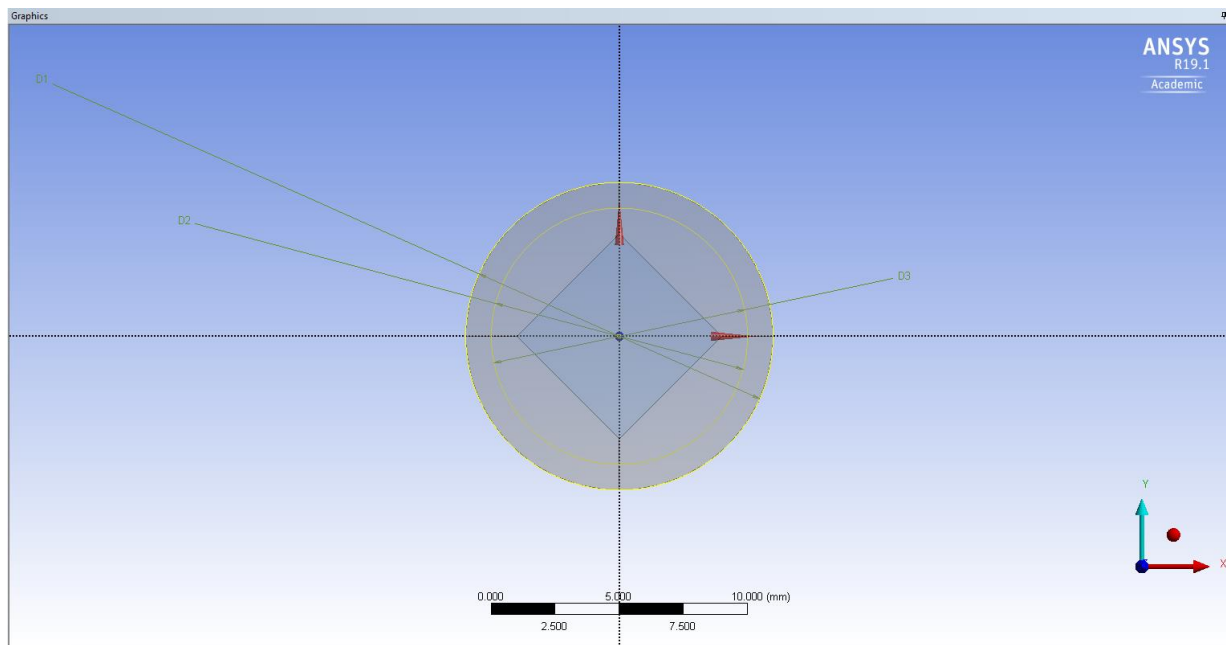
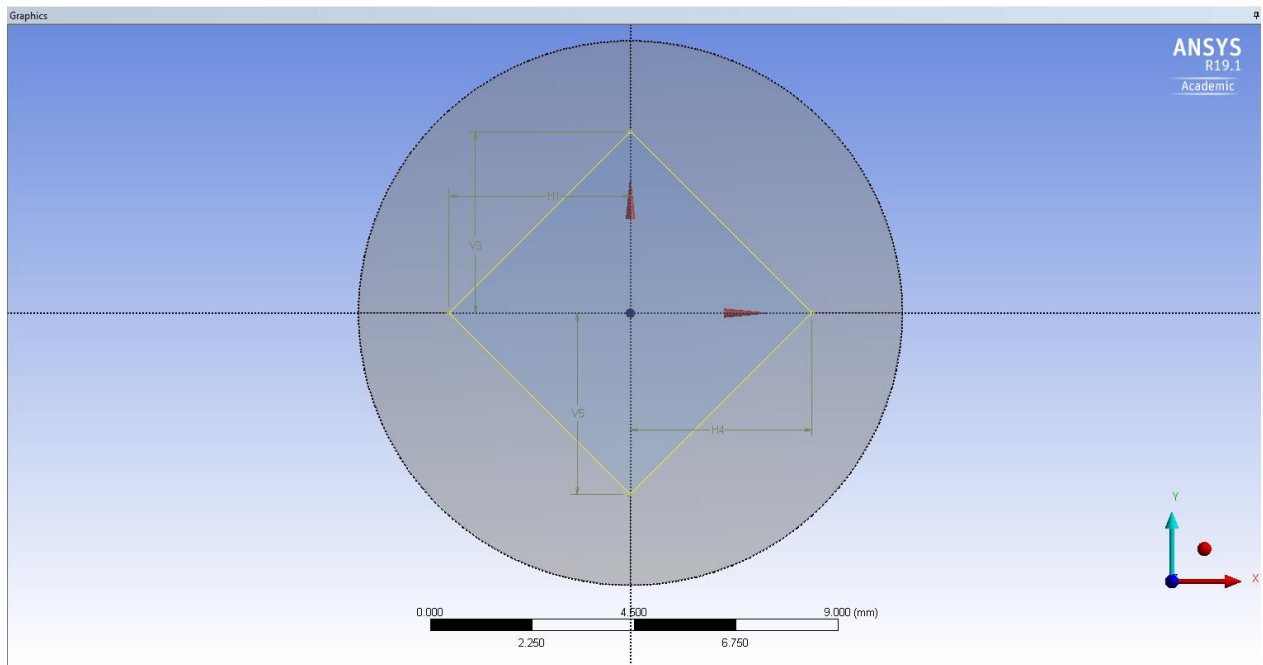


Figure 23 - Showing the sketch used to create the outer portion of the cylinder



*Figure 24 - Showing the sketch and dimensions used to create the central prism*

The five volumes (the prism, and four cylindrical sectors less the prism area) were extruded to a length of 50 mm. This length was also arbitrarily chosen. The geometry was then split into two volumes (the central prism as one volume/body, and all other sections as one volume/body).

### 5.3.2 Mesh Controls

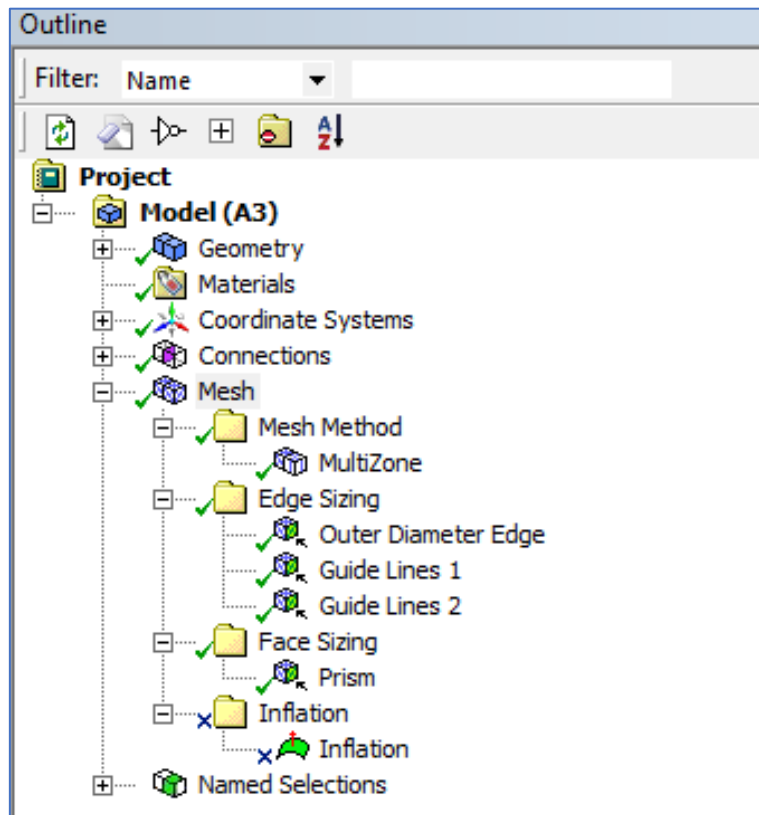


Figure 25 - The ANSYS Meshing tree, showing the structure of the mesh

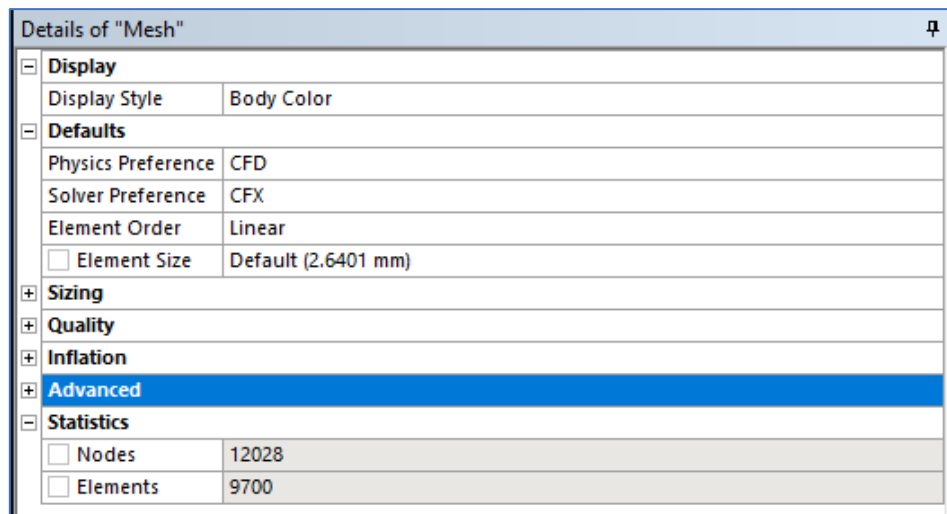


Figure 26 - The details tab of the mesh overview

The details tab has some global mesh settings such as solver and physics preference. It also displays some information about the current mesh such as the number of nodes and elements.

The chart below summarises the differences between each physics and solver preference that can be selected in the mesh details.

Meshing Control	Physics Preference							
	Mechanical		Nonlinear Mechanical	Electromagnetic	CFD			Explicit
	Mechanical APDL Solver	Rigid Body Dynamics Solver			CFX-Solver	FluentSolver	Polyflow Solver	
Relevance Center	Coarse	Coarse	N/A	Medium	Coarse	Coarse	Coarse	Medium
Element Size	Default	Default	N/A	Default	Default	Default	Default	Default
Initial Size Seed	Active Assembly	Active Assembly	N/A	Active Assembly	Active Assembly	Active Assembly	Active Assembly	Active Assembly
Smoothing	Medium	Medium	N/A	Medium	Medium	Medium	Medium	High
Transition	Fast	Fast	N/A	Fast	Slow	Slow	Slow	Slow
Span Angle Center	Coarse	Coarse	Coarse	Coarse	Fine	Fine	Fine	Coarse
Size Function	Curvature for shell models; otherwise Adaptive	Curvature for shell models; otherwise Adaptive	Curvature	Adaptive	Curvature	Curvature	Curvature	Curvature for shell models; otherwise Adaptive
Transition Ratio	0.272	0.272	0.272	0.272	0.77	0.272	0.272	0.272
Inflation Algorithm	Pre	Pre	Post	Pre	Pre	Pre	Pre	Pre
Collision Avoidance	Stair Stepping	Stair Stepping	Stair Stepping	Stair Stepping	Stair Stepping	Layer Compression	Stair Stepping	Stair Stepping
Shape Checking	Standard Mechanical	Standard Mechanical	Nonlinear Mechanical	Electromagnetics	CFD	CFD	CFD	Explicit
Element Midsize Nodes	Program Controlled	Dropped (Read-only)	Program Controlled	Kept	Dropped	Dropped	Dropped	Dropped

Figure 27 - Selecting different physics preferences can have a large impact on the final mesh generated [26]

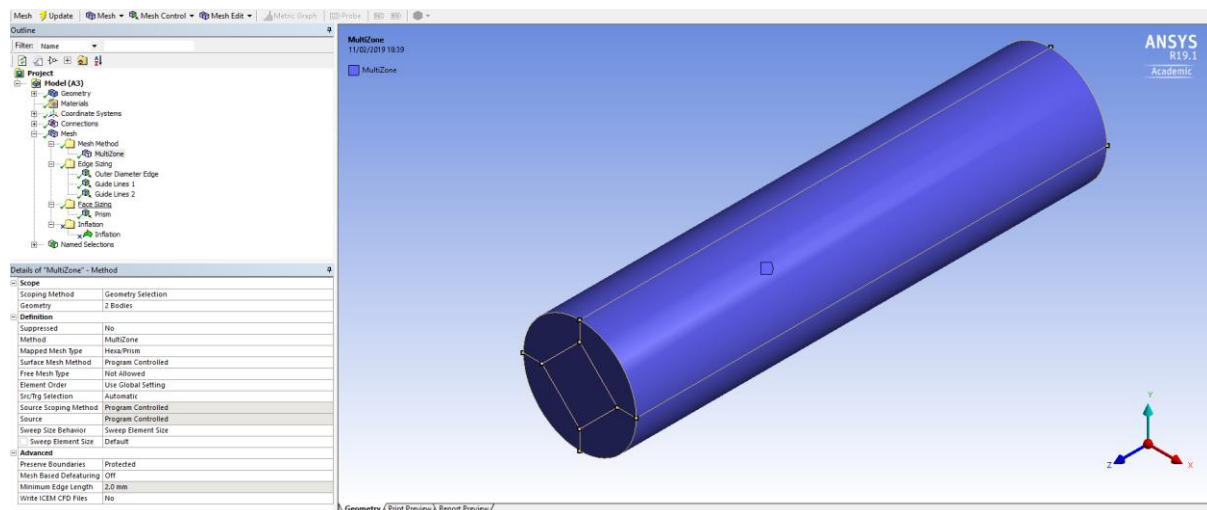


Figure 28 - Isometric view of the model showing the guide lines used for the mesh sizing

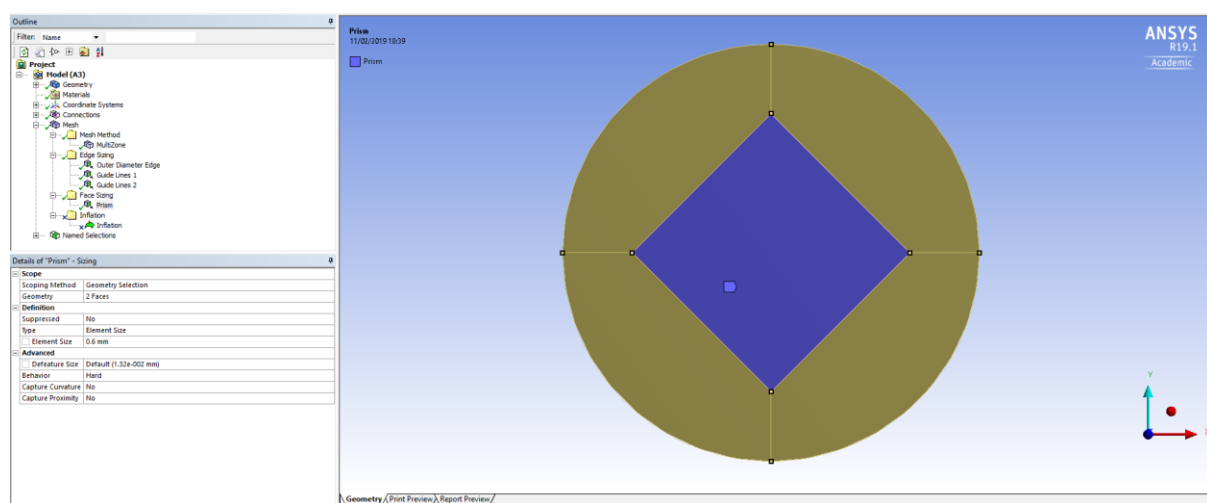


Figure 29 - The face sizing used on the central prism

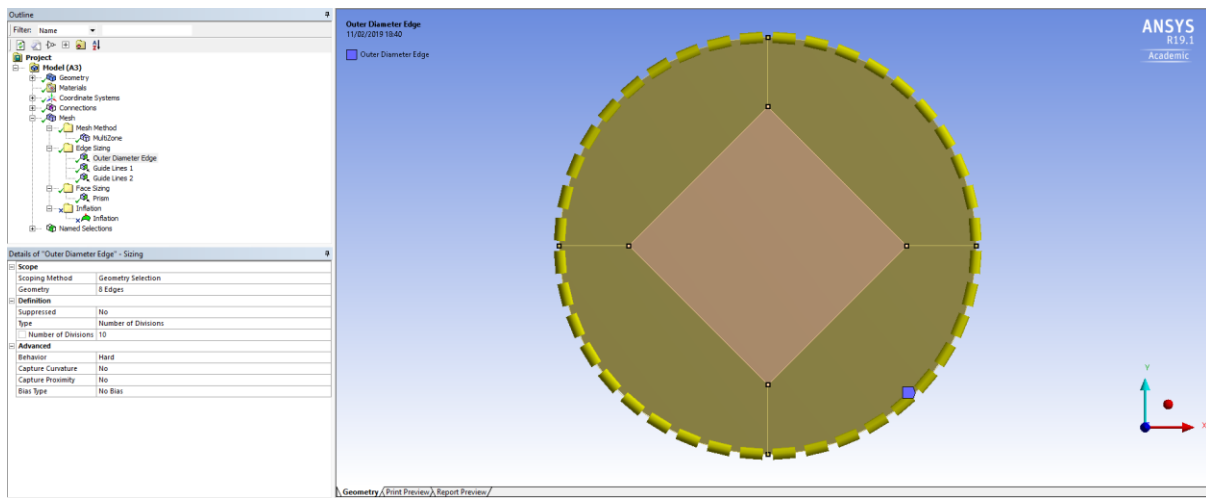


Figure 30 - The edge sizing method used on the outer circular edge

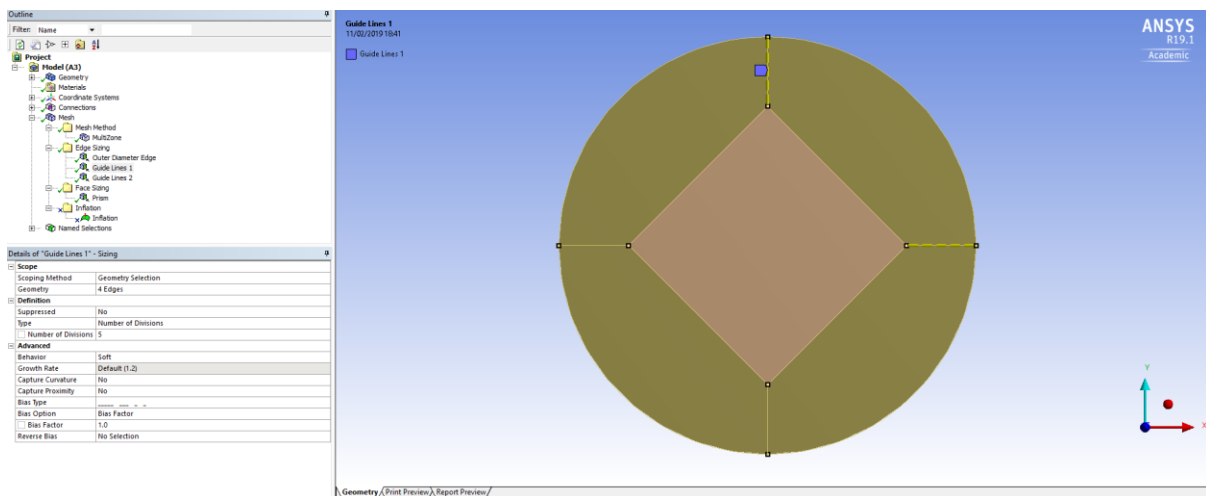


Figure 31 - The edge sizing method used on the top and right guide lines

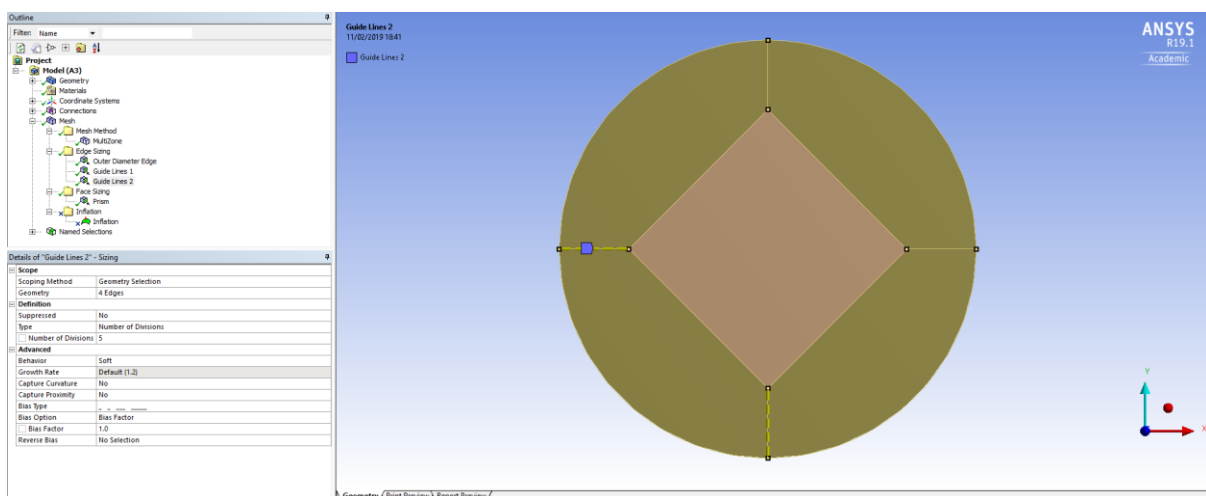


Figure 32 - The edge sizing method used on the bottom and left guide lines

### 5.3.3 Final Meshes

The five final meshes can be seen below. For each, a view normal to the inlet face and an isometric cutaway view showing the internal mesh is shown.

#### 5.3.3.1 Mesh 1 - 28,661 Nodes

Mesh 1 consisted of 28,661 nodes and 6,000 elements.

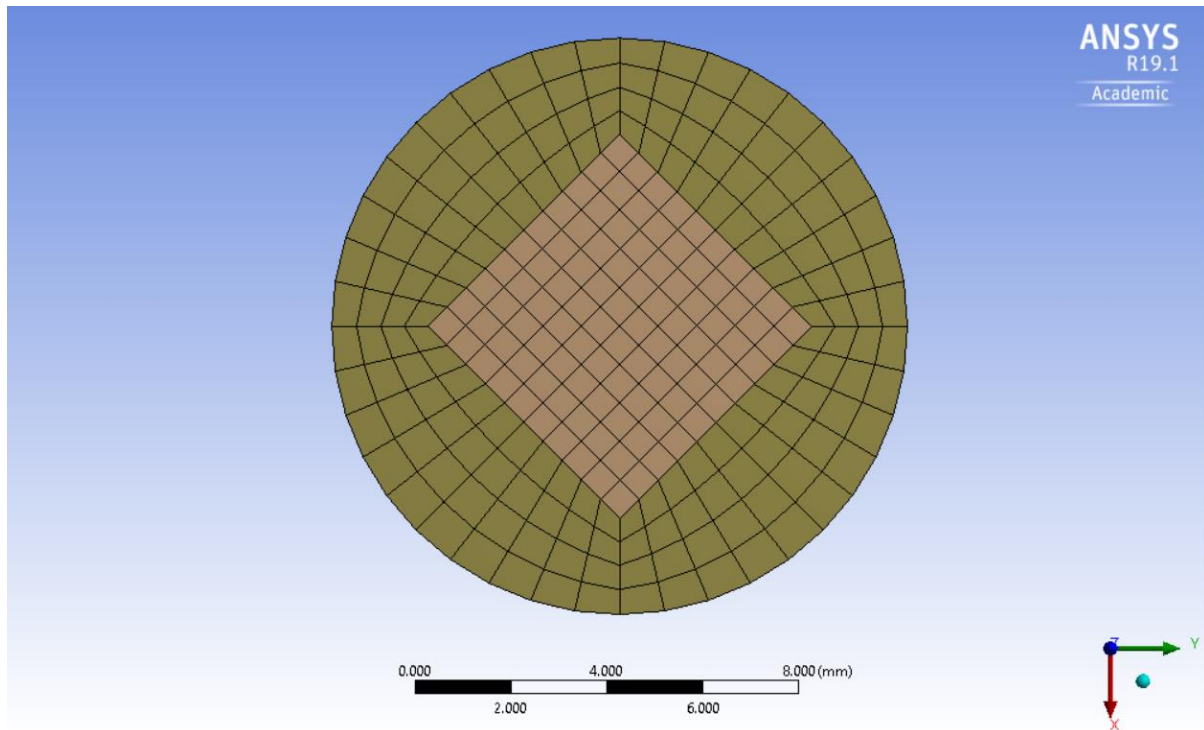


Figure 33 - Front view of mesh 1

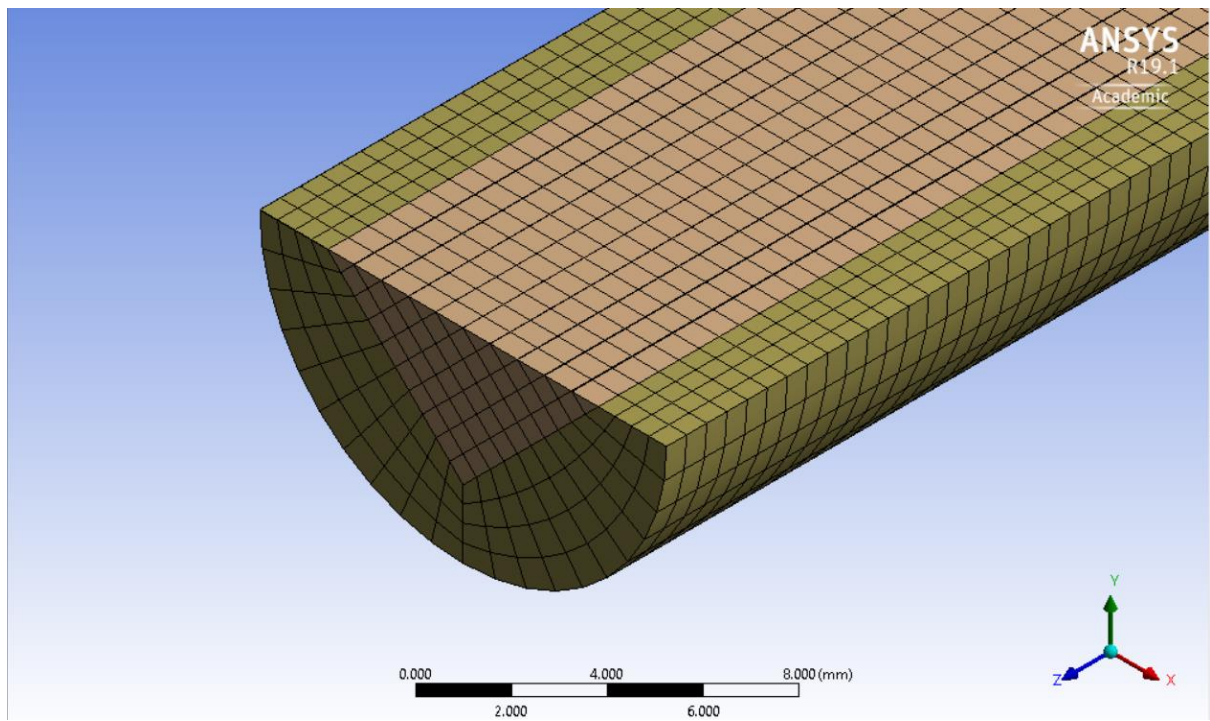


Figure 34 - Isometric view showing cutaway of mesh 1

### 5.3.3.2 Mesh 2 - 97,888 Nodes

Mesh 2 consisted of 97,888 nodes and 85,140 elements

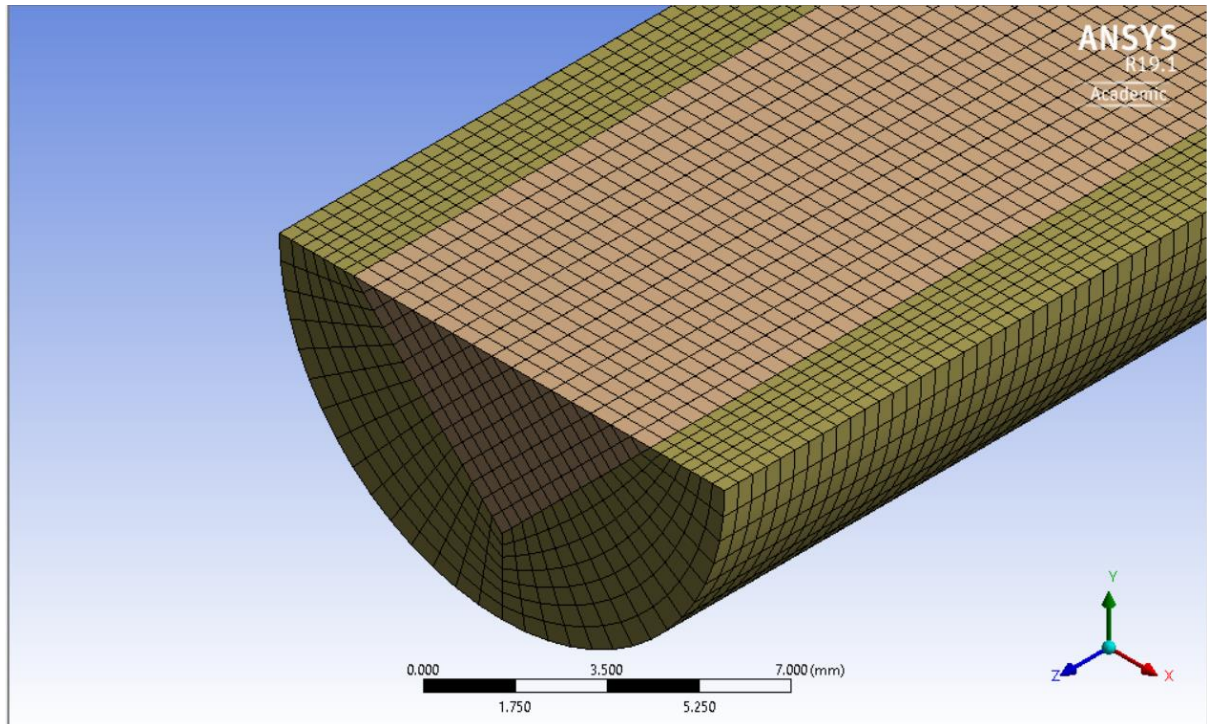


Figure 35 - Front view of mesh 2

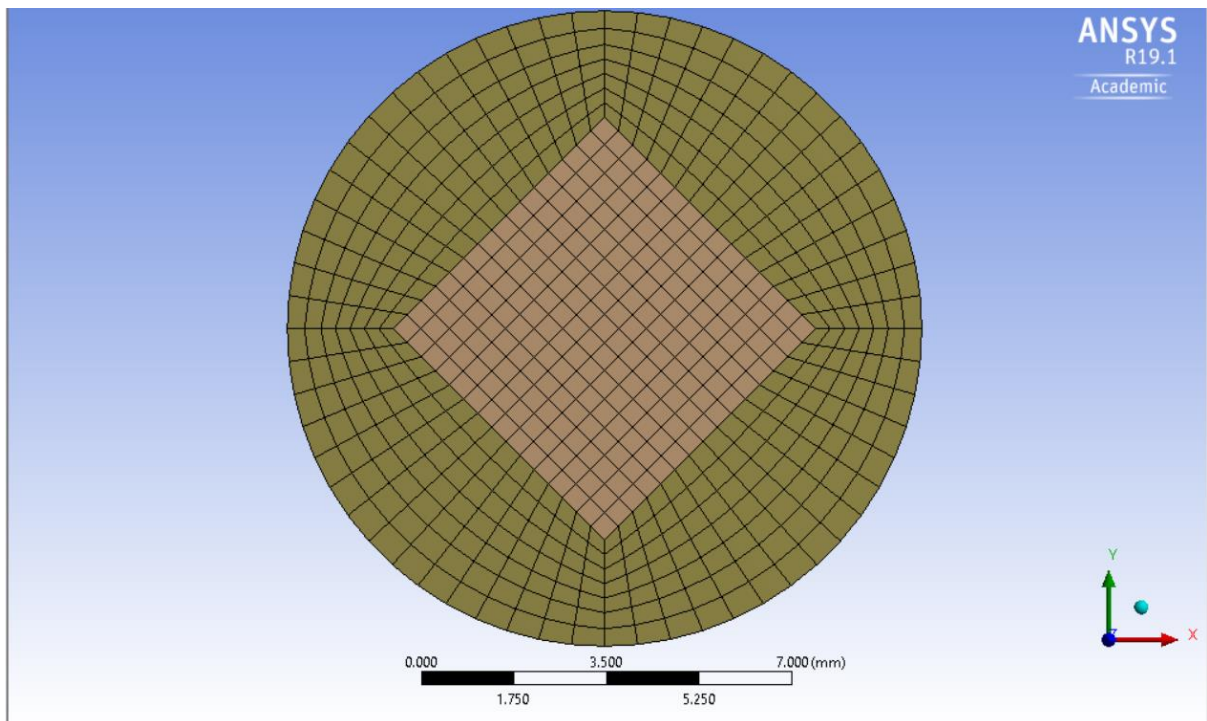


Figure 36 - Isometric view showing cutaway of mesh 2

### 5.3.3.3 Mesh 3 - 223,200 Nodes

Mesh 3 consisted of 223,200 nodes and 199,227 elements.

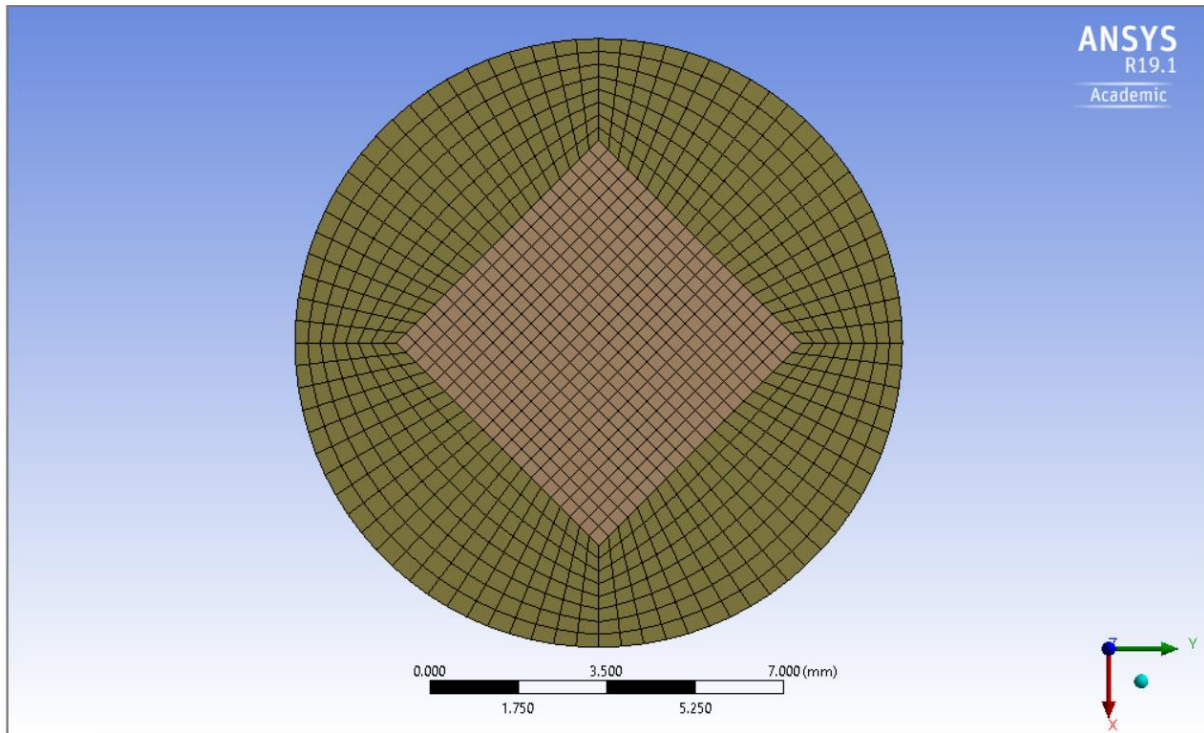


Figure 37 - Front view of mesh 3

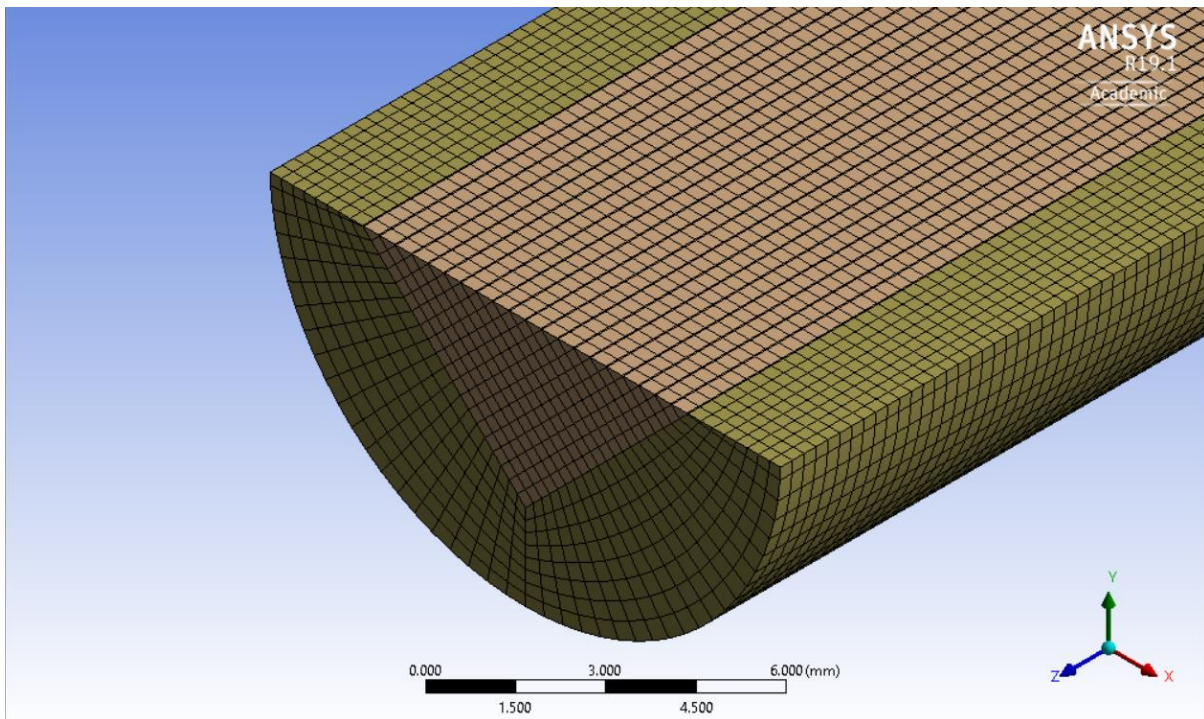


Figure 38 - Isometric view showing cutaway of mesh 3

#### 5.3.3.4 Mesh 4 - 318,612 Nodes

Mesh 4 consisted of 318,612 nodes and 289,271 elements.

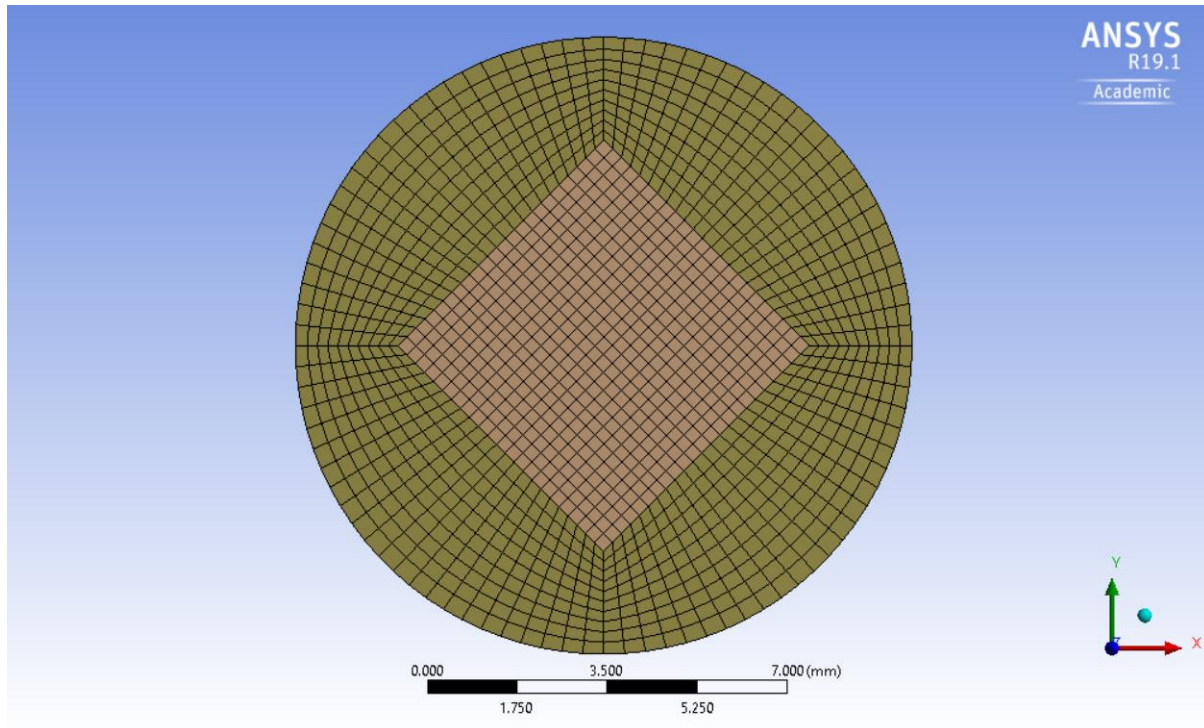


Figure 39 - Front view of mesh 4

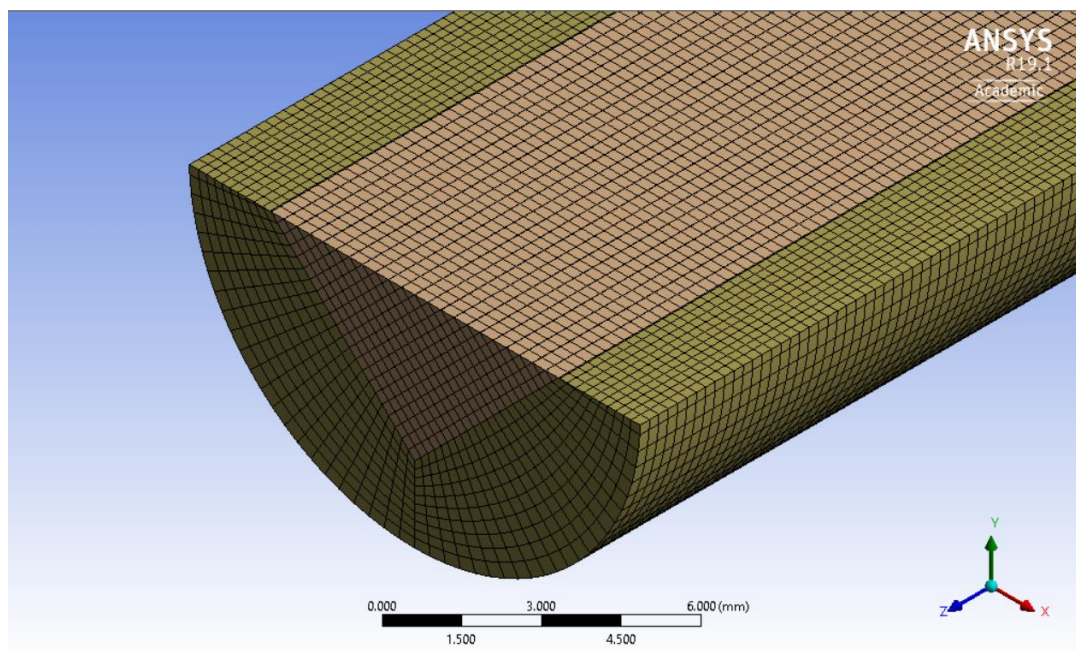


Figure 40 - Isometric view showing cutaway of mesh 4

### 5.3.3.5 Mesh 5 - 498,178 Nodes

Mesh 5 consisted of 498,178 nodes and 460,356 elements.

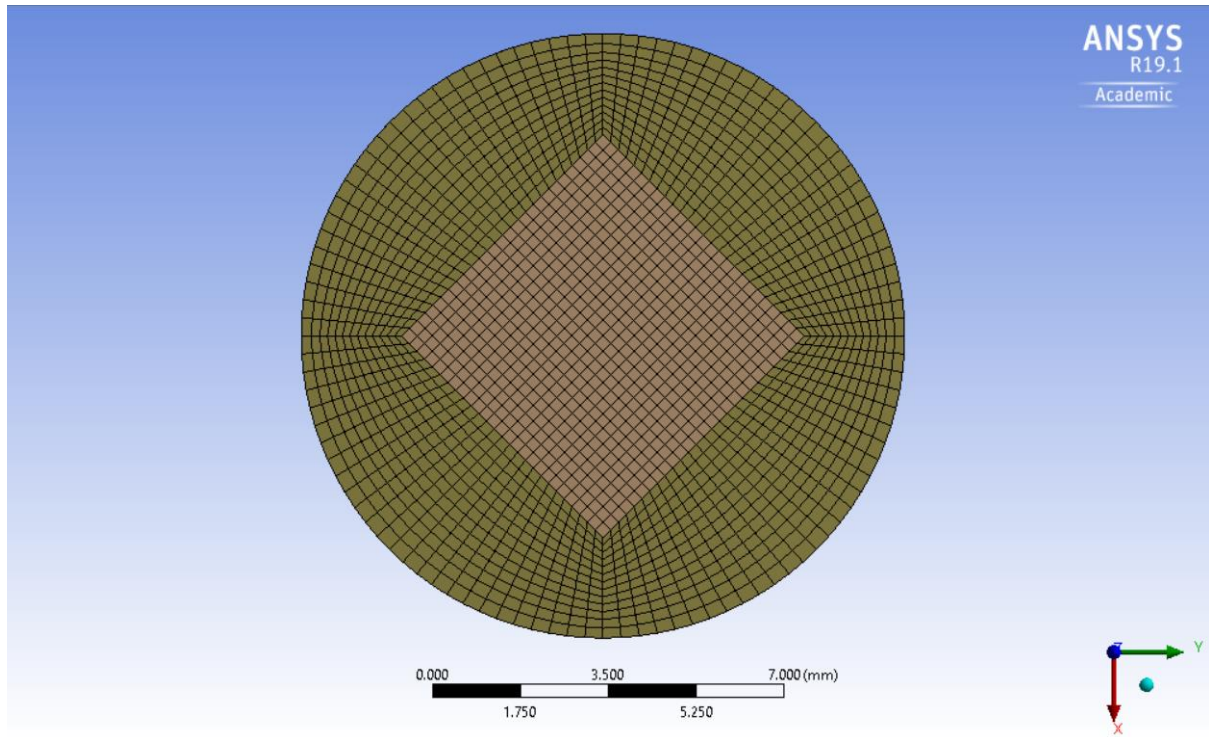


Figure 41 - Front view of mesh 5

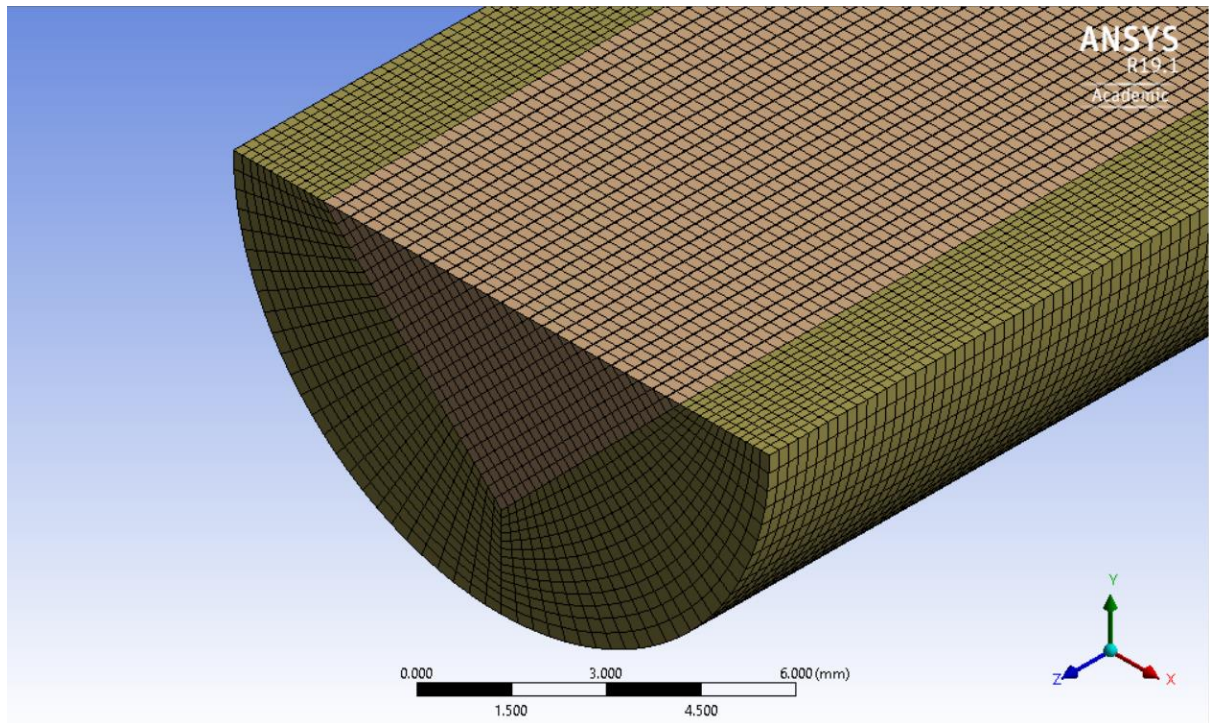


Figure 42 - Isometric view showing cutaway of mesh 5

## 5.4 THEORETICAL CALCULATIONS

The calculations were completed by hand and then rewritten in Word using the formulae provided in both “Fluid Mechanics: Fundamentals & Applications” by John M. Cimbala and Yunus A. Cengel [27], and in the course notes provided for Fluid Mechanics MECH4004, by Professor Fergal Boyle.

The variables listed in the below table were used, based on the properties of the fluid that was used in the FDA PIV experiments.

More calculations could have been carried out for this section of pipe, however for the purposes of this study these were the only values needed to validate the model.

Given Info			
Diameter	$D$	0.012 12	$m$ $mm$
Area	$A$	0.0001131 113.1	$m^2$ $mm^2$
Length	$L$	0.05 50	$m$ $mm$
Density	$\rho$	1056	$kg/m^3$
Dynamic Viscosity	$\mu$	3.50E-03	$kg/ms$
Reynolds Number	$R_e$	500	

Table 4 - The assumed information about the pipe and fluid

### 5.4.1 Hand Calculations

#### 5.4.1.1 Velocity

$$R_e = \frac{\rho V_{Avg} D}{\mu}$$

(Eqn. 5)

$$\Rightarrow V_{Avg} = \frac{R_e \cdot \mu}{\rho d} = \frac{(500) \cdot (0.0035)}{(1056) \cdot (0.012)} = 0.1381 \text{ m/s}$$

$$\therefore V_{Max} = 2 \cdot V_{Avg} = 2 \cdot (0.1381) = 0.2762 \text{ m/s}$$

#### 5.4.1.2 Volume Flow Rate

$$Q = V_{Avg} \cdot A = (0.1381) \left( \frac{\pi D^2}{4} \right) = (0.1381) \left( \frac{\pi (0.012)^2}{4} \right) = 0.000015619 \text{ m}^3/\text{s}$$

(Eqn. 6)

#### 5.4.1.3 Mass Flow Rate

$$\dot{m} = Q \cdot \rho = (0.000015619)(1056) = 0.0165 \text{ kg/s}$$

(Eqn. 7)

#### 5.4.1.4 Darcy Friction Factor

$$f = \frac{64}{R_e} = 0.1280$$

(Eqn. 8)

#### 5.4.1.5 Pressure Drop

$$\Delta P = f \frac{L}{D} \cdot \frac{\rho V_{Avg}^2}{2} = (0.1280) \left( \frac{0.05}{0.012} \right) \left( \frac{(1056)(0.1381)^2}{2} \right) = 5.3705 \text{ Pa}$$

(Eqn. 9)

#### 5.4.1.6 Head Loss Due to Friction

$$h_{friction} = f \frac{L}{D} \frac{V^2}{2g} = (0.1280) \left( \frac{0.05}{0.012} \right) \left( \frac{0.138^2}{2 \cdot (9.81)} \right) = 5.1768 \times 10^{-4} \text{ m}$$

(Eqn. 10)

### 5.4.2 Excel Workbook Calculations

In addition to the hand calculations, an Excel workbook was also created, in order to make calculating flow information about the pipe easy, should any of the properties change.

Pipe Info			
Diameter	$D$	0.012 12	$m$ $mm$
Area	$A$	0.0001131 113.1	$m^2$ $mm^2$
Length	$L$	0.05 50	$m$ $mm$

Fluid Info			
Density	$\rho$	1056	$kg/m^3$
Dynamic Viscosity	$\mu$	3.50E-03	$kg/ms$

Fluid Flow Information			
Average Velocity	$V_{avg}$	0.138	$m/s$
Max Velocity	$V_{Max}$	0.276	$m/s$
VFR	$Q$	0.000015619 15619	$m^3/s$ $mm^3/s$
MFR	$\dot{m}$	0.0165 16.5	$kg/s$ $g/s$
Reynolds Number	$R_e$	500.00	
Darcy Friction Factor	$f$	0.128	
$h_{friction}$ Pressure Drop	$h_L$ $\Delta P$	0.050 5.371	$m$ $Pa$

Figure 43 - The workbook created to keep track of multiple theoretical calculations

## 5.5 MODEL SETUP

### 5.5.1 Working Fluid

The working fluid in this model was designed to mimic the fluid that was used in the physical FDA testing i.e. a mixture of water and glycerine, with density = 1056 kg/m<sup>3</sup>, and dynamic viscosity = 0.0035 kg/ms. This fluid was created in ANSYS Workbench by duplicating the properties of water at 25°C and changing the required values. Many of the properties and characteristics remained unchanged as they were not used in the simulation (e.g. radiation and buoyancy properties). This material was then renamed to “Water and Glycerin” mix so that it could be used in future models.

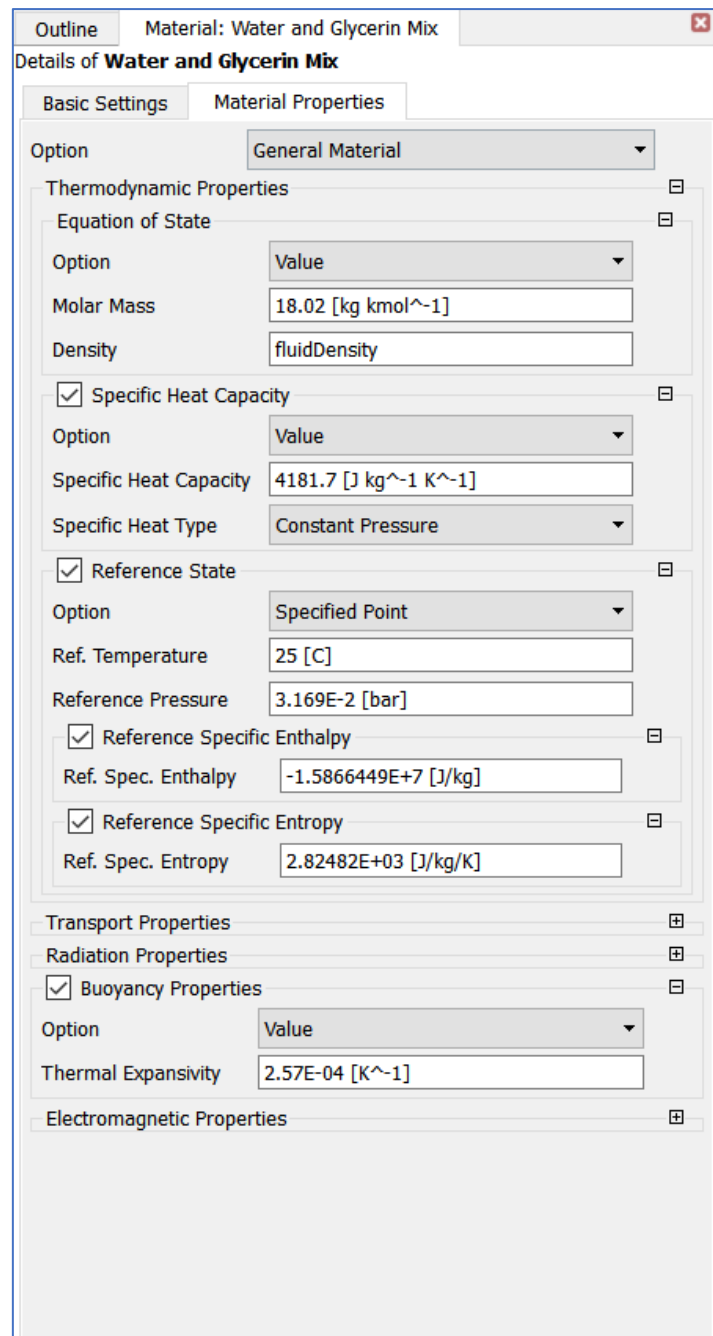


Figure 44 - The properties settings for the new fluid

This material was then selected as the working fluid in the domain.

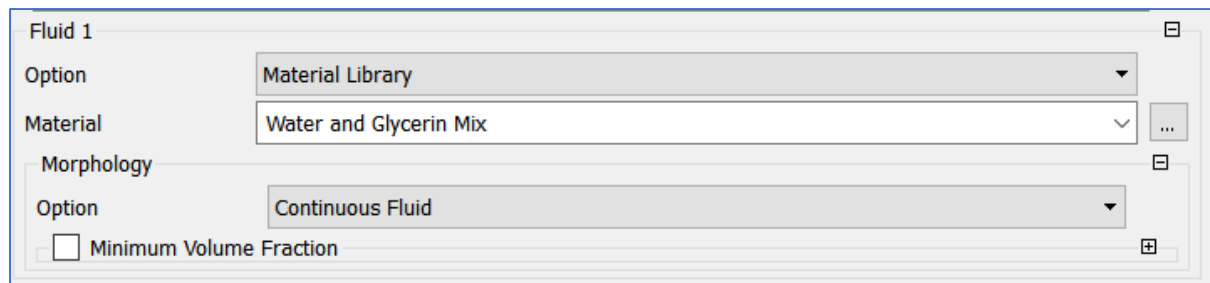


Figure 45 - The fluid selection menu

### 5.5.2 Boundary Conditions

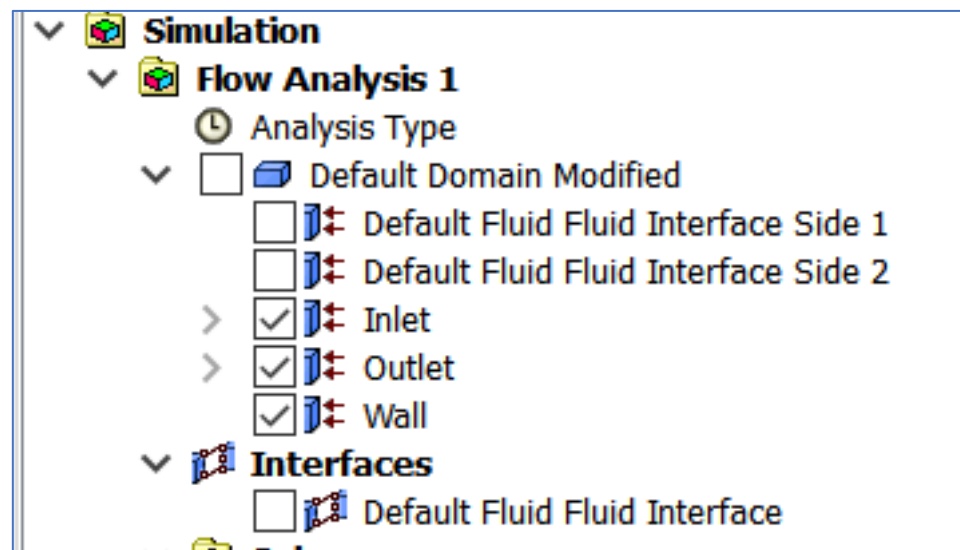


Figure 46 - Outline tree structure in CFX-Pre

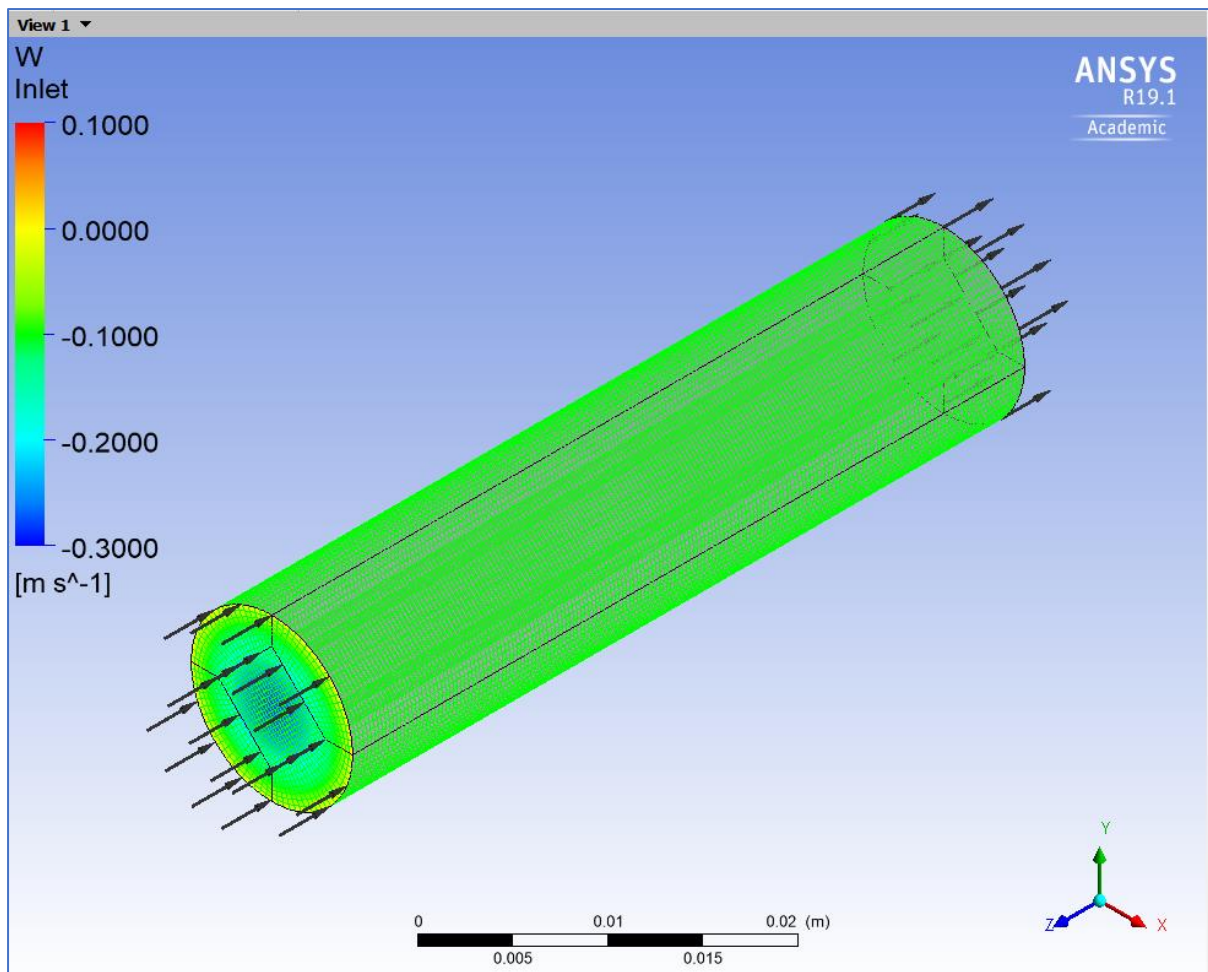


Figure 47 - Isometric view of the model with all boundaries highlighted in green. The black vector arrows show the inlet and outlet of the fluid domain.

#### 5.5.2.1 Inlet

The inlet boundary was defined using a mass and momentum method, and cartesian velocity components. As the flow was assumed to be fully laminar, the velocity profile that was previously calculated was input in the -Z direction (W component). This can be seen in the figure below. Flow in the X and Y directions was assumed to be 0, due to the laminar nature of the flow.

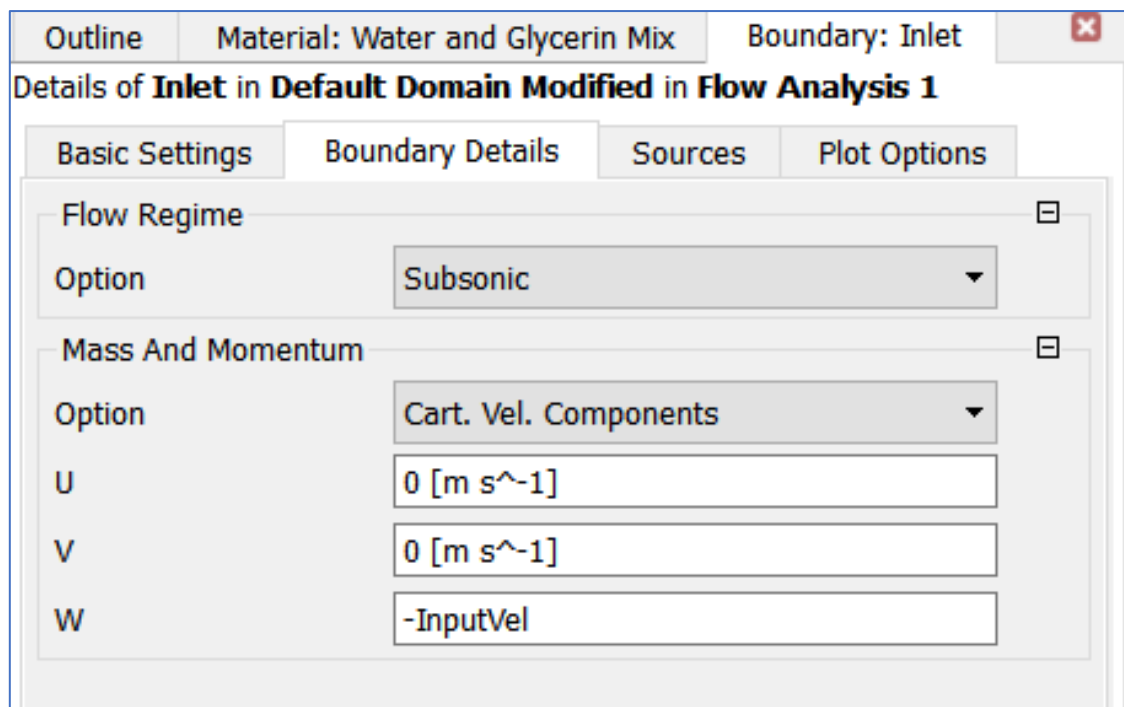


Figure 48 - The inlet boundary details

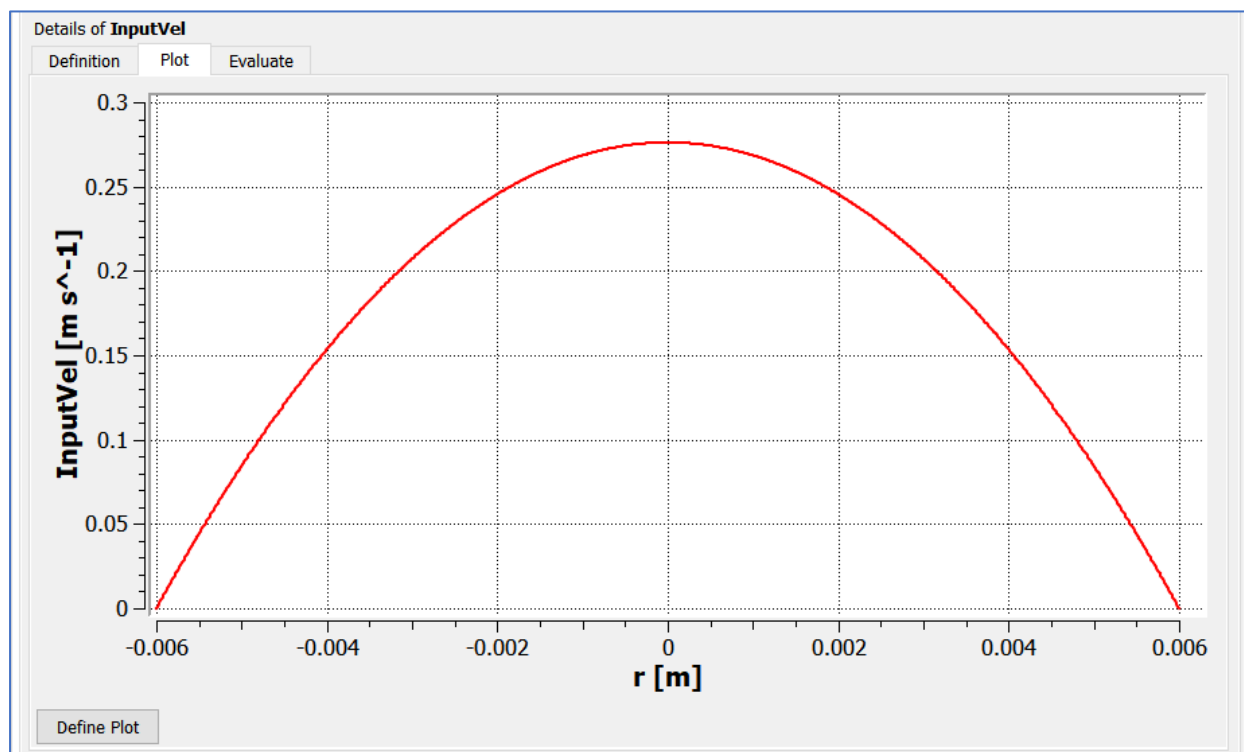


Figure 49 - The inlet velocity profile shown plotted within CFX-Pre using CEL

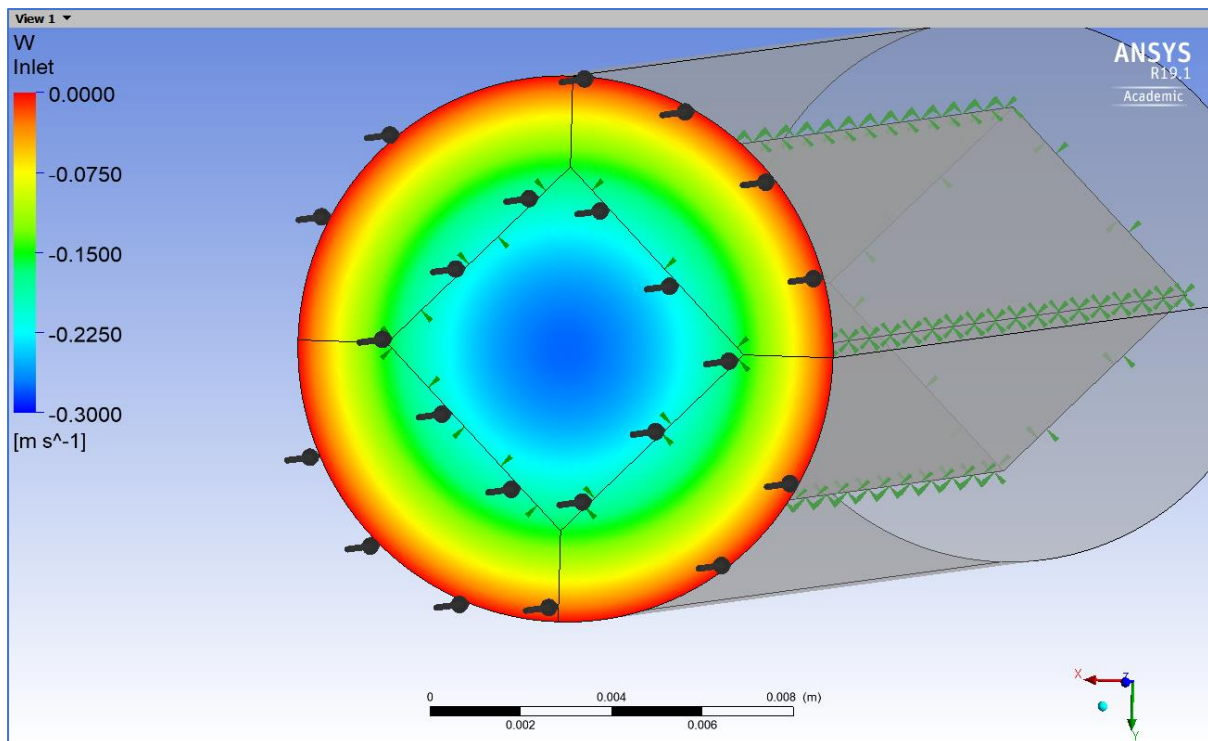


Figure 50 - A boundary contour plot showing the velocity profile of the fluid as it enters the domain. Note - red denotes a minimum velocity and blue denotes a maximum velocity

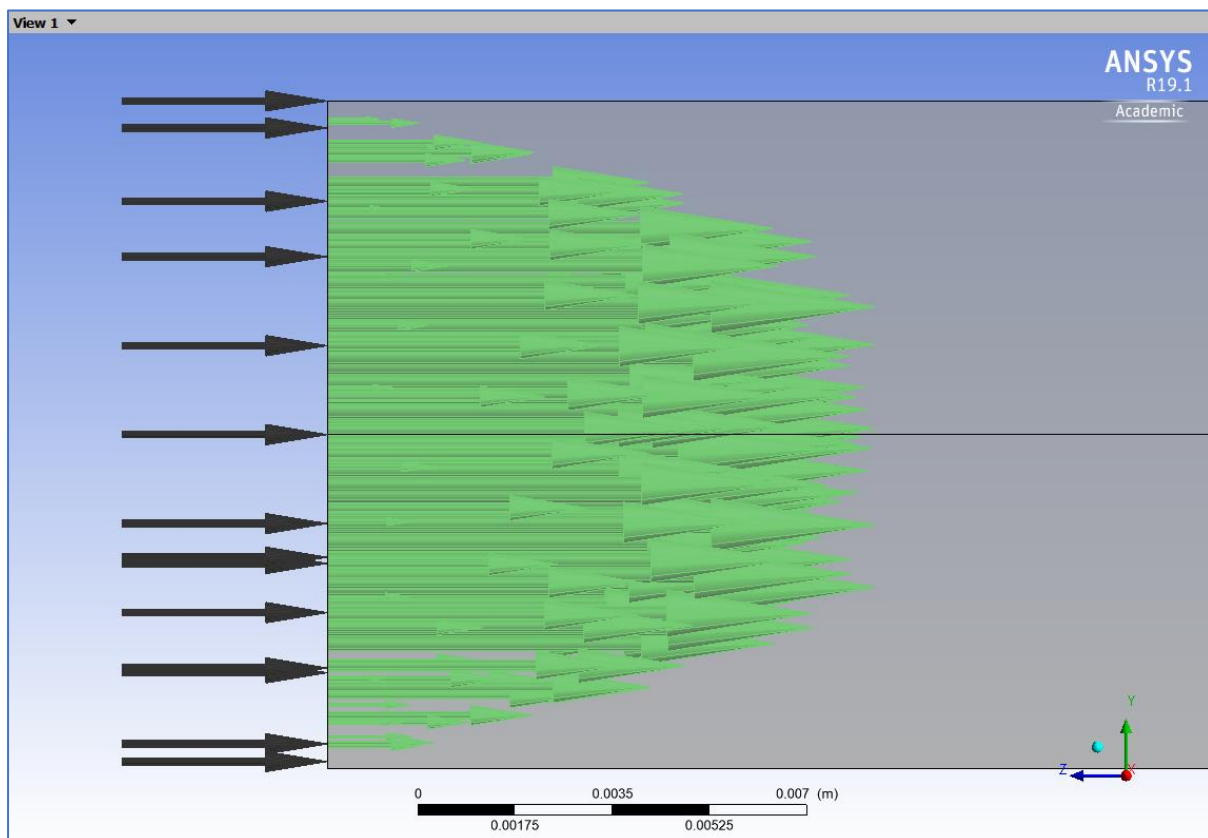


Figure 51 - The inlet velocity profile plotted using vector arrows

### 5.5.2.2 Outlet

The outlet boundary was defined using an average static pressure method, under the mass and momentum section. The relative pressure was set to 0 Pa, and the pressure profile blend was left at the default value of 0.05.

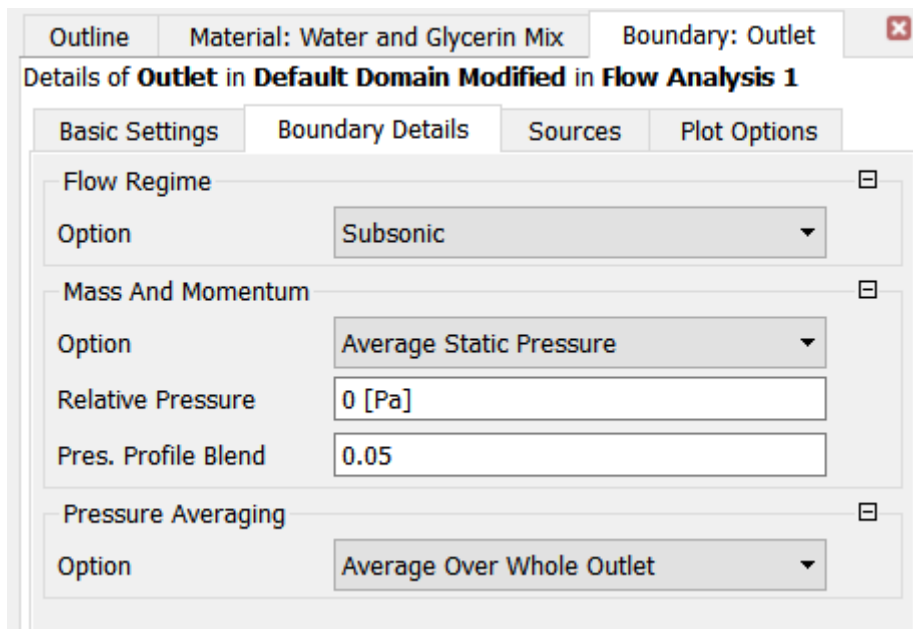


Figure 52 - The outlet boundary details

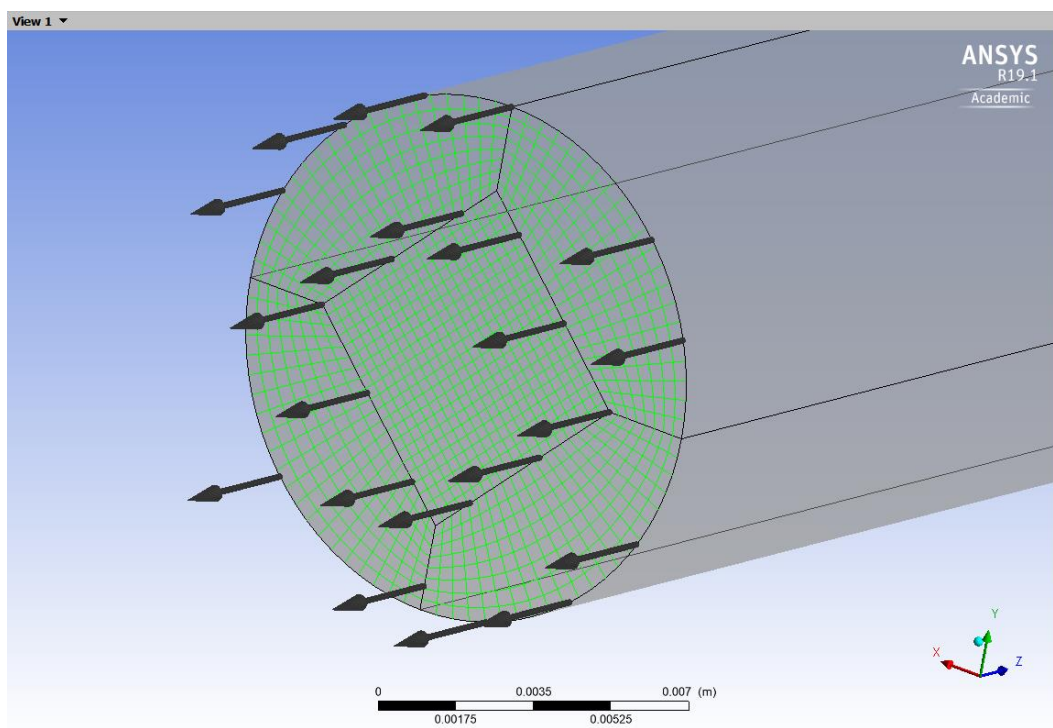


Figure 53 - A closeup of the outlet boundary

### 5.5.2.3 Walls

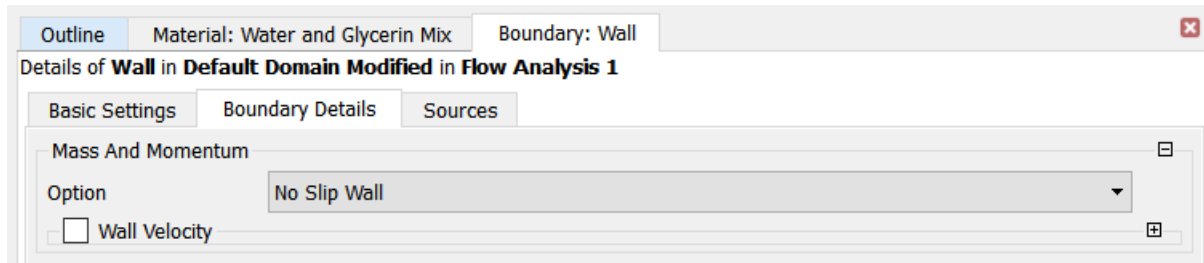


Figure 54 - The wall boundary details

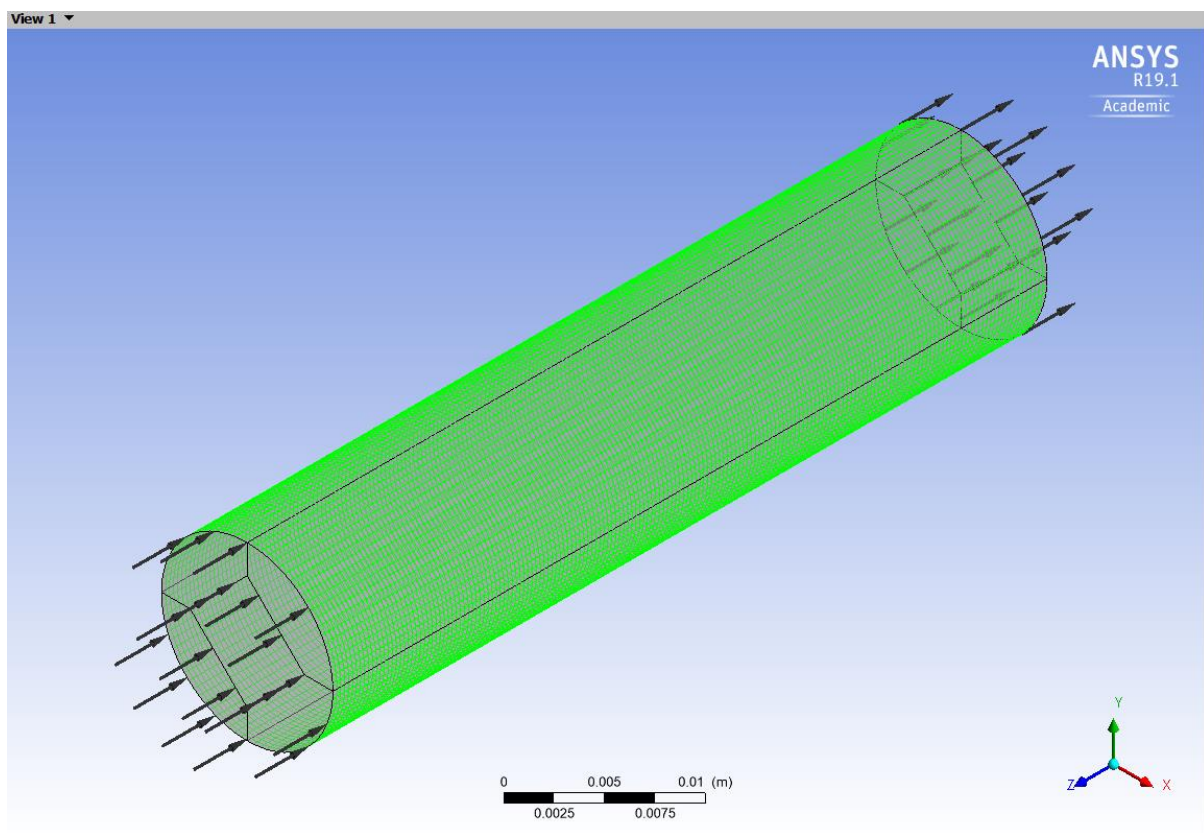


Figure 55 - Isometric view highlighting the wall boundary in green

### 5.5.3 Solver Control

The main method that was used to determine solution convergence was setting an RMS residual target of  $1 \times 10^{-7}$ . This low value was chosen, as it would add convergence confidence without adding much solution wall clock time (due to the fully developed, laminar flow characteristics of the model).

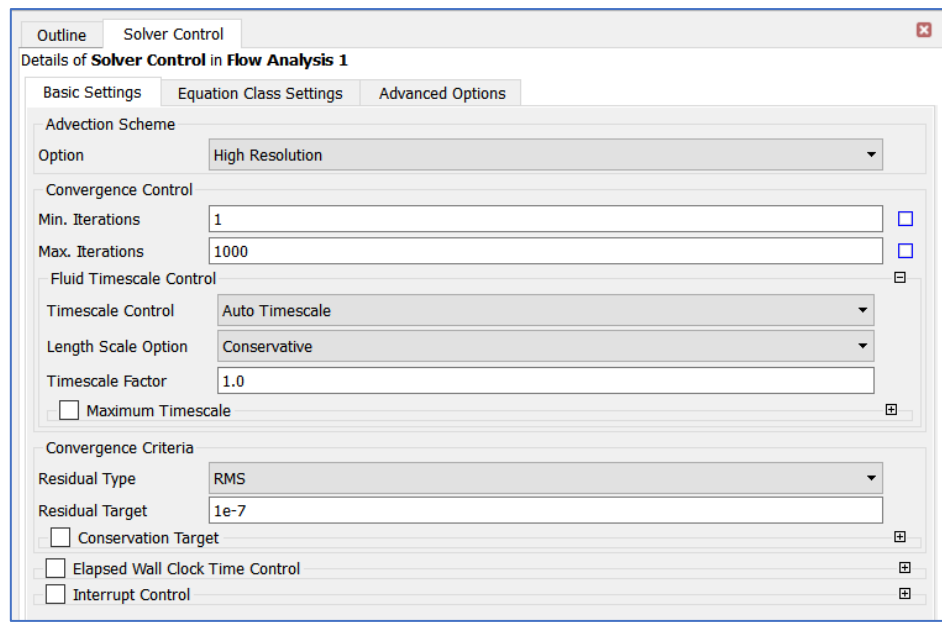


Figure 56 - The solver control menu

#### 5.5.4 Expressions

Custom user variables can be created in CFX, by using the CFX Expression Language (CEL). Custom variables were used to set up the model, and to make data extraction easier once the model had been solved.

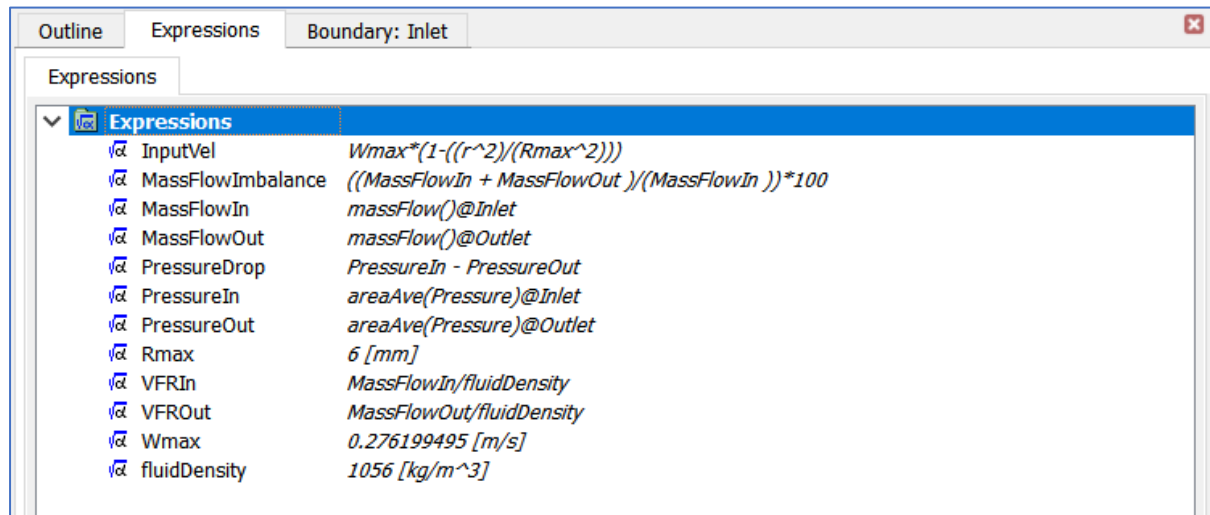


Figure 57 - The CEL expressions used for this model

As the flow is fully laminar, the input velocity profile can be described as a function written in CEL. This can be seen under the title of “InputVel”.

## 5.6 SOLUTION

There were 2 computers used to create and solve this CFD model at various points in time, the majority of the work was done on a desktop PC which consisted of an Intel i7 - 3820 CPU running at 3.3 - 3.6 GHz, with 16 GB of DDR3 RAM running at 1333 MHz. The second system was a Dell XPS-13 (9350) laptop, which had an Intel i5 - 6200U CPU running at 2.4 - 2.8 GHz, along with 8 GB of DDR3L RAM with a clock speed of 1880 MHz. CFX allows the user to easily adjust the number of CPU cores that can be used when solving the model, which means that systems with more CPU cores can be used to solve models in a much shorter amount of time. The screenshots below were taken on the laptop, which has 2 physical CPU cores, with each one being split into 2 virtual cores.

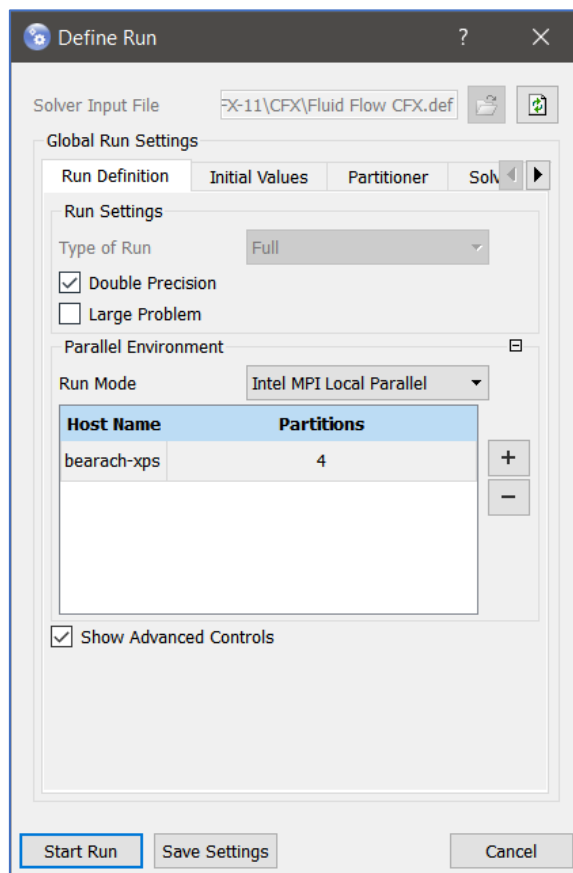


Figure 58 - The "Define Run" dialog box allows the user to easily set the number of CPU cores to be used when solving the CFD code. Along with the option of "Double Precision" mode and "Large Problem" mode

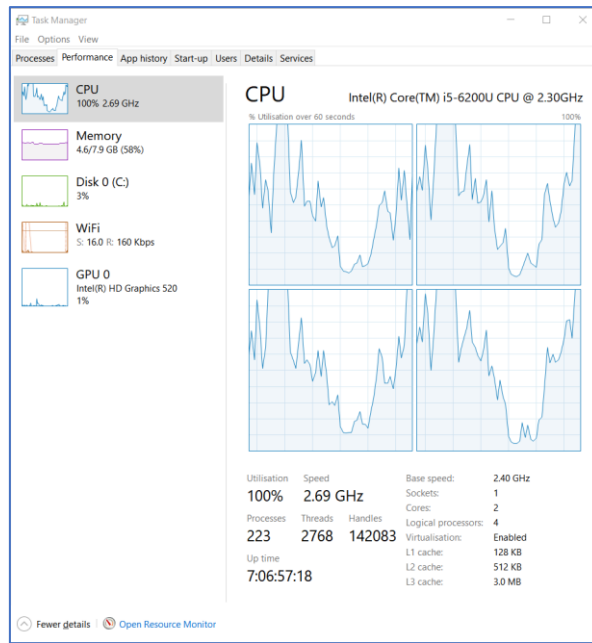


Figure 59 - Windows Task Manager showing the laptop CPU under 100% load on all 4 virtual CPU cores while solving a CFD model

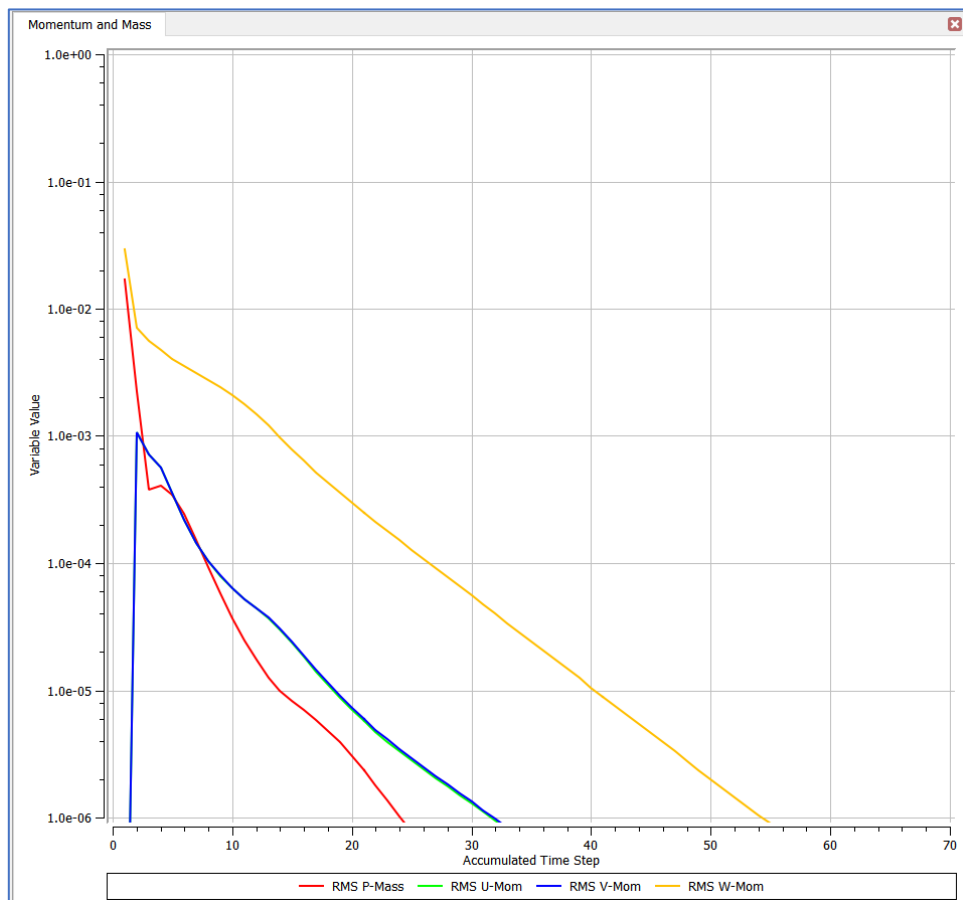


Figure 60 - The RMS values plotted against the accumulated time step of the crudest mesh

```

Total wall clock time: 6.777E+01 seconds
      or: (          0:          0:          1:    7.774 )
            (        Days:     Hours: Minutes: Seconds )

```

Figure 61 - The total wall clock time needed for the crudest mesh to achieve RMS values of  $1 \times 10^{-7}$

```

=====
OUTER LOOP ITERATION =   70                      CPU SECONDS = 2.609E+02
-----
|      Equation      | Rate | RMS Res | Max Res | Linear Solution |
+-----+-----+-----+-----+
| U-Mom           | 0.91 | 6.9E-09 | 1.2E-07 |      8.8E-02  OK|
| V-Mom           | 0.90 | 7.3E-09 | 1.7E-07 |      6.4E-02  OK|
| W-Mom           | 0.88 | 9.9E-08 | 1.8E-06 |      2.1E-02 OK|
| P-Mass          | 0.92 | 1.6E-08 | 3.8E-07 |  4.7  8.7E-02 OK|
+-----+-----+-----+-----+
CFD Solver finished: Tue Feb 12 16:10:52 2019
CFD Solver wall clock seconds: 5.9695E+01
=====
Termination and Interrupt Condition Summary
=====
CFD Solver: All target criteria reached
(Equation residuals)
=====
```

Figure 62 - The final iteration of the crudest mesh, showing that convergence of the RMS residuals was achieved

## 5.7 MODEL VALIDATION

The metrics used to determine a valid model were the pressure drop across the length of the pipe, and the mass flow rate/ imbalance in the domain.

As can be seen from the tabulated results calculated in Excel, the pressure drop ( $\Delta P$ ) between the inlet and the outlet of the pipe vary from a maximum of -1.3% on Mesh 1, to a minimum of -0.71% on Mesh 5. While not perfect, these results do quite agree with the theoretical value of 5.37 Pa.

As for the mass flow rate, it varies from a maximum of 0.17% with Mesh 1, to a minimum of 0.02% on Mesh 5. These results agree very well with the theoretical results. Along with the low variation from the theoretical value, all of these meshes achieved a mass flow imbalance of 0%, with the mass flow rate through the inlet and outlet being exactly equal.

Mesh Metrics	Mesh 1	Mesh 2	Mesh 3	Mesh 4	Mesh 5	Units
Inlet Pressure	5.30	5.32	5.32	5.32	5.33	Pa
Outlet Pressure	1.45E-05	1.60E-06	1.22E-06	9.46E-07	1.23E-06	
$\Delta P$	5.30	5.32	5.32	5.32	5.33	
% Change	0	0.33%	0.10%	-0.05%	0.23%	
Theoretical Value	5.3705					Pa
Variation from Theory	-1.30%	-0.98%	-0.88%	-0.93%	-0.71%	-
$\dot{m}_{in}$	0.01652	0.01650	0.01650	0.01650	0.01650	kg/s
$\dot{m}_{out}$	-0.01652	-0.01650	-0.01650	-0.01650	-0.01650	
$\Delta \dot{m}$	0	0	0	0	0	
$\dot{m}_{imbal}$	0%	0%	0%	0%	0%	
Theoretical Value	0.016493					kg/s
Variation from Theory	0.17%	0.07%	0.04%	0.03%	0.02%	-

Table 5 - Table created in Excel that was used to compare the model values with theoretical values

## 5.8 MESH CONVERGENCE STUDY

### 5.8.1 Mesh Details

Five meshes were created, starting with approximately 30,000 elements, and increasing to approximately 500,000 elements (which is the element limit placed on CFD models in the ANSYS student licence). The details of the mesh sizings used on each can be seen in the table below.

		Mesh 1	Mesh 2	Mesh 3	Mesh 4	Mesh 5	Units
Edge Sizing	Outer Diameter	10	15	21	23	26	Divisions    mm
	Guide Lines 1	5	7	8	10	13	
	Guide Lines 2	5	7	8	10	13	
	Prism Length	0.6	0.38	0.28	0.25	0.22	
Face Sizing	Prism	0.6	0.38	0.28	0.25	0.22	mm
Number of Longitudinal Elements		83	132	179	200	227	
Number of Nodes		28,661	97,888	223,200	318,612	498,178	
Number of Elements		6,000	85,140	199,227	289,271	460,356	

Table 6 - The mesh sizing chart created in Excel

The primary metric used to establish mesh convergence was that of the pressure drop across the length of the pipe (i.e.  $\Delta P = P_{\text{Inlet}} - P_{\text{Outlet}}$ ). The mass flow imbalance was going to be the secondary mesh convergence metric used, however all 5 meshes achieved a mass flow imbalance of 0%. This was due to the laminar and fully developed flow regime through the pipe.

A convergence tolerance of 1% was used to determine convergence. That is, if the pressure drop across the length of the pipe varies by under 1% from one mesh to another, convergence has been achieved.

The variables of interest (pressure drop, mass flow rate, volume flow rate) were set up as CEL expressions, which were then defined as ANSYS Workbench output parameters. Output parameters can easily be viewed in Workbench, which makes copying the data into an Excel sheet simple.

## 5.8.2 Mesh Convergence Results

Outline of All Parameters				
	A	B	C	D
1	ID	Parameter Name	Value	Unit
2	Input Parameters			
*	New input parameter	New name	New expression	
4	Output Parameters			
5	28,661 Nodes (B1)			
6	P7	PressureDrop	5.3005	Pa
7	P8	VFRImbalance	2.3252E-05	
8	P9	MassFlowImbalance	2.2548E-05	
9	P28	MassFlowIn	0.016522	kg s^-1
10	P29	MassFlowOut	-0.016522	kg s^-1
11	P30	PressureIn	5.3005	Pa
12	P31	PressureOut	8.1945E-06	Pa
13	100,000 Nodes (D1)			
14	P13	PressureDrop	5.3179	Pa
15	P14	VFRImbalance	0	
16	P32	PressureIn	5.318	Pa

Figure 63 - Screenshot from Workbench showing the output parameters table view

Mesh Metrics	Mesh 1	Mesh 2	Mesh 3	Mesh 4	Mesh 5	Units
Inlet Pressure	5.30	5.32	5.32	5.32	5.33	Pa
Outlet Pressure	1.45E-05	1.60E-06	1.22E-06	9.46E-07	1.23E-06	
$\Delta P$	5.30	5.32	5.32	5.32	5.33	
% Change	0	0.33%	0.10%	-0.05%	0.23%	
Theoretical Value	5.3705					
Variation from Theory	-1.30%	-0.98%	-0.88%	-0.93%	-0.71%	-
$\dot{m}_{in}$	0.01652	0.01650	0.01650	0.01650	0.01650	kg/s
$\dot{m}_{out}$	-0.01652	-0.01650	-0.01650	-0.01650	-0.01650	
$\Delta \dot{m}$	0	0	0	0	0	
$\dot{m}_{imbal}$	0%	0%	0%	0%	0%	-
Theoretical Value	0.016493					kg/s
Variation from Theory	0.17%	0.07%	0.04%	0.03%	0.02%	-

Table 7 - Tabulated results from the 5 meshes

### 5.8.2.1 Pressure Drop

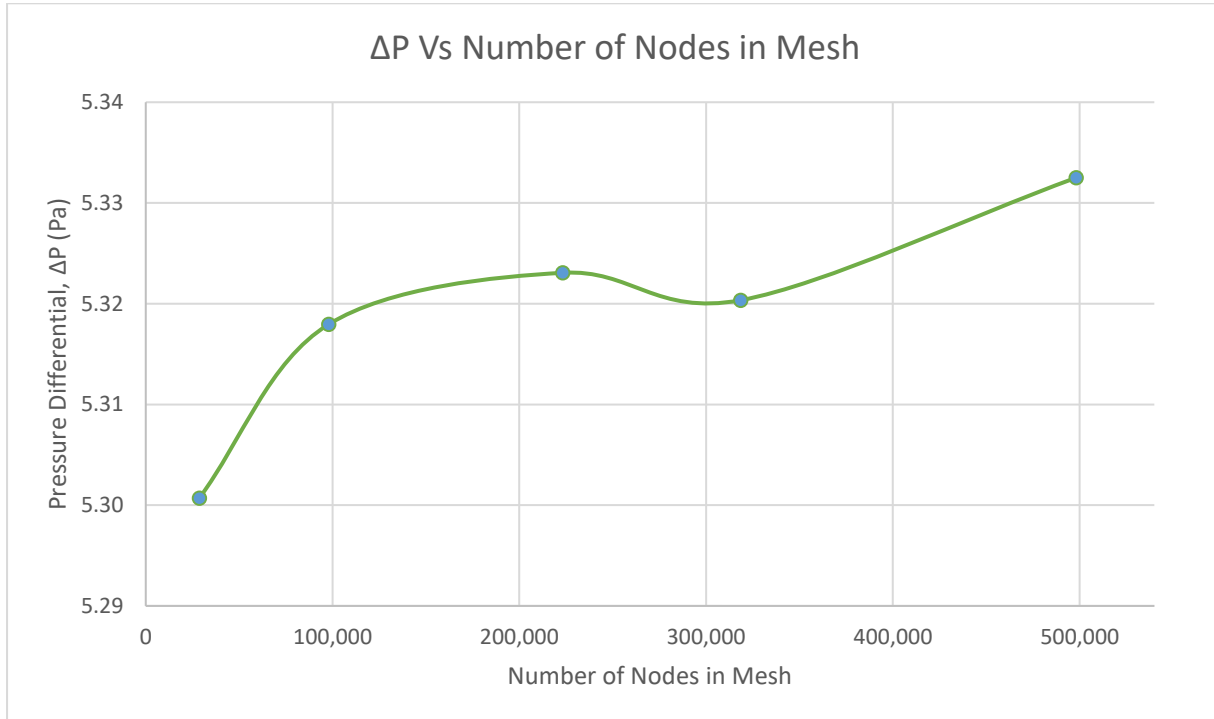
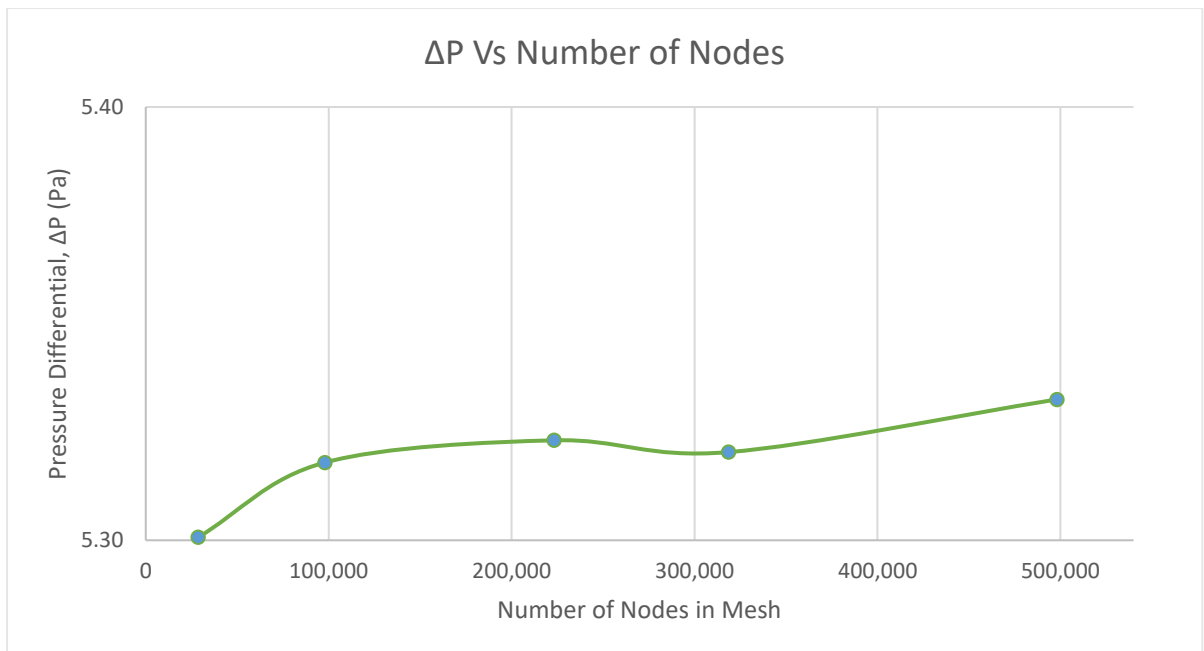


Figure 64 - Plot of pressure drop against number of nodes in mesh

When the pressure differential is plotted against the number of nodes in the mesh, it can be seen that there is an overall trend upwards, as the number of nodes increases. However, the percentage change between these results varies from a maximum of 0.33% between the first and second meshes, to a minimum of -0.05% between the third and fourth meshes. Due to the scale of the Y axis, these results may appear at first to vary quite a bit.



*Figure 65 - Plot of pressure drop against number of nodes in mesh (with adjusted Y axis)*

When the scale of the Y axis on the plot is changed to have a range of 0.1 Pa, the differences appear much more realistic.

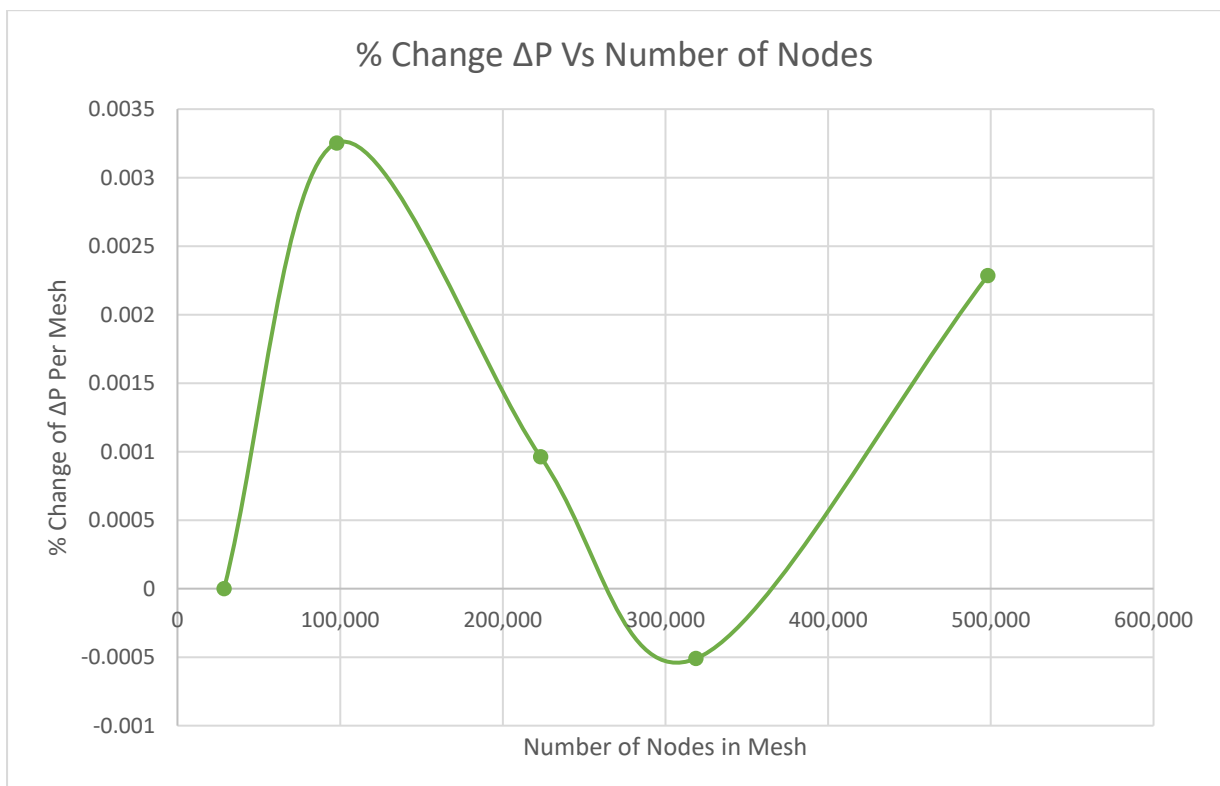


*Figure 66 - Plot of the % change in pressure drop against mesh size*

### 5.8.2.2 Mass Flow Rate

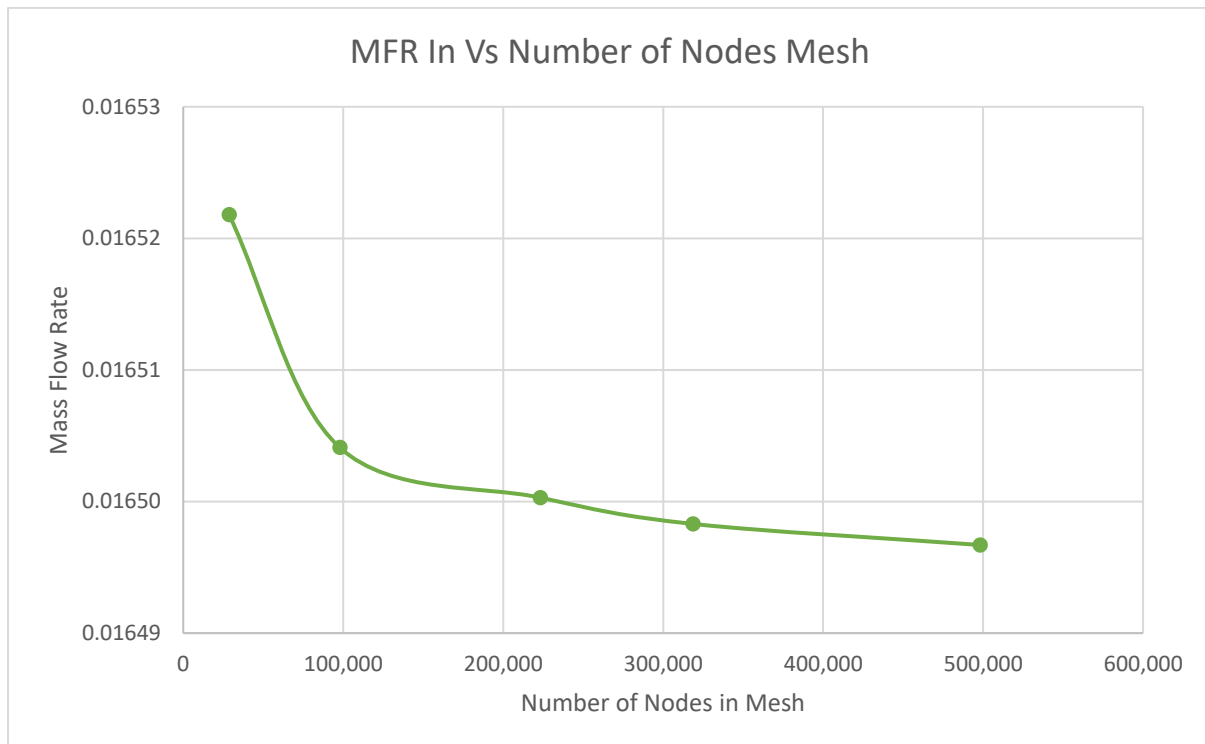


Figure 67 - Plot of mass flow rate against mesh size

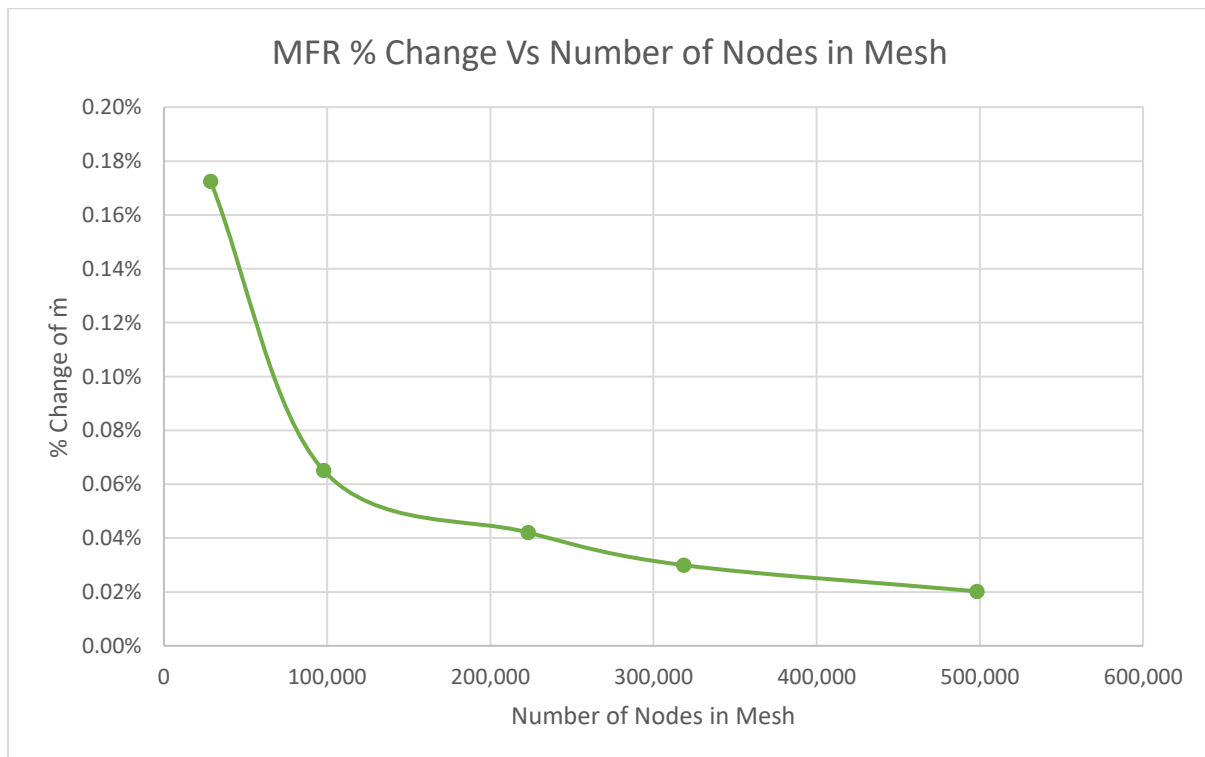
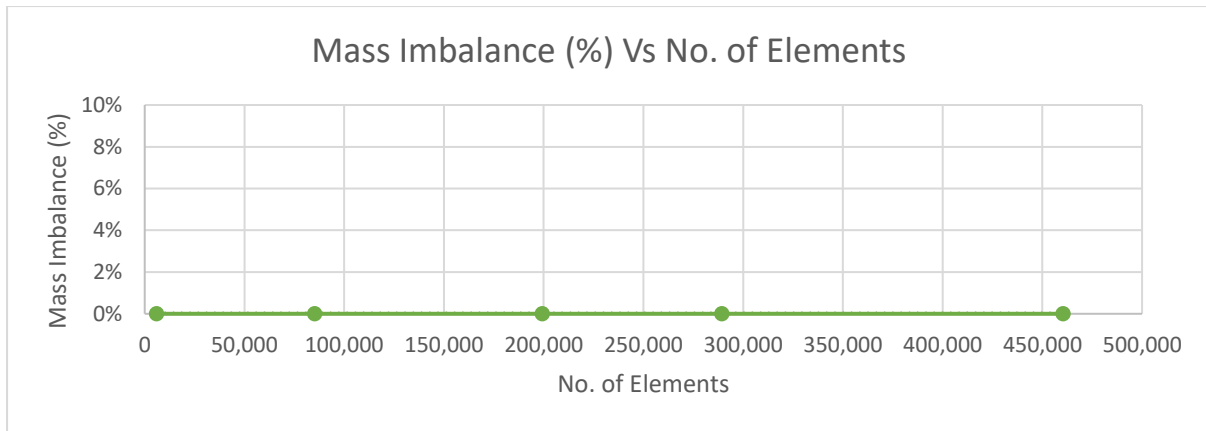


Figure 68 - Plot showing the % change in mass flow rate against size of mesh



*Figure 69 - Plot showing the mass imbalance plotted against mesh size*

As the mass imbalance for all meshes was 0%, using the mass imbalance as a mesh convergence metric was not possible.

### 5.8.3 Conclusion

Mesh convergence was achieved with the first mesh used, as changes in the pressure drop were under the 1% tolerance chosen between the first and second mesh.

## 5.9 CONCLUSION

In conclusion, ANSYS Workbench was used to create an accurate model of fluid flow through a 12 mm diameter pipe. This was verified using pipe theory (pressure drop), and then a mesh convergence study was carried out, with the crudest mesh created staying within the 1% convergence tolerance limit.

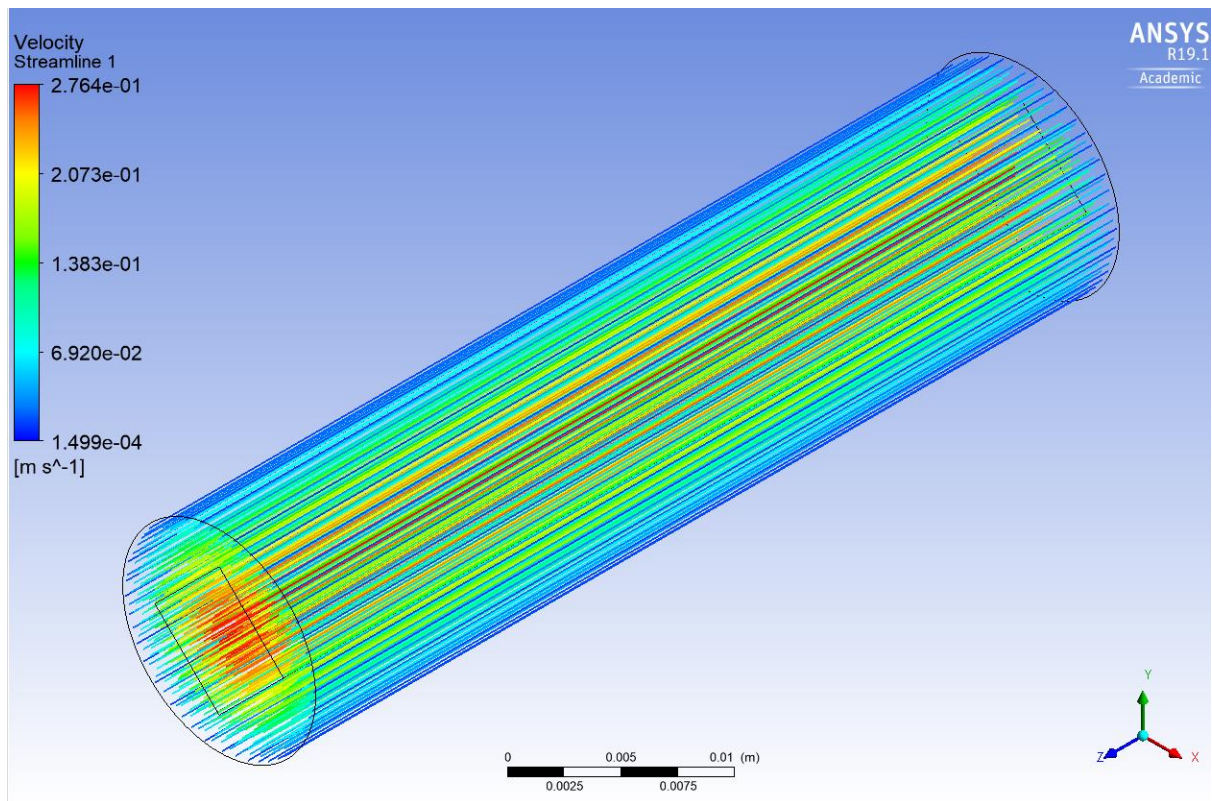


Figure 70 - Isometric view showing streamlines coloured by velocity

# Chapter 6

## FINAL MODEL

### 6.1 INTRODUCTION

This chapter will detail the design of the final model, covering the steps that were taken to create the geometry, mesh, model setup, and model solution.

### 6.2 GEOMETRY

The geometry was created using the dimensioned drawings provided on the FDA Round Robin website ([www.nciphub.org](http://www.nciphub.org)) and the modelling was done in Solidworks 2018. Once the part had been saved as a Solidworks part file (.SLDPRT), it was then saved as a STEP (.STEP) file, which could then be imported into Workbench.

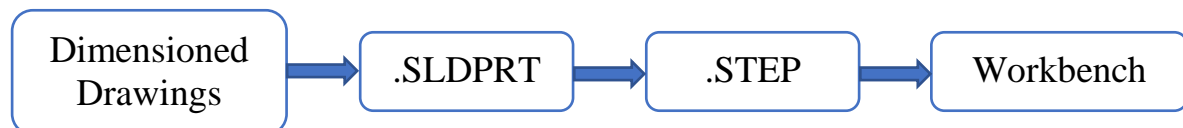


Figure 71 - Flowchart showing the steps taken to create the geometry

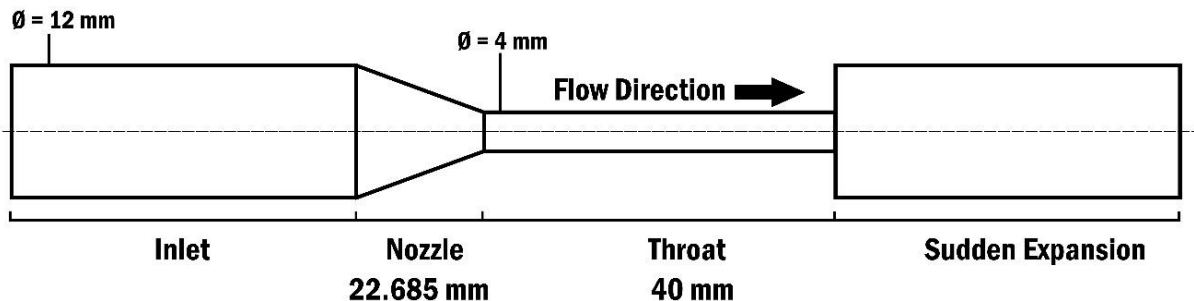


Figure 72 - Benchmark #1 geometry

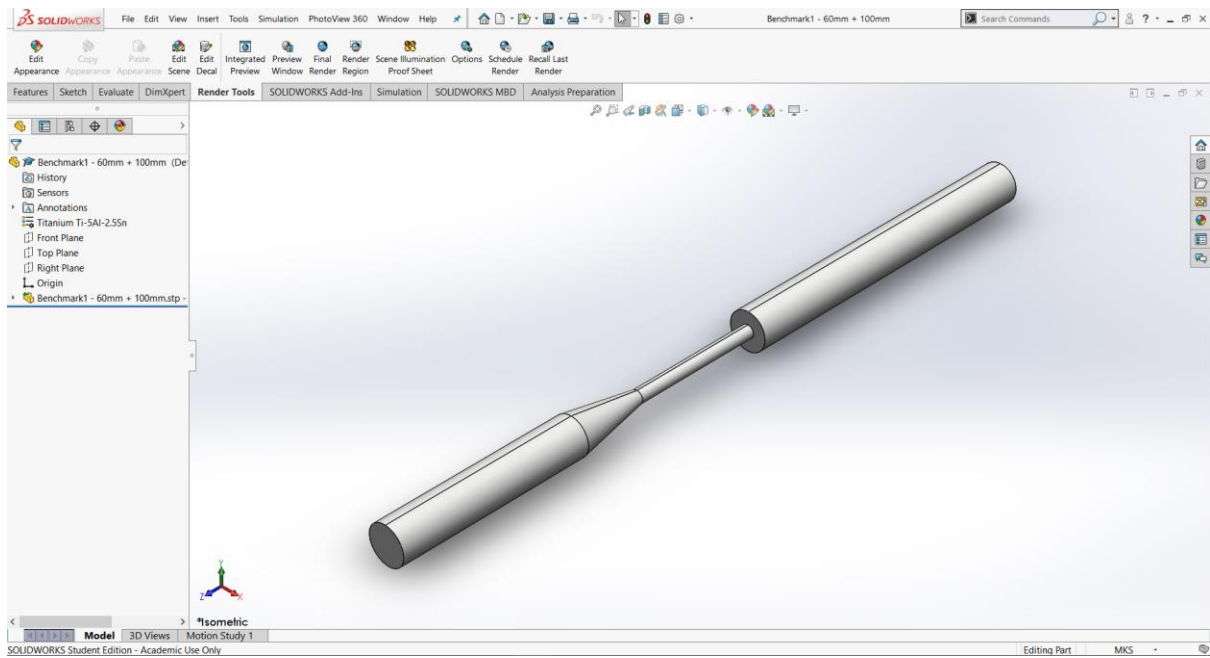


Figure 73 - The geometry modelled in Solidworks

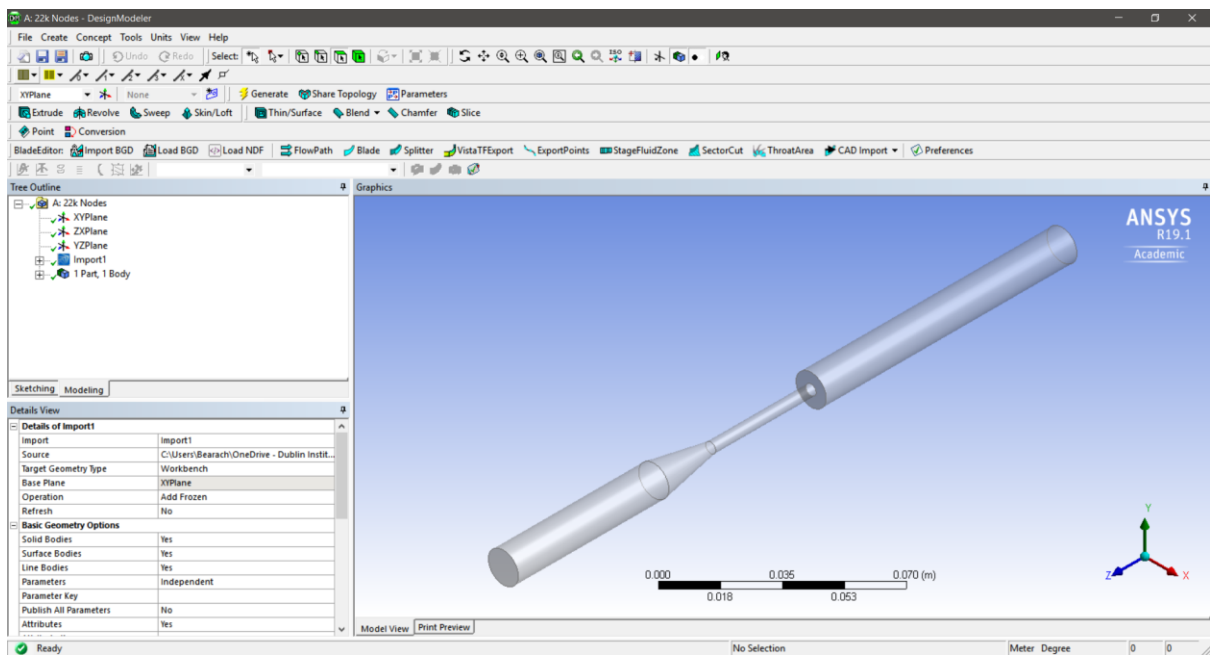


Figure 74 - The geometry opened in Design Modeler after being imported to Workbench

## 6.3 MESH

There were five meshes created, in order for a mesh convergence study to be carried out. The meshes used the same format with the only difference between each of them being the element

sizing. The main limitation on the resolution of the meshes that could be used in this project was the node limit placed on the ANSYS student licence of 512,000 nodes for CFD simulations. As with the earlier model, all meshing was completed in ANSYS Meshing.

### 6.3.1 Mesh Controls

Due to the more complex nature of the geometry, less stringent mesh controls were placed on the final geometry than the simple pipe test case. Some meshing methods similar to the ones used in the previous test case were attempted, however the meshes that those methods yielded were not adequate. As a result of this, a simpler mesh was used that did not use a H grid method.

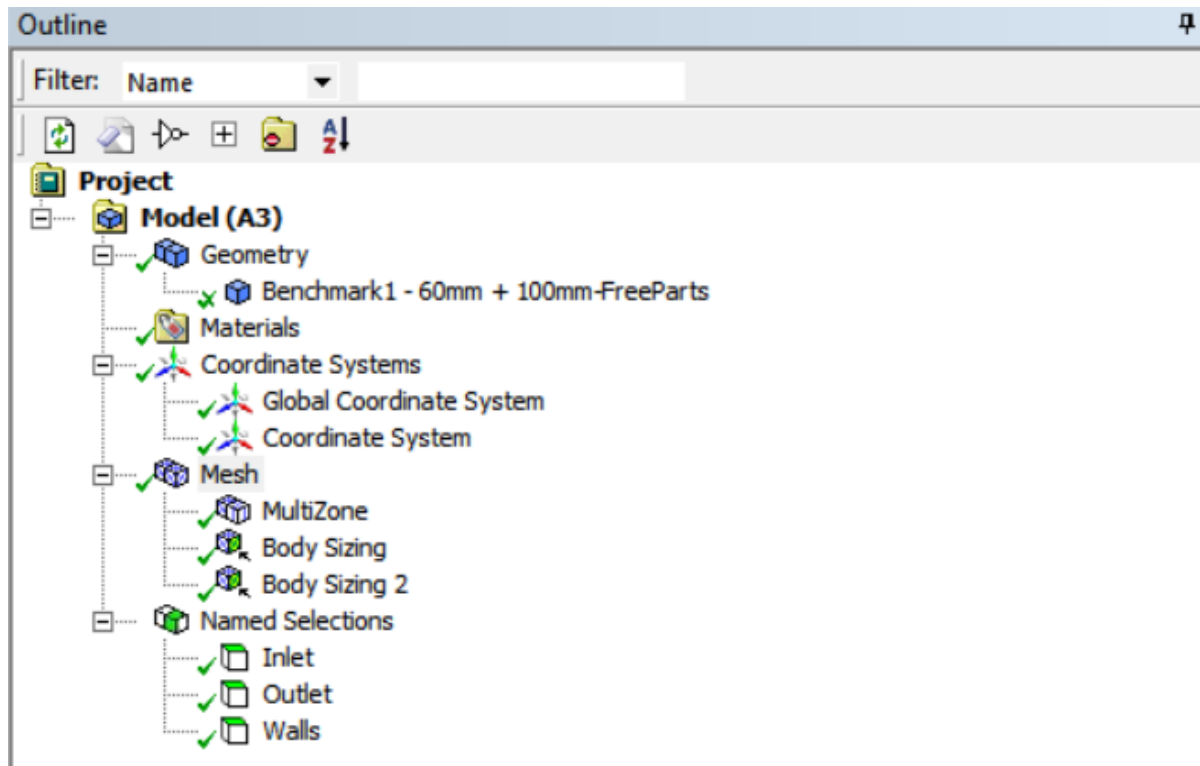


Figure 75 - The outline tree in ANSYS Meshing

Details of "Mesh"	
<input type="checkbox"/>	<b>Display</b>
Display Style	Body Color
<input type="checkbox"/>	<b>Defaults</b>
Physics Preference	CFD
Solver Preference	CFX
Element Order	Linear
<input type="checkbox"/> Element Size	Default (11.167 mm)
<input checked="" type="checkbox"/>	<b>Sizing</b>
<input checked="" type="checkbox"/>	<b>Quality</b>
<input checked="" type="checkbox"/>	<b>Inflation</b>
<input checked="" type="checkbox"/>	<b>Advanced</b>
<input type="checkbox"/>	<b>Statistics</b>
<input type="checkbox"/> Nodes	28807
<input type="checkbox"/> Elements	25284

Figure 76 - Mesh details

### 6.3.2 Area of Interest

The main area of interest that required an increased level of detail is the area around the sudden expansion. To increase the level of detail in this area, a smaller element sizing was used on this area using a sphere of influence method. The sphere had a radius of 34 mm, in order to encompass all of the areas after the sudden expansion where CFD results were compared with experimental results.

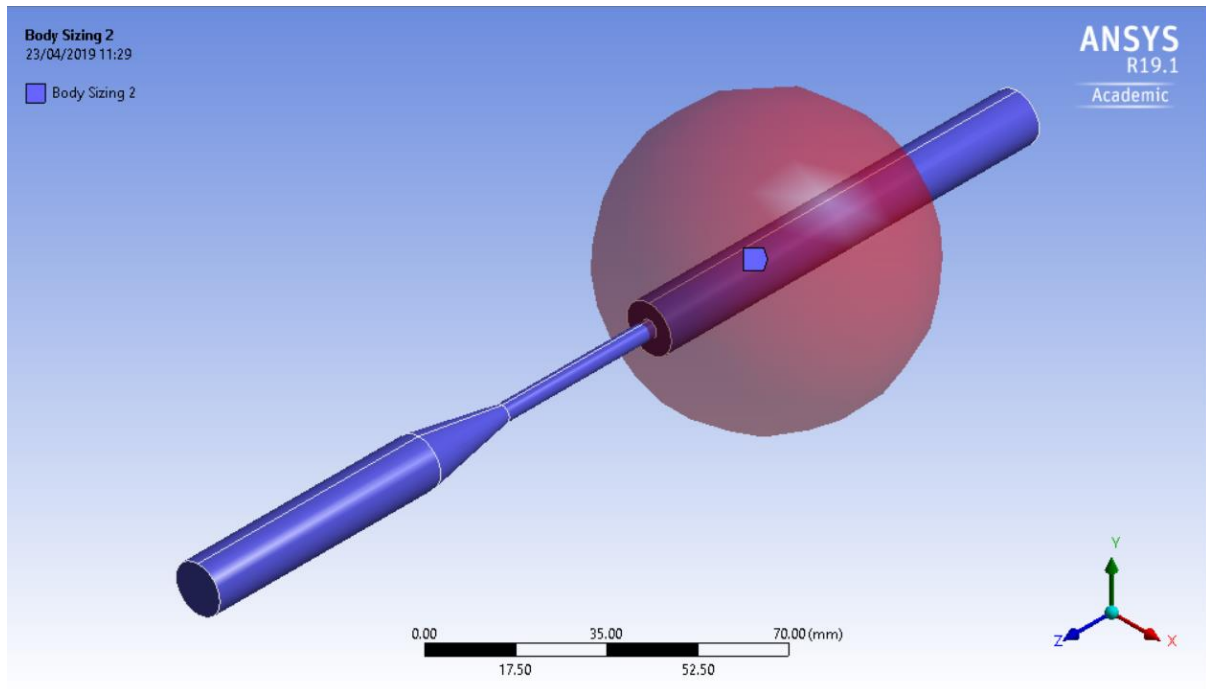


Figure 77 - Sphere of influence body sizing around the area of interest

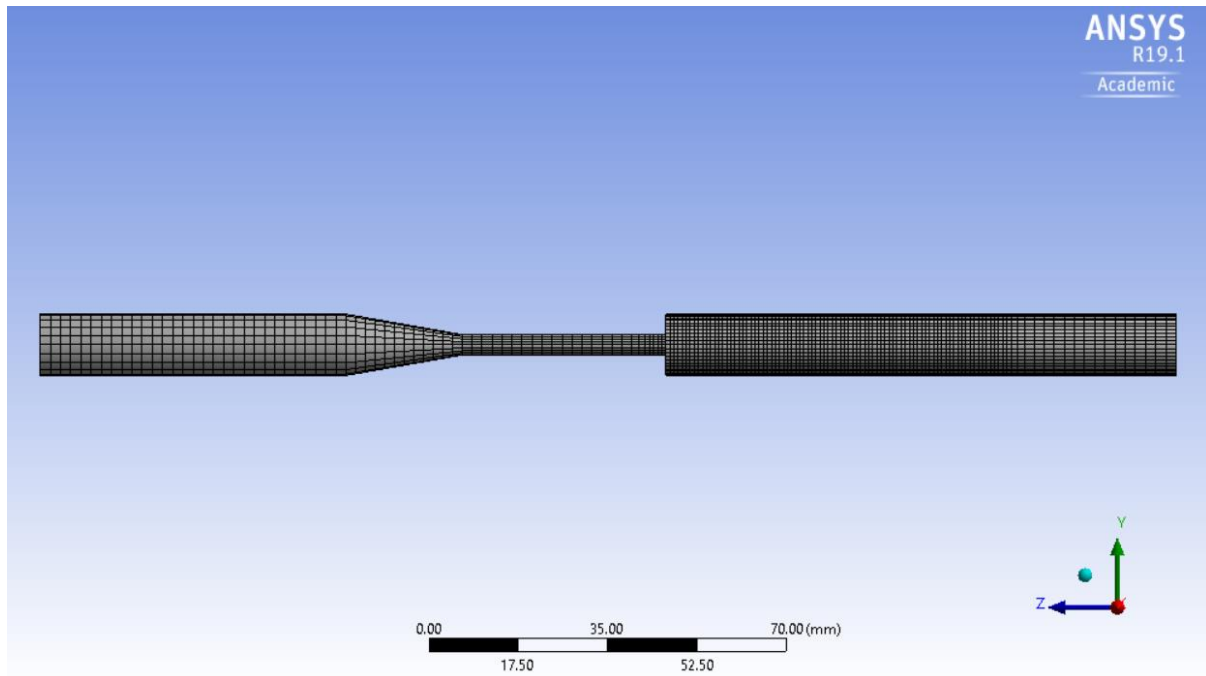


Figure 78 - Profile view of the mesh

### 6.3.3 Final Meshes

Details of the final meshes can be seen summarised below, along with screenshots of each mesh.

Mesh Metrics	Mesh 1	Mesh 2	Mesh 3	Mesh 4	Mesh 5	Units
Number of Nodes	28,807	96,332	212,634	358,666	510,794	-
Number of Elements	25,284	87,198	195,220	332,540	476,234	
Body Sizing 1	2.00	1.60	1.30	0.70	0.55	mm
Body Sizing 2	0.80	0.45	0.32	0.28	0.25	mm

*Table 8 - The sizing and element/node counts for each of the final meshes*

### 6.3.3.1 Mesh 1

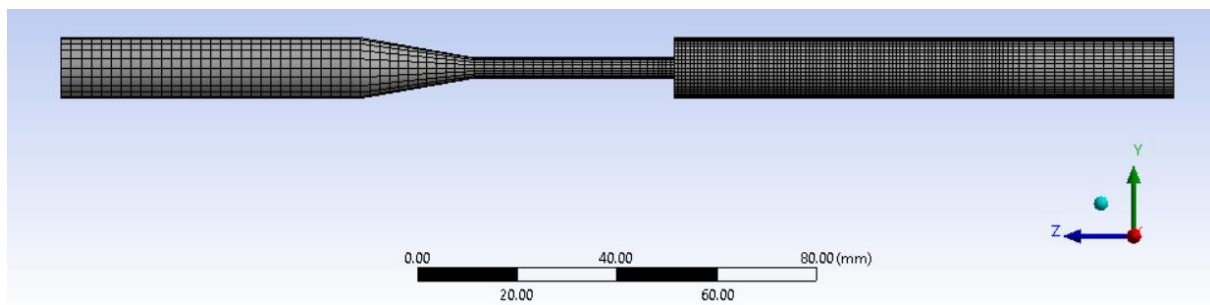


Figure 79 - Profile view of mesh 1

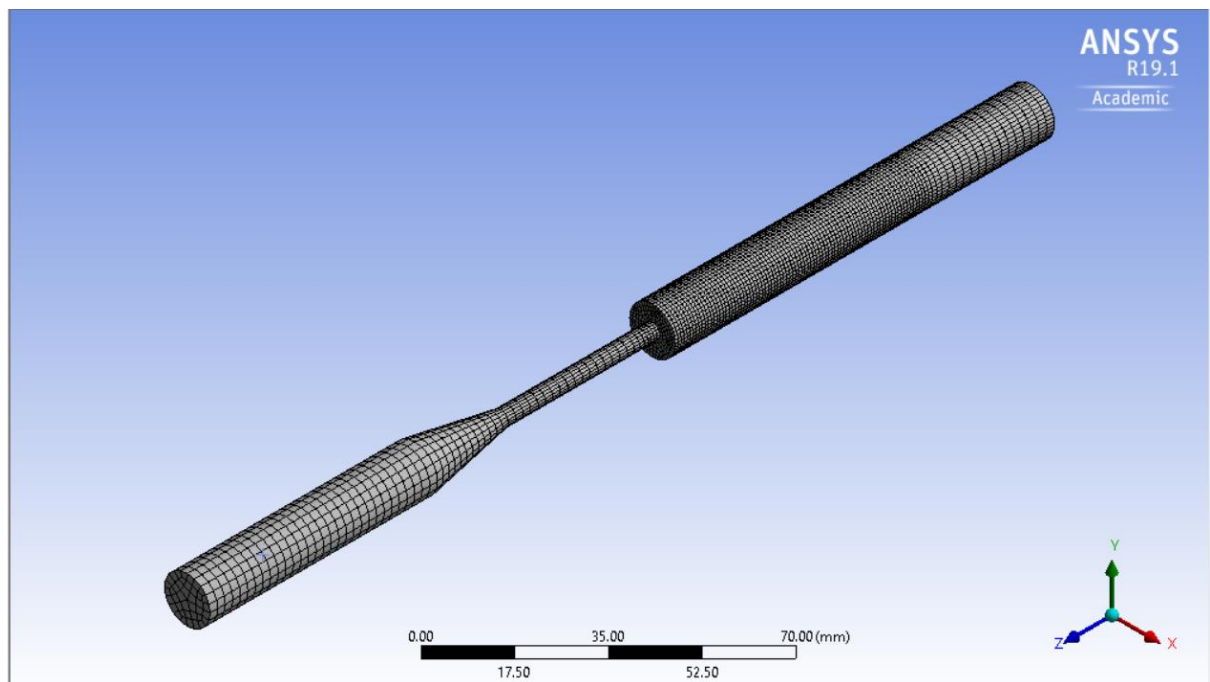


Figure 80 - Isometric view of mesh 1

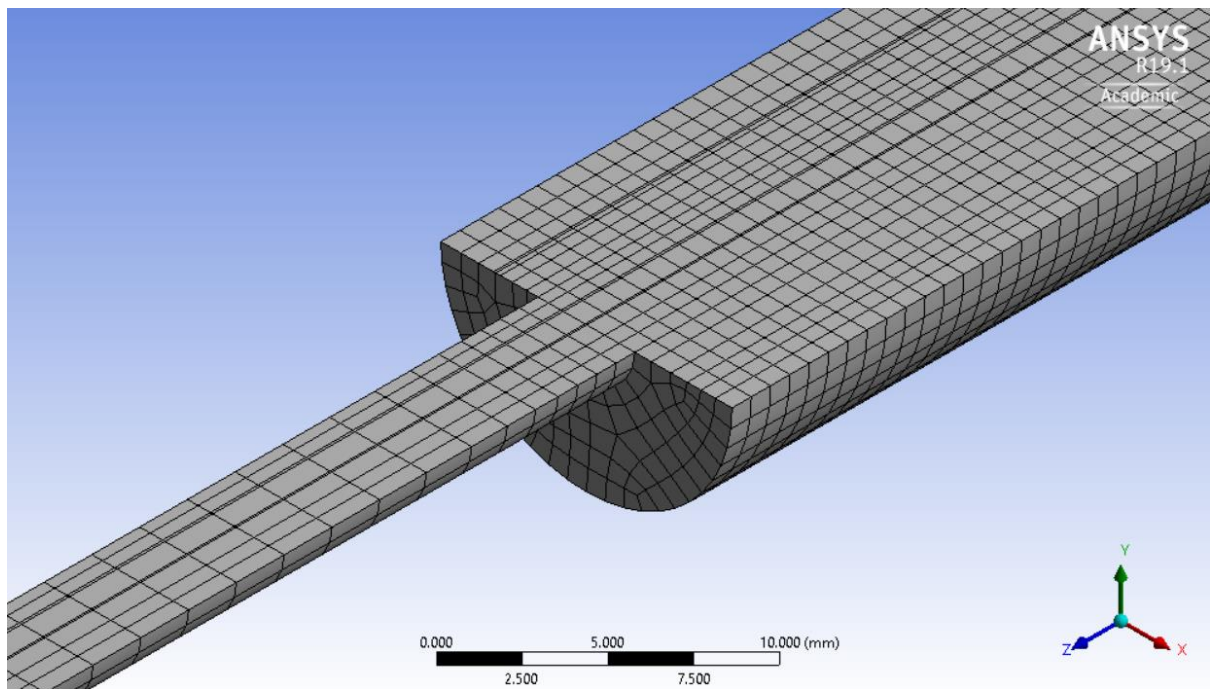


Figure 81 - Isometric cutaway view of mesh 1

#### 6.3.3.2 Mesh 2

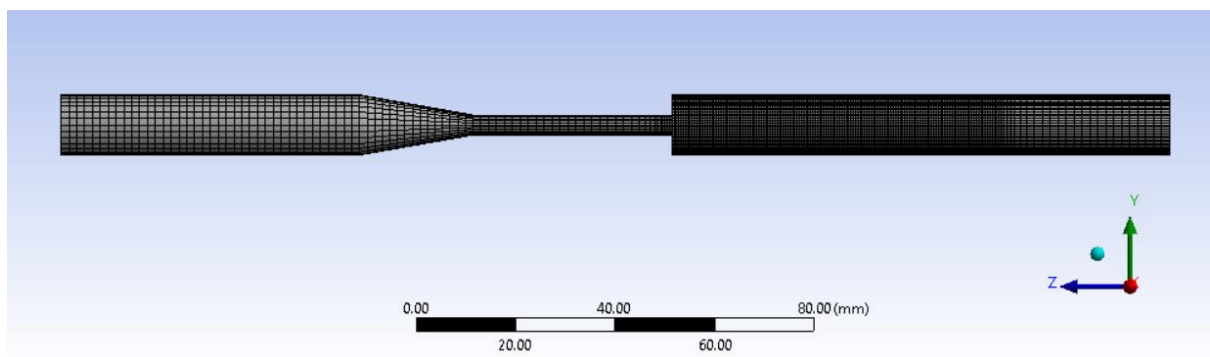


Figure 82 - Profile view of mesh 2

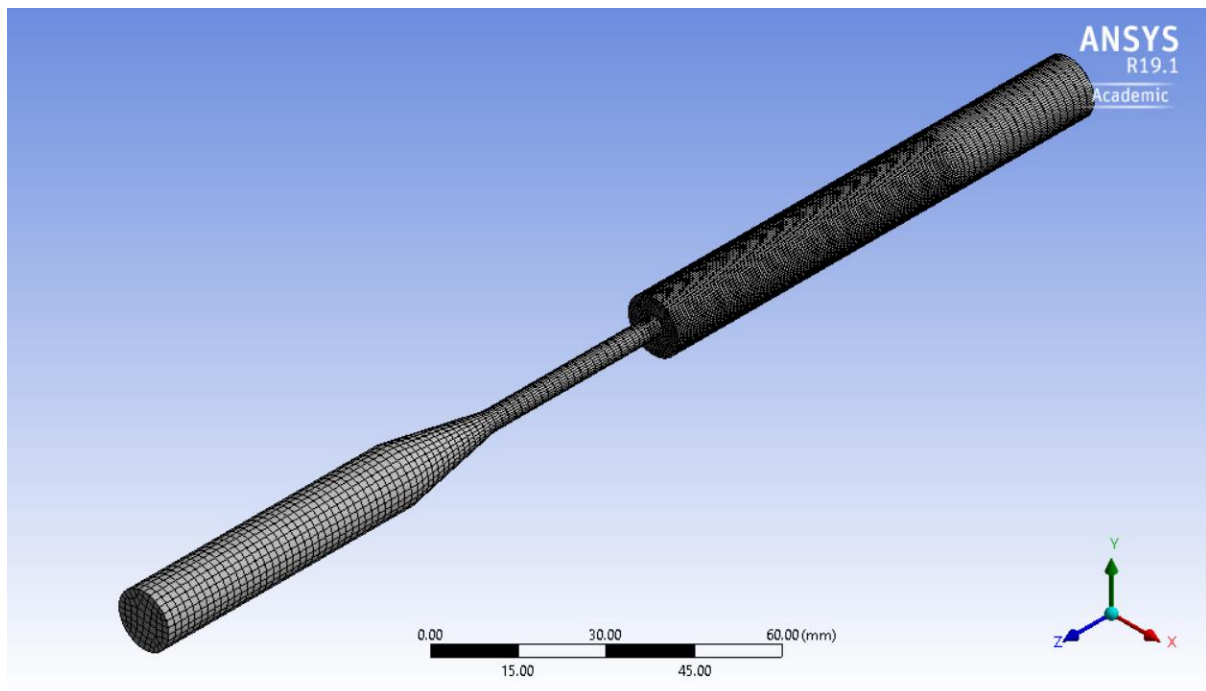


Figure 83 - Isometric view of mesh 2

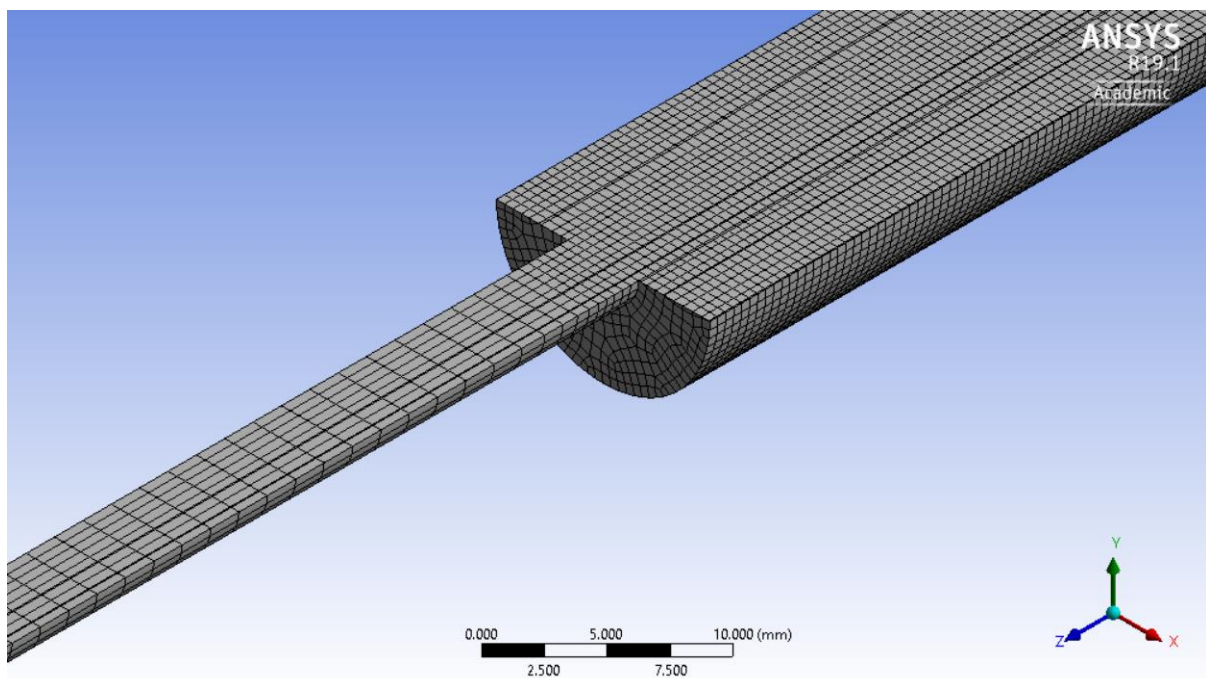


Figure 84 - Isometric cutaway view of mesh 2

### 6.3.3.3 Mesh 3

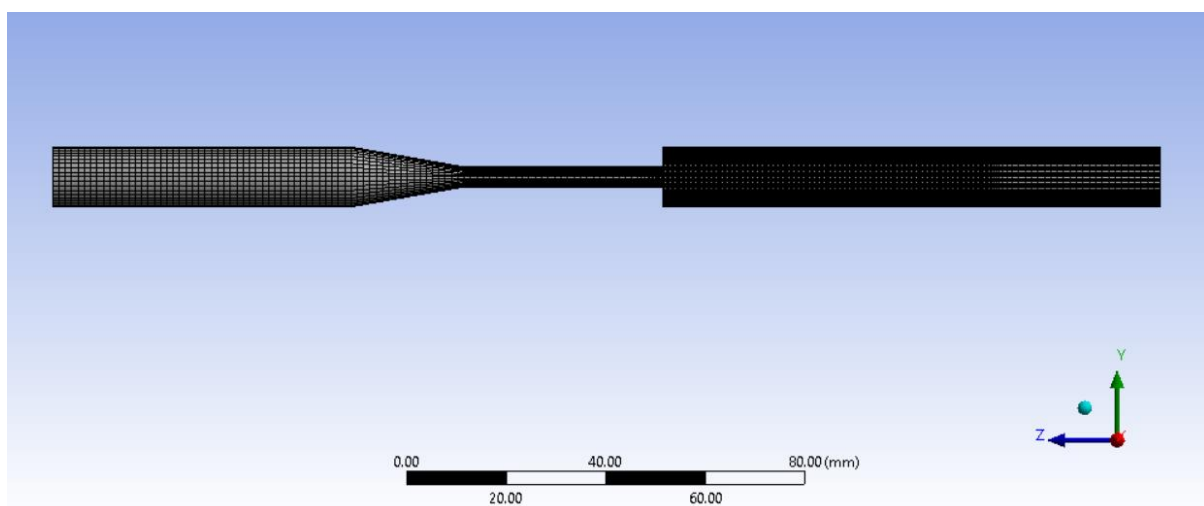


Figure 85 - Profile view of mesh 3

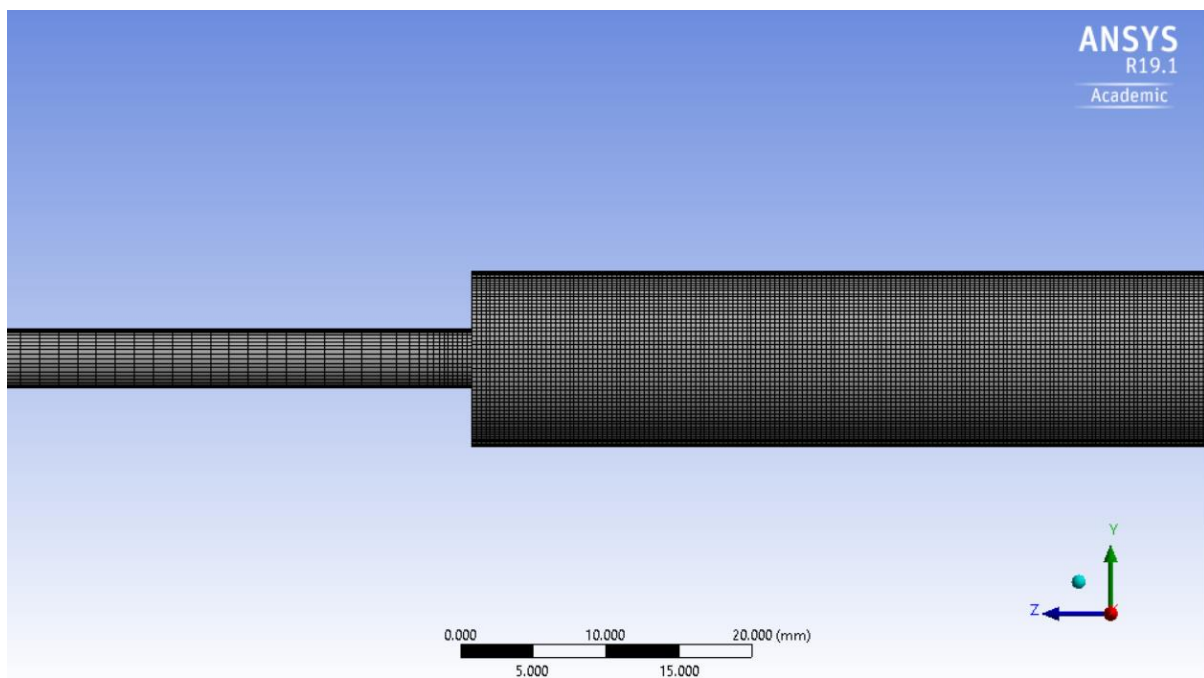


Figure 86 - Profile view of mesh 3

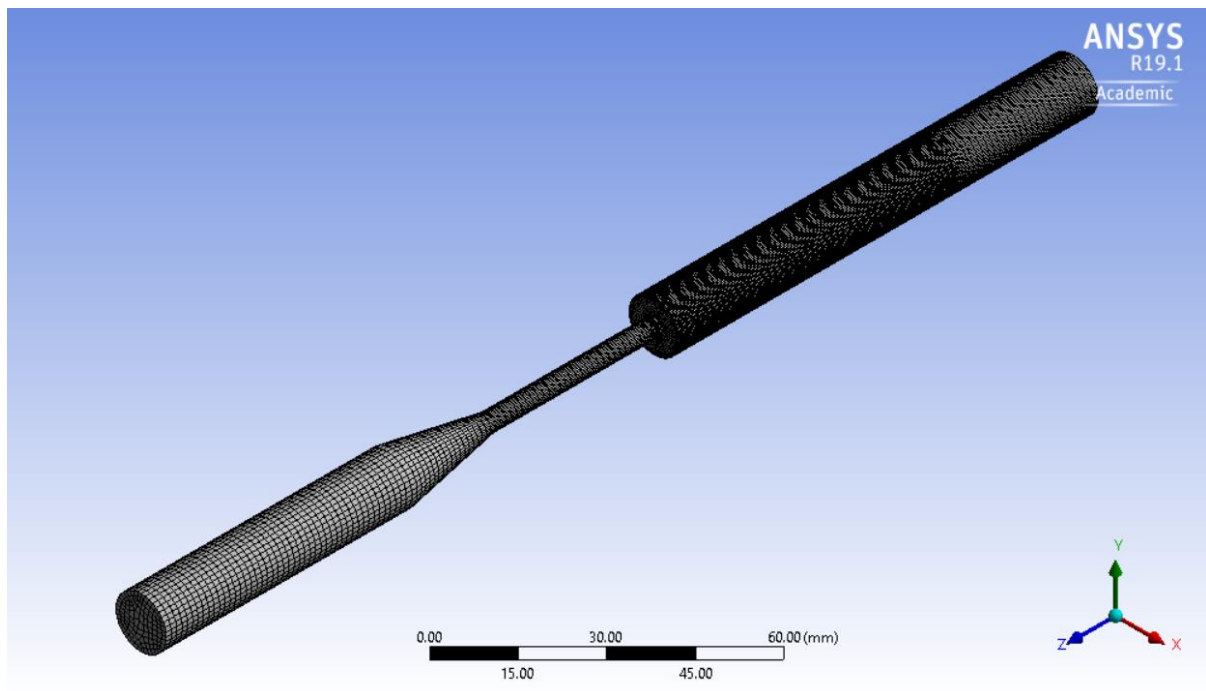


Figure 87 - Isometric view of mesh 3

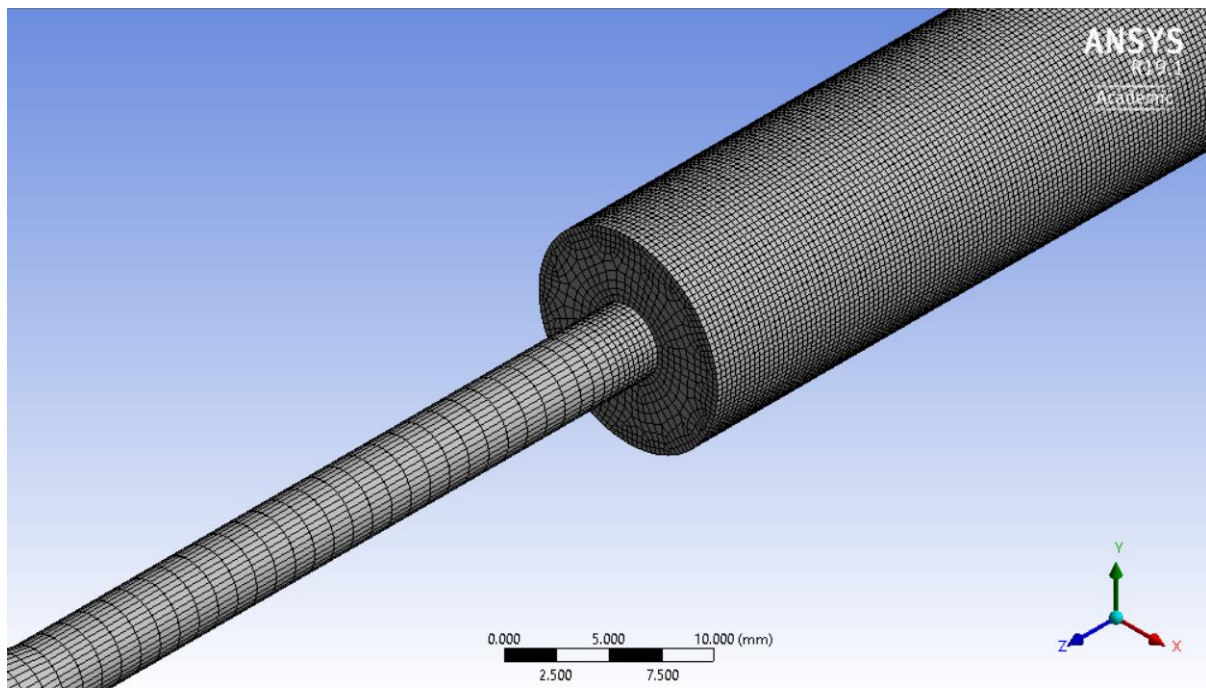


Figure 88 - Isometric view of mesh 3

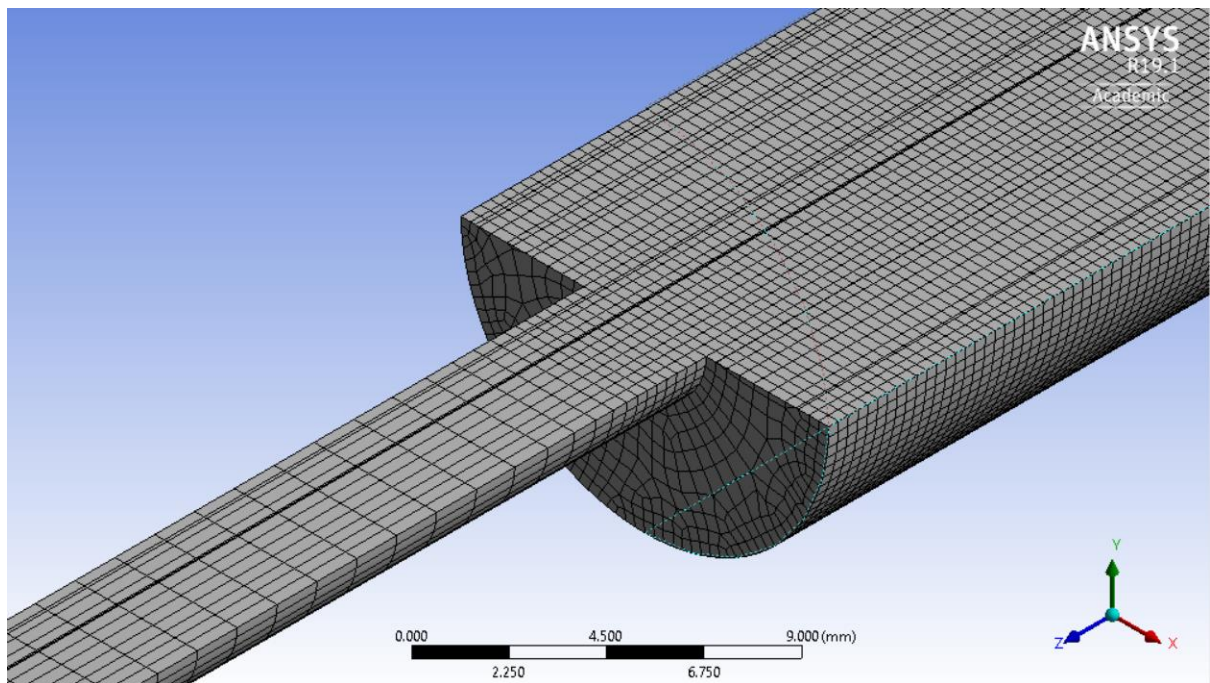


Figure 89 - Isometric cutaway view of mesh 3

#### 6.3.3.4 Mesh 4

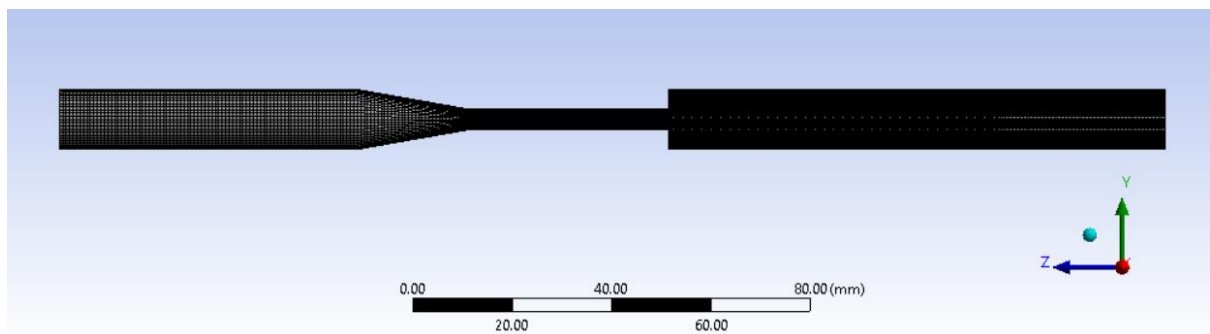


Figure 90 - Profile view of mesh 4

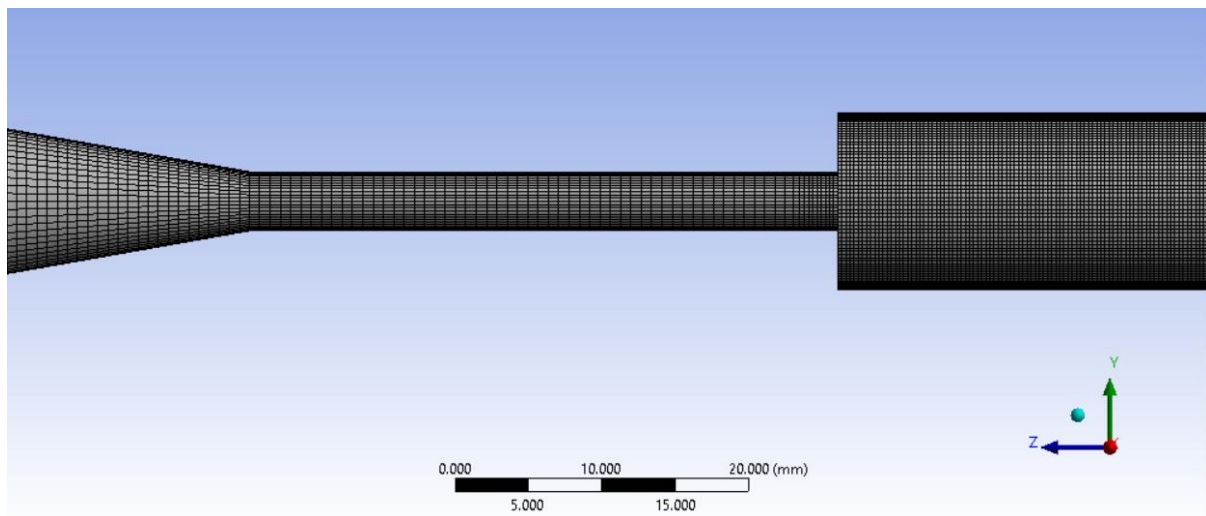


Figure 91 - Profile view of mesh 4

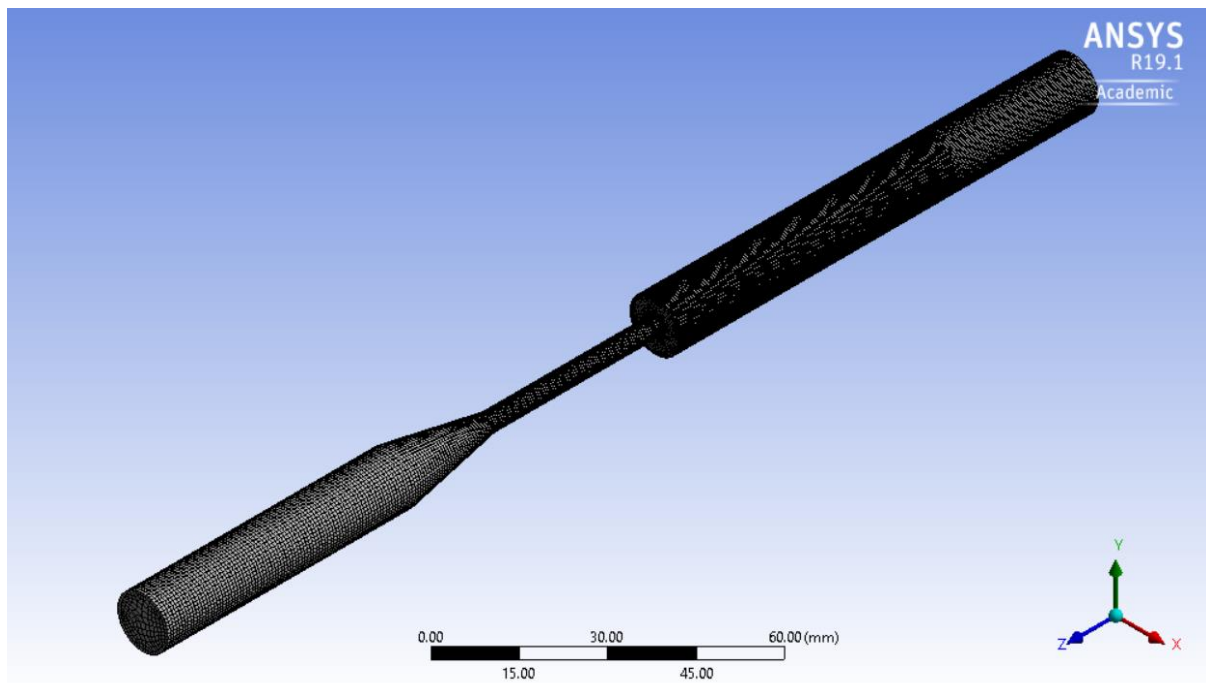


Figure 92 - Isometric view of mesh 4

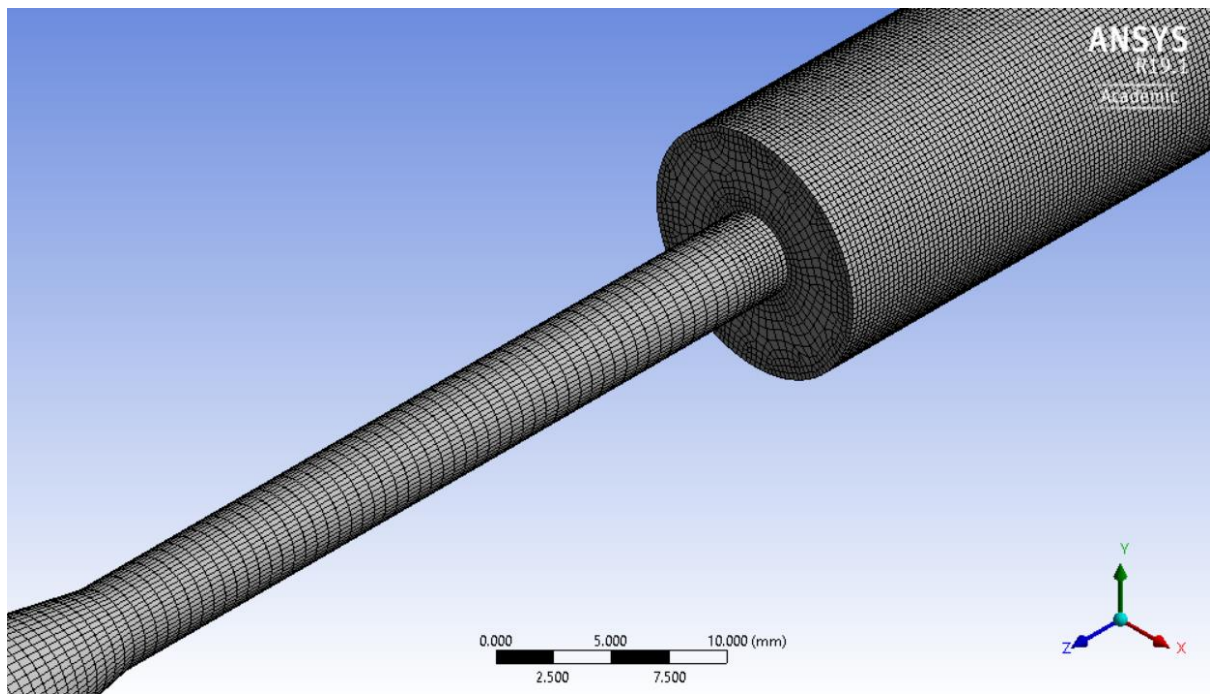


Figure 93 - Isometric view of mesh 4

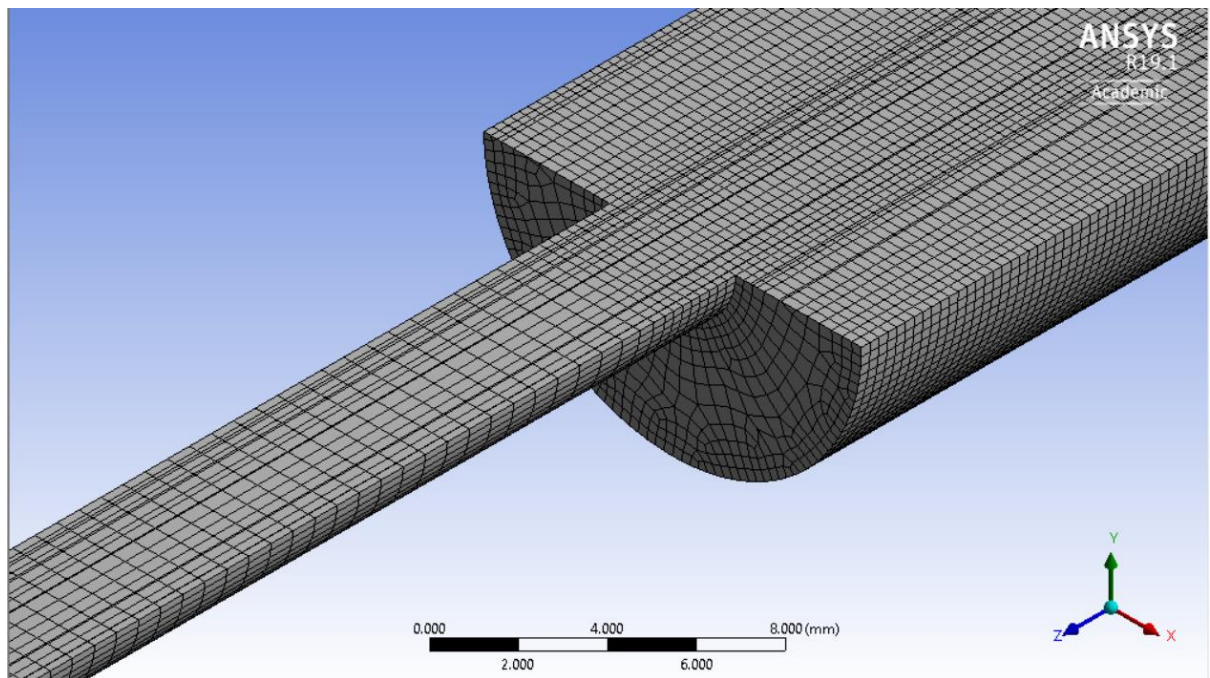


Figure 94 - Isometric cutaway view of mesh 4

### 6.3.3.5 Mesh 5

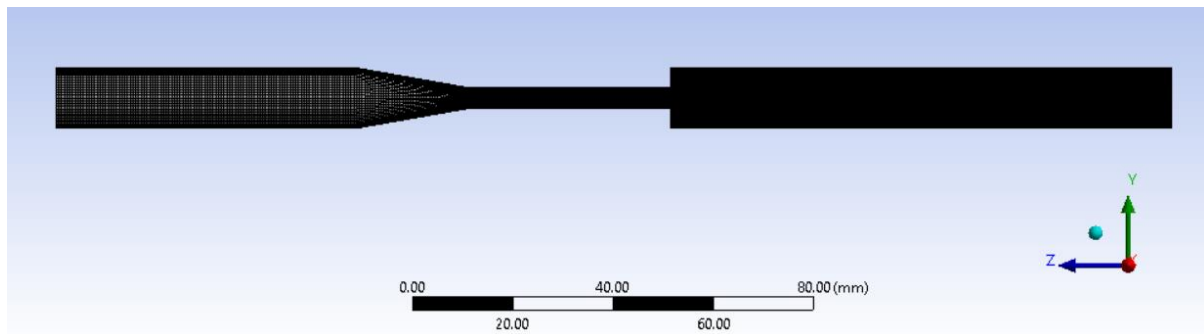


Figure 95 - Profile view of mesh 5

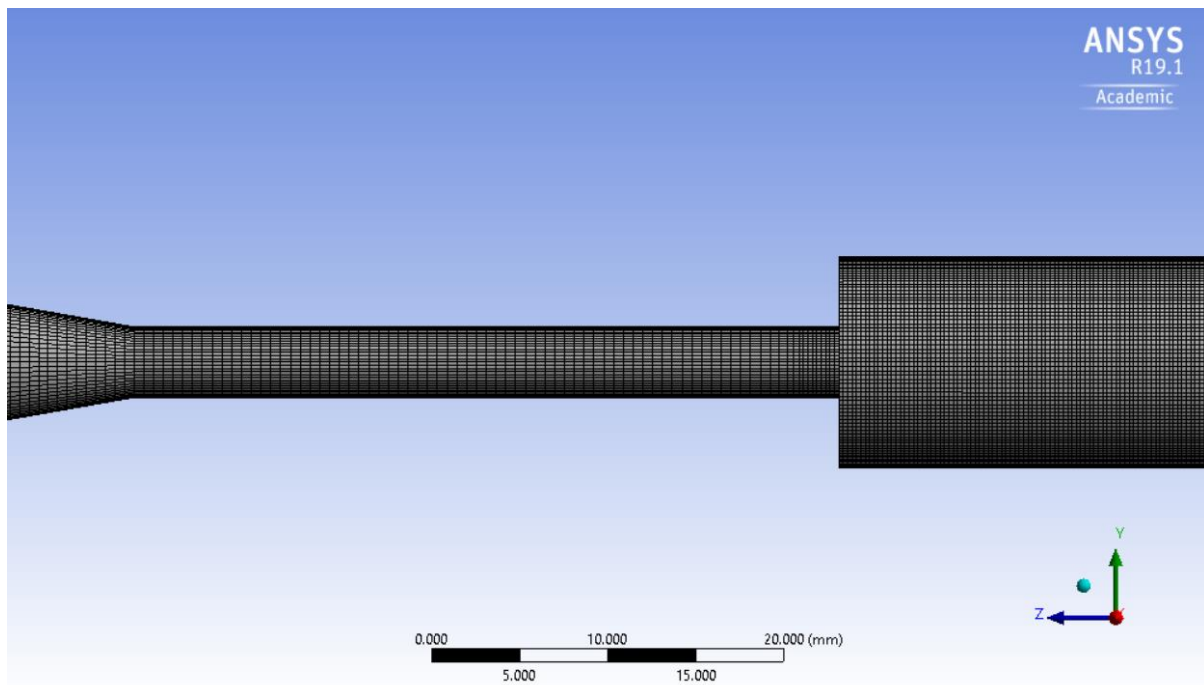


Figure 96 - Profile view of mesh 5

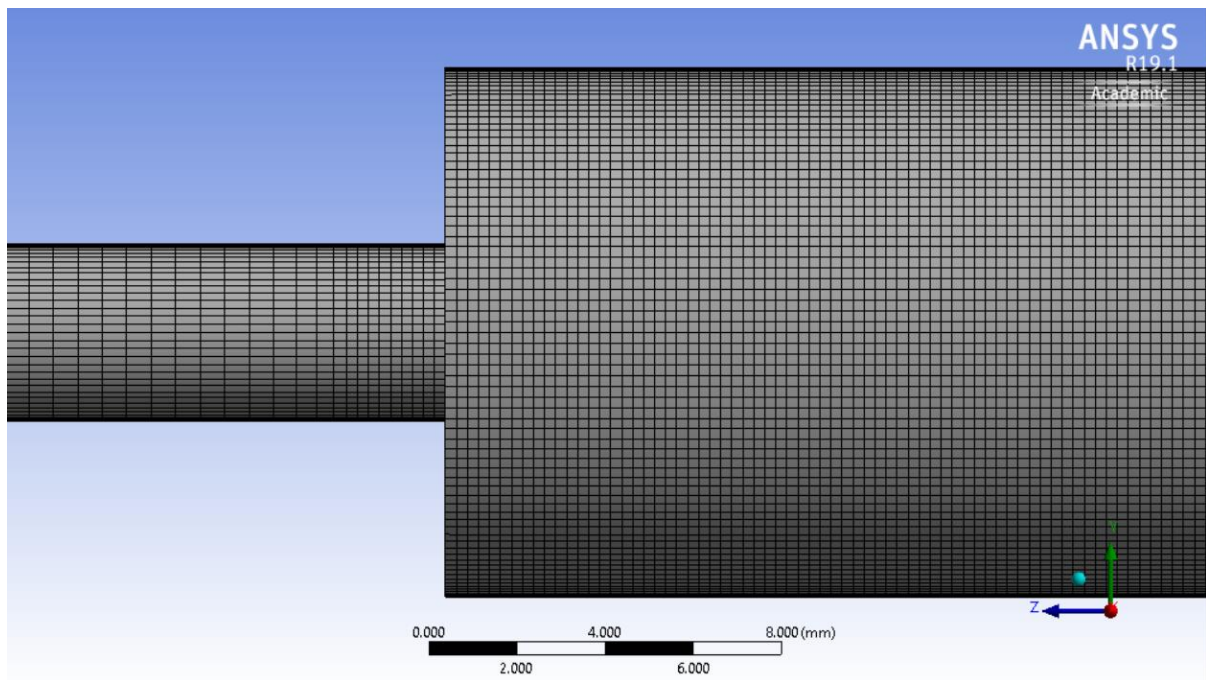


Figure 97 - Profile view of mesh 5

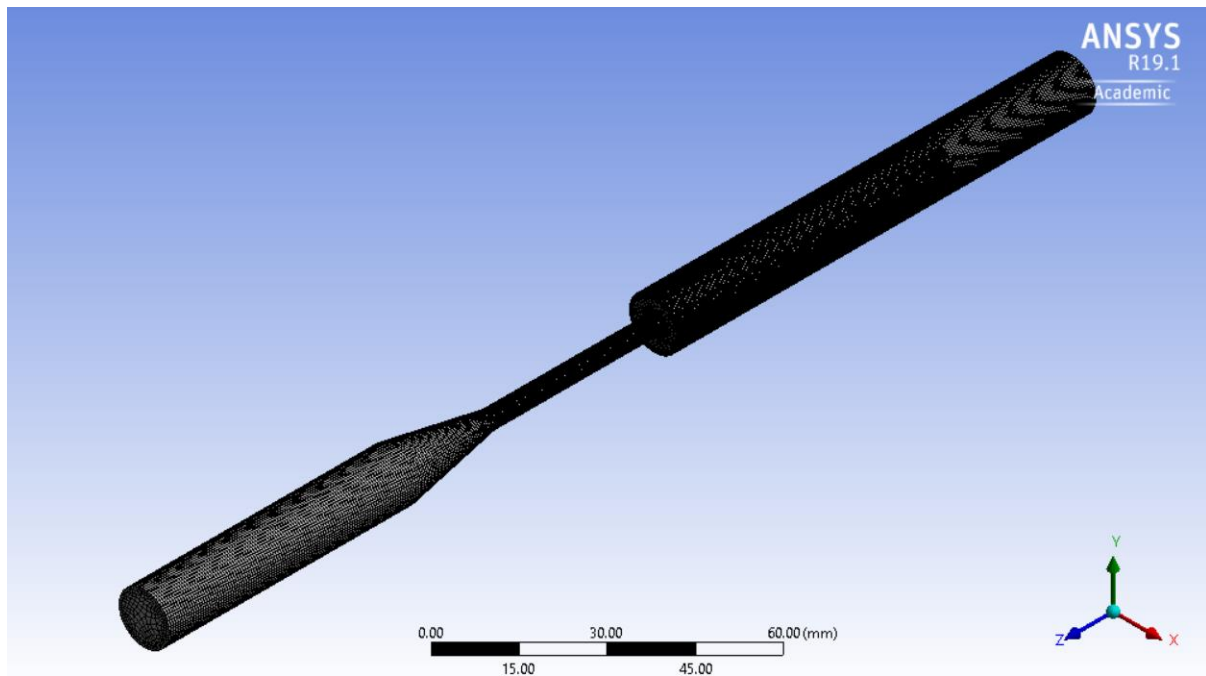


Figure 98 - Isometric view of mesh 5

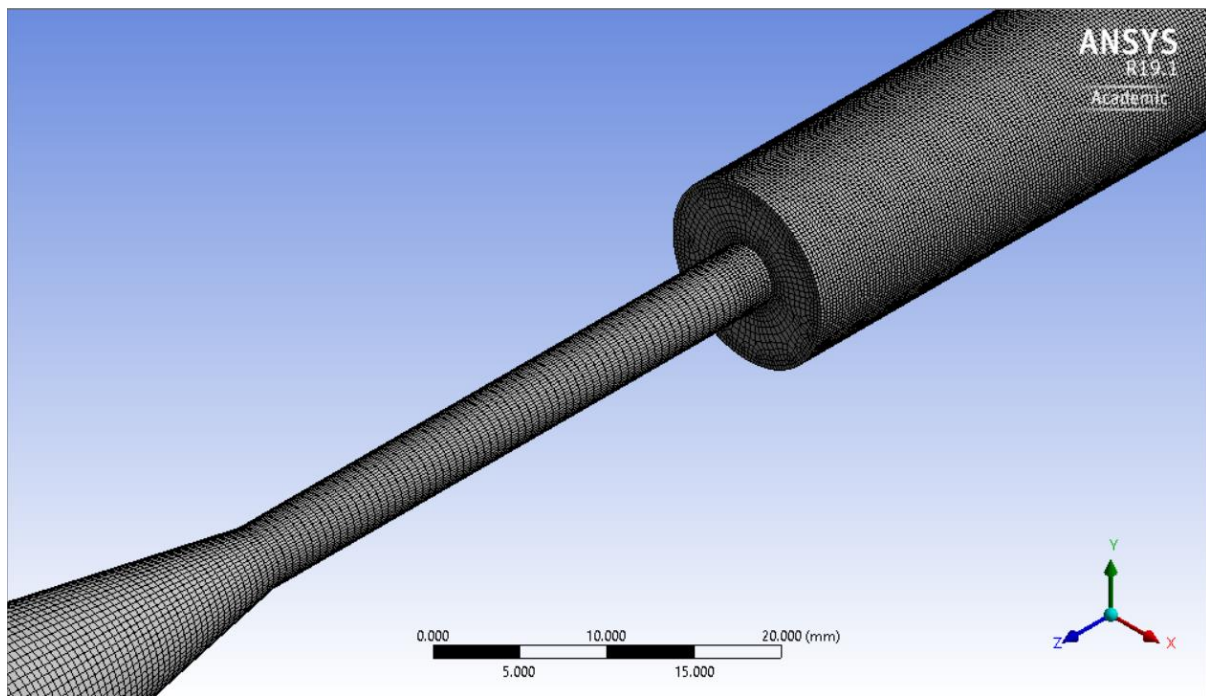


Figure 99 - Isometric view of mesh 5

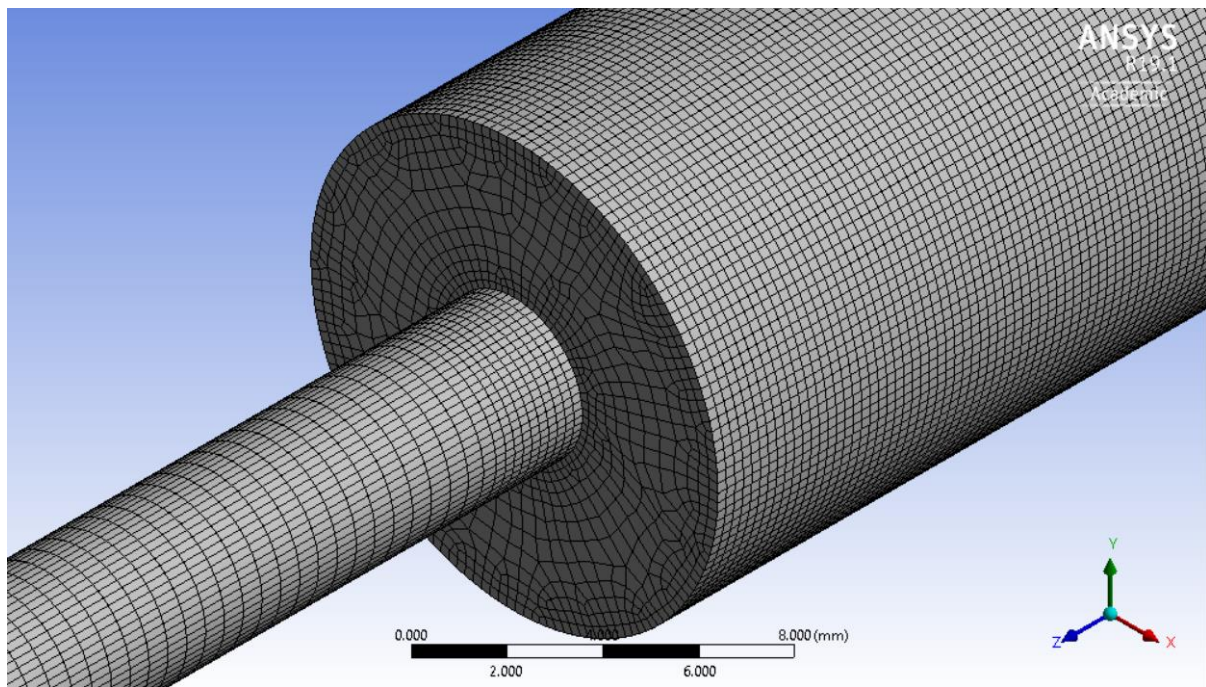


Figure 100 - Isometric view of mesh 5

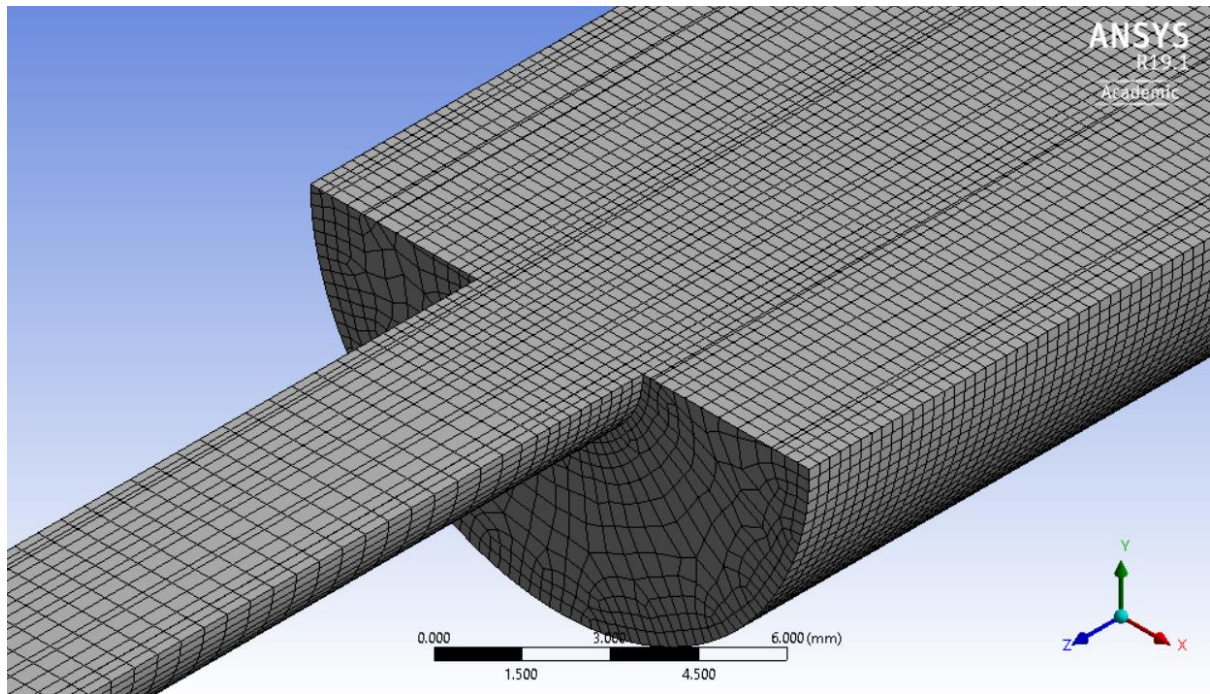


Figure 101 - Isometric cutaway view of mesh 5

## 6.4 MODEL SETUP

### 6.4.1 Working Fluid

The working fluid for this model is the same as for the simple pipe model. Details of the set up can be seen in section “5.5.1 Working Fluid”.

### 6.4.2 Theoretical Calculations

The given Reynolds number at the throat  $Re_{\text{Throat}} = 500$ , equates to a Reynolds number at the inlet of  $Re_{\text{Inlet}} = 167$ . This was used to calculate the inlet velocity profile.

#### 6.4.2.1 Velocity at Inlet

$$\Rightarrow V_{Avg} = \frac{R_e \cdot \mu}{\rho d} = \frac{(167) \cdot (0.0035)}{(1056) \cdot (0.012)} = 0.046125 \text{ m/s}$$

$$\therefore V_{Max} = 2 \cdot V_{Avg} = 2 \cdot (0.046125) = 0.092251 \text{ m/s}$$

#### 6.4.2.2 Volume Flow Rate

$$Q = V_{Avg} \cdot A = (0.046125) \left( \frac{\pi D^2}{4} \right) = (0.046125) \left( \frac{\pi (0.012)^2}{4} \right) = 5.22 \times 10^{-6} \text{ m}^3/\text{s}$$

#### 6.4.2.3 Mass Flow Rate

$$\dot{m} = Q \cdot \rho = (5.22 \times 10^{-6}) (1056) = 5.51 \times 10^{-3} \text{ kg/s}$$

#### 6.4.2.4 Velocity Profile

### 6.4.3 Boundary Conditions

The inlet, outlet and walls boundary conditions for the model are explained here.

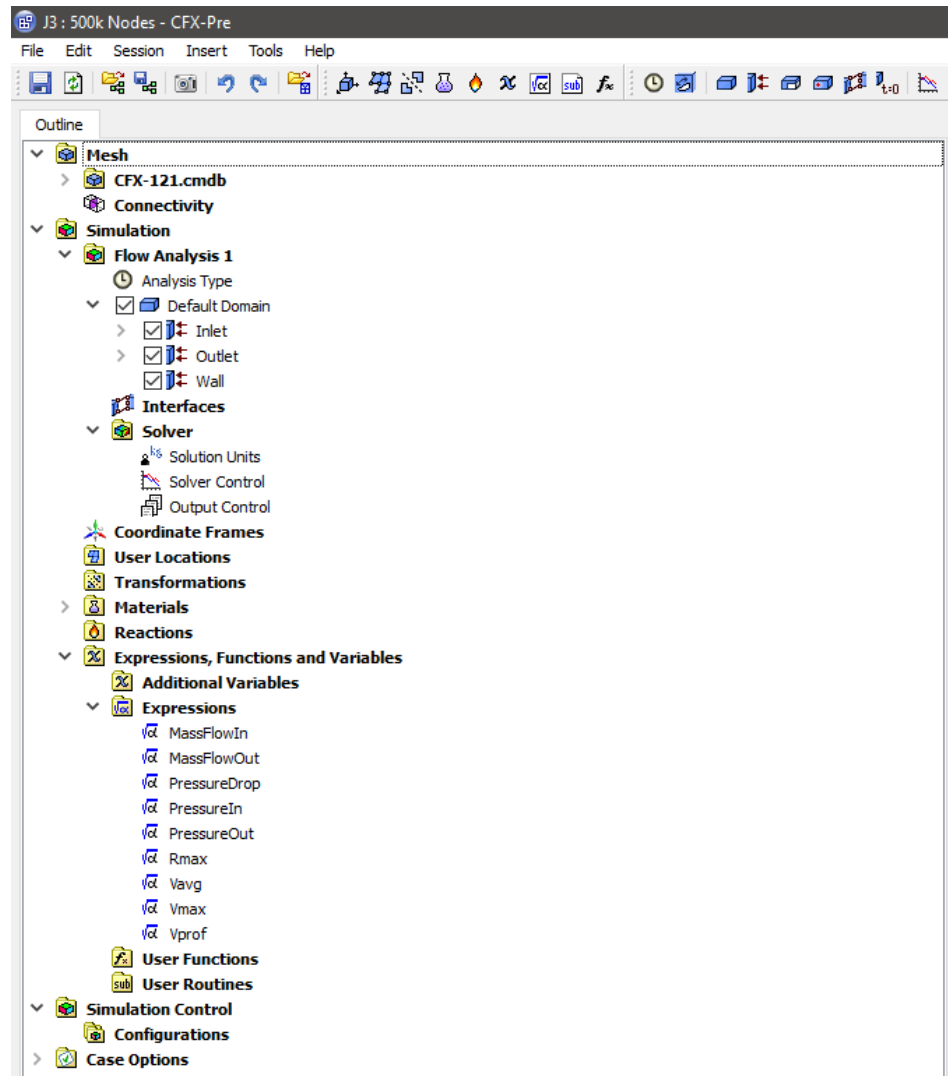


Figure 102 - Outline tree structure in CFX-Pre

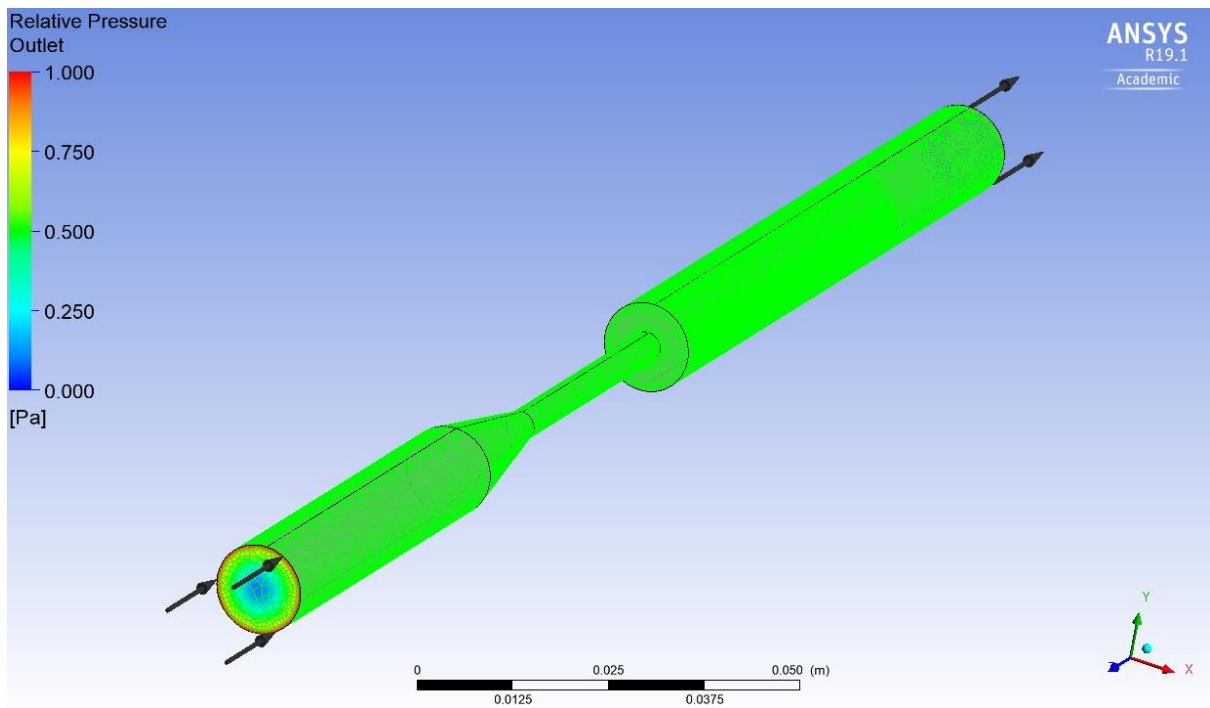


Figure 103 - Isometric view of the model with all boundaries highlighted in green. The black vector arrows show the inlet and outlet of the fluid domain.

#### 6.4.3.1 Inlet

The inlet boundary was defined using a mass and momentum method, and cartesian velocity components. As the flow was assumed to be fully laminar, the velocity profile that was previously calculated was input in the -Z direction (W component). This can be seen below in figure 35. Flow in the X and Y directions was assumed to be 0, due to the laminar nature of the flow.

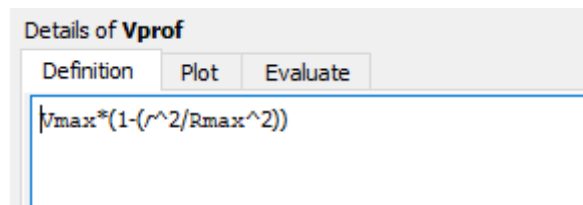


Figure 104 - The CEL expression used to define the inlet velocity profile

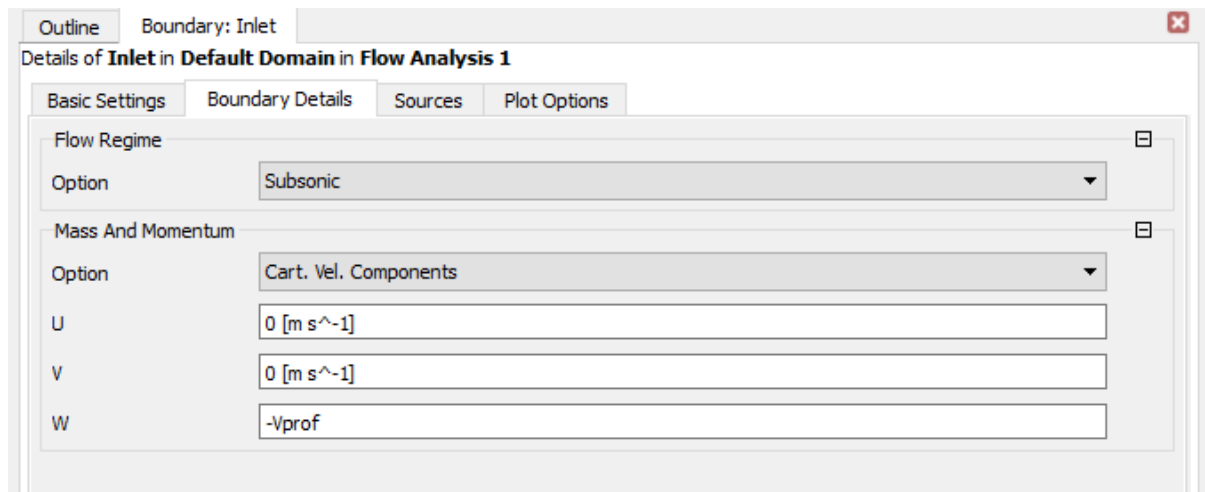


Figure 105 - The inlet boundary details

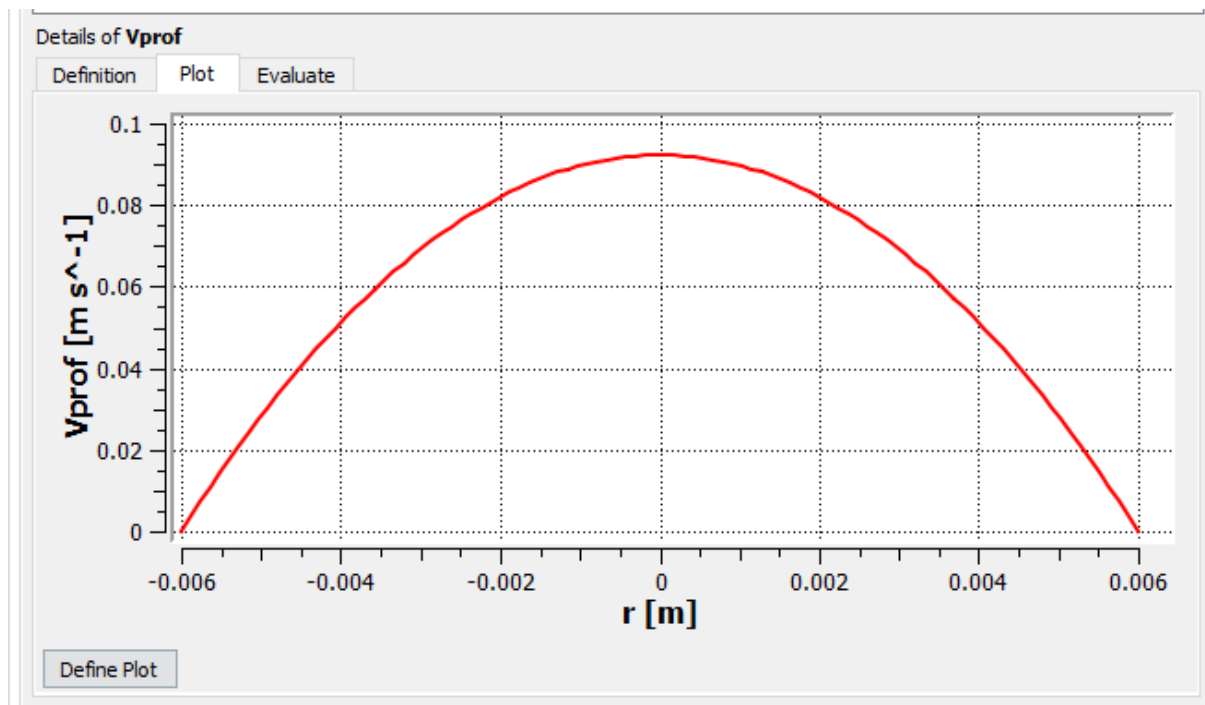


Figure 106 - The inlet velocity profile shown plotted within CFX-Pre using CEL

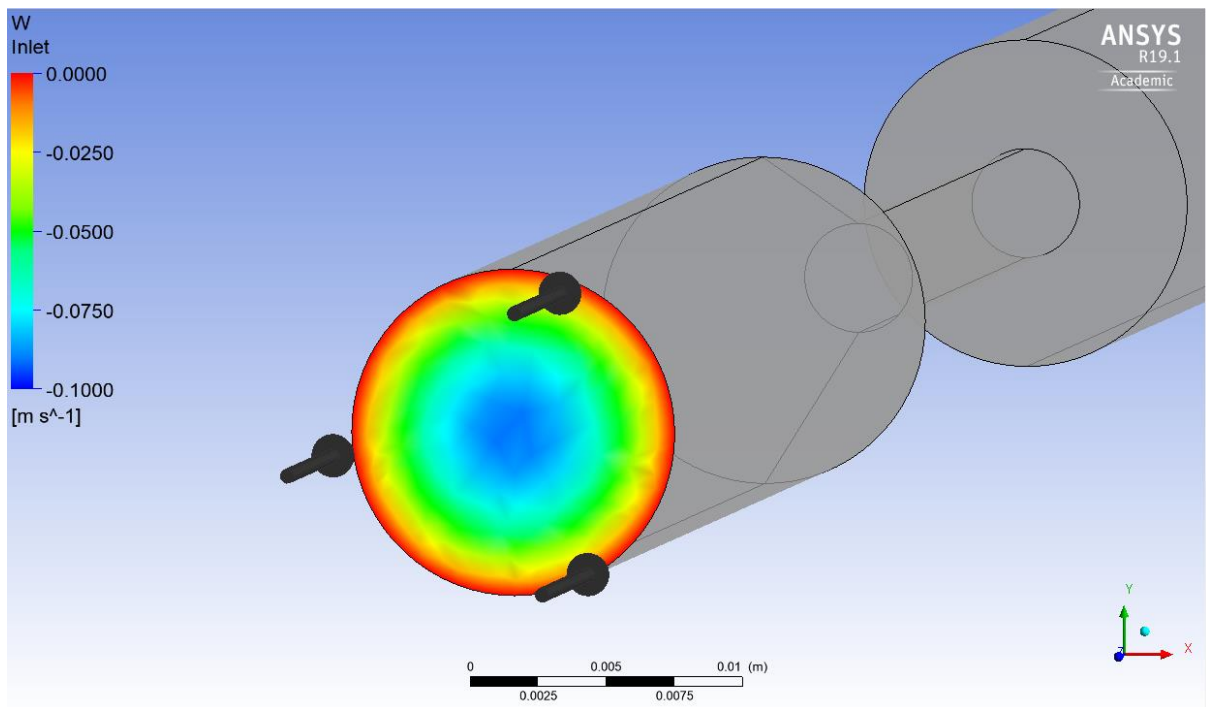


Figure 107 - A boundary contour plot showing the velocity profile of the fluid as it enters the domain. Note - red denotes a minimum velocity and blue denotes a maximum velocity

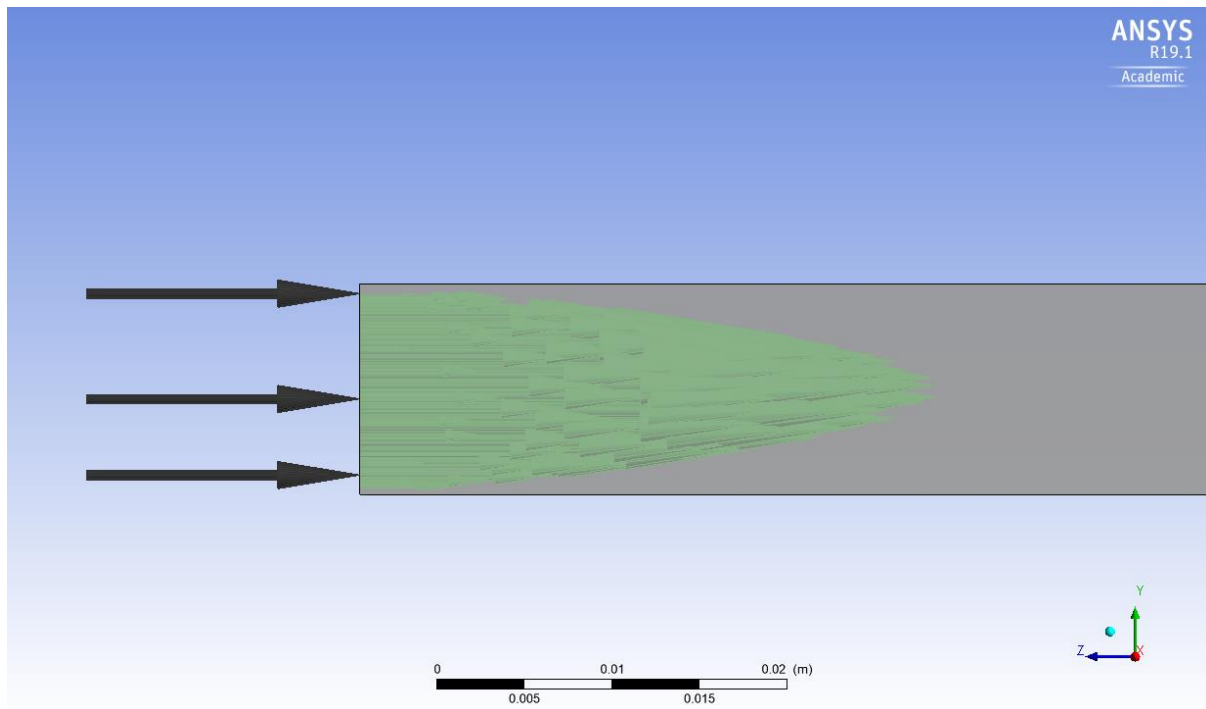


Figure 108 - The inlet velocity profile plotted using vector arrows

#### 6.4.3.2 Outlet

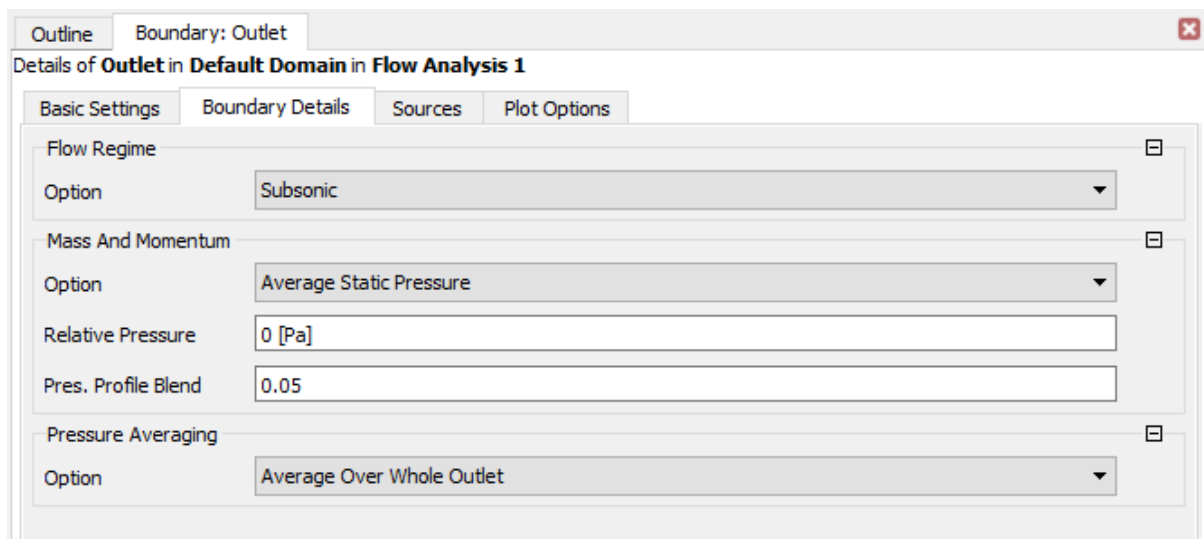


Figure 109 - The outlet boundary details

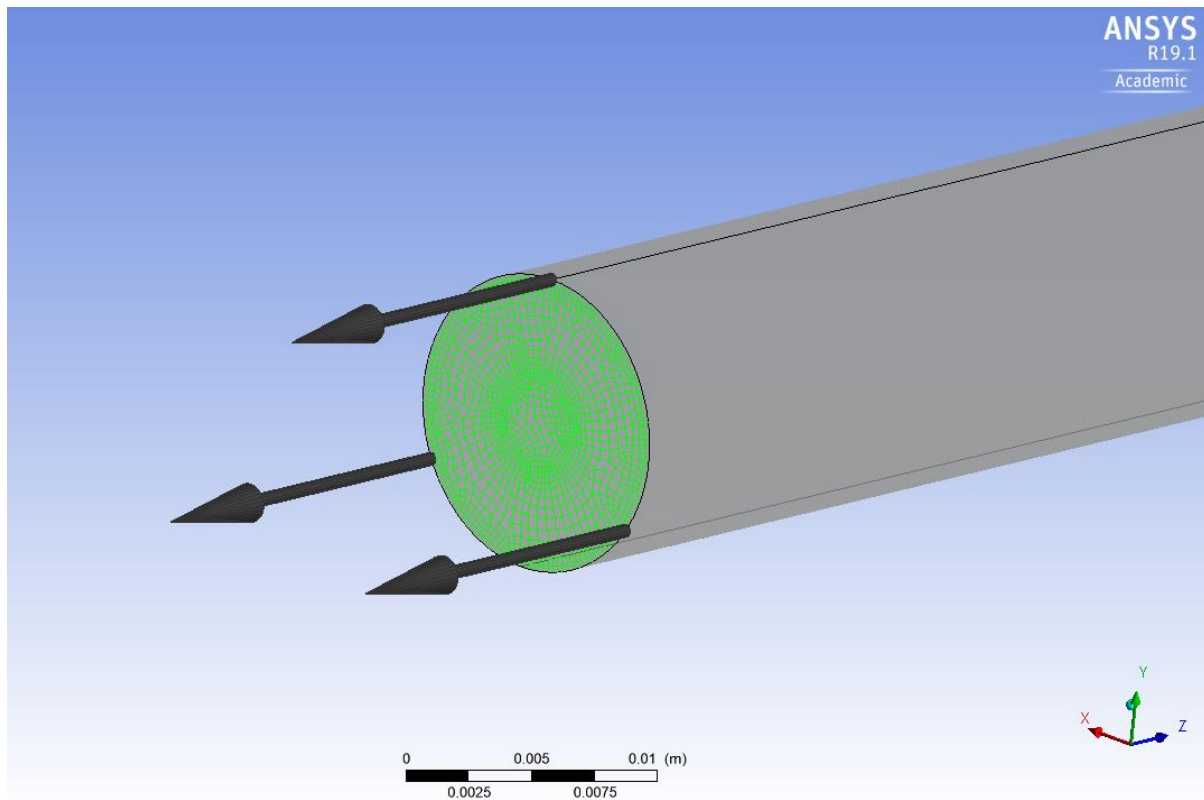


Figure 110 - A closeup of the outlet boundary

#### 6.4.3.3 Walls

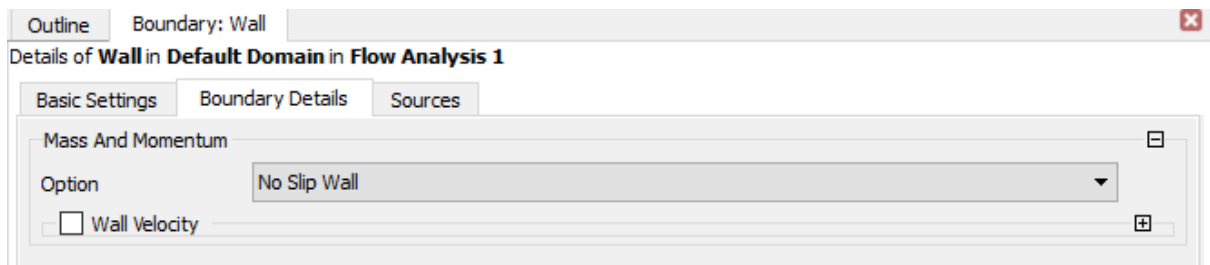


Figure 111 - The wall boundary details

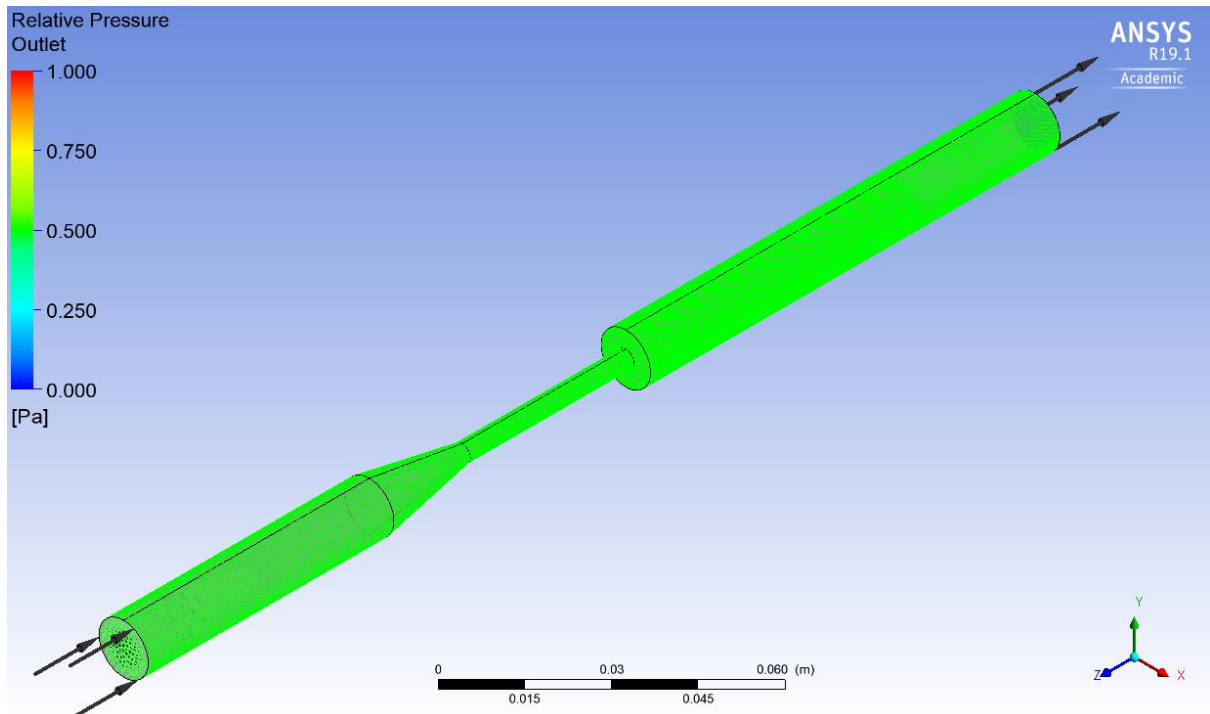


Figure 112 - Isometric view highlighting the wall boundary in green

#### 6.4.4 Solver Control

The main method that was used to determine solution convergence was setting an RMS residual target of  $1 \times 10^{-8}$ . This low value was chosen, as it would add convergence confidence without adding much solution wall clock time (due to the fully developed, laminar flow characteristics of the model). The maximum number of iterations was set to 10,000, to allow the solver to run until it reached the RMS residual target. However, on all mesh sizes convergence was achieved within a 400 - 500 iterations.

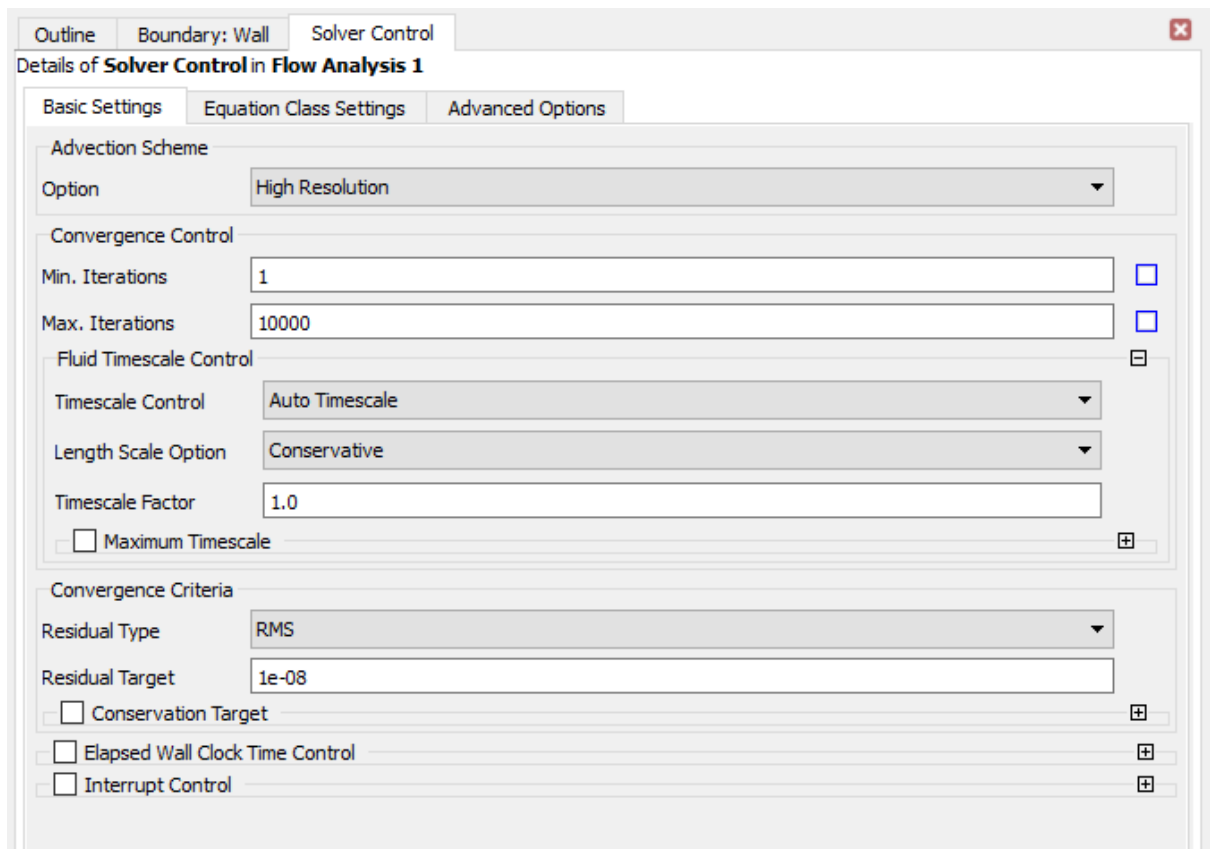


Figure 113 - The solver control menu

#### 6.4.5 Expressions

Custom user variables can be created in CFX, by using the CFX Expression Language (CEL). Custom variables were used to set up the model, and to make data extraction easier once the model had been solved. The expressions used can be seen below.

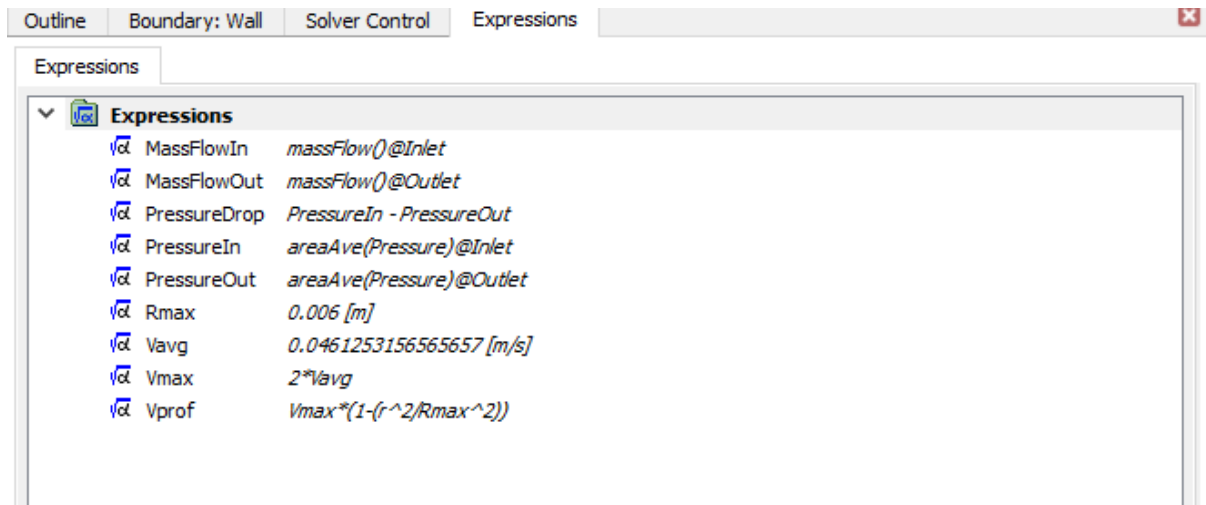
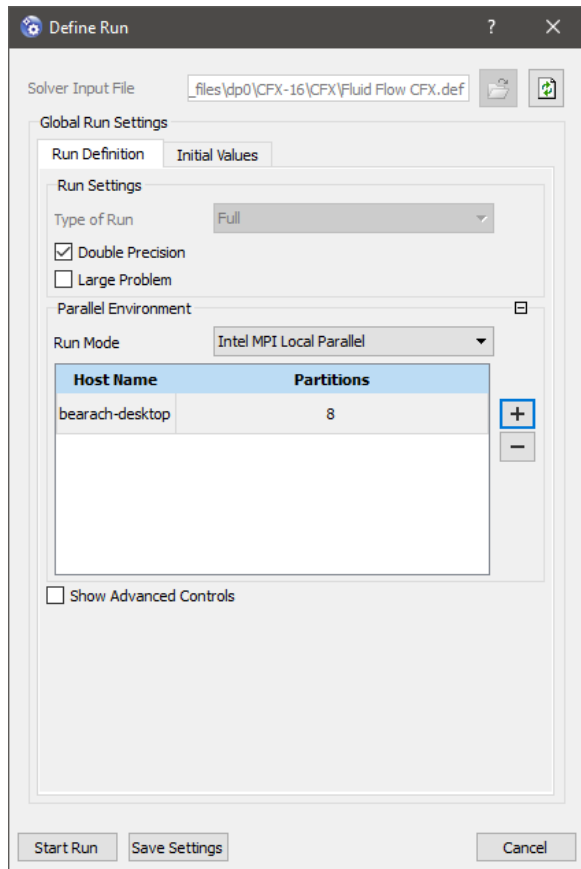


Figure 114 - The CEL expressions used for this model

## 6.5 MODEL SOLUTION

The computer used to solve this model consisted of an Intel i7 - 3820 CPU running at 3.3 - 3.6 GHz, with 16 GB of DDR3 RAM running at 1333 MHz. This CPU has 4 physical cores using Intel's "Hyperthreading" architecture, meaning that the CPU has 8 virtual cores. As such, the CFX solver can be set to fully utilise all of these 8 virtual cores.



*Figure 115 - The "Define Run" dialog box allows the user to easily set the number of CPU cores to be used when solving the CFD code. Along with the option of "Double Precision" mode and "Large Problem" mode.*

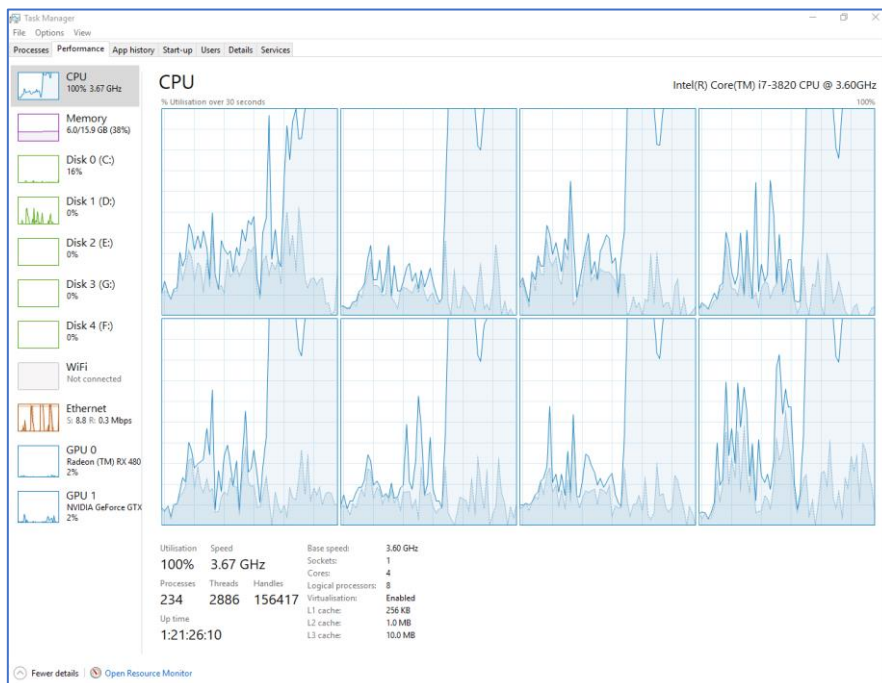


*Figure 116 - Windows Task Manager showing the laptop CPU under 100% load on all 8 virtual CPU cores while solving a CFD model*

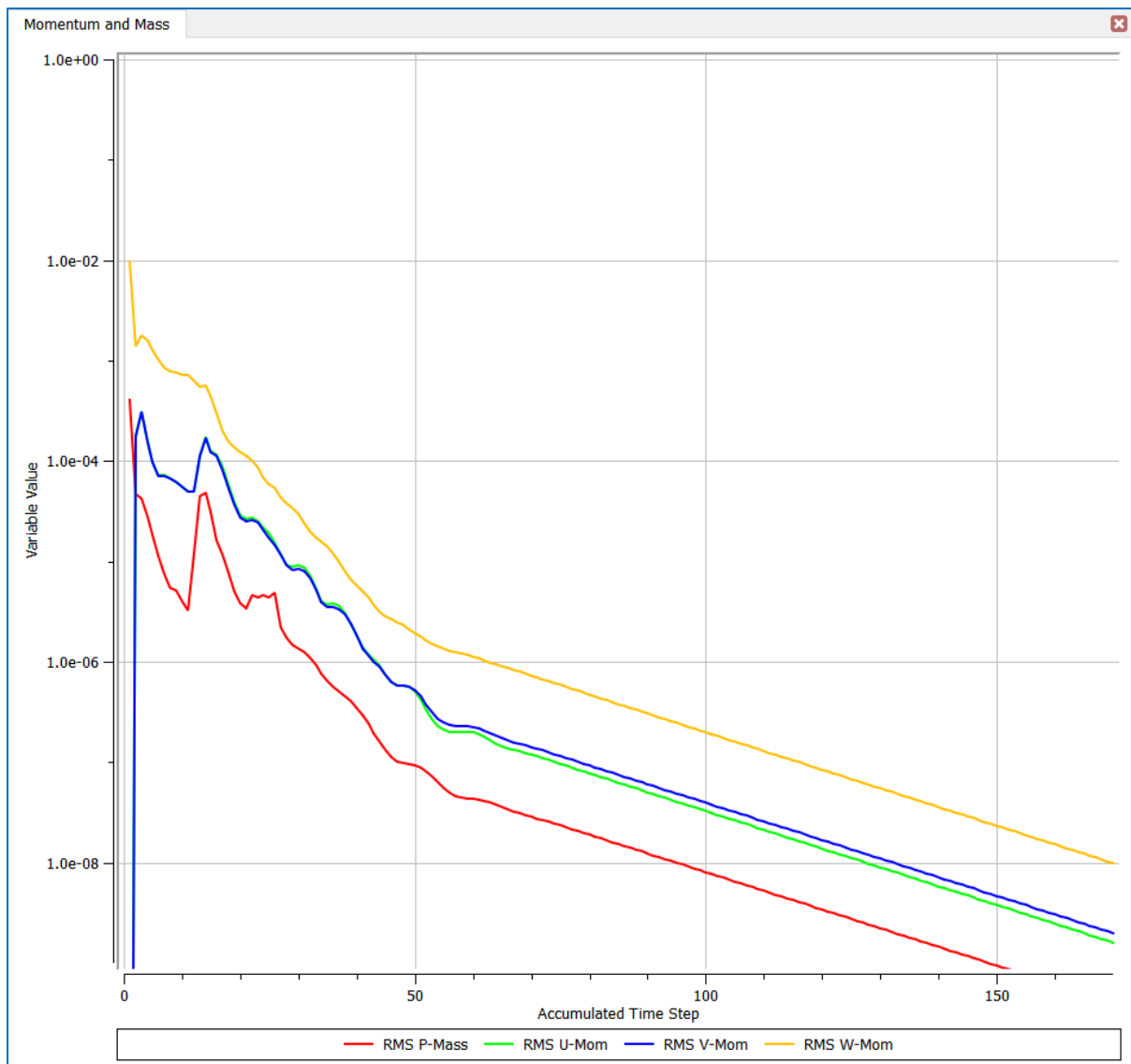


Figure 117 - - The RMS values plotted against the accumulated time step for the final mesh

```

+-----+
|          CPU Requirements of Numerical Solution - Total          |
+-----+



Subsystem Name           Discretization      Linear Solution
                         (secs.   %total)    (secs.   %total)

-----
Momentum and Mass       4.57E+03   72.4 %     1.11E+03   17.6 %
-----
Subsystem Summary        4.57E+03   72.4 %     1.11E+03   17.6 %

File Reading             1.59E+00   0.0 %
Search Calculations      7.99E-03   0.0 %
Variable Updates         5.44E+02   8.6 %
File Writing              2.40E+01   0.4 %
Miscellaneous             6.25E+01   1.0 %
-----
Total                   6.31E+03

+-----+
|          Job Information at End of Run                         |
+-----+



Job finished: Thu Apr 25 15:13:52 2019

Total wall clock time: 1.577E+03 seconds
or: (          0:          0:         26:     17.456 )
      (     Days:    Hours: Minutes: Seconds )



--> Final synchronization point reached by all partitions.
End of solution stage.

+-----+
| The results from this run of the ANSYS CFX Solver have been   |
| written to C:/Users/Bearach/OneDrive - Dublin Institute of    |
| Technology/2. Thesis Files/1. Final Assessment/Project Files/Ansys |
| Files/Final Models/Draft 3 (March 14th)/Draft 3 (March        |
| 14th)_pending/dp0_CFX_4_Solution_4/Fluid Flow CFX_001.res   |
+-----+



This run of the ANSYS CFX Solver has finished.

```

Figure 118 - The total wall clock time needed for the crudest mesh to achieve RMS values of  $1 \times 10^{-8}$

## 6.6 MESH CONVERGENCE

Similar to the previous modelling case of the pipe, a mesh convergence tolerance of 1% was selected, with the primary mesh convergence metric again being the pressure drop along the length of the geometry ( $\Delta P = P_{Inlet} - P_{Outlet}$ ). Mass flow ( $\dot{m}$ ) was also used to determine convergence.

### 6.6.1 Mesh Details

The table below summarises the results from each different mesh and compares those results with theory.

Mesh Metrics	Mesh 1	Mesh 2	Mesh 3	Mesh 4	Mesh 5	Units
<b>Number of Nodes</b>	28,807	96,332	212,634	358,666	510,794	-
<b>Number of Elements</b>	25,284	87,198	195,220	332,540	476,234	
<b>Inlet Pressure</b>	242.65	260.67	275.19	285.14	287.94	<i>Pa</i>
<b>Outlet Pressure</b>	-4.1054	-3.6559	-3.2536	-1.71206	-1.34254	
$\Delta P$	246.76	264.32	278.44	286.85	289.29	
<b>Diff</b>	-246.76	17.57	14.12	8.41	2.44	
<b>% Change</b>	0	7.12%	5.34%	3.02%	0.85%	-
$\dot{m}_{in}$	0.00555	0.00553	0.00552	0.00551	0.00551	<i>kg/s</i>
$\dot{m}_{out}$	-0.00555	-0.00554	-0.00552	-0.00551	-0.00551	
$\Delta \dot{m}$	-9.4E-07	-5.22E-06	0	-1E-08	-7E-08	
$\dot{m}_{imbal}$	0.017%	0.094%	0.000%	0.000%	0.001%	
<b>Theoretical Value</b>	0.005509					<i>kg/s</i>
<b>Variation from Theory</b>	0.74%	0.40%	0.21%	0.11%	0.07%	-

Table 9 - Mesh convergence study results

### 6.6.2 Mesh Convergence Results

The mesh convergence results for both pressure and mass flow can be seen below.

#### 6.6.2.1 Pressure

The plot below shows the number of nodes in the mesh plotted against the pressure drop from inlet to outlet. In combination with the table summarising the results, it can be seen that the pressure drop achieves the mesh convergence tolerance of 1% on the final mesh.

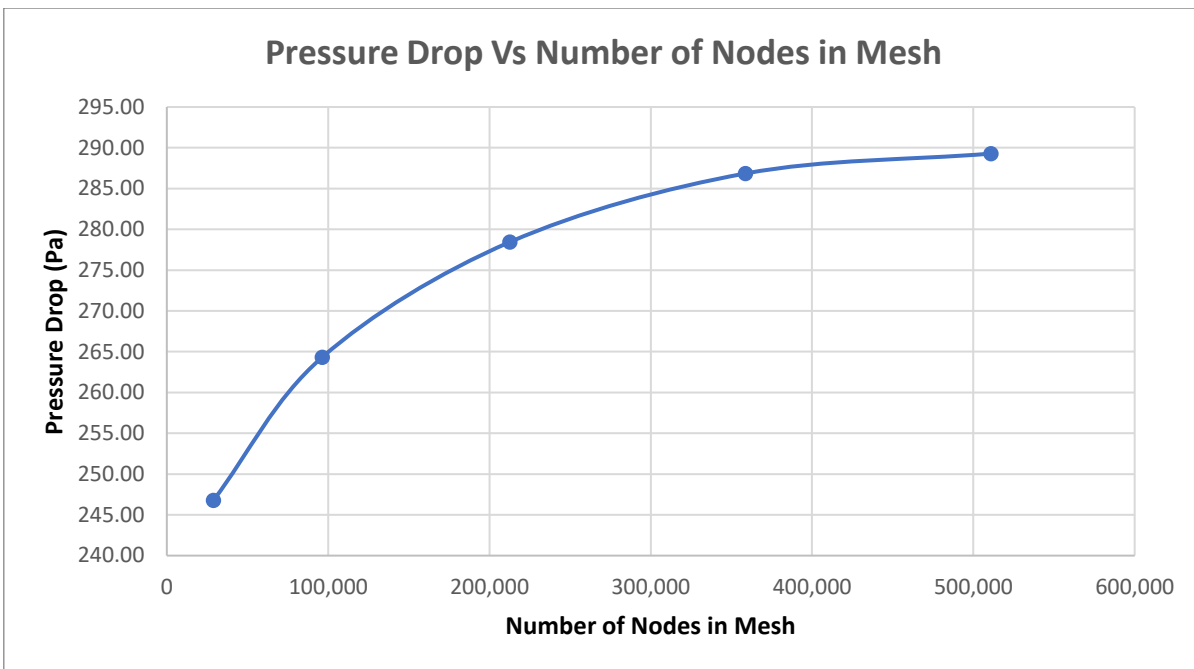


*Figure 119 - Pressure drop plotted against number of nodes in mesh*

#### 6.6.2.2 Mass Flow Rate

The plots below show that variation of mass flow rate is under 1% for all of the meshes.

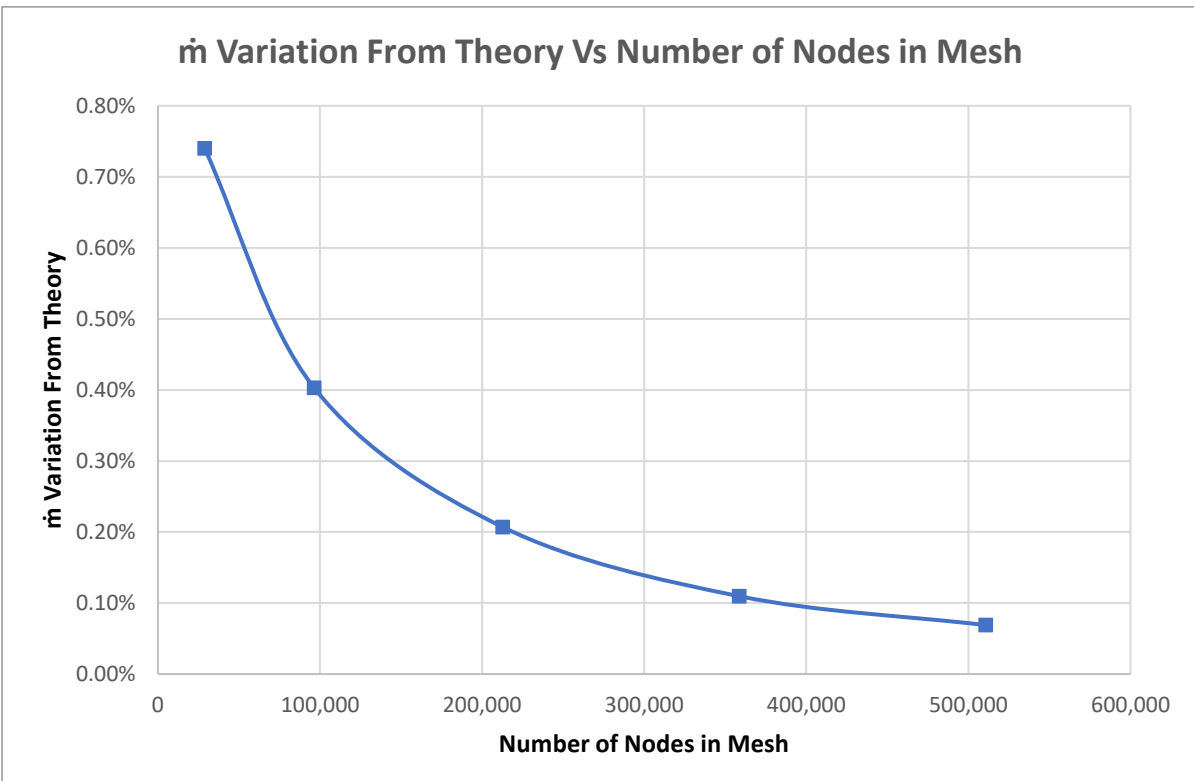


*Figure 120 - Variation from theoretical mass flow rate Vs number of nodes in mesh*

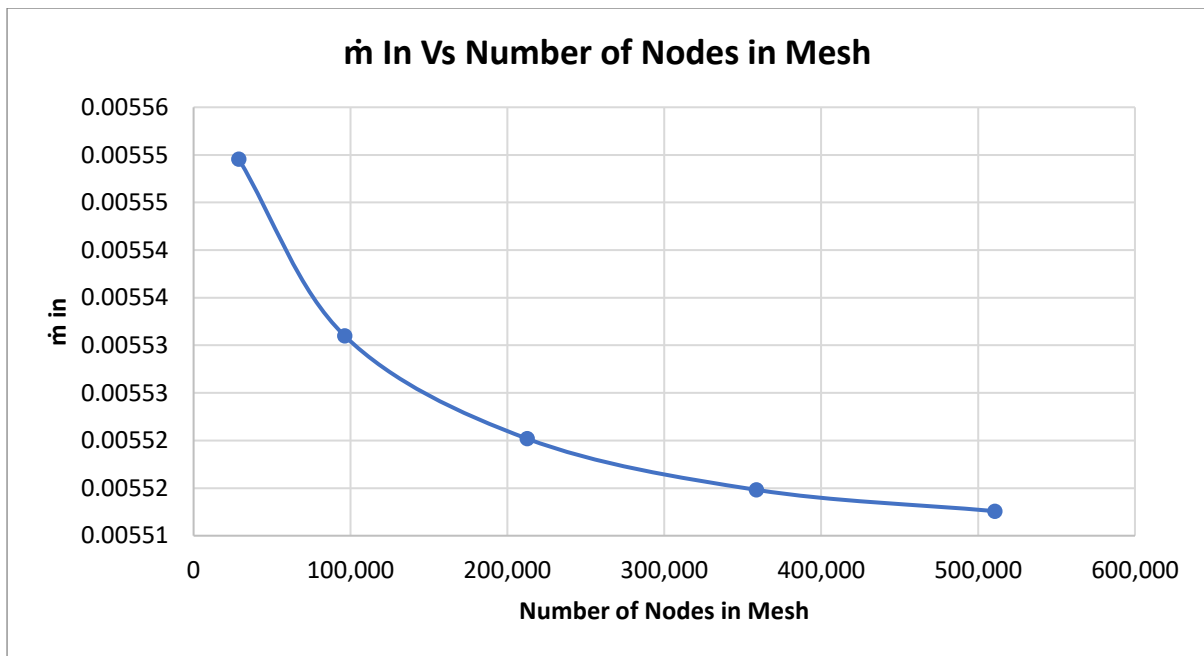


*Figure 121 - Variation in mass flow flow rate Vs number of nodes in mesh*

### 6.6.3 Conclusion

In conclusion, ANSYS Workbench was used to create a model of fluid flow through the Benchmark #1 geometry, and then a mesh convergence study was carried out. The finest mesh that was created (Mesh 5) achieved mesh convergence, staying within the 1% mesh convergence tolerance.

# Chapter 7

## RESULTS

### 7.1 VELOCITY

Below the axial velocity contour plots from the CFD model can be seen for each of the 12 locations along the Z axis. These velocity profiles will then be compared against the experimental results.

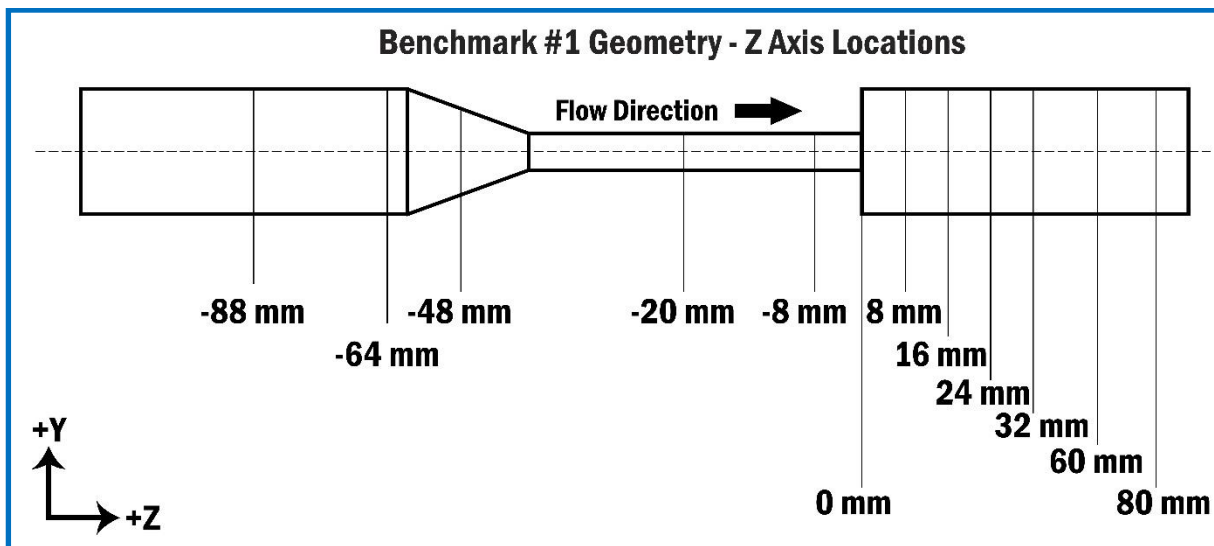


Figure 122 - Geometry showing the 12 slice locations

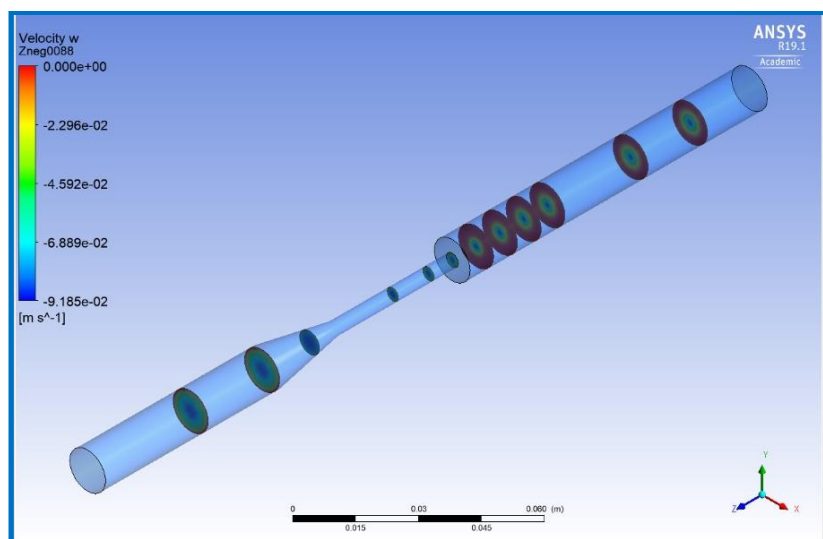


Figure 123 - Showing the 12 slices in CFD post

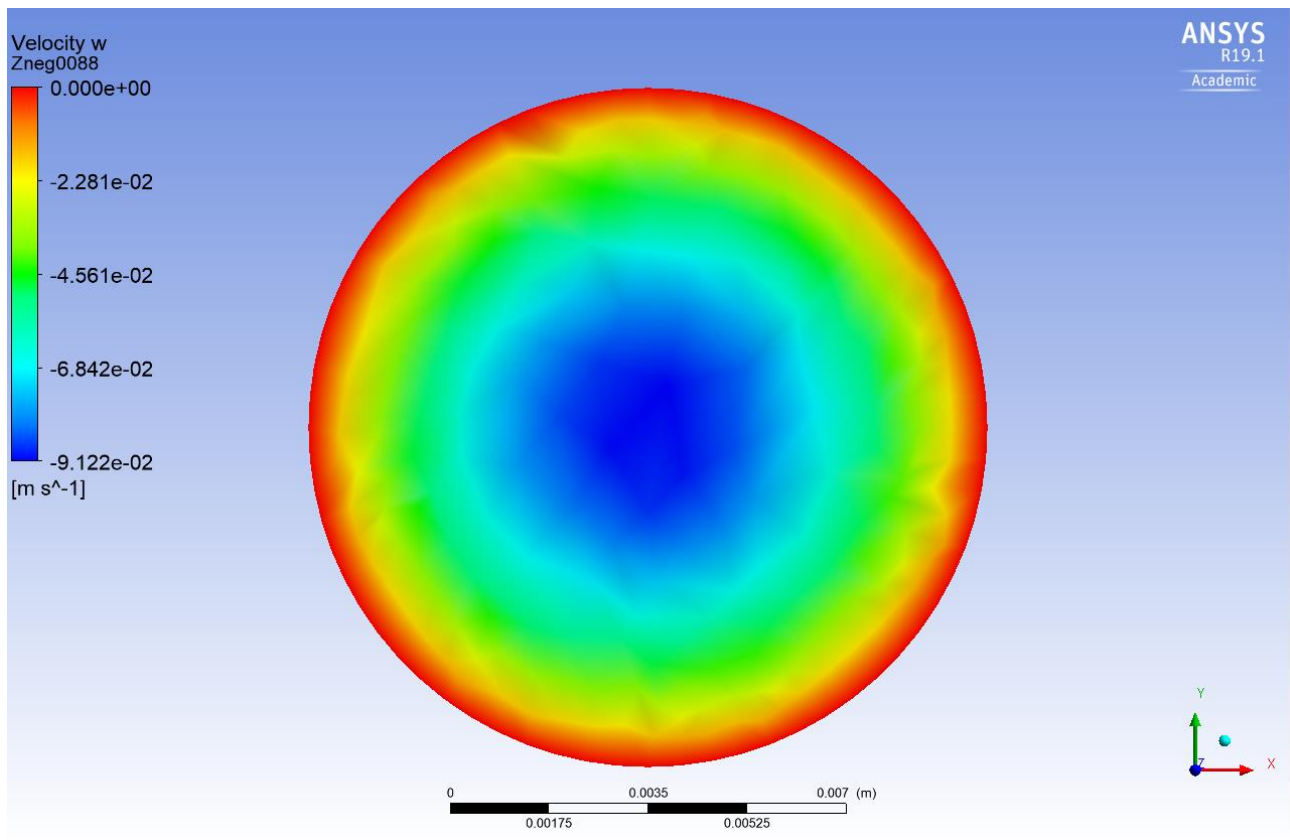


Figure 124 - Axial velocity at  $Z = -0.088\text{ m}$

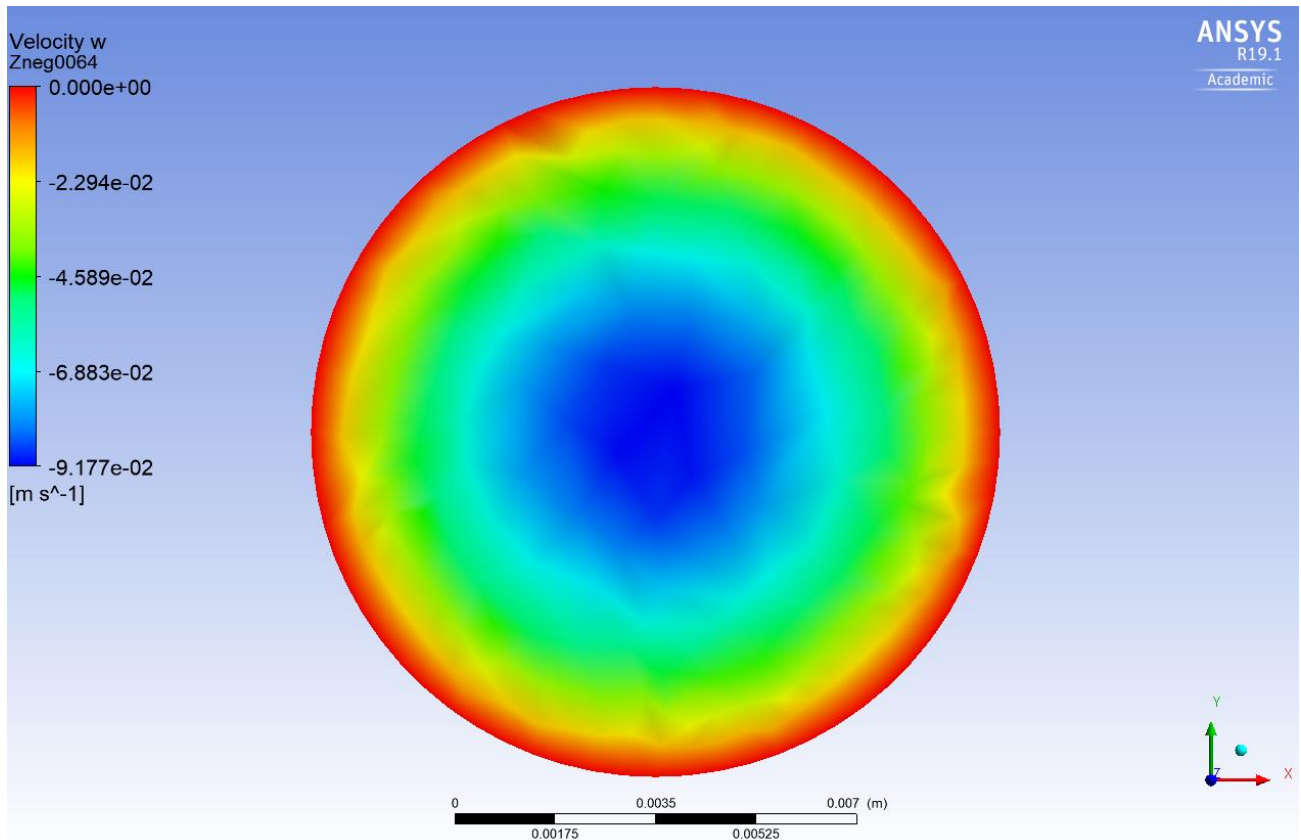


Figure 125 - Axial velocity at  $Z = -0.064\text{ m}$

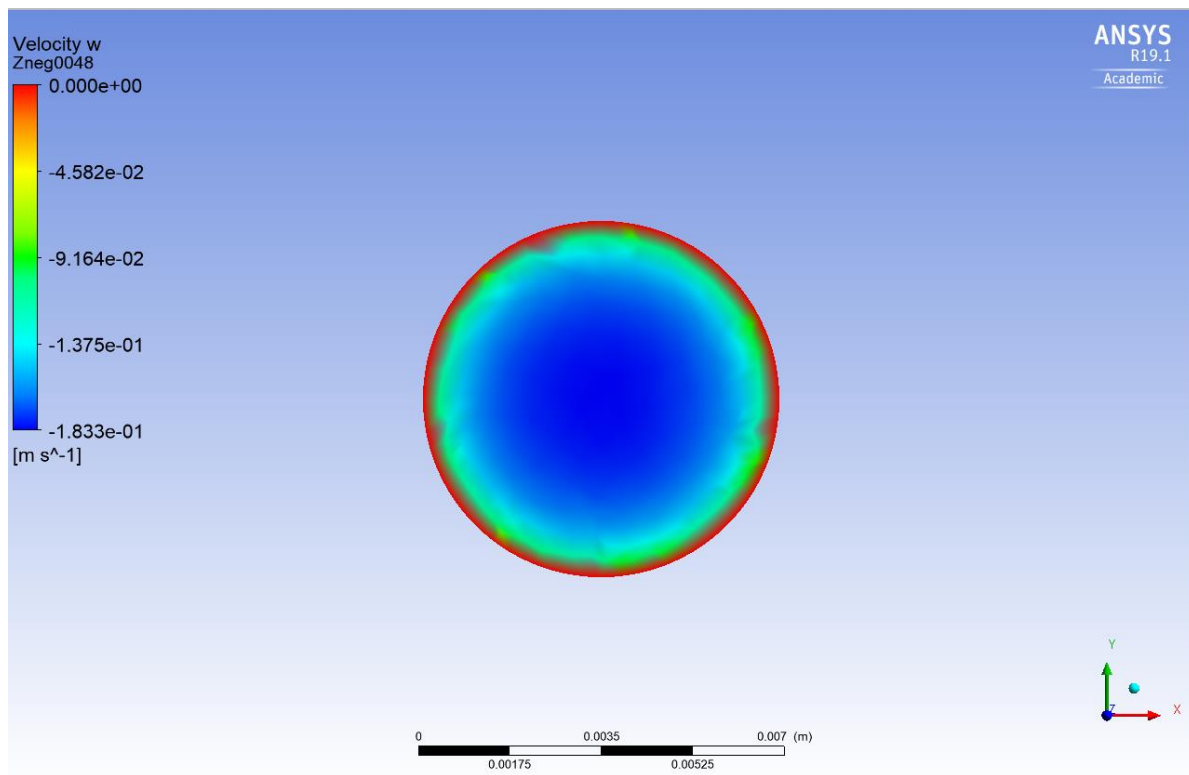


Figure 126 - Axial velocity at  $Z = -0.048 \text{ m}$

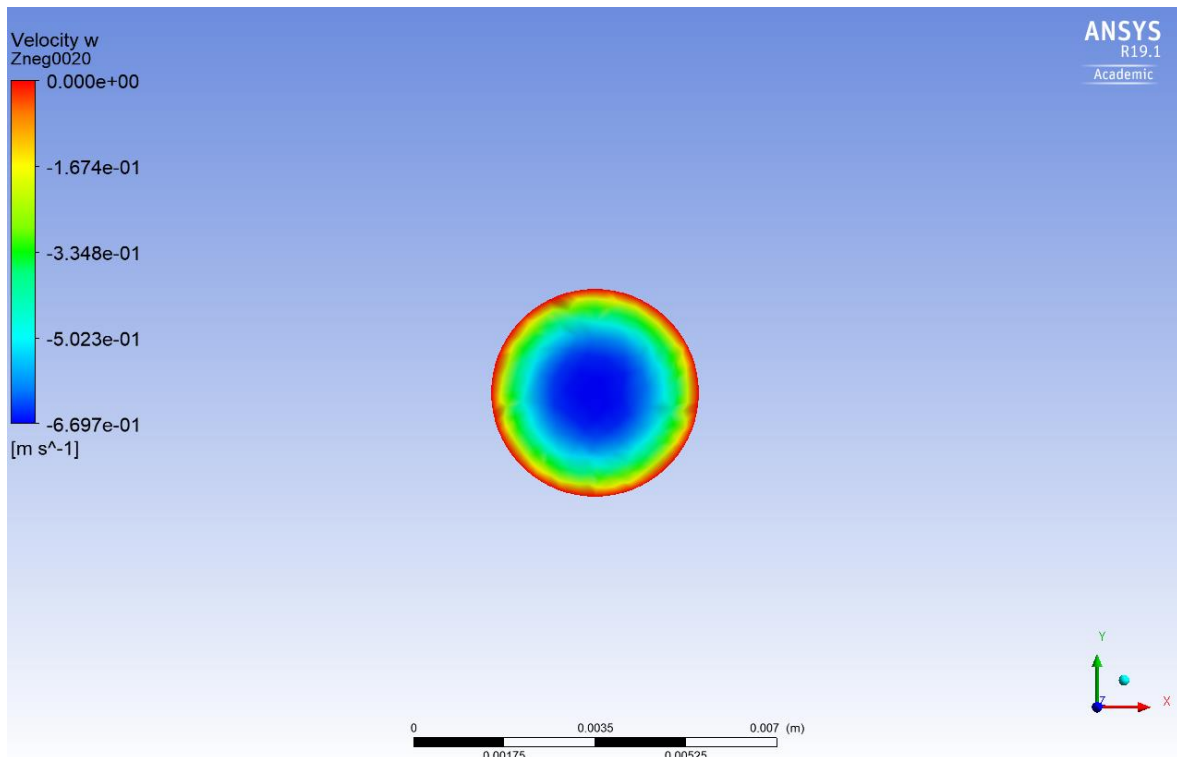


Figure 127 - Axial velocity at  $Z = -0.02 \text{ m}$

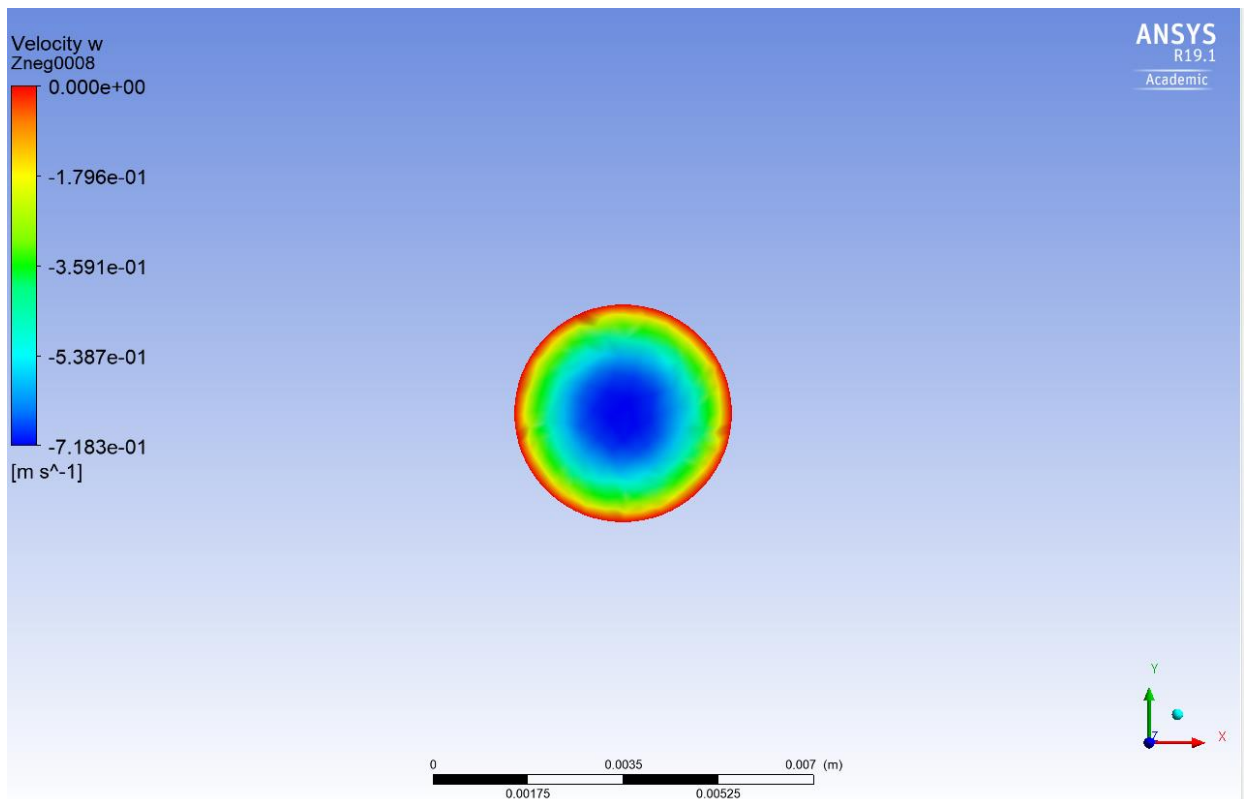


Figure 128 - Axial velocity at  $Z = -0.008 \text{ m}$

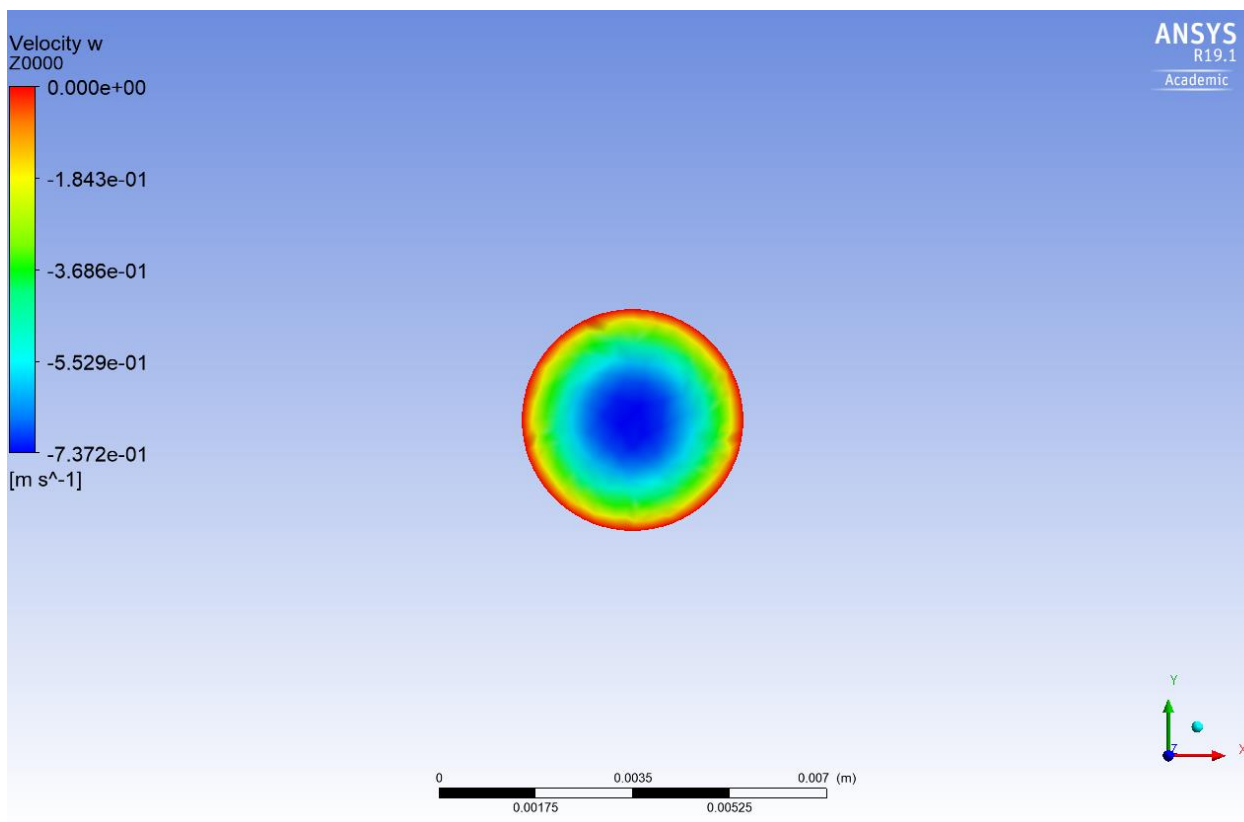


Figure 129 - Axial velocity at  $Z = 0.0 \text{ m}$

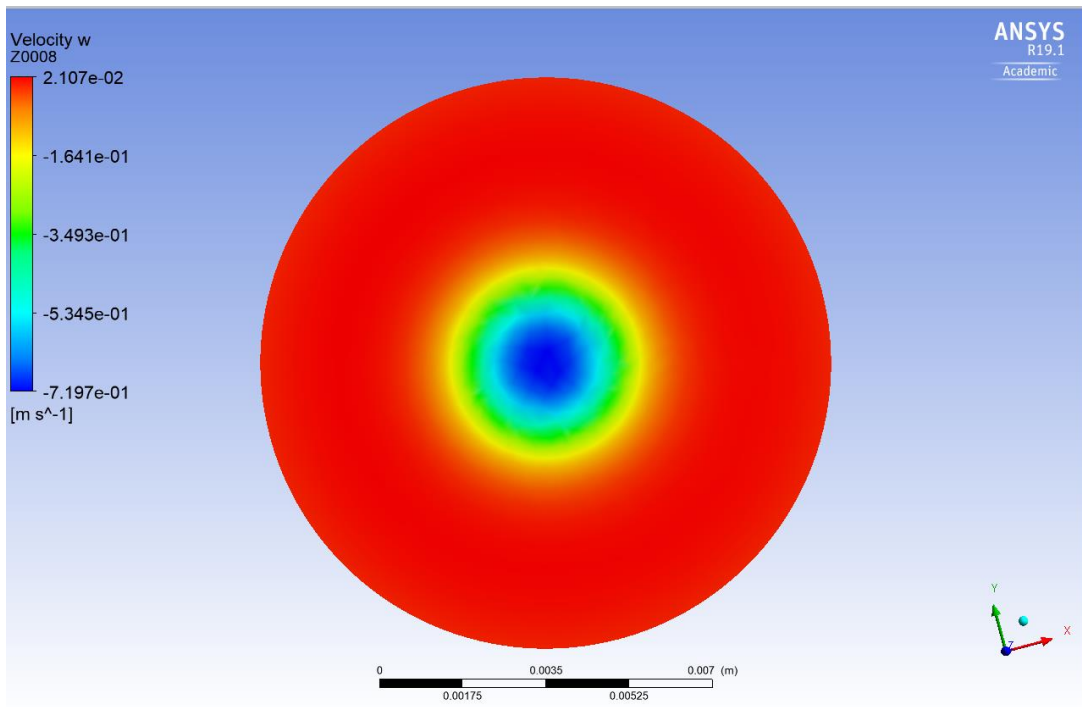


Figure 130 - Axial velocity at  $Z = 0.008\text{ m}$

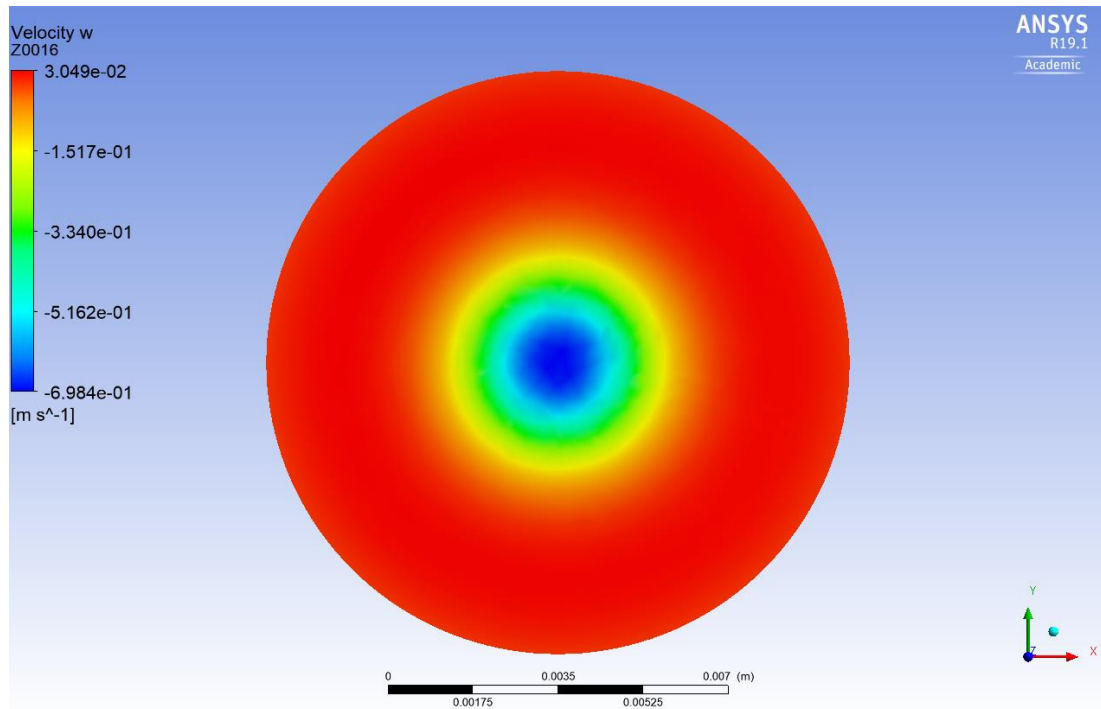


Figure 131 - Axial velocity at  $Z = 0.016\text{ m}$

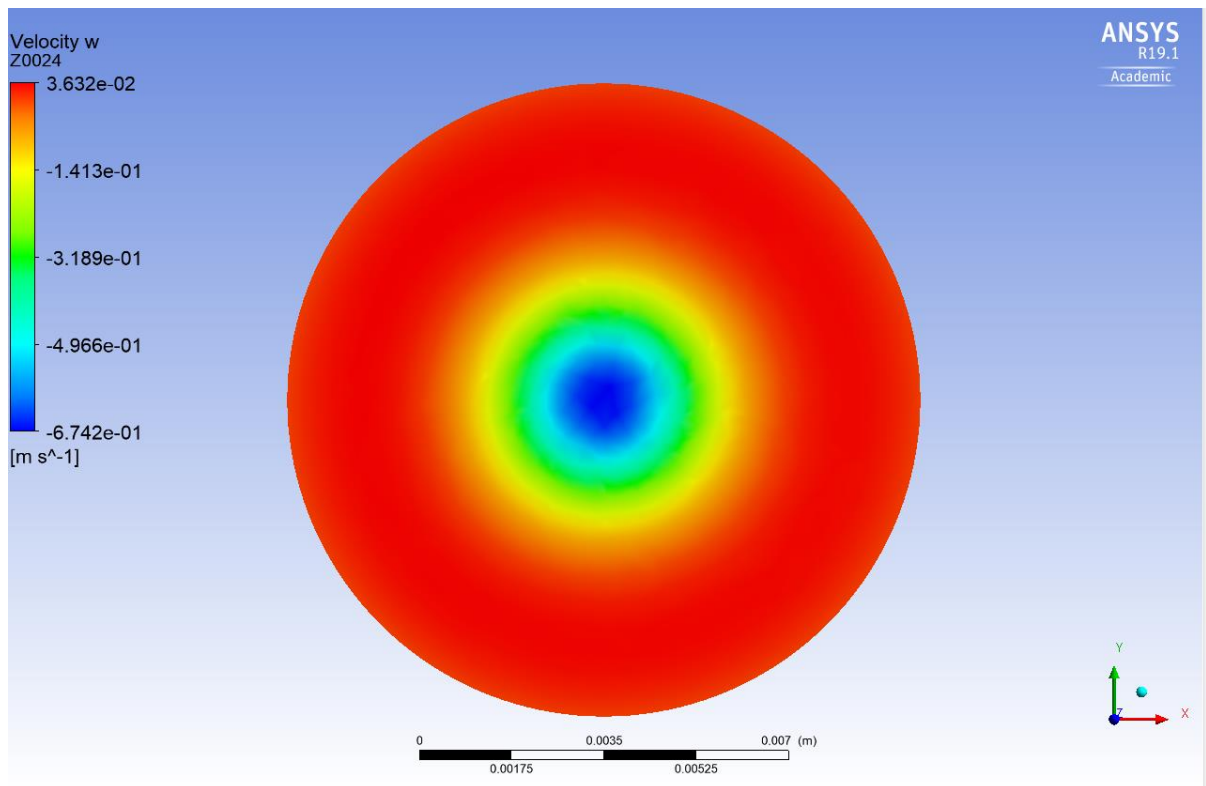


Figure 132 - Axial velocity at  $Z = 0.024$  m

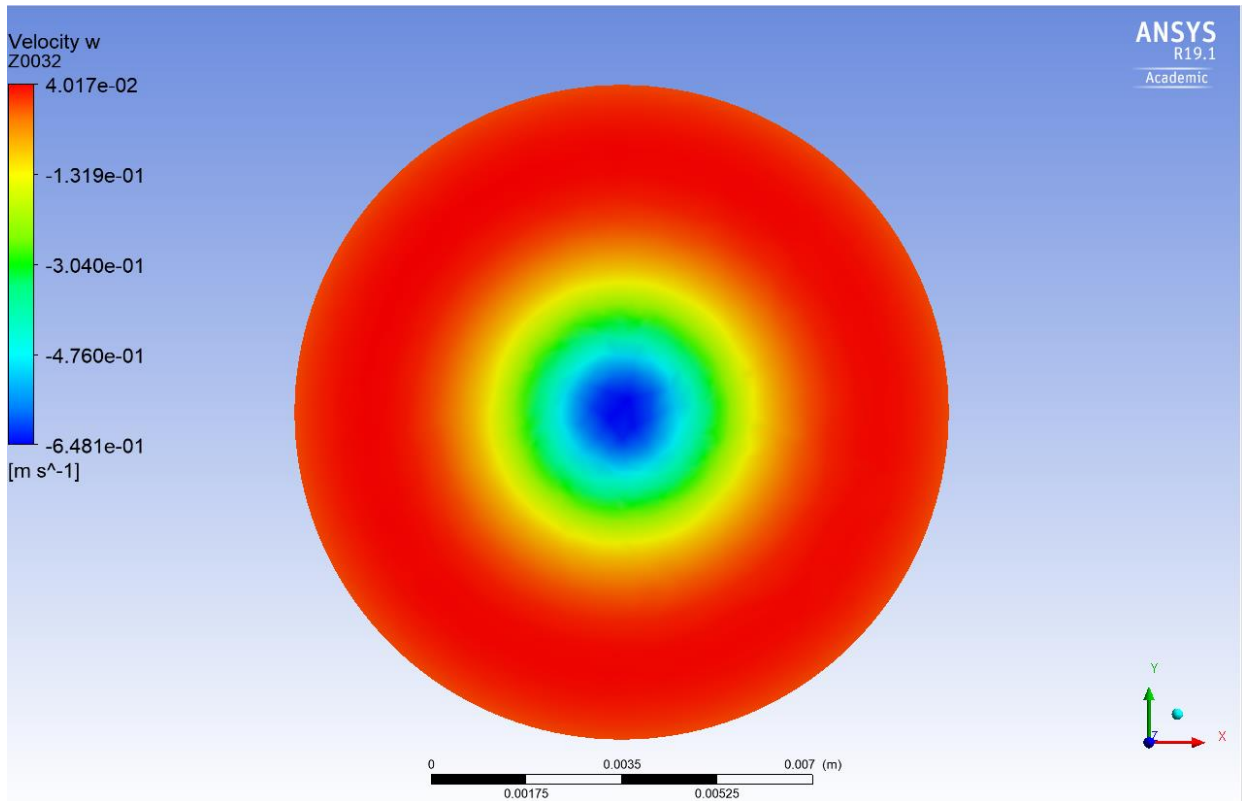


Figure 133 - Axial velocity at  $Z = 0.032$  m

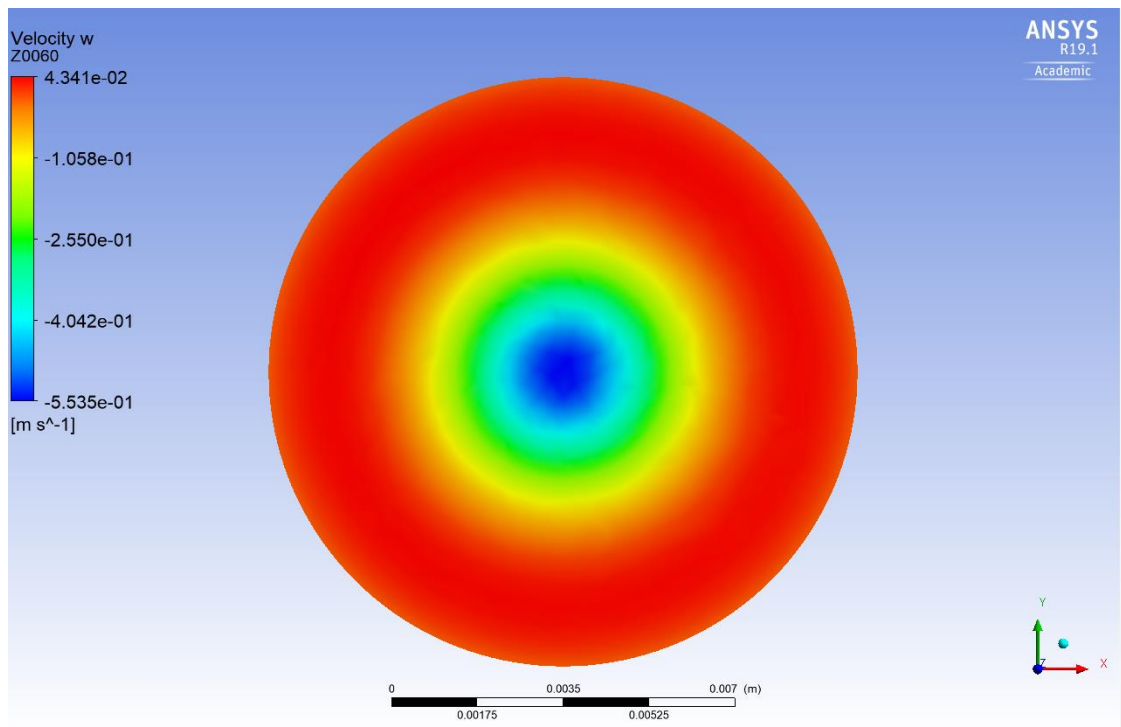


Figure 134 - Axial velocity at  $Z = 0.060\text{ m}$

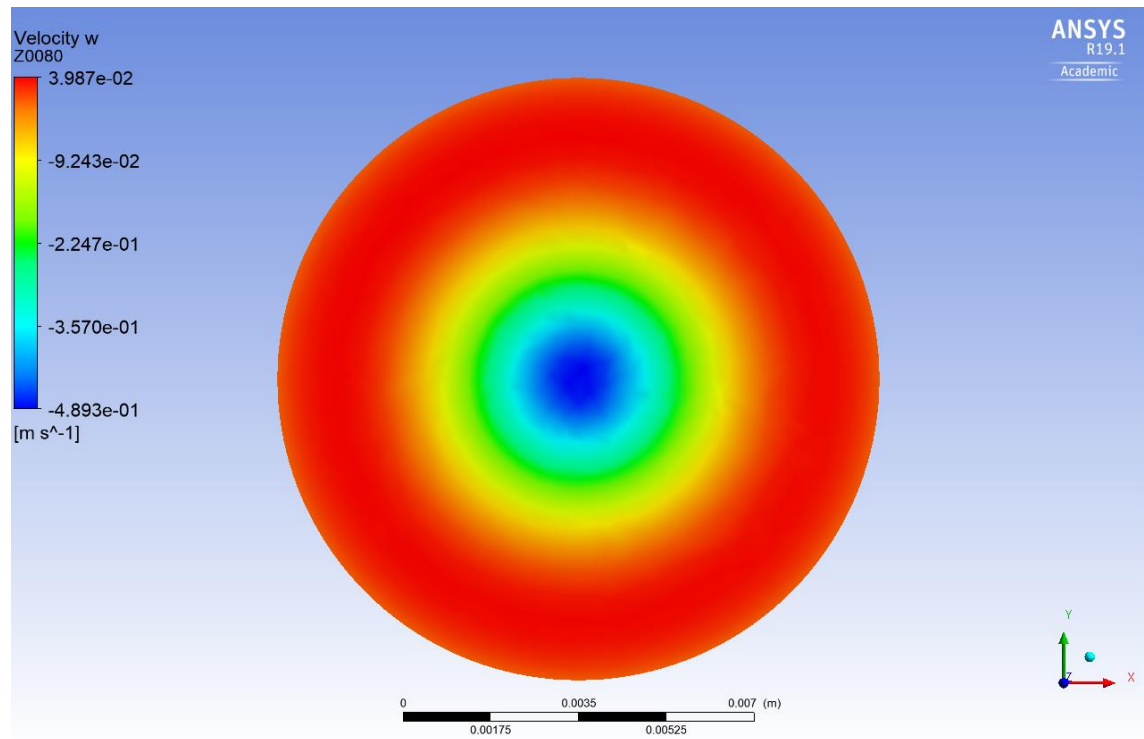


Figure 135 - Axial velocity at  $Z = 0.088\text{ m}$

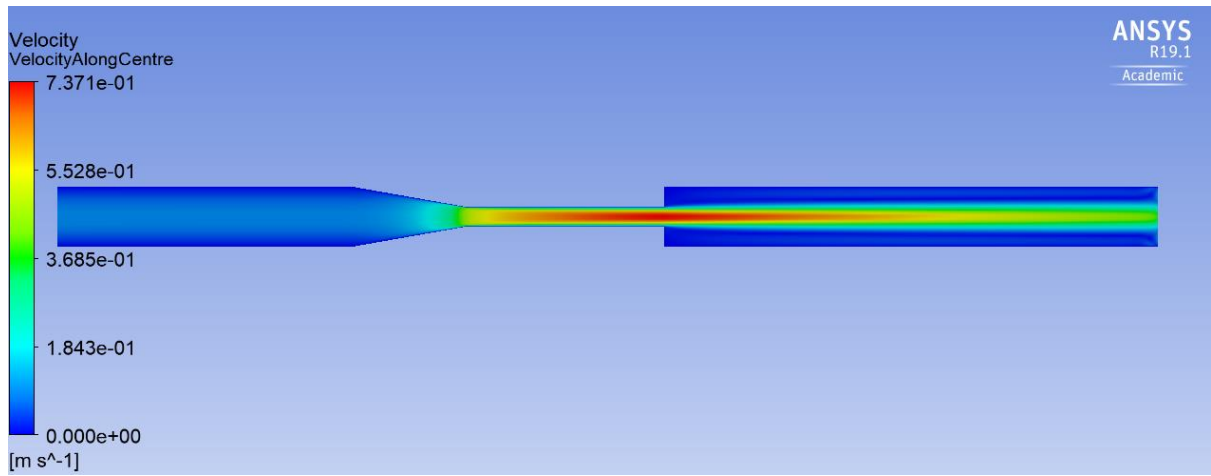


Figure 136 - Slice showing the velocity along the centre of the geometry

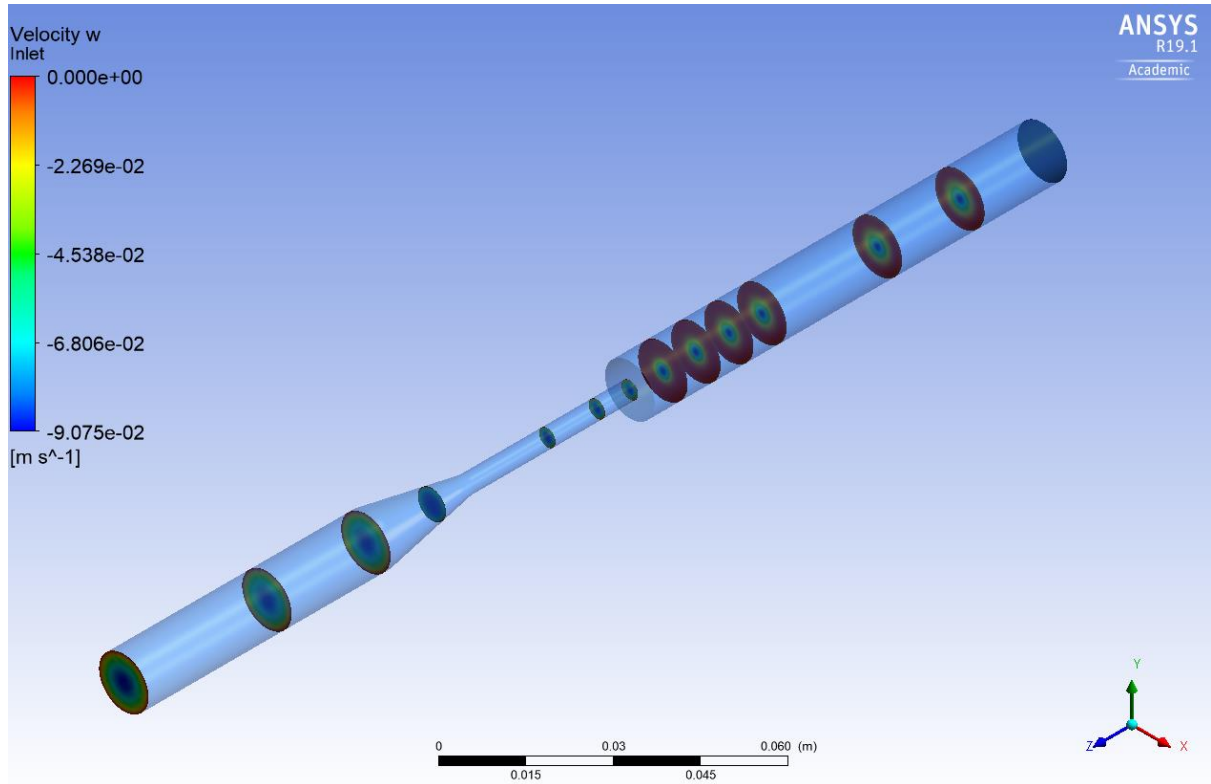


Figure 137 - The 12 axial velocity profile locations that will be compared against the experimental measurements

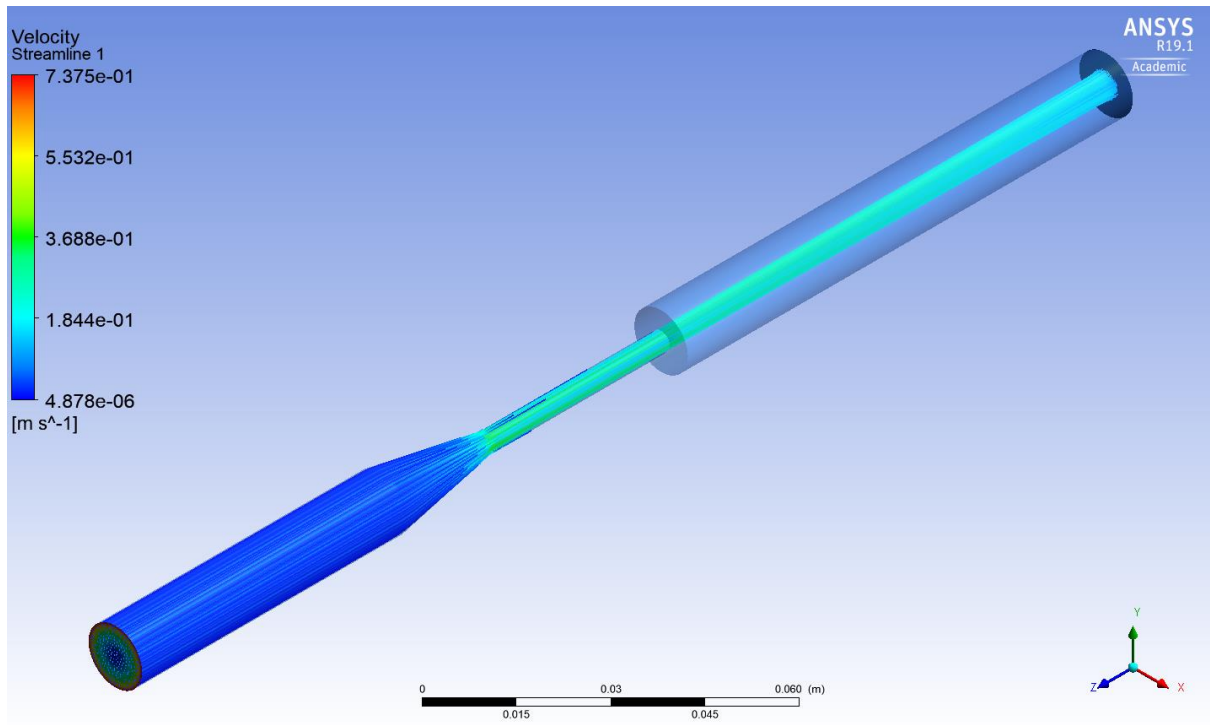


Figure 138 - Streamline visualisation that coloured to show velocity

## 7.2 PRESSURE

Below, a centreline slice of the geometry can be seen, coloured to show variation in pressure along the length of the geometry. The pressure can be seen to change from approximately 288 Pa at the inlet, to approximately 0 Pa at the outlet.

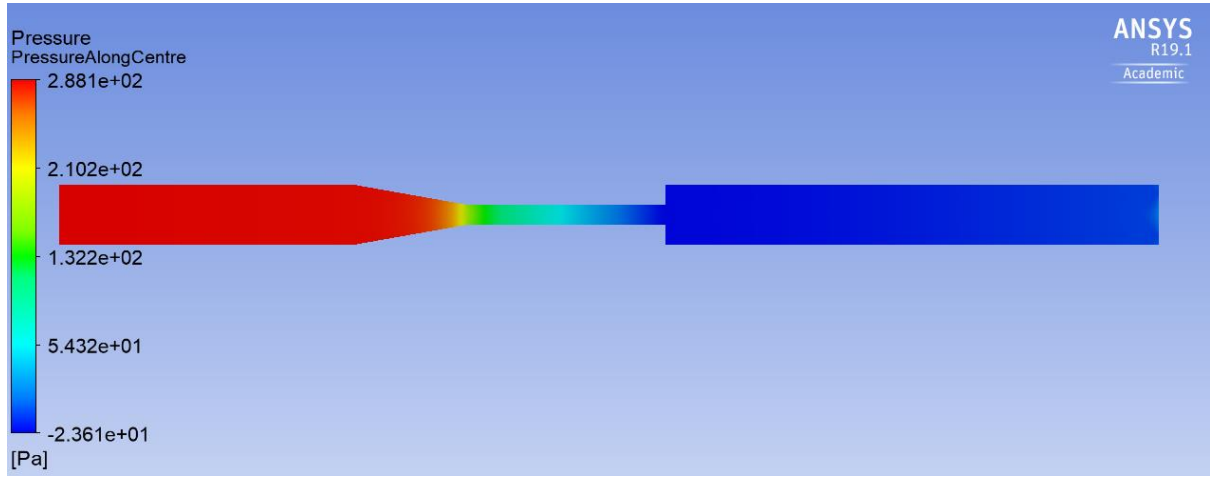


Figure 139 - Pressure along the centreline of geometry

## 7.3 RESULTS VALIDATION

The results generated from the CFD was validated against the experimental results. The comparisons of which can be seen below.

### 7.3.1 Centreline Velocity

Here, the velocity along the centreline is compared between the CFD model and the experimental measurements from 3 of the FDA labs.

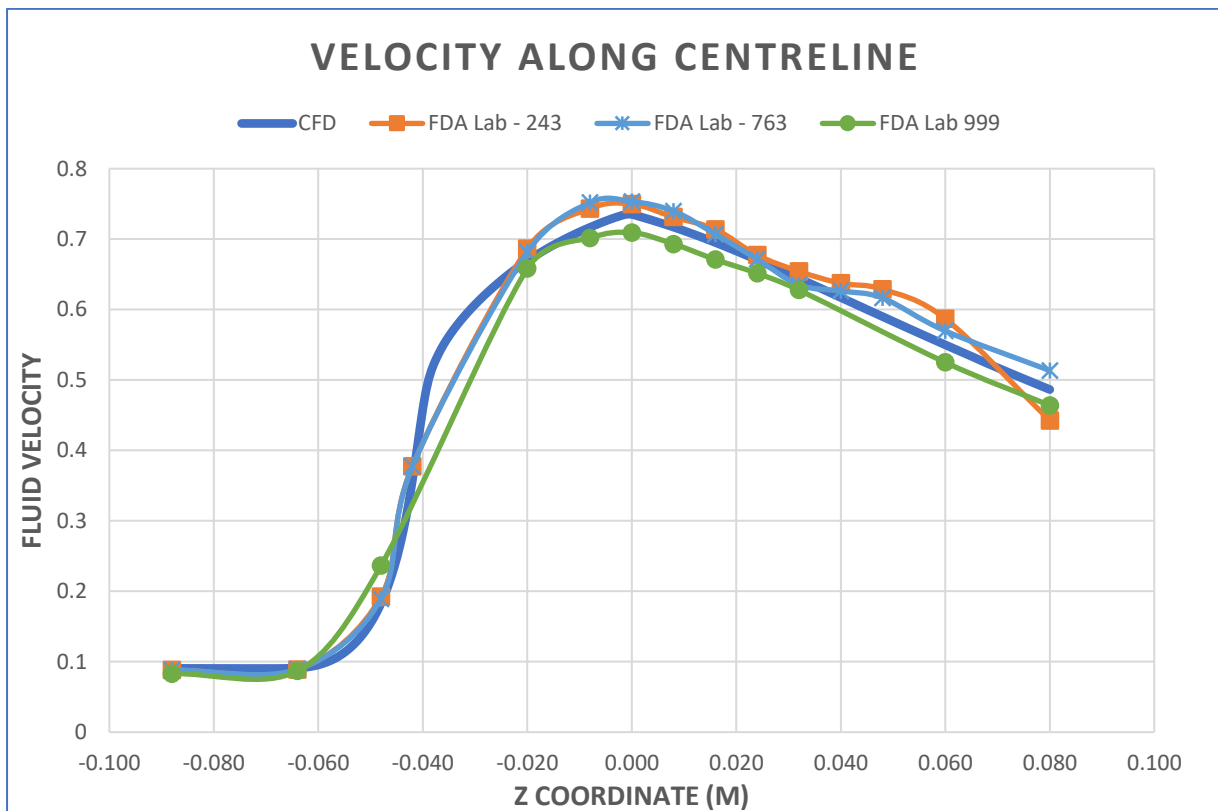


Figure 140 - Centreline velocity, comparison of CFD and experimental

CFD		763		% Difference
Z [m]	Velocity [m s^-1]	Z [m]	Velocity [m s^-1]	
-0.088	0.0906	-0.088	0.0880	<b>2.84</b>
-0.064	0.0910	-0.064	0.0892	<b>1.99</b>
-0.048	0.1833	-0.048	0.1890	<b>-3.07</b>
-0.042	0.3613	-0.042	0.3774	<b>-4.37</b>
-0.020	0.6688	-0.020	0.6815	<b>-1.89</b>
-0.008	0.7169	-0.008	0.7518	<b>-4.75</b>
0.000	0.7351	0.000	0.7534	<b>-2.46</b>
0.008	0.7169	0.008	0.7398	<b>-3.14</b>
0.016	0.6953	0.016	0.7070	<b>-1.66</b>
0.024	0.6705	0.024	0.6714	<b>-0.14</b>
0.032	0.6439	0.032	0.6350	<b>1.40</b>
0.040	0.6172	0.040	0.6264	<b>-1.49</b>
0.048	0.5898	0.048	0.6163	<b>-4.41</b>
0.060	0.5499	0.060	0.5696	<b>-3.52</b>
0.080	0.4864	0.080	0.5134	<b>-5.39</b>

Table 10 - Centreline velocity CFD Vs PIV

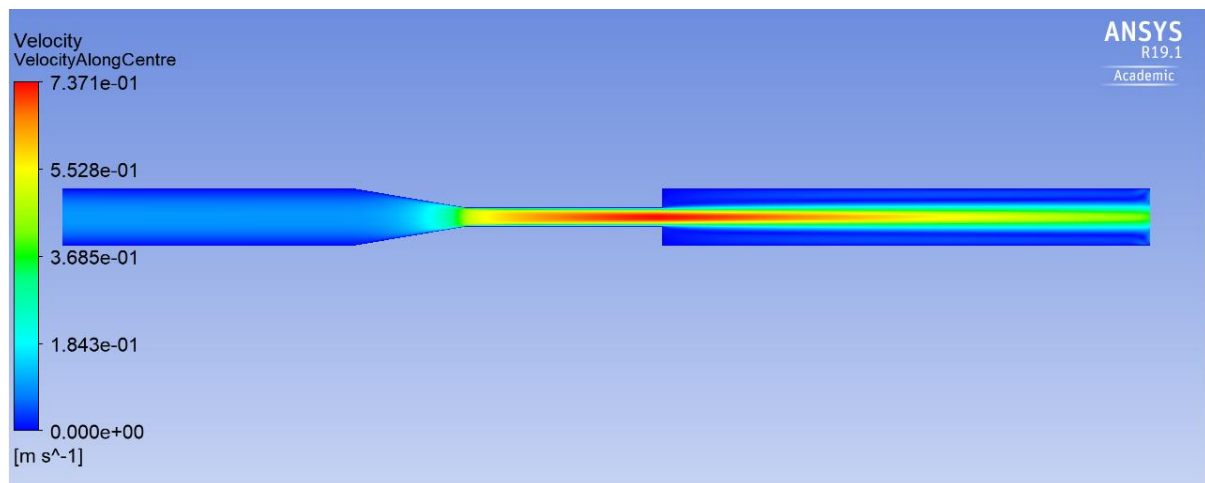


Figure 141 - Centreline slice of velocity

### 7.3.2 Centreline Pressure

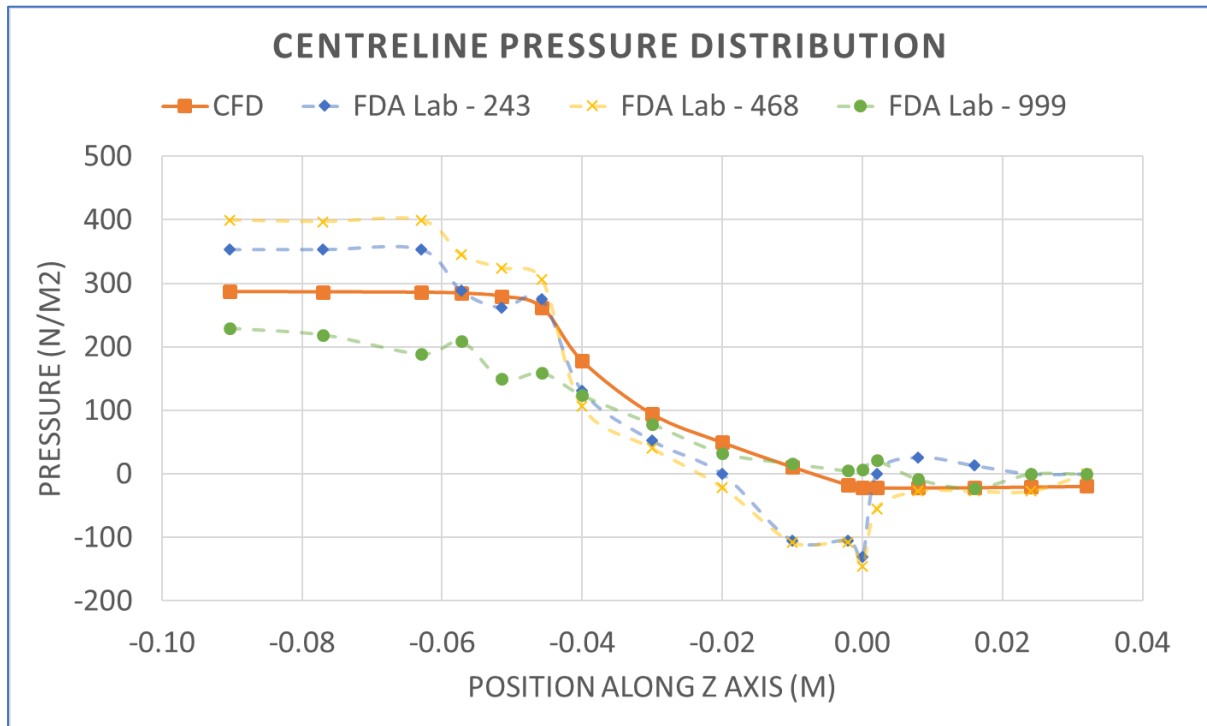


Figure 142 - Centreline pressure distribution

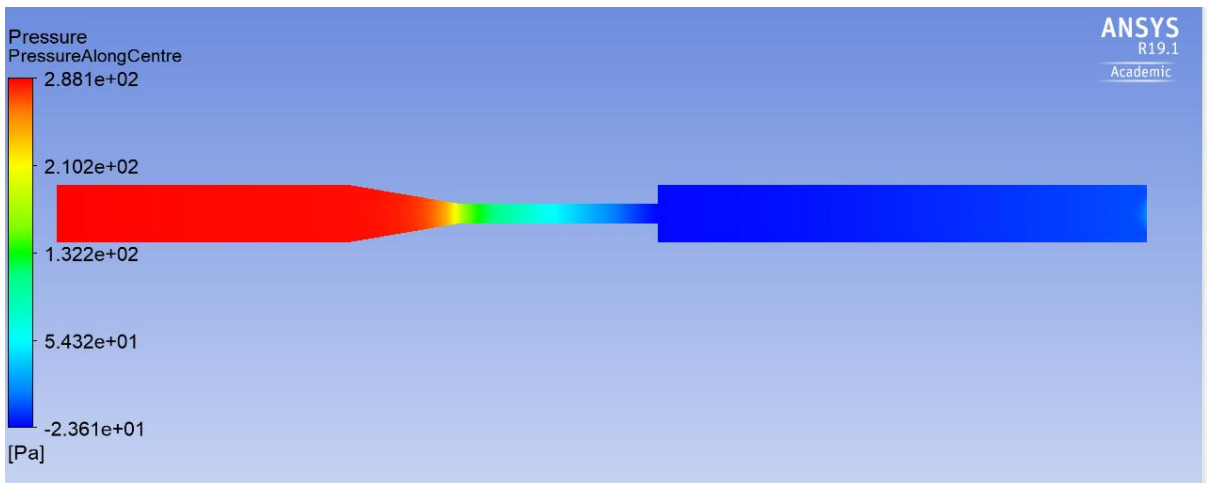


Figure 143 - Centreline slice of pressure

	468	CFD	
Position on Z Axis (m)	Pressure (N/m <sup>2</sup> )		% Difference
-0.09032	399	287	-33
-0.07696	397	286	-32
-0.06299	399	286	-33
-0.05723	345	285	-19
-0.05149	324	280	-14
-0.04575	306	264	-15
-0.04001	106	170	46
-0.03000	40	94	81
-0.01999	-22	50	508
-0.01001	-107	11	-246
-0.00203	-107	-17	-144
0.00000	-145	-22	-147
0.00203	-55	-22	-86
0.00800	-28	-22	-23
0.01600	-28	-21	-25
0.02400	-28	-20	-29
0.03200	-	-19	-

Table 11 - Centreline pressure - CFD Vs Experimental

### 7.3.3 Wall Pressure

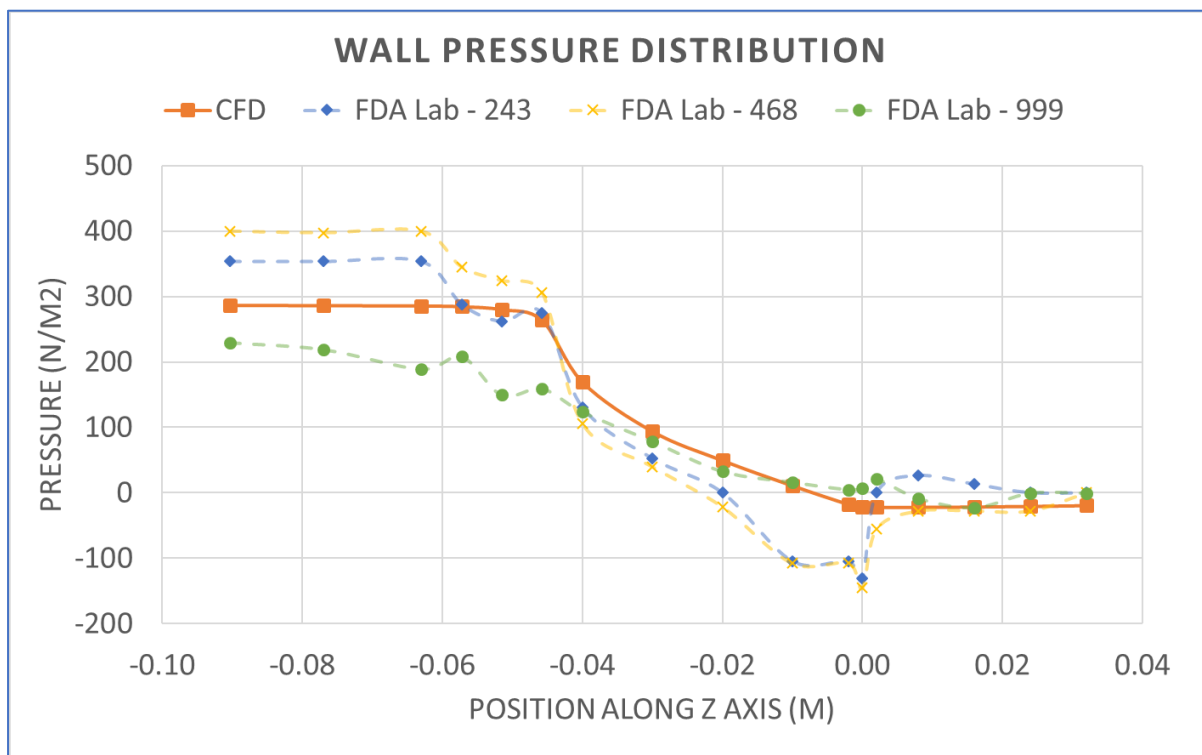


Figure 144 - Wall pressure distribution along the length of the geometry

### 7.3.4 Axial Velocity Slices

In each plot below, the CFD results are shown in orange, while the experimental measurements from one of the FDA labs (Lab 297) are shown in blue. The dataset from lab 297 was chosen at random.

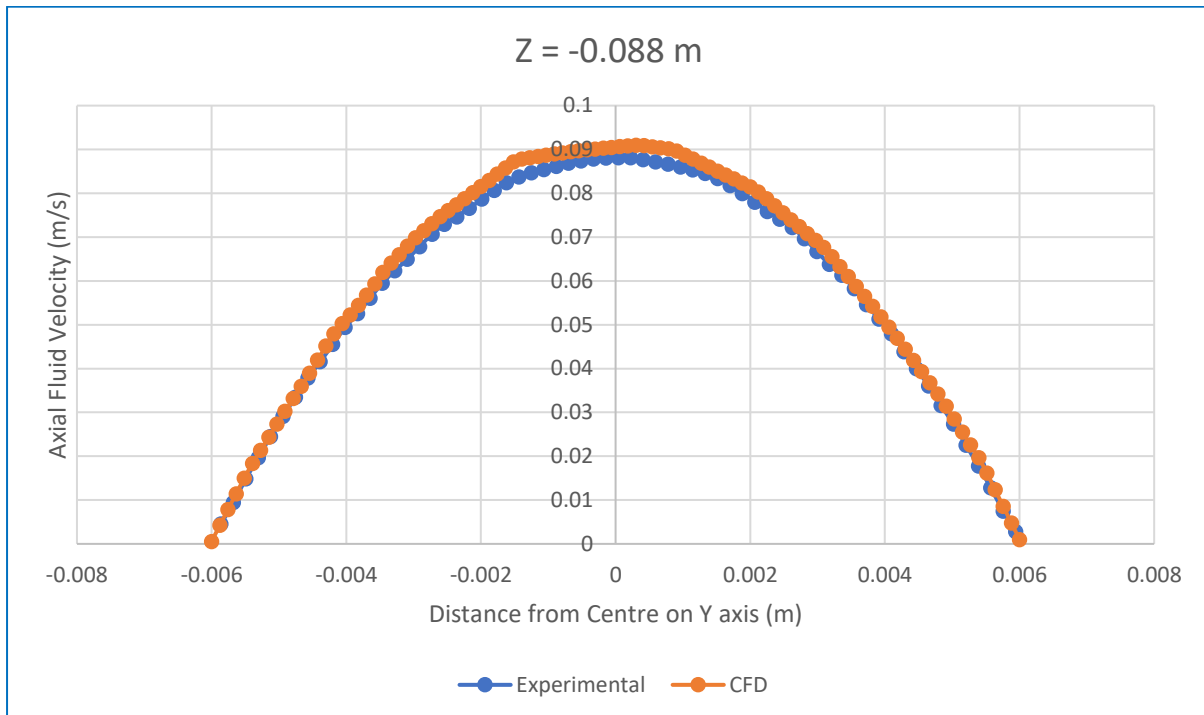


Figure 145 - CFD vs experimental velocity @ Z = -0.088 m

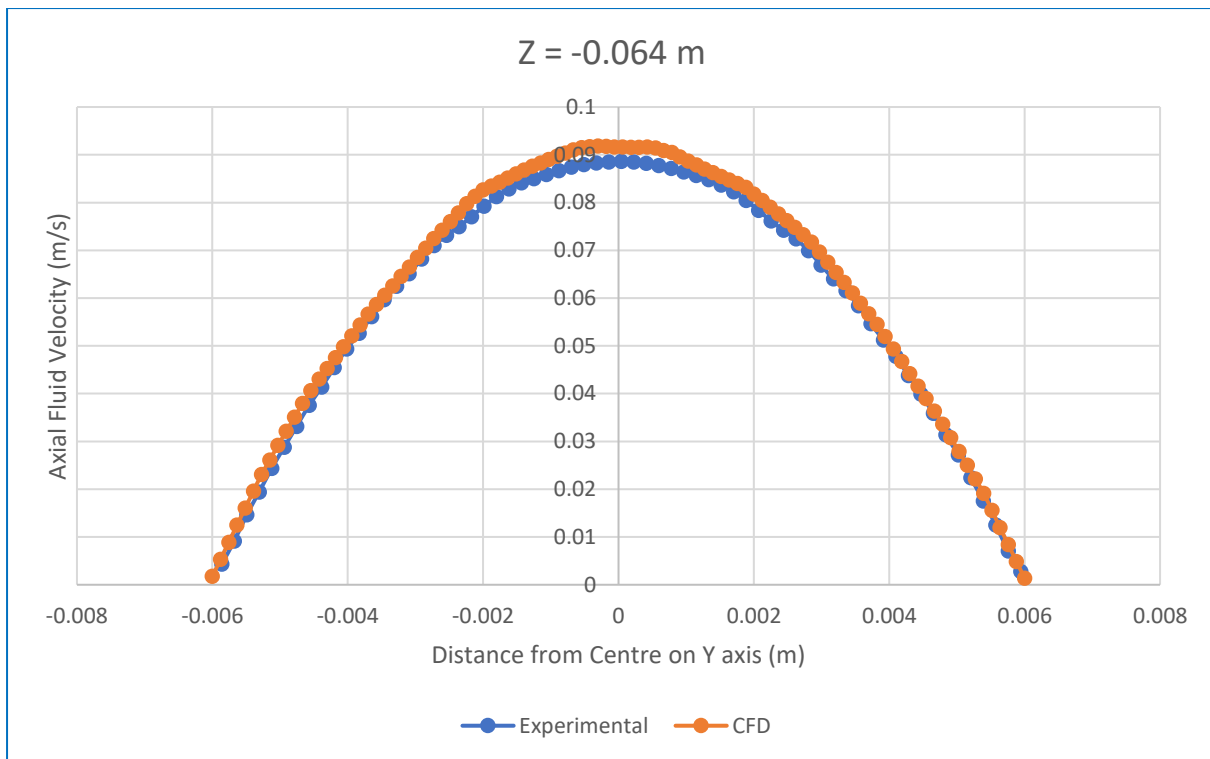


Figure 146 - CFD vs experimental velocity @  $Z = -0.064 \text{ m}$

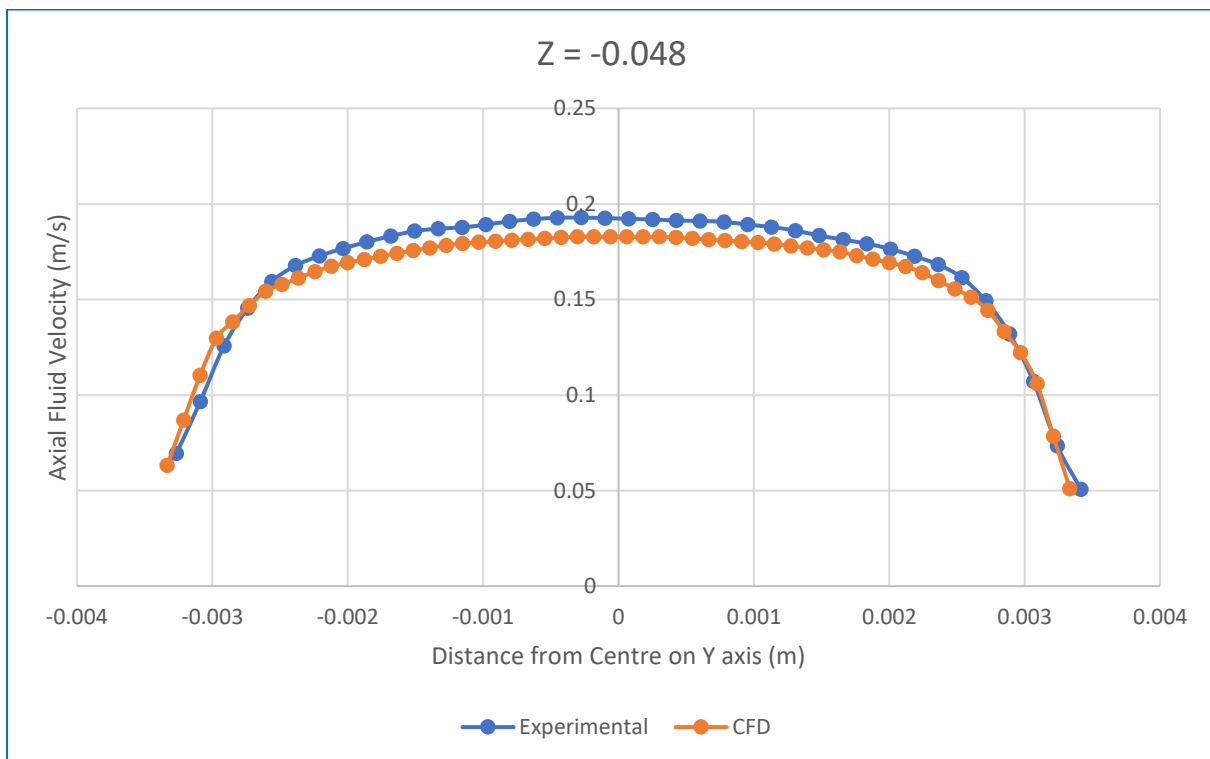


Figure 147 - CFD vs experimental velocity @  $Z = -0.048 \text{ m}$

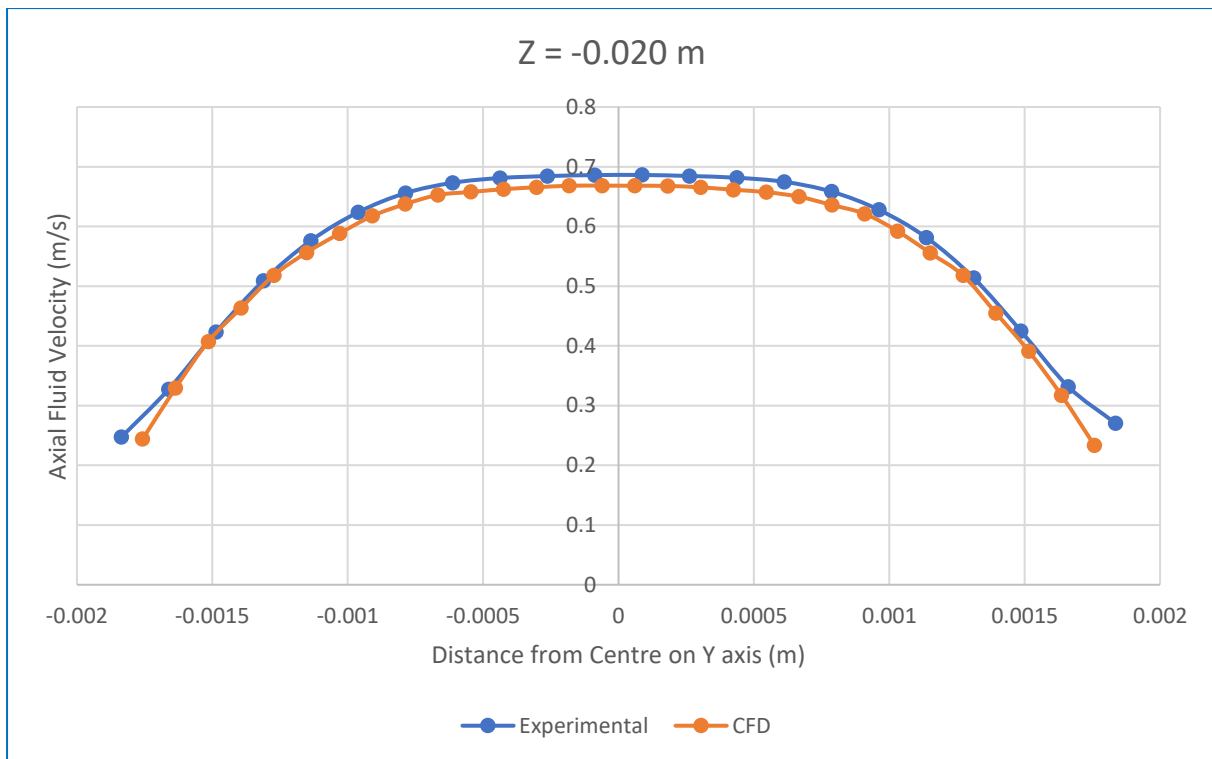


Figure 148 - CFD vs experimental velocity @  $Z = -0.020 \text{ m}$

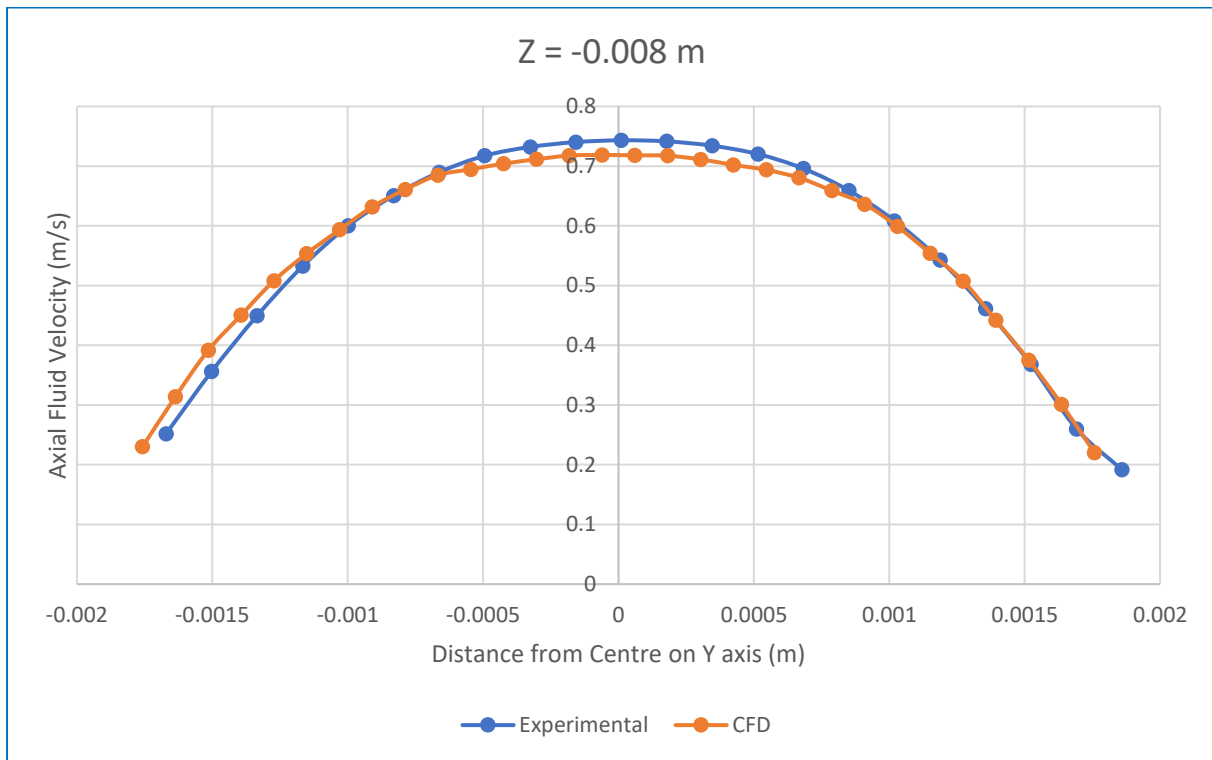


Figure 149 - CFD vs experimental velocity @  $Z = -0.008 \text{ m}$

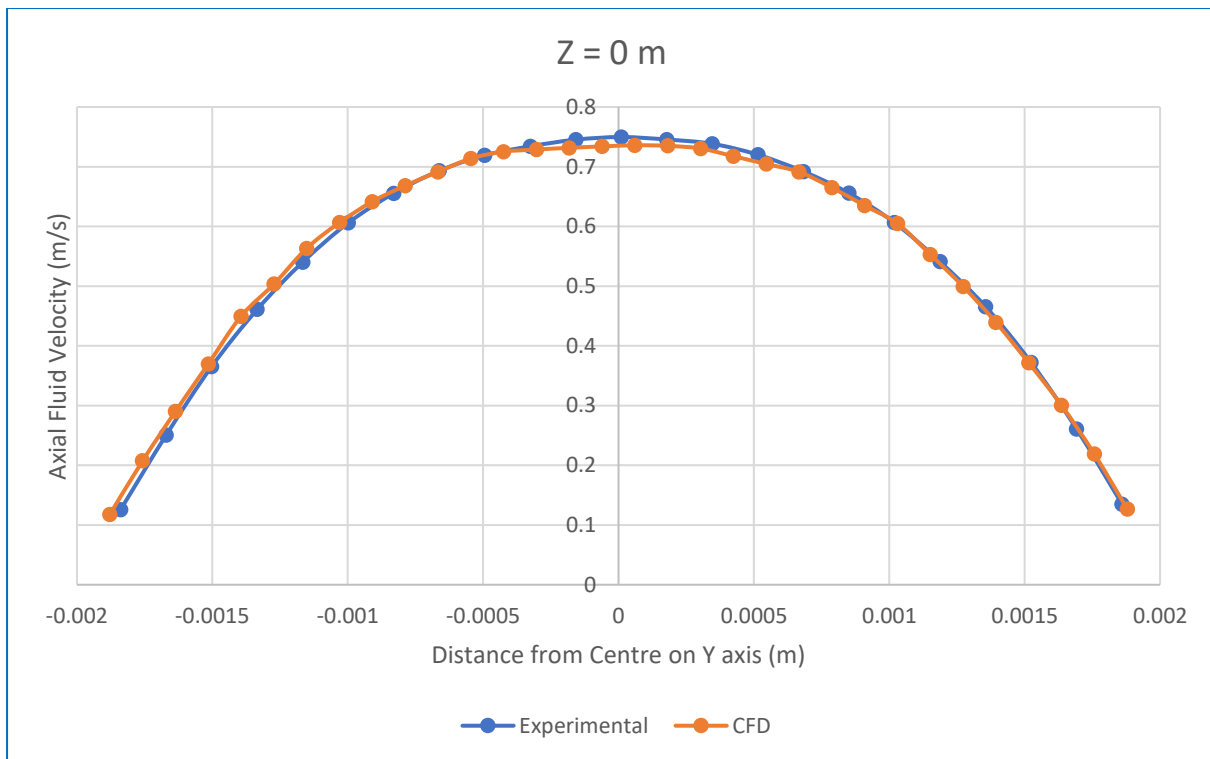


Figure 150 - CFD vs experimental velocity @  $Z = 0.000 \text{ m}$

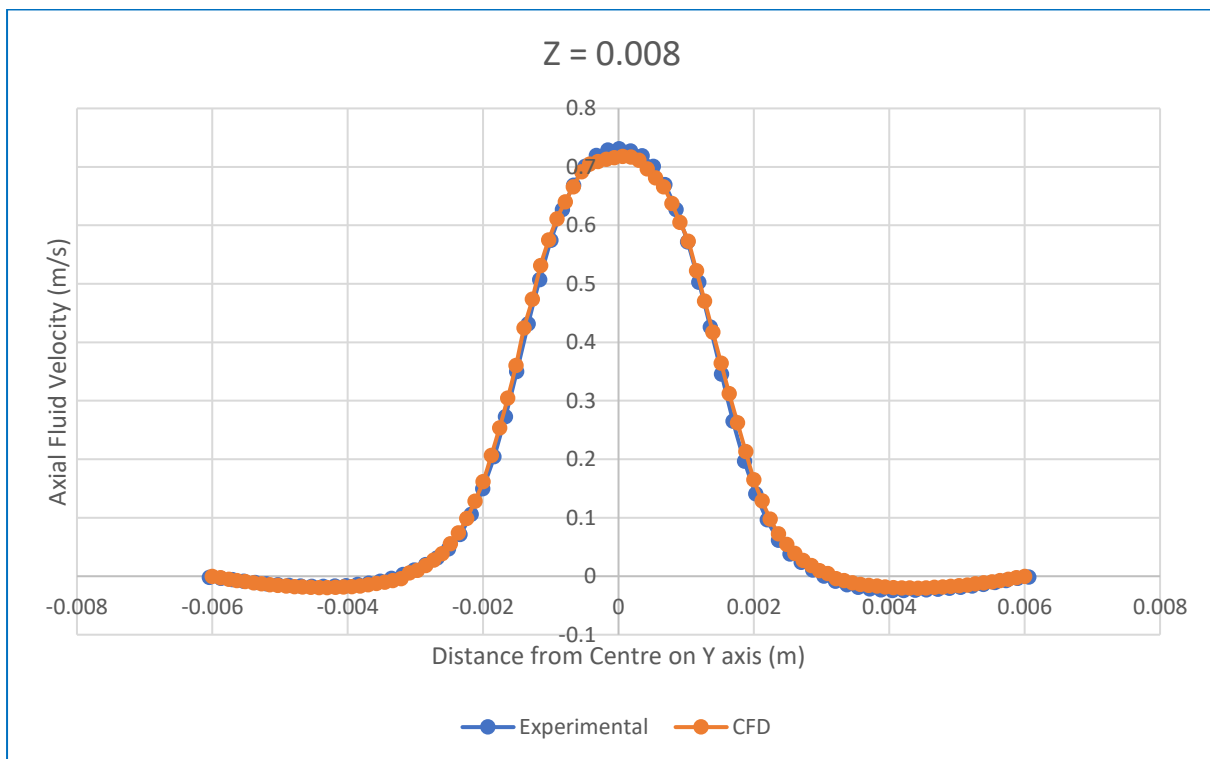


Figure 151 - CFD vs experimental velocity @  $Z = 0.008 \text{ m}$

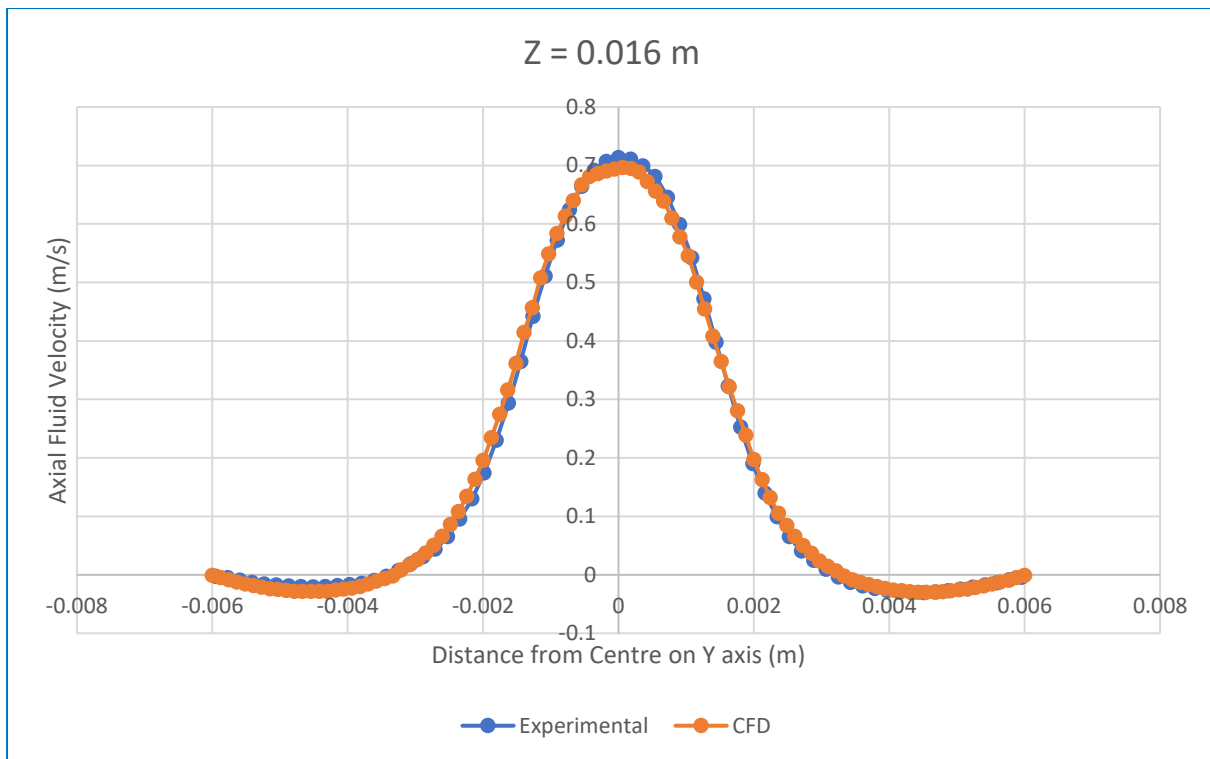


Figure 152 - CFD vs experimental velocity @  $Z = 0.016 \text{ m}$

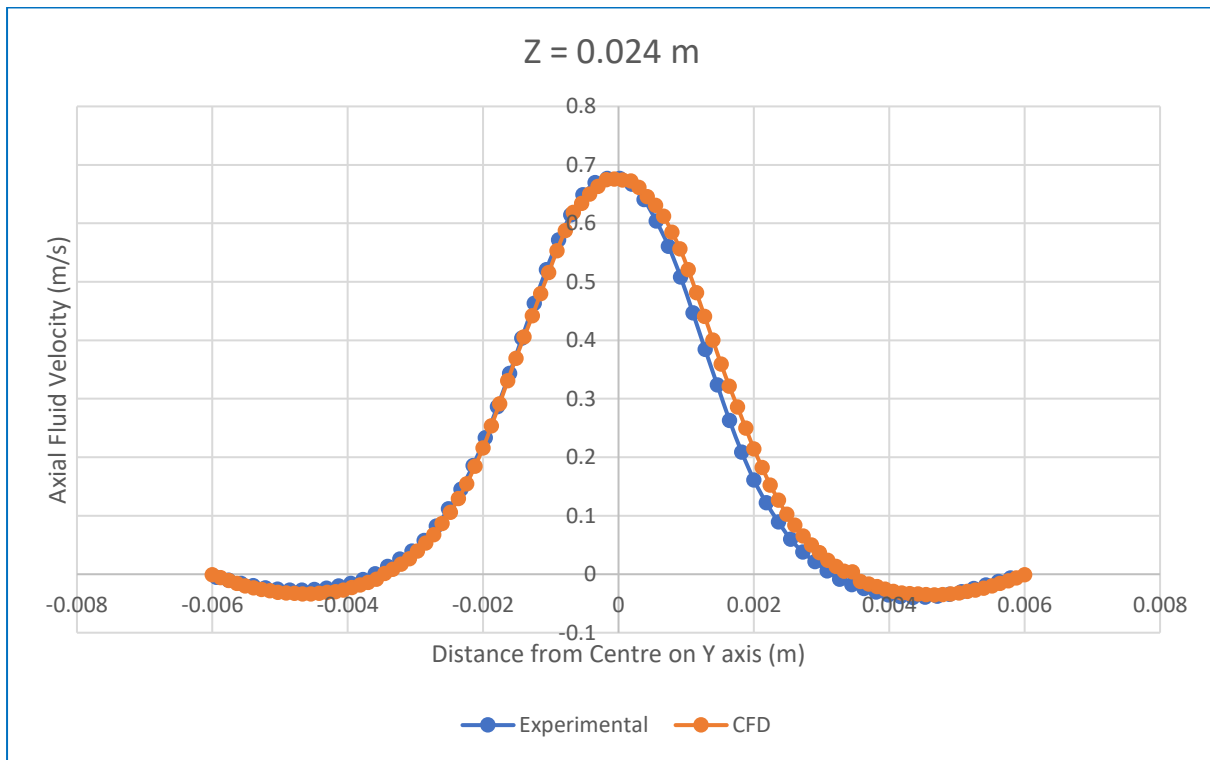


Figure 153 - CFD vs experimental velocity @  $Z = 0.024 \text{ m}$

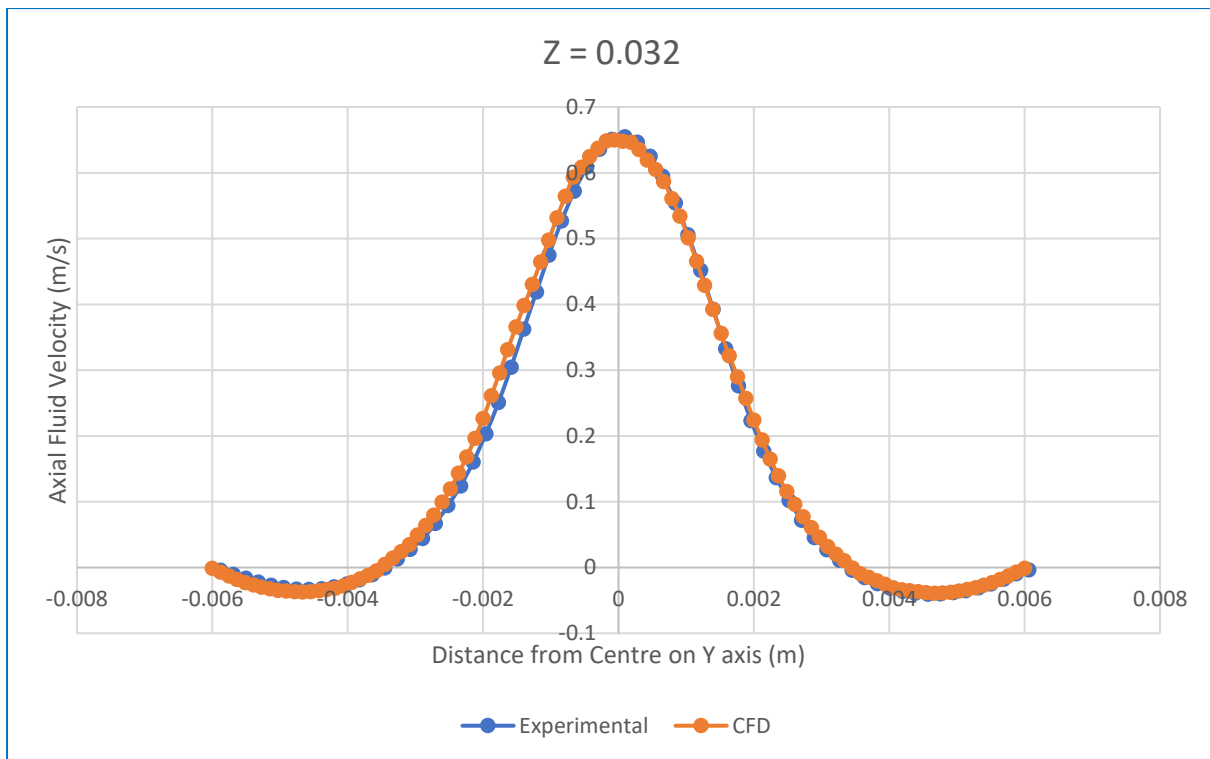


Figure 154 - CFD vs experimental velocity @  $Z = 0.032\text{ m}$

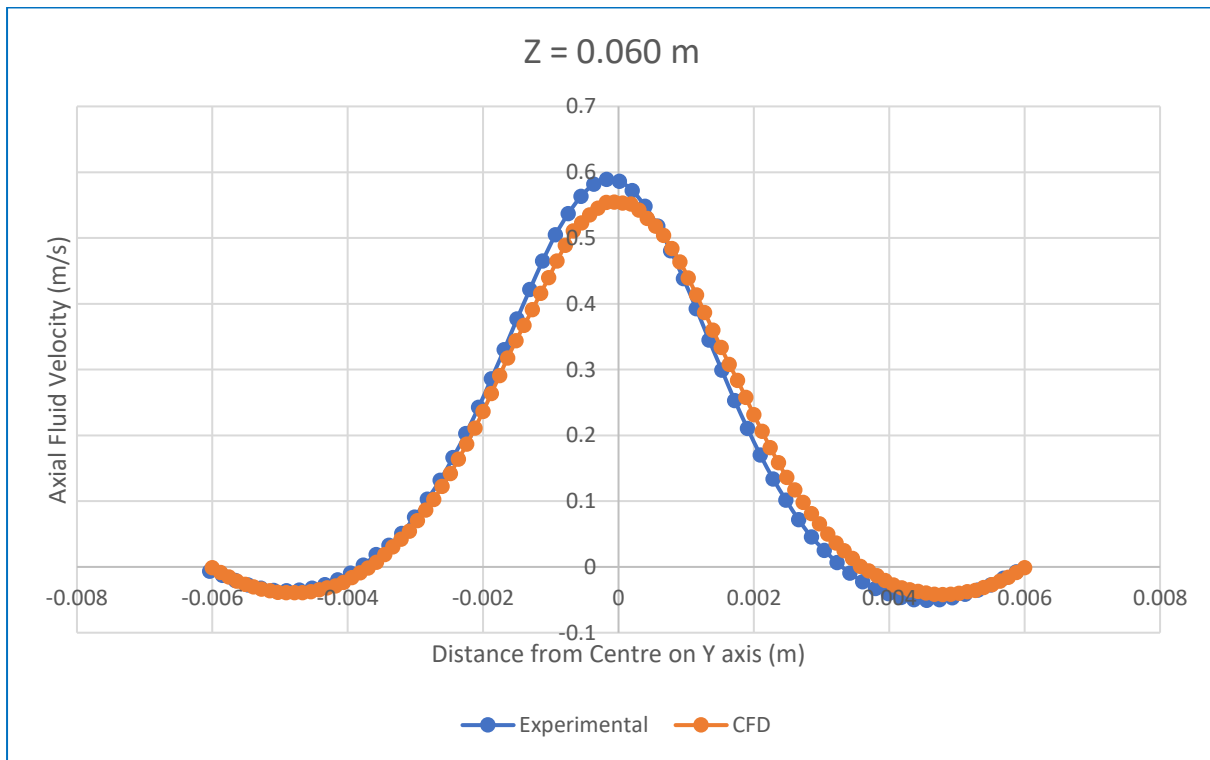
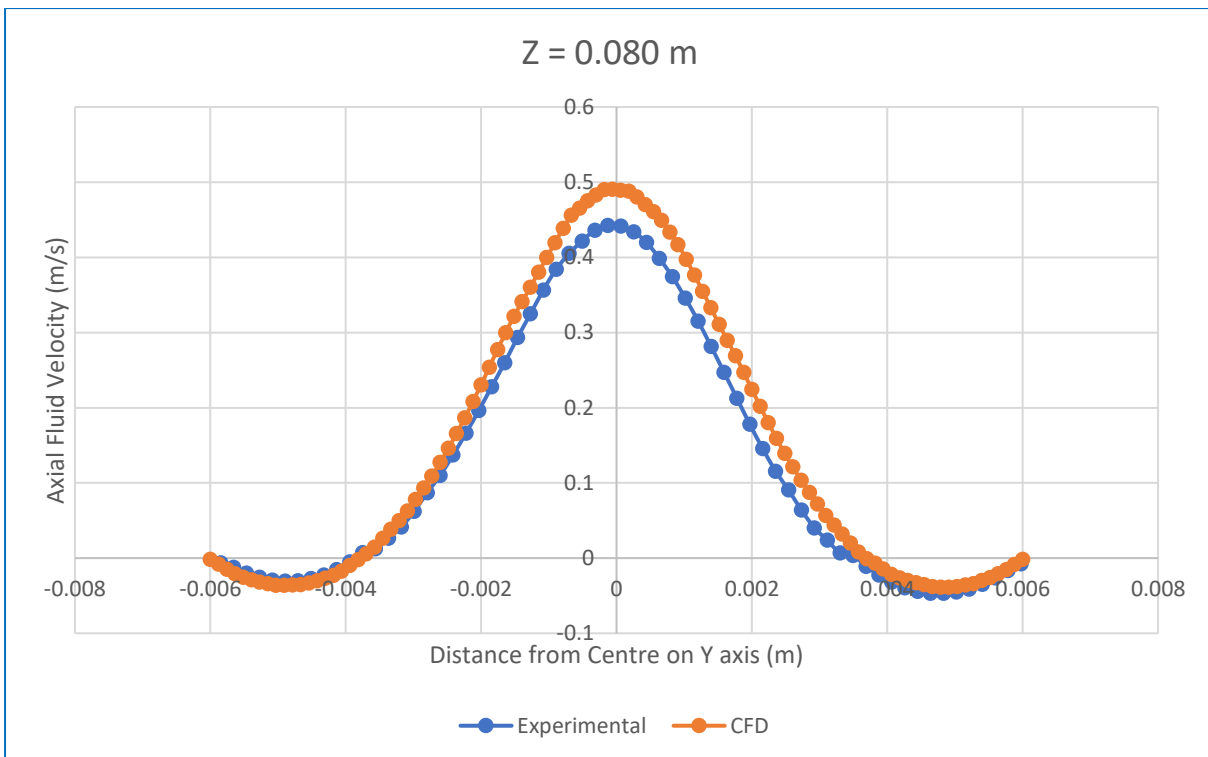


Figure 155 - CFD vs experimental velocity @  $Z = 0.060\text{ m}$



*Figure 156 - CFD vs experimental velocity @  $Z = 0.080 \text{ m}$*

# Chapter 8

## CONCLUSIONS & RECOMMENDATIONS

### 8.1 CONCLUSIONS

The aim of this project was to create a true to life CFD model of fluid flow through the FDA Round Robin Benchmark #1 geometry.

The primary conclusion that can be drawn from the work completed for this project is that an accurate CFD model of an internal blood flow problem can be created. While the model that was designed was not actually based on a blood flow problem through a medical device, as has been previously discussed, the FDA study was designed from the ground up to mimic a real world medical device.

ANSYS CFX proved to be a reliable CFD solver, that can be highly customised and adapted to a given problem. CFX yielded velocity results that are extremely close to the experimentally recorded measurements.

A mesh convergence tolerance of 1% was set, this mesh convergence tolerance was achieved on Mesh 5, using the pressure drop and mass flow rates as the mesh convergence metrics.

#### 8.1.1 Comparison of Results

##### 8.1.1.1 Velocity along centreline

- The CFD results are all within  $\pm 5.4\%$  of the value of the FDA lab 763 experimental measurements.

##### 8.1.1.2 Pressures Along Centreline

- The pressures vary not only between the CFD results and the experimental measurements, but even within the different FDA experiments there is massive variation between the different labs.
- Despite the numerical differences, the overall trend of the CFD pressure drop lines up with the experimental measurements.

### 8.1.1.3 Axial Velocity Slices

- The axial velocity slices show extremely good agreement with the experimental measurements, as can be seen in the graphical comparisons in chapter 7.

## 8.2 RECOMMENDATIONS

This section deals with possible areas in which the project could progress. Areas that could provide a better understanding of the content or provide a more detailed analysis of the content in question.

### 8.2.1 Normalised Pressure Comparison

A better way of comparing the pressures taken from the CFD model and the experiments may be to use a normalisation formula to normalise the pressures, so that the trends can be examined in greater detail. The absolute value of the pressures on its own does not mean much, and that is what has been compared in this project.

### 8.2.2 Further Test Cases

As this report only covers the test case when the Reynolds number within the throat is equal to 500, further test cases could be completed. The datasets provided by the FDA include experimental measurements for five different test cases (i.e. five different Reynolds numbers).

Case	Re
Case 1	500
Case 2	2000
Case 3	3500
Case 4	5000
Case 5	6500

Table 12 - The experimental test cases

Due to the transitional/turbulent nature of the flows in all cases except for Case 1, a completely different modelling setup would need to be used.

#### 8.2.2.1 Fluid Inlet

As the flow may no longer be assumed to be laminar, the method of inputting the velocity profile into the model would have to be changed.

One potential method for inputting the velocity may be using the volume/mass flow rate through the domain. By first calculating the mass flow rate through the system, a second model specified using the given Reynolds number and corresponding mass flow rate would be created. This model would have the same diameter as the geometry input; however the mass flow would be specified as a plug (i.e. constant velocity across the diameter). This model would then be extended in length to allow the flow to fully develop. Once the flow is fully developed, the velocity profile can be exported directly into the full Benchmark #1 geometry.

#### *8.2.2.2 Inflation Layers*

As there is transitional/turbulent flow expected in the other test cases, inflation layers should be used on the meshes. Inflation layers are needed on simulations containing turbulent flow, as due to the turbulent nature of the flow, greater resolution is needed at the walls of the domain. [28]

### **8.2.3 Two Dimensional Simulations**

As the Benchmark #1 geometry is axisymmetric, a 2D simulation may be performed on it. This may possibly give similar results to the 3D simulation that was completed in this project, while being much less computationally demanding to solve. However there are a number of potential issues that a 2D simulation may cause.

The first issue is that ANSYS CFX, which this project was completed in does not have a 2D solver, it can only solve 3D meshes. This would mean that the model would have to be solved in another CFD solver, such as ANSYS Fluent, or OpenFoam.

The second potential issue with a 2D simulation, is that the flow through the sudden expansion may encounter the Coandă effect, which could cause the flow to attach to one of the walls. As the flow through the sudden expansion is a case of bounded jet flow [29] [30], it may be reasonable to expect the Coandă effect to be seen in a 2D simulation. In which case, a 3D simulation may then be needed to see in better detail what is happening within the system.

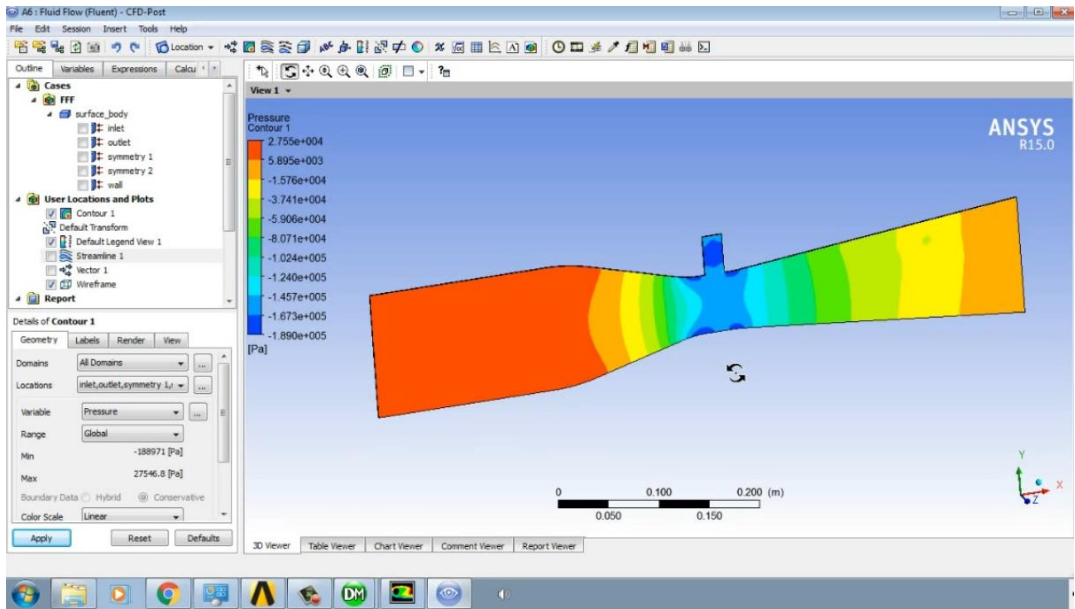


Figure 157 - An example of a 2D simulation created in ANSYS Fluent [31]

#### 8.2.4 Wedge Simulations

As previously stated, CFX does not have the ability to perform 2D simulations. As such, if one wishes to perform a 2D simulation within CFX, a small wedge of the axisymmetric geometry can be used in conjunction with symmetry planes in order to simulate a 2D geometry, which can then be extrapolated out, into a 3D geometry in CFD Post. The mesh for this setup would be 1 element thick, hence giving a near 2D mesh.

The CFX 2017 User's Guide suggests a 10° wedge of the axisymmetric model should be used if a 1 element thick 3D mesh is being used. [26]

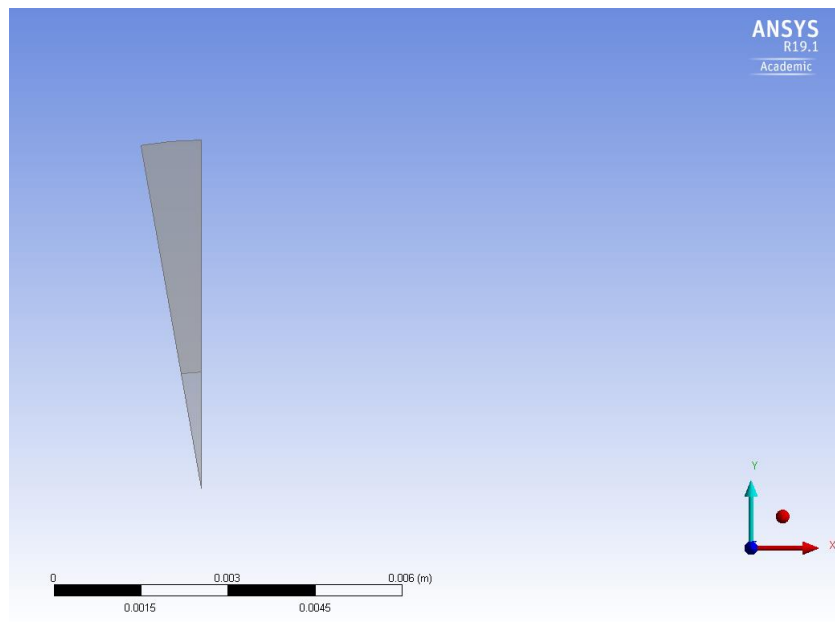


Figure 158 - View of the 10 degree wedge of the geometry

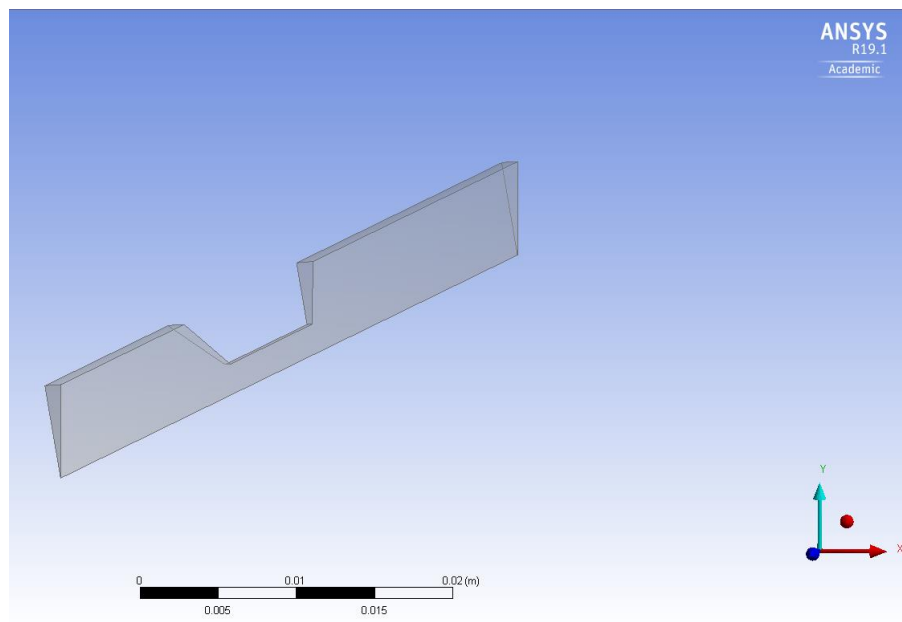
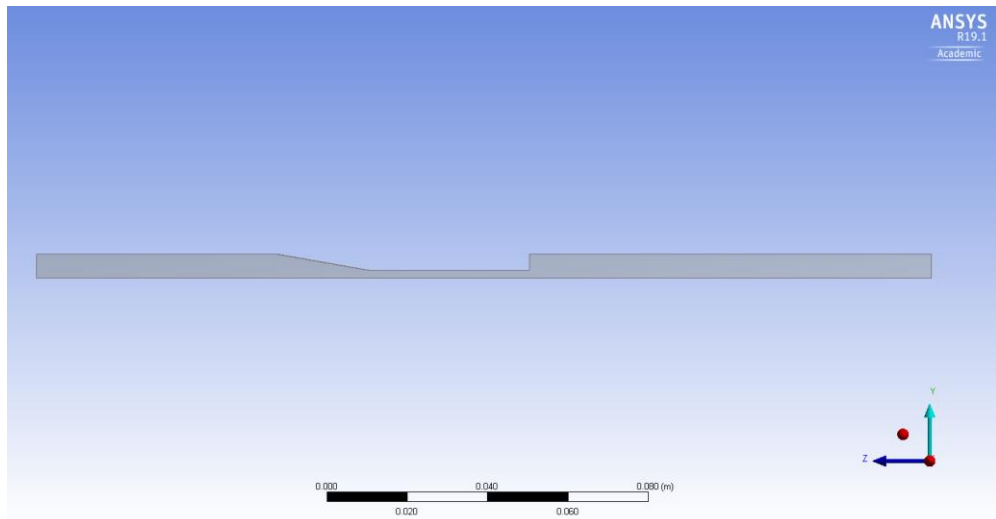


Figure 159 - View of the 10 degree wedge of the geometry



*Figure 160 - Profile view of the 10 degree wedge of the geometry*

### 8.2.5 Larger Meshes

Larger meshes may be used to potentially increase the accuracy of the model, however as a mesh convergence tolerance of 1% was already reached within the 512,000 node limit, in order to use a higher node count mesh, a more mesh convergence tolerance would need to be used also.

### 8.2.6 More Strict Convergence Criteria

One area that could be explored is the effect of more strict model solution convergence criteria. The RMS values that were used on the final model was  $1 \times 10^{-8}$ , which is already much lower than the RMS settings recommended in the CFX user's guide [26]. However, a smaller RMS target may provide slightly better results.

### 8.2.7 Critical Path Initiative

The round robin study that this project focuses on was just one of many studies within the FDA's "Critical Path Initiative", the initiative was launched in 2004 and continues to be updated with new studies which aims to "transform the way FDA regulated medical products are developed, evaluated, and manufactured" [32]. As such, there is further studies within this initiative that CFD can be applied to, and there will be more added in future.

# REFERENCES

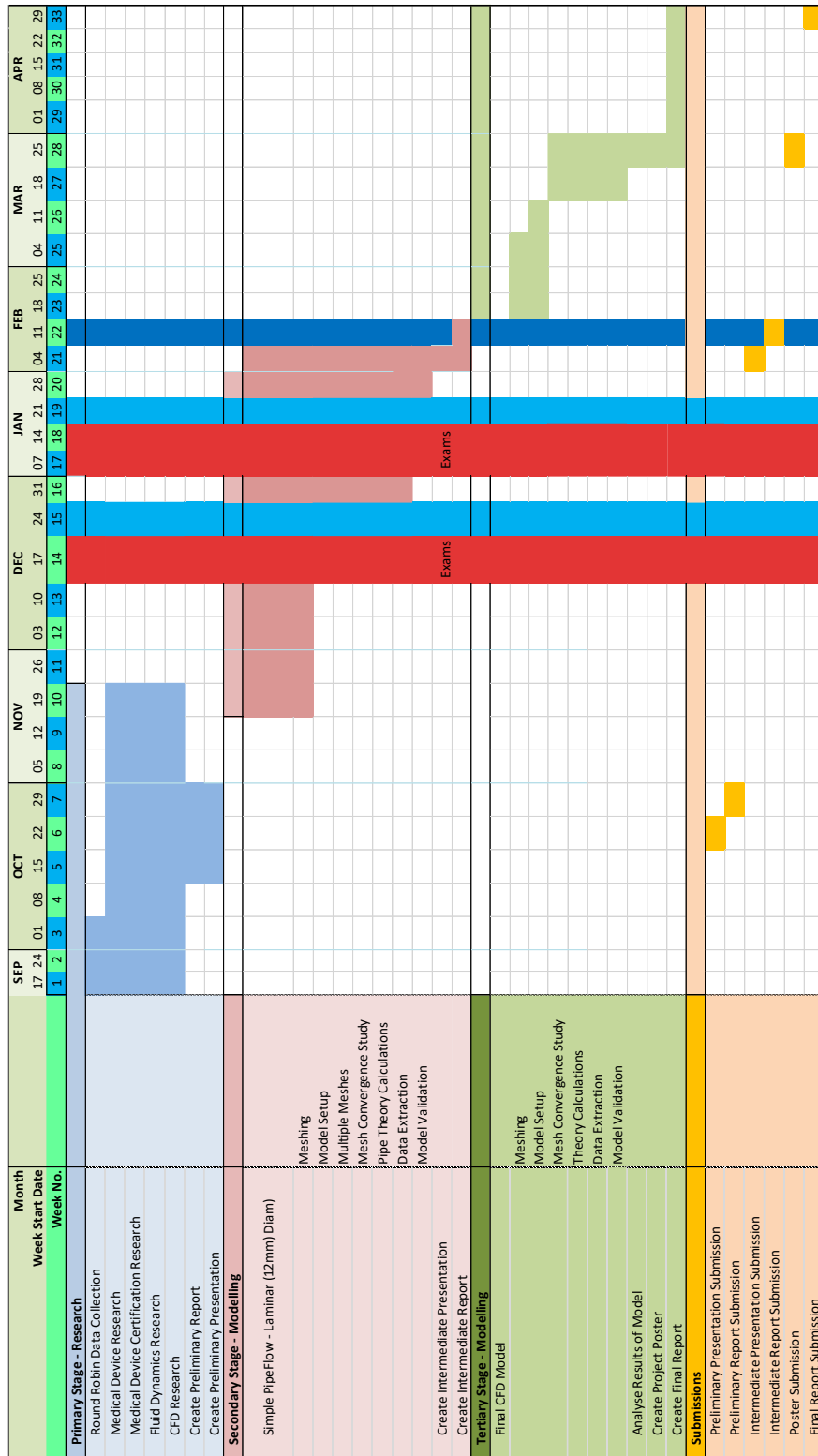
- [1] S. P. E. B. G. H. P. G. M. R. V. D. S. M. K. D. S. B. M. M. M. a. M. R. Stewart, “Assessment of CFD Performance in Simulations of an Idealized Medical Device: Results of FDA's First Computational Interlaboratory Study,” *Cardiovascular Engineering and Technology*, pp. 139-160, 2012.
- [2] Health Products Regulatory Authority, “Regulatory Information,” 1 November 2018. [Online]. Available: <http://www.hpra.ie/homepage/medical-devices/regulatory-information>.
- [3] BMP Medical, “What’s the Difference Between the FDA Medical Device Classes?,” 2 February 2018. [Online]. Available: 2018.
- [4] US FDA, “Class I / II Exemptions,” 22 March 2018. [Online]. Available: <https://www.fda.gov/medicaldevices/deviceregulationandguidance/overview/classifyyourdevice/ucm051549.htm>.
- [5] US FDA, “Classify Your Medical Device,” 31 August 2018. [Online]. Available: <https://www.fda.gov/medicaldevices/deviceregulationandguidance/overview/classifyyourdevice/ucm2005371.htm>.
- [6] S. T. J. M. M. K. B. R. G. A. F. A. A. DEUTSCH, “Experimental Fluid Mechanics of Pulsatile Artificial Blood Pumps,” *Annual Review of Fluid Mechanics*, pp. 65-86, 2006.
- [7] F. Sotiropoulos, “Computational Fluid Dynamics for Medical Device Design: Are We There Yet?,” *Cardiovascular Engineering and Technology (CVET)*, vol. 3, no. 2, pp. 137-138, 2012.
- [8] I. C. F. D. P. R. R. P. Chien-Jung Huang, “CFD Validations with FDA Benchmarks of Medical Devices Flows,” in *15th International LS-Dyna Users Conference*, Detroit, 2018.

- [9] A. A. J. M. B. M. C. B. Miquel Trias, “FDA’s Nozzle Numerical Simulation Challenge: Non-Newtonian Fluid Effects and Blood Damage,” *PLOS ONE*, vol. 9, no. 3, pp. 1-114, 2014.
- [10] F. Sotiropoulos, “Computational Fluid Dynamics for Medical Device Design and Evaluation: Are We There Yet?,” *Cardiovascular Engineering and Technology*, vol. 3, no. 2, pp. 137-138, 2012.
- [11] ANSYS, Inc, “ANSYS CFX Reference Guide,” ANSYS, Inc, Canonsburg, 2013.
- [12] W. M. H.K. Versteeg, “Navier-Stokes Equations for a Newtonian Fluid,” in *An Introduction to Computational Fluid Dynamics: The Finite Volume Method*, Essex, Longman Scientific & Technical, 1995, pp. 21-24.
- [13] NASA, “Navier-Stokes Equations: 3 Dimensional - Unsteady,” NASA, Washing D.C., 2015.
- [14] Z. Warsi, “Conservation form of the Navier-Stokes equations in general nonsteady coordinates,” *AIAA Journal*, vol. 19, no. 2, pp. 240-242, 1981.
- [15] Ansys, Inc., “CFX Documentation,” 30 January 2016. [Online]. Available: [https://www.sharcnet.ca/Software/Ansys/17.0/en-us/help/ai\\_sinfo/cfx\\_intro.html](https://www.sharcnet.ca/Software/Ansys/17.0/en-us/help/ai_sinfo/cfx_intro.html). [Accessed 30 October 2018].
- [16] S. A. Orszag, “Analytical theories of turbulence,” *Journal of Fluid Mechanics*, pp. 363-386, 1970.
- [17] U. Piomelli, “Wall-layer models for large-eddy simulations,” *Progress in Aerospace Sciences*, vol. 44, no. 6, pp. 437-446, 2008.
- [18] J. Smagorinsky, “General Circulation Experiments with the Primitive Equations,” *Monthly Weather Review*, vol. 91, no. 3, pp. 99-164, 1963.
- [19] U.S. Food and Drug Administration (FDA), “Computational Round Robin #1 (Nozzle),” 19 January 2017. [Online]. Available: [https://nciphub.org/wiki/FDA\\_CFD/ComputationalRoundRobin1Nozzle](https://nciphub.org/wiki/FDA_CFD/ComputationalRoundRobin1Nozzle).

- [20] US Food & Drug Administration, “Computational Round Robin #1 (Nozzle),” 19 January 2017. [Online]. Available: [https://nciphub.org/wiki/FDA\\_CFD/ComputationalRoundRobin1Nozzle](https://nciphub.org/wiki/FDA_CFD/ComputationalRoundRobin1Nozzle).
- [21] US FDA, “Computational Round Robin 2 (Pump),” 24 March 2017. [Online]. Available: [https://nciphub.org/wiki/FDA\\_CFD/ComputationalRoundRobin2Pump](https://nciphub.org/wiki/FDA_CFD/ComputationalRoundRobin2Pump).
- [22] PolyFab, “Clear PVC Cone,” 13 January 2013. [Online]. Available: <http://www.polyfab.org/clear-pvc-cone.htm>.
- [23] bardiche1989, “Particle Imaging Velocimetry,” 1 March 2011. [Online]. Available: <https://www.youtube.com/watch?v=wFZ8b4u-pUA>.
- [24] W. T. a. E. J. Stamhuis, “PIVlab – Towards User-friendly, Affordable and Accurate Digital Particle Image Velocimetry in MATLAB,” *Journal of Open Research Software*, pp. 2-10, 2014.
- [25] W. L. A. B. M. F. OBERKAMPF, “Measures of agreement between computation and experiment: Validation metrics,” *Journal of Computational Physics - Special issue: Uncertainty quantification in simulation science* , pp. 5-36, 2006.
- [26] ANSYS, Inc, “CFX 17.2 User's Guide,” ANSYS, Inc, Canonsburg, 2016.
- [27] J. C. a. Y. A. Cengel, “Flow In Pipes,” in *Fluid Mechanics: Fundamentals and Applications*, McGraw Hill Education, 2010, pp. 321-332.
- [28] K. Chaitanya, “Boundary Layer Modeling using Inflation Layers,” CADFEM India, 4 July 2017. [Online]. Available: <http://www.cadfem.in/blog/organic/fbu/modeling-boundary-layer-inflation/>. [Accessed 5 April 2019].
- [29] S. H. N. M. S. H. B. & G. L. P. Ali Assoudi, “Experimental and numerical study of an offset jet with different velocity and offset ratios,” *Engineering Applications of Computational Fluid Mechanics*, vol. 1, no. 9, pp. 490-512, 2015.
- [30] M. N. Tsutomu Nozaki, “Experimental Study of Turbulence Properties For A Bounded Jet Flow,” Kagoshima National College of Technology, Kagoshima, 1990.

- [31] A. Kaushal, “Ansystutorial - CFD Of Venturi 2D Using Fluid Flow (Fluent) Module,” Grabcad Community, 16 September 2017. [Online]. Available: <https://grabcad.com/tutorials/ansys-tutorial-cfd-of-venturi-2d-using-fluid-flow-fluent-module>. [Accessed 31 March 2019].
- [32] FDA, “Critical Path Initiative,” 23 April 2018. [Online]. Available: <https://www.fda.gov/science-research/science-and-research-special-topics/critical-path-initiative>. [Accessed 20 April 2019].
- [33] Boston Scientific, “REBEL™ Platinum Chromium Coronary Stent System,” 13 May 2015. [Online]. Available: <http://www.bostonscientific.com/en-US/products/stents--coronary/rebel-platinum-chromium-coronary-stent-system.html>.

# Appendix A - GANTT CHART



# Appendix B - FDA DATASET

PIV_Sudden_Expansion_500_243 - Notepad					
File	Edit	Format	View	Help	
dataset-comment	plot-profile-axial-velocity-at-z	-0.088	plot-profile-axial-vi		
dataset-description	Sudden Expansion 500	-0.005861663	0.00452241	-0.005861663	
dataset-orientation	Sudden Expansion	-0.005677225	0.00940381	-0.005677225	
dataset-reynolds	500	-0.005492787	0.0148128	-0.005492787	0.0146127
dataset-laminar-turbulent		-0.005308348	0.0196668	-0.005308348	0.0196668
dataset-experiment	1	-0.00512391	0.024505	-0.00512391	0.0243296
dataset-code	243	-0.004939471	0.0290719	-0.004939471	0.0287821
dataset-experiment	1	-0.004755033	0.0334977	-0.004755033	0.0331538
geometry-flow-z-direction	1	-0.004570595	0.0378235	-0.004570595	0.0378235
geometry-throat-outlet-expansion-type	sudden	-0.004386156	0.0415471	-0.004386156	0.0415471
geometry-sudden-z	0	-0.004201718	0.0455057	-0.004201718	0.0454488
fluid-density	1056	-0.004017279	0.0493745	-0.004017279	0.0493512
fluid-viscosity	0.0035	-0.003832841	0.052565	-0.003832841	0.0526048
fluid-volumetric-flow-rate		5.21E-06	-0.003648403	0.056018	-0.003648403
plot-wall-distribution-pressure		-0.003463964	0.0595093	-0.003463964	0.0595093
17		-0.003279526	0.0623217	-0.003279526	0.062458
-0.09032	353.372	-0.003095087	0.064921	-0.003095087	0.0650765
-0.07696	353.372	-0.002910649	0.0678361	-0.002910649	0.0681499
-0.06299	353.372	-0.002726211	0.0706533	-0.002726211	0.0709753
-0.05723	287.933	-0.002541772	0.072908	-0.002541772	0.0731361
-0.05149	261.757	-0.002357334	0.074629	-0.002357334	0.0749763
-0.04575	274.845	-0.002172895	0.0765356	-0.002172895	0.0770419
-0.04001	130.879	-0.001988457	0.0786739	-0.001988457	0.0792404
-0.03	52.3514	-0.001804019	0.0806922	-0.001804019	0.081228
-0.01999	0	-0.00161958	0.0824392	-0.00161958	0.0828729
-0.01001	-104.703	-0.001435142	0.0837074	-0.001435142	0.0840979
-0.00203	-104.703	-0.001250703	0.0846836	-0.001250703	0.0850118
0	-130.879	-0.001066265	0.0853694	-0.001066265	0.0858579
0.00203	0	-0.000881826	0.086145	-0.000881826	0.0866663
0.008	26.1757	-0.000697388	0.0868308	-0.000697388	0.0873768
0.016	13.0879	-0.00051295	0.087372	-0.00051295	0.087955
0.024	0	-0.000328511	0.0877995	-0.000328511	0.0883017
0.032	0	-0.000144073	0.088064	-0.000144073	0.0885127
plot-z-distribution-pressure		0.000040366	0.0881386	0.000040366	0.0881386
17		0.000224804	0.0880811	0.000224804	0.0884764
-0.09032	353.372	0.000409242	0.0876974	0.000409242	0.0881846
-0.07696	353.372	0.000593681	0.0871843	0.000593681	0.0877495
-0.06299	353.372	0.000778119	0.0866211	0.000778119	0.0871185
-0.05723	287.933	0.000962558	0.0860107	0.000962558	0.0864245
-0.05149	261.757	0.001146996	0.0853119	0.001146996	0.0856592
-0.04575	274.845	0.001331434	0.0845315	0.001331434	0.0847727
-0.04001	130.879	0.001515873	0.0833621	0.001515873	0.0836765
-0.03	52.3514	0.001700311	0.0817637	0.001700311	0.0822638
-0.01999	0	0.00188475	0.0799475	0.00188475	0.0804257
-0.01001	-104.703	0.002069188	0.0779771	0.002069188	0.0783354
-0.00203	-104.703	0.002253626	0.0758587	0.002253626	0.0761465
0	-130.879	0.002438065	0.0740583	0.002438065	0.0741974
0.00203	0	0.002622503	0.0722105	0.002622503	0.072377
0.008	26.1757	0.002806942	0.0696489	0.002806942	0.0699271

Dataset from FDA Lab 243

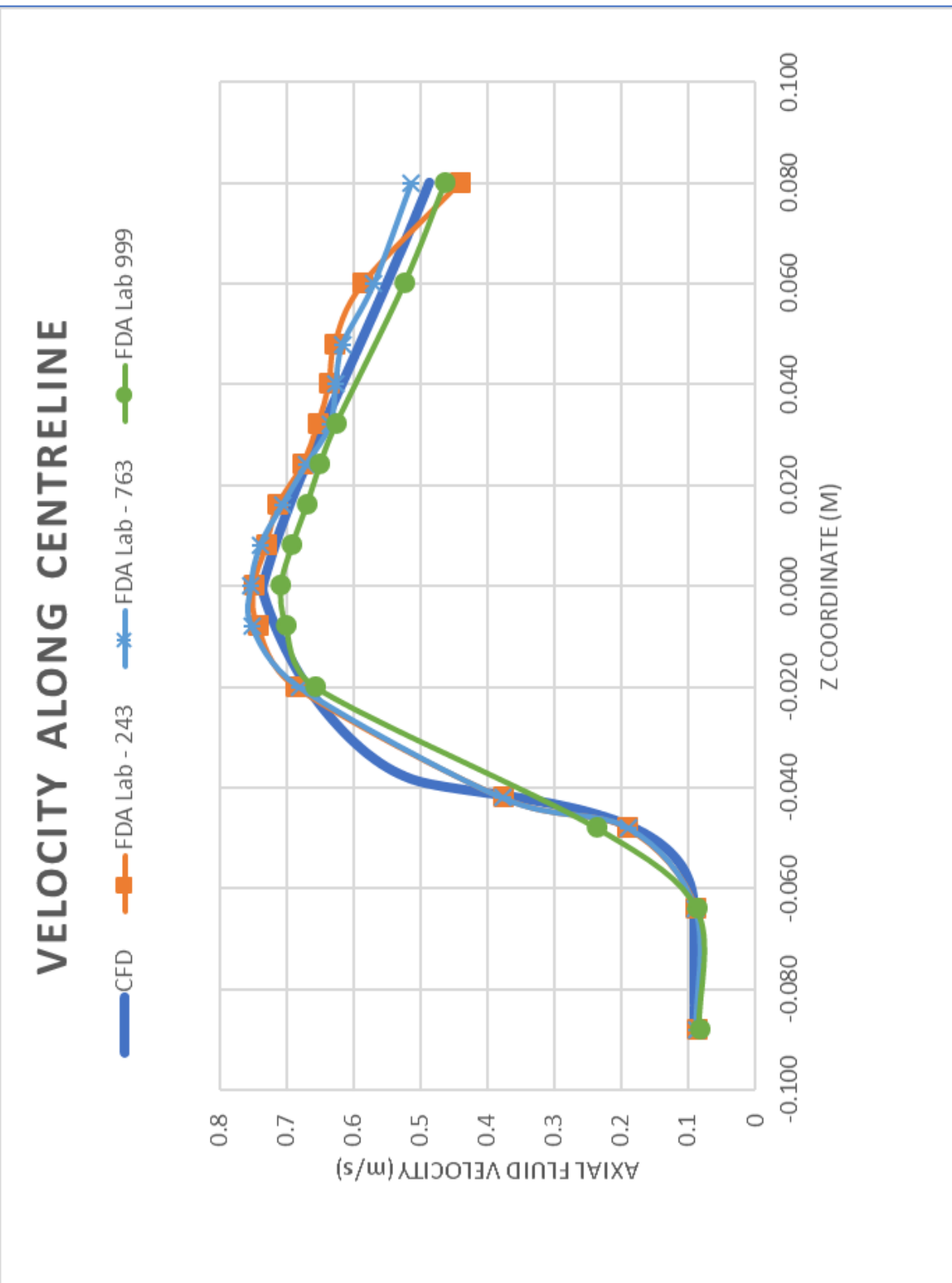
# Appendix C - CFD DATASET

A1	:		X	✓	f <sub>x</sub>
1	A	B	C	D	E
2	[Name]				
3	Centreline Velocity				
4					
5	[Data]				
6	X [ m ]	Y [ m ]	Z [ m ]	Velocity [ m s <sup>-1</sup> ]	
7	0.00E+00	0.00E+00	-1.47E-02	9.06E-02	
8	0.00E+00	0.00E+00	-1.64E-02	9.05E-02	
9	0.00E+00	0.00E+00	-1.81E-02	9.05E-02	
10	0.00E+00	0.00E+00	-1.98E-02	9.05E-02	
11	0.00E+00	0.00E+00	-2.15E-02	9.05E-02	
12	0.00E+00	0.00E+00	-2.32E-02	9.05E-02	
13	0.00E+00	0.00E+00	-2.49E-02	9.04E-02	
14	0.00E+00	0.00E+00	-2.66E-02	9.04E-02	
15	0.00E+00	0.00E+00	-2.83E-02	9.04E-02	
16	0.00E+00	0.00E+00	-3.00E-02	9.04E-02	
17	0.00E+00	0.00E+00	-3.17E-02	9.04E-02	
18	0.00E+00	0.00E+00	-3.34E-02	9.04E-02	
19	0.00E+00	0.00E+00	-3.50E-02	9.04E-02	
20	0.00E+00	0.00E+00	-3.67E-02	9.06E-02	
21	0.00E+00	0.00E+00	-3.84E-02	9.10E-02	
22	0.00E+00	0.00E+00	-4.01E-02	9.20E-02	
23	0.00E+00	0.00E+00	-4.18E-02	9.40E-02	
24	0.00E+00	0.00E+00	-4.35E-02	9.73E-02	
25	0.00E+00	0.00E+00	-4.52E-02	1.02E-01	
26	0.00E+00	0.00E+00	-4.69E-02	1.09E-01	
27	0.00E+00	0.00E+00	-4.86E-02	1.19E-01	
28	0.00E+00	0.00E+00	-5.03E-02	1.31E-01	
29	0.00E+00	0.00E+00	-5.20E-02	1.47E-01	
30	0.00E+00	0.00E+00	-5.37E-02	1.68E-01	
31	0.00E+00	0.00E+00	-5.54E-02	1.96E-01	
32	0.00E+00	0.00E+00	-5.71E-02	2.32E-01	
33	0.00E+00	0.00E+00	-5.88E-02	2.81E-01	
34	0.00E+00	0.00E+00	-6.05E-02	3.49E-01	
35	0.00E+00	0.00E+00	-6.22E-02	4.35E-01	

Dataset from extracted CFD velocity data

## Appendix D -

### FINAL MODEL CENTRELINE VELOCITY



## Appendix E -

### FINAL MODEL CENTRELINE PRESSURE

